The Hong Kong Polytechnic University

Department of Civil and Environmental Engineering

INTEGRATED DATA ANALYSIS AND CHARACTERIZATION OF PHOTOCHEMICAL OZONE IN SUBTROPICAL HONG KONG

By

LING ZHENHAO

A Thesis Submitted in Partial Fulfilment of the Requirements
for the degree of Doctor of Philosophy

October 2013

CERTIFICATE OF ORGINALITY

I hereby declare that this thesis is my own work and that, to the best of my knowledge and belief, it reproduces no material previously published or written, nor material that has been accepted for the award of any other degree or diploma, except where due acknowledgement has been made in the text.

_____ (Signed)

LING ZHENHAO_____ (Name of student)

Abstract

To understand the photochemical O_3 pollution at different elevations in mountainous areas, and to provide a conceptual description of O_3 pollution in Hong Kong, a number of field campaigns were undertaken in different locations in Hong Kong and the inland PRD region, which were followed by in-depth data analysis and model simulation.

Intensive field measurements were concurrently conducted for the first time at a mountain site (TMS) and an urban site at the foot of the mountain (TW) from September to November 2010. The mixing ratios of air pollutants were greater at TW than those at TMS, except for O_3. The relatively higher levels of O_3 at TMS were attributed to the combined influence of NO titration, vertical meteorological conditions, regional transport and mesoscale circulations. The photochemical O_3 formation at TMS was mostly influenced by VOCs, with measurable influence of NO_x, while O_3 production at TW was generally limited by the concentrations of VOCs. By using a photochemical box model coupled with master chemical mechanism (PBM-MCM), the photochemical reactivity at the above two sites were investigated. It was found that slightly higher HO_2 concentrations were found at TMS, while much higher OH concentrations were estimated at TW, suggesting that the HO_x cycling processes were different at the two sites due to the differences of O_3 and its precursors. The O_3 formation was dominated by the reaction of HO_2 + NO at the two sites, while O_3 was mainly destroyed by the reactions of OH + NO_2 at TW, and by the O_3 photolysis and the reaction of O_3 + HO_2 at TMS. Furthermore, more O_3 could be produced for each radical generated at TMS.

Since VOCs are the most important chemicals contributing to high O_3 production in Hong Kong and the inland PRD region, identification of VOC sources and

quantification of source contributions could provide valuable information for the formulation and implementation of O_3 pollution control measures. A new reactivity-based approach, combining the Positive Matrix Factorization (PMF) model with an observation-based model (OBM), was developed in this study. A new parameter, i.e., Relative Incremental Reactivity (RIR) – weighted value, considering both the emissions and reactivity of VOCs, was used to evaluate the contributions of VOC sources and the major species to O_3 formation. In the inland PRD region, ten VOC sources were identified, while seven sources were identified in Hong Kong. Among all the sources, vehicular- and solvent-related emissions contributed significantly to ambient VOCs. In addition, the RIR-weighted values indicated that the O_3 formation in inland PRD and Hong Kong was controlled by a small number of VOC species in specific sources. Sensitivity analysis on the basis of relative O_3 reduction efficiency (RORE) indicated that the O_3 reduction was the most effective when the identified VOC sources and the major species from these sources were cut by certain percentages.

Finally, to formulate and implement effective control strategies for O_3 pollution, a conceptual model was developed for the first time in Hong Kong based on the integrated data analysis at Tung Chung (TC) in Hong Kong between 2005 and 2010. By comparing meteorological parameters between O_3 and non-O_3 episode days, it was found that high temperatures, strong solar radiation, low wind speeds and relative humidity, northeasterly and/or northwesterly prevailing winds were favorable for the O_3 formation, while tropical cyclones were most conducive to the occurrence of O_3 episodes. Backward trajectories simulation and graphical illustration of O_3 pollution suggested that super-regional and regional transport were other factors that contributed to high O_3 levels in Hong Kong. The photochemical O_3 formation,

generally VOC-limited in Hong Kong, was controlled by a small number of VOCs, which were mainly from solvent usage and vehicular emissions.

Overall, the results of this study suggested that mesoscale circulations had a significant influence on the distributions of air pollutants in mountainous areas in Hong Kong, and the cycling processes among radicals, the production and destruction of O_3 were different at the mountain and urban sites due to the different levels of O_3 and its precursors. It is recommended that before the formulation and implementation of VOC control strategies, the abundance and reactivity of each VOC in each source should be considered. This study has provided an alternative way to more efficiently alleviate O_3 pollution by controlling specific VOCs in certain VOC sources and highlighted the importance of monitoring these VOCs.

The novelty of this study

In this study, to investigate the characteristics of photochemical air pollutants and the impact factors for the O_3 variations at different elevations in mountainous areas in Hong Kong, concurrent field measurements were firstly conducted at the mountain site (Mt. Tai Mo Shan, TMS) and the low-elevation urban site (Tsuen Wan, TW) in Hong Kong from September to November 2010. A newly developed photochemical box model coupled with master chemical mechanism (PBM-MCM) was applied to and constrained by the above full suite of air pollutants at TMS and TW to understand chemical mechanisms of photochemical reactivity under the influence of different levels of O_3 and precursors, including the HO_x budget, the OH chain length, and calculated O_3 production for the first time in Hong Kong.

Previous studies demonstrated that the O_3 formation was generally VOC-limited in Hong Kong, where most of the VOC control measures were mass-based. As such, a new reactivity-based method, combining the PMF and an observation-based model (OBM), was firstly developed based on the data collected in the inland PRD. This reactivity-based method was further used to investigate the roles of VOC sources in the O_3 formation in the urban area of Hong Kong, and the implications for VOC control policy were emphasized by considering both reactivity and abundance of VOC sources.

Finally, to obtain a full picture of O_3 pollution in Hong Kong, a conceptual model based on the 6-year monitoring data at Tung Chung (TC) was firstly developed by investigating the influence of meteorological conditions, O_3-precursors relationship and sources of O_3 precursors in 2005-2010. The significance of the conceptual modeling results to the future O_3 control policy formulation and implementation was highlighted.

PUBLICATIONS

1. **Ling, Z.H.**, Guo, H*., Cheng, H.R., Yu, Y.F., 2011. Sources of ambient volatile organic compounds and their contributions to photochemical ozone formation at a site in the Pearl River Delta, southern China. Environmental Pollution, 159, 2310-2319.

2. **Ling, Z.H.**, Guo, H*., Zheng, J.Y., Louie, P.K.K., Cheng, H.R., Jiang, F., Cheung, K., Wong, L.C., Feng, X.Q., 2013. Establishing a conceptual model for photochemical ozone pollution in subtropical Hong Kong. Atmospheric Environment, 76, 208-220.

3. Guo, H*., **Ling, Z.H.**, Cheung, K., Jiang, F., Wang, D.W., Simpson, I.J., Barletta, B., Meinardi, S., Wang, T.J., Wang, X.M., Saunders, S.M., Blake, D.R., 2013. Characterization of photochemical pollution at different elevations in mountainous areas in Hong Kong. Atmospheric Chemistry and Physics 13, 3881-3898.

4. **Ling, Z.H.** and Guo, H*., 2013. Contribution of VOC sources to photochemical ozone formation and its control policy implication in Hong Kong. Environmental Science and Policy, 10.1016/j.envsci.2013.12.004.

5. **Ling, Z.H.**, Guo, H*., Lam, S.H.M, Saunders, S.M., 2013. Atmospheric photochemical reactivity and ozone production at two sites in Hong Kong: Application of a photochemical box model with master chemical mechanism (PBM-MCM). In preparation.

6. Guo, H*., **Ling, Z.H.**, Cheung, K., Wang, D.W., Simpson, I.J., Blake, D.R., 2012. Observations of isoprene, methacrolein (MAC) and methyl vinyl ketone (MVK) at a mountain site in Hong Kong. Journal of Geophysical Research-Atmosphere 117, D19303, doi: 10.1029/2012JD017750, 2012.

7. Guo, H*., **Ling, Z.H.**, Simpson, I.J., Blake, D.R., Wang, D.W., 2012. Acetone in the atmosphere of Hong Kong: Abundance, sources and photochemical precursors, Atmospheric Environment 65, 80-88, 10.1016/j.atmosenv.2012.10.027.

8. Guo, H., Cheng, H.R., **Ling, Z.H.**, Louie, P.K.K., Ayoko, G.A., 2011. Which emission sources are responsible for the volatile organic compounds in the atmosphere of Pearl River Delta? Journal of Hazardous Materials 188, 116-124.

9. Feng, X.Q., Peng, K., **Ling, Z.H.**, Zheng, J.Y*., Guo, H., 2012. Source apportionments and characteristics of VOCs from 2005 to 2010 in Hong Kong. Acta Scientiae Circumstantiae 32, 12, 1-8.

10. Guo H.*, Wang D.W., Cheung, K., **Ling Z.H.**, Chan, C.K., Yao, X.H., 2012. Observation of aerosol size distribution and new particle formation at a mountain site in subtropical Hong Kong, Atmospheric Chemistry and Physics 12, 9923–9939, 2012.

11. Lam, S.H.M., Saunders, S.M., Guo, H*., **Ling, Z.H.**, Jiang, F., Wang, X.M., Wang, T.J., 2013. Modelling VOC source impacts on high ozone episode days observed at a mountain summit in Hong Kong under the influence of mountain-valley breezes. Atmospheric Environment 81, 166-176.

12. Gao, B., Guo, H., Wang, X.M., Zhao, X.Y., **Ling, Z.H.**, Zhang, Z., Liu, T.Y., 2013. Tracer-based source apportionment of polycyclic aromatic hydrocarbons in PM2.5 in Guangzhou, southern China, using positive matrix factorization (PMF). Environmental Science and Pollution Research 20, 4, 2398-2409.

13. Gao, B., Guo, H*., Wang, X.M., Zhao, X.Y., **Ling, Z.H.**, Zhang, Z., Liu, T.Y., 2012. Polycyclic aromatic hydrocarbons in PM2.5 in Guangzhou, southern China: Spatiotemporal patterns and emission sources. Journal of Hazardous Materials 239-240, 78-87.

CONFERENCE PRESENTATIONS

1. Ling, Z.H., Guo, H. (2010). Preliminary evaluation of airborne bioaerosols at livestock farms in the Pearl River Delta region, China. The 1st International Confrence on Sustainable Urbanization ICSU 2010, 15-17 December, 2010, Hong Kong.

2. Ling, Z.H., Guo, H. (2011). Relationship between ozone and its precursors at a mountain site and an urban site in Hong Kong. The 3rd International Workshop on Regional Air Quality Improvement in Rapidly Developing Economic Regions, 12-13 November, 2011, Guangzhou.

3. Ling, Z.H., Guo, H. (2012). Characterization of photochemical pollution at different elevations in mountainous areas in Hong Kong, the 1st GIGCAS-HKPOLYU Joint Workshop on Environmental Science and Engineering, 3rd November, 2012.

4. Ling, Z.H., Guo, H. (2012). Source contribution to photochemical ozone formation in Hong Kong, the 19th conference on Environmental Science and Technology in China, 2012, Qingdao.

5. Ling, Z.H., Guo, H. (2013). Simulations of a newly developed photochemical box model with master chemical mechanisms (PBM-MCM), the 12th International Conference on Atmospheric Sciences and Applications to Air Quality, 2013, Seoul, Korea.

6. Ling, Z.H., Guo, H. (2014). Atmospheric photochemical reactivity and ozone production at two sites in Hong Kong: application of a photochemical box model with master chemical mechanism (PBM-MCM). The 4th International Workshop on Regional Air Quality Management in Rapidly Developing Economic Regions, 2014, Hong Kong.

ACKNOWLEDGEMENTS

I would like to express my deepest gratitude to my supervisor Dr. GUO Hai for his constant encouragement, guidance, and providing me with an excellent atmosphere for doing research. I appreciate his vast knowledge and skill in many areas, and his assistance in writing thesis.

Very special thanks go to Prof. ZOU Shichun of Sun Yet-sen University for his guidance and support during my PhD study.

I must thank my friends, particularly Liu Qian, Cheng Hairong, Luo Chunling, Wang Zhe, Xu Likun, Guo Jia, Xu Zheng, Zhou Shenzhen, Chao Qiaozhi, Yan Chao, Huang Yu, Wang Dawei, Wang Nan, Yan Huanghuang, Cheung Kalam, Ou Jiamin and Liu Bo, for their support and care which helped me overcome setbacks and stay focused on my graduate study.

I would also like to thank my family for their support through my entire life and in particular, I must acknowledge my wife and daughter. Without their love and encouragement, I would not have finished this thesis. Paticular thanks to my dear wife. She took good care of my family and my daughter, and supported me regardless of up or down. I owed her a lot. May this thesis be a special gift to her.

Thanks god for providing me such a special trip in my life, guiding me, helping me and protecting me.

Finally, this project was supported by Hong Kong Polytechnic University PhD scholarship (RPHU), Hong Kong Research Grant Council of the Hong Kong Special Administrative Region (PolyU 5179/09E) and Environment and Conservation Fund (No. 7/2009).

Contents

LIST OF FIGURES

LIST OF TABLES

Chapter 1 Overview

1.1 Introduction

Ozone (O_3), a major component of photochemical smog which impairs visibility and human health, is formed by a complex series of chemical reactions involving (hydrogen oxide radical) HO_x radicals, i.e., hydroxyl radical (OH) and hydroperoxyl radical (HO_2), volatile organic compounds (VOCs) and nitrogen oxides (NO_x) in the presence of sunlight (Seinfeld and Pandis, 2006). In the troposphere, O_3 plays important roles in determining the oxidative capacity of the atmosphere, affecting human and vegetation health, and influencing the radiation budget of the atmosphere (NCR, 1991). In recent years, with increasing recognition of the adverse impact of O_3 on human health, a series of control measures have been implemented in Hong Kong and the rest of the Pearl River Delta (PRD) region to reduce O_3 and its precursors (GDEMC and HKEPD, 2005 – 2012; Cheng et al., 2010a, b; Zheng et al., 2010a). Though the concentrations of O_3 precursors have been reducing gradually in last decades, the concentration of O_3 is still increasing and high levels of O_3 were frequently observed in Hong Kong and the rest of Pearl River Delta (PRD) region (Wang et al., 2009; HKEPD, 2010, 2012a). For instance, Zheng et al. (2010a) demonstrated that there were 3 – 5 ppbv increases in 1 h-average O_3 levels and 8 – 11 ppbv increases in 1 h-max O_3 levels in 2007 compared to the values in 2006 across the PRD region. Moreover, a 14-year continuous study provides clear evidence that O_3 levels in the background atmosphere of South China have exhibited a slow rising trend since 1994 (Wang et al., 2009). Therefore, investigation of characteristic of O_3 is urgently needed for effectively controlling O_3 pollution in this area.

The dependence of O_3 formation on VOCs and NO_x has classified the O_3-precursors relationships into two categories: VOC-limited and NO_x-limited.

Previous studies have reported that the O_3 formation in the urban areas of Hong Kong and the inland PRD was generally VOC-limited (So and Wang, 2004; Huang et al., 2005; Zhang et al., 2007, 2008; Cheng et al., 2010a, b; Zheng et al., 2010a). Therefore, identification of VOC sources and quantification of source contributions could provide important information on reducing VOC emissions, which will result in O_3 reduction. The sources of VOCs have been investigated in Hong Kong and the inland PRD by using different methods. For instance, Guo et al. (2011a) applied the Positive Matrix Factorization (PMF) model to investigate VOC sources in Hong Kong and the inland PRD region, reporting that vehicular emissions and solvent use were the two major contributors to ambient VOCs. Using the same approach, Lau et al. (2010) identified 9 sources of VOCs at four sites in Hong Kong in 2002 – 2003 and 2006 – 2007, concluding that vehicle and marine vessel related sources and liquefied petroleum gas (LPG) were the most significant local sources. However, most of previous studies of the source identification and evaluation regarded each individual VOC as equally important to the O_3 formation, without considering the actual difference in O_3 formation potentials of individual compounds. Hence, the relative importance of potential VOC sources to the O_3 formation still remains unclear in this region.

Various measures have been implemented to reduce VOC emissions in Hong Kong and the inland PRD but most of the control strategies implemented were based on mass-based approaches, focusing on the control of the weight of total VOC emitted. Though measurability and practicality are the major advantage of the mass-based approach, it does not consider the O_3 formation potentials of VOCs (Avery et al., 2006). If heavier VOCs with lower photochemical reactivity were replaced by lighter VOCs with higher photochemical reactivity the O_3 pollution would be worse, as the

more reactive VOCs would increase the photochemical O_3 formation (HKEPD, 2010; Derwent et al., 2007a). Reactivity-based methods using MIR (maximum incremental reactivity) and OFP (O_3 formation potential) can overcome the limitation by considering the contributions of VOC species to photochemical O_3 (Chang et al., 2005; Derwent et al., 1998; Carter, 1994; Chameides et al., 1992), but the two methods simply estimate O_3 formation under optimum or ideal conditions. Consequently, a new reactivity-based method, considering both the emissions and the reactivity of VOCs, is urgently needed for better understanding the roles of VOCs in O_3 formation in Hong Kong and the inland PRD, where serious O_3 pollution is frequently observed.

Though many studies on photochemical O_3 have been conducted in Hong Kong and the inland PRD in recent years (Lam et al., 1998; Chan et al., 1998a, b; Lee et al., 2002; So and Wang, 2003; Huang et al,, 2005, 2006; Wang et al., 2006; Guo et al., 2009; Wang et al., 2009), these studies focused on the levels and spatial and temporal variations of O_3, the O_3-precursors relationships, and the influence of meteorology on O_3. The photochemical reactivity of O_3, its precursors, free radicals, and intermediate products, which could provide valuable insights into the formation and abatement of O_3 pollution, were poorly understood in this region. In addition, the photochemical reactivity may be different due to the variations of O_3, its precursors, and meteorological conditions in different areas, especially in this region where the topography and physical features are complex (AFCD, 2008). For further policy implementation of regional policies to alleviate photochemical O_3 problem, it is necessary to understand the photochemistry of O_3 and its precursors in different areas.

In addition to the emissions of its precursors, meteorological conditions have significant influence on O_3 pollution. High temperature, intense solar radiation, low winds and relative humidity are favorable for photochemical O_3 formation. Tropical

cyclones have been found to be mostly conducive to the occurrence of high O_3 mixing ratios in PRD (Lam et al., 2004, Huang et al., 2005, Jiang et al., 2008). In addition to the above meteorological parameters, long-range transport could also induce high O_3 levels observed in Hong Kong and the inland PRD region. Guo et al. (2009) investigated the O_3 characteristic at a suburban site in PRD and found that the high O_3 mixing ratios there were associated with air masses from Eastern China. Based on data simulated by the Weather Research and Forecasting (WRF) model, Jiang et al. (2010) reported that the weather conditions induced regional transport of O_3 pollution occurred in the fall of 2007.

It has been well known that in addition to long-range transport, mesoscale circulations like mountain-valley/sea-land breezes, play important roles in redistributing air pollution in mountainous/coastal regions. The coastline and the mountains combine to give a terrain with many complex physical features in Hong Kong. The role of sea-land breezes in air pollution transport has been well-studied (Zhang and Zhang, 1997; Liu et al., 2000; Ding et al., 2004). For instance, Ding et al. (2004) studied the impact of sea-land breeze on transporting air pollutants during an O_3 episode in the PRD region and concluded that cross-border transport and sea-land breeze did play a critical role in air-quality deterioration in the PRD region. There were relatively few Hong Kong studies focusing on mountain-valley breezes, even though they are almost certainly very important to air pollution transport in Hong Kong, where topography and physical features are complex and where about 75% of the land area is hilly (AFCD, 2008). In addition, there were very few studies conducting field measurements at mountain sites, especially concurrent measurements at the foot and summit of the mountain in this region.

Through the results of this study, it could be found that meteorological conditions, i.e., high temperature, strong solar radiation, low wind speed, northerly winds, regional transport and mesoscale circulations have significant influence on O_3 pollution in Hong Kong. In particular, tropical cyclones were mostly conducive to the occurrence of high O_3 mixing ratios in this region. In addition, regional transport and mesoscale circulations could have significant influence on the redistribution of air pollutants in subtropical Hong Kong. Furthermore, the O_3 formation was generally VOC-limited at the urban environment, while measurable influence of NO_x could be also found at the mountain site in Hong Kong. Controlling vehicular- and solvent-related emissions could alleviate the O_3 pollution throught reducing VOCs in Hong Kong and the inland PRD region. Moreover, the investigation of photochemical reactivity indicated that the HO_x cycling processes and O_3 fomration were different at TMS and TW due to different levels of precursors, and the longer OH chain length suggested that more O_3 could be produced for each radical that is produced at TMS. Overall, these results are expected to provide additional support to alleviate the O_3 pollution in the PRD region.

1.2 Aims and objectives

An intensive field measurement was carried out simultaneously at the mountain site and an urban site at the foot of the mountain in Hong Kong from September to November 2010. The high quality measurement data from this concurrent field measurement, together with data from another field measurement in the inland PRD, enable a set of comprehensive analysis of the characteristics and the impact factors of O_3 pollution and the O_3-precursors relationships at different elevations, the influence of mesoscale circulations on the distributions of air pollutants, the similarities and differences of photochemical reactivity under the influence of different levels of O_3

and its precursors, and the contributions of VOC sources to O_3 formation in Hong Kong. In addition, data from a 6-year monitoring campaign at Tung Chung provide us with an opportunity to develop a conceptual model for the O_3 pollution in Hong Kong.

The major objectives of this study are therefore as follows:

- Characterize the O_3 pollution and investigate the impact factors that influence the variations of O_3 pollution at different elevations in Hong Kong;
- Investigate the influence of mesoscale circulation/regional transport on air pollutants and the relationships between O_3 and its precursors at different elevations in Hong Kong.
- Develop a new reactivity-based method to evaluate the contributions of VOC sources to O_3 formation in Hong Kong and the inland PRD region.
- Investigate the similarities and differences of photochemical reactivity under different relative concentrations of O_3 and precursors at two sites in Hong Kong.
- Develop a conceptual model for the O_3 pollution in Hong Kong.

1.3 Structure of the thesis

The thesis is composed of nine chapters as follows:

1) Chapter 1 provides the background and the major research objectives of this study.

2) Chapter 2 presents a brief literature review on the characteristics and the impact factors of O_3 pollution, the characteristics of O_3 precursors, the O_3-precursors relationships and the photochemical oxidation.

3) Chapter 3 describes the methodology used in this study, including the description of sampling sites, measurement techniques, data analysis, quality control, quality assurance (QA/QC) and model description.

4) Chapter 4 gives an overview of the variations of O_3 pollution and its impact factors and the O_3-precursors relationships at different elevations in Hong Kong.

5) Chapter 5 develops a new reactivity-based method to investigate the roles of VOC sources in O_3 formation based on the data collected in the inland PRD region.

6) Chapter 6 applies the new reactivity-based method to the Hong Kong dataset to investigate the contributions of VOC sources to O_3 formation and provide suggestions for O_3 control in Hong Kong.

7) Chapter 7 investigates the photochemical reactivity under the influence of the different levels of O_3 and its precursors at two sites in Hong Kong.

8) Chapter 8 presents the development of a conceptual model of O_3 pollution in Hong Kong.

9) Chapter 9 highlights the major findings, the significant contributions and the implications of the study.

Chapter 2 Literature Review

2.1 Photochemical ozone formation

Ozone (O_3), a major constituent of photochemical smog, is a key trace gas in the atmosphere. The O_3 layer in the upper atmosphere (stratosphere) is beneficial, preventing potentially damaging electromagnetic radiation from reaching the Earth's surface. However, in the lower atmosphere (troposphere, 0 – 10 km), O_3 plays important roles in atmospheric chemistry, climate change, and air quality (NRC, 1991; Godish, 2004). Owing to its adverse health effects, tropospheric O_3 has become one of the most studied topics in recent decades (Bell et al., 2004; Mauzerall and Wang, 2001; Zheng et al., 2010a).

Ozone in the troposphere is determined by the downward transport of stratospheric air (Stohl, et al., 2003), dry deposition on the earth's surface and series of photochemical reactions involving volatile organic compounds (VOCs) and nitrogen oxides (NO_x) in the presence of sunlight. The mechanisms of photochemical reactions resulting in O_3 formation are summarized below. Figure 2.1 presents the details of the chemistry for the oxidation of a generic saturated hydrocarbon, RH (i.e., an alkane), into its first-generation oxidized products, while reactions R1 – R9 show the simplified mechanism for the process of O_3 formation initiated by both saturated and unsaturated hydrocarbons with OH radical (Jenkin and Clemitshaw, 2000).

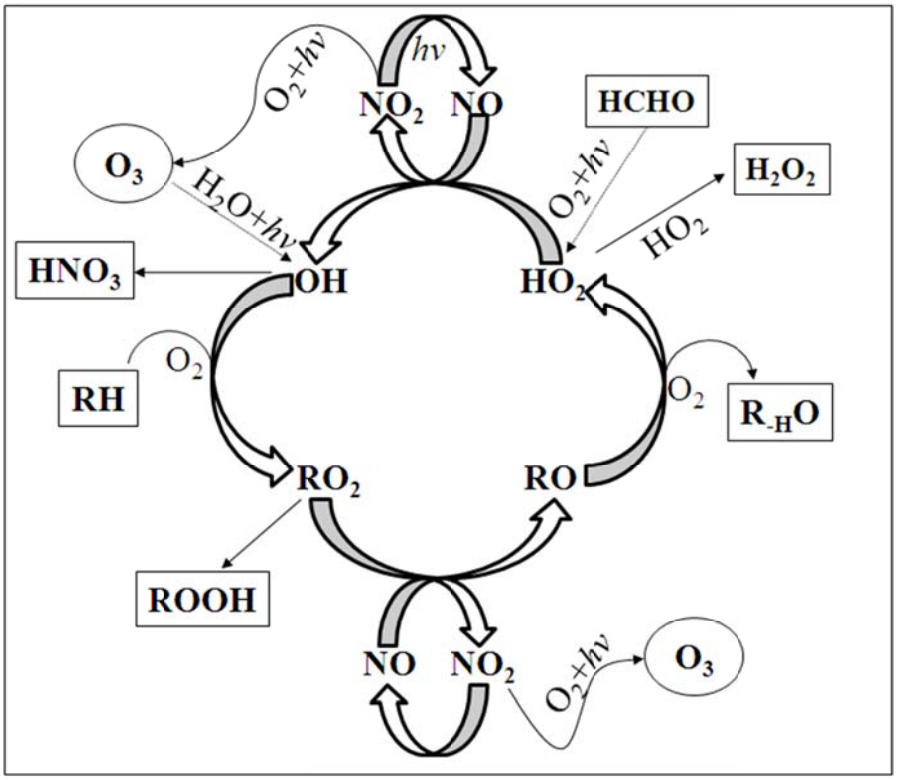

Figure 2.1 Schematic representation of the free radical-catalyzed oxidation of a generic saturated hydrocarbon, RH, to its first generation oxidized product, $R_{-H}O$. The key role played by the NO_x species in the chain-propagating process, which leads to the generation of O_3 as a by-product, is also illustrated. The major sources and sinks of the free radicals are also shown (Jenkin and Clemitshaw, 2000)

(R1) $RH + OH\cdot \rightarrow R\cdot + H_2O$

(R2) $R\cdot + O_2 + M \rightarrow RO_2\cdot + M$

(R3) $RO_2\cdot + NO \rightarrow RO\cdot + NO_2$

(R4) $RO\cdot + O_2 \rightarrow R_{-H}O + HO_2\cdot$

(R5) $HO_2\cdot + NO \rightarrow OH\cdot + NO_2$

(R6) $NO_2 + h\nu \rightarrow NO + O\cdot$

(R7) $O\cdot + O_2 + M \rightarrow O_3 + M$

Net: $RH + 4O_2 + h\nu \rightarrow RCHO + 2H_2O + 2O_3$

The OH radical, formed primarily via the photolysis of O_3, initiates the reaction sequence. Then the OH radical reacts with both saturated and unsaturated hydrocarbons to form alkyl proxy radicals ($RO_2\cdot$), efficiently converting NO to NO_2. Finally, photochemical O_3 is formed by the subsequent photolysis of NO_2. It should be noted that the formation of $RO_2\cdot$ is the rate-limiting step for the above photochemical reactions. The net reaction for the above mechanisms converts one molecule of the saturated and/or unsaturated hydrocarbons to ketones and aldehydes, forming two molecules of O_3. In addition, O_3 can also be generated from CO oxidation via

(R8) $CO + OH\cdot \rightarrow CO_2 + H\cdot$

(R9) $H\cdot + O_2 \rightarrow HO_2$

followed by (R5), (R6), and (R7).

Although VOCs and NO_x have been confirmed to be key precursors of photochemical O_3 production, it is difficult to determine whether O_3 production during specific events is associated with NO_x-sensitive chemistry or VOC-sensitive chemistry, due to its complicated chemistry processes which depend on meteorological parameters and concentrations of VOCs and NO_x. The rate of O_3 production (ppb h^{-1}) as a function of NO_x and VOCs concentrations is shown in Figure 2.2 (Sillman, 1999). The isopleths plot shows that the rate of O_3 formation is a nonlinear function of VOC and NO_x concentrations in the atmosphere, depending on the relative concentrations of VOCs and NO_x. When NO_x is low, the rate of O_3 formation increases with the increase of NO_x in a near-linear fashion. As NO_x increases, the rate of increase in O_3 formation slows and eventually reaches a local maximum. At higher NO_x concentrations, the rate of O_3 formation would decrease with the increase of NO_x. The line representing the local maxima for the rate of O_3 formation (the “ridge line”) can be thought of as a dividing line separating two

different photochemical regimes. In the NO_x-sensitive regime below the ridge line, O_3 increases with the increase of NO_x and shows relatively little change in response to increased VOCs. In the VOC-sensitive (or NO_x-saturated) regime, O_3 increases with the increase of VOCs and decreases with the increase of NO_x. So the ratio of VOCs to NO_x is an important parameter to evaluate whether the production of O_3 is controlled by NO_x or VOCs, and high VOC/NO_x ratios generally correspond to NO_x-limited and low VOC/NO_x ratios correspond to VOC-limited. Thus, the development of an effective O_3 abatement strategy in a given urban area requires an in-depth understanding of the two key O_3 precursor relationships: 1) the relative concentrations of NO_x and VOCs in the area (e.g. VOCs : NO_x ratio), and 2) the mix of reactive VOCs present in the atmosphere.

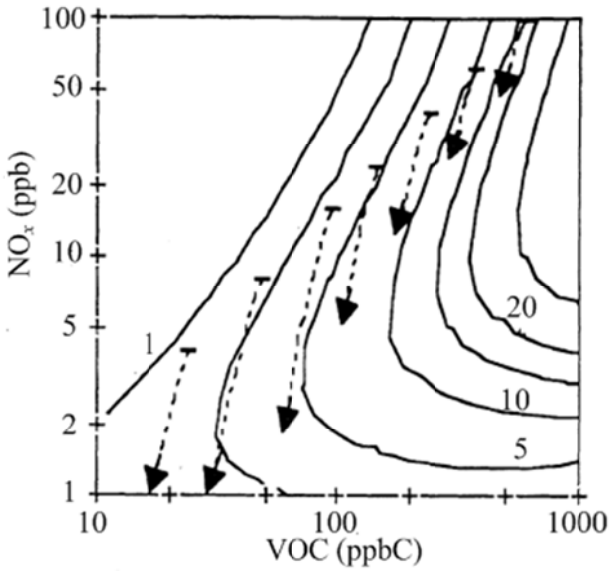

Figure 2.2 Isopleths giving net rate of ozone production (ppb/h, solid lines) as a function of VOC (ppbC) and NO_x (ppb) for mean summer daytime meteorology and clear skies. The solid lines represent production rates of 1, 2.5, 5, 10, 15, 20 and 30 ppb/h. The dashed lines and arrows show the calculated evolution of VOC and NO_x concentrations in a series of air parcels over an 8 h period (9 am-5 pm), each with initial VOC/NO_x = 6 and speciation typical of urban centers in the US, based on calculations shown in Milford et al. (1994)

2.2 Ambient concentration and characteristics of ozone

Extensive O_3 studies have been conducted to characterize tropospheric O_3 in different locations all over the world (Chan et al., 1998a; Jacob et al., 1999; Hidy, 2000; Kleinman, 2000; Solomon et al., 2000; Jaffe et al., 2003; Vingarzan and Taylor, 2003; Chou et al., 2006; Oltmans et al., 2006; Derwent et al., 2007b; Jaffe and Ray, 2007; Krzyscin et al., 2007; Jenkin, 2008; Guo et al., 2009; Kurokawa et al., 2009; Shao et al., 2009a, b; Tanimoto et al., 2009; Tarasova et al., 2009; Wang, T. et al., 2009; Wang, Y. et al., 2011). In general, the O_3 levels and characterisitics varied temporally and spatially due to the fact that the O_3 concentration in any given area results from a combination of formation, transport, destruction and deposition.

The magnitude and patterns of O_3 vary in different areas because of the complex interactions of chemical and meteorological factors. Previous research indicates that ground-level O_3 concentrations are strongly influenced by the changes in anthropogenic emissions of O_3 precursors, regional transport and atmospheric circulations (Ryerson et al., 2003; Pochanart et al., 2003; Zellweger et al., 2003; Parrish et al., 2004, 2009; Chang et al., 2005; Jaffe and Ray, 2007; Oltmans et al., 2008; Guo et al., 2009; Wang et al., 2009; Zheng et al., 2009a, b; Gilge et al., 2010; Fiore et al., 2011). Below shows the detailed literature review of the ambient O_3 concentrations and characteristics.

2.2.1 Atmospheric oxidation chemistry and O_3 productions

As described above, the O_3 formation in the atmosphere involves the chemistry of atmospheric radicals, particularly the hydroxyl radical (OH) and it's chemical relative hydroperoxyl radical (HO_2). It was found that the photolysis of O_3, nitrous acid (HONO), oxygenated VOCs (OVOCs) and hydroperoxide (H_2O_2) are the primary sources for the HO_x, including OH and HO_2 in the atmosphere (Ren et al., 2013).

Investigating the atmospheric oxidation chemistry can provide detailed information of the O_3 formation mechanism. Therefore, many studies have been conducted to characterize the atmospheric oxidation and O_3 production in different locations (Ren et al., 2006, 2008, 2013; Mao et al., 2009, 2010; Hofzumahaus et al., 2009; Dusanter et al., 2009; Shirley et al., 2006; Sommariva et al., 2004; Martinez et al., 2003). Most of the studies were conducted in North America and focused on the abundance of OH and HO_2 by measurements, in addition to using different models with different mechanisms to investigate the HO_x budget and O_3 calculation. In general, unexplained high concentrations of OH were observed in the presence of high VOC mixing ratios and low to moderate NO_x levels in rural forested North America (Rent et al., 2008) and above the tropical rainforest in Surinam (Lelieveld et al., 2008). On the other hand, different variations were found in the urban areas. For example, Ren et al. (2006) conducted a field measurement of OH and HO_2 radicals in New York City. They found that OH and HO_2 levels in the winter of 2004 were much higher than those observed in the summer of 2001. The average maximum daytime mixing ratios in winter 2004 were 0.05 pptv for OH and 0.7 pptv for HO_2, which were about one fifth of the levels in the summer of 2001. Furthermore, a zero-dimension chemical model with the regional atmospheric chemical mechanism (RACM) was constrained by the measured parameters to investigate the HO_x chemistry in the urban environment. Though the model reproduced the daytime OH well, it under-predicted the HO_2 during the whole day, which may be caused by the missed HO_x production in the model.

Similar results suggested by the lower HO_2/OH ratio in the model were also found in other urban areas in North America, e.g. Mexico City (Dusanter et al., 2009; Shirley et al., 2006). The lower HO_2/OH ratio suggested that model may overestimate

the HO_2 to OH propagation rate or a process converting OH into HO_2 may be missing from the chemical mechanism when the NO mixing ratios were higher than 5 ppbv. The model results indicated that photolysis of HONO and HCHO was the major contributor to HO_x production during the daytime, while the reactions of O_3 and alkenes dominated at night. Mao et al. (2010) compared the photochemical activity of four sampling campaigns in North America: TEXAQS2000 (Houston, 2000), NYC2001 (New York City, 2001), MCMA2003 (Mexico City, 2003) and TRAMP2006 (Houston 2006). They found that the photochemical reactivity was associated with the relative dependence of O_3 precursors, i.e. VOCs and NO_x. However, a problematic result of greater OH production than OH loss during morning rush hour was found in all four sutides, which may be related to the under-predicted HO_2 in high NO_x conditions. In addition to the abundance of HO_x, the measurement of OH reactivity provides a useful tool to investigate atmospheric photochemistry. In the Inter-continental Chemical Transport Experiment-B (INTEX-B) campaign, the measured OH reactivity was higher than the OH reactivity calculated from the total measurements of all OH reactants. The higher OH reactivity was most likely related to some highly reactive VOCs that had HCHO as an oxidation production.

In the PRD region, limited studies have been conducted to characterize the atmospheric oxidation (Hua et al., 2008; Hofzumahaus et al., 2009; Lou et al., 2010; Lu et al., 2012). Hofzumahaus et al. (2009) measured the OH abundance at the Guangzhou Backgarden site in the PRD region. The most striking feature of their findings is the high average OH concentration of 15×10^6 cm^{-3} around noon, although a large OH reactivity of about 20 s^{-1} was found. Lou et al. (2010) presented the atmospheric OH reactivity at the same site and found that the OH reactivity, k_{OH} exhibited a pronounced diurnal profile with a mean maximum value of 50 s^{-1} at

daybreak and a mean minimum value of 20 s^{-1} at noon. The comparison between the measured reactivity and the calculated k_{OH} from measured trace gases revealed a missing reactivity of about a factor of 2 at day and night. The contributions for the calculated OH reactivity of different reactants indicated that anthropogenic pollutants, including CO, NO_x, light alkenes and aromatic hydrocarbons dominated the OH reactivity at night, while it was stongly influenced by local biogenic emissions of isoprene during the day. In addition, a box model constrained by the measured data could reproduce the observed OH reactivity well and suggested that the unmeasured secondary chemistry products, i.e. aldehydes and ketones, were the main cause of the discrepancy between the calculated and measured OH reactivity.

2.2.2 Long-term trends of ozone

Investigation of long-term trends of O_3 could provide useful information for evaluating the impact of O_3 on human health, vegetation, and climate change. The long-term trends of O_3 in the given areas are determined by the trends of background levels and regional changes. The increase of industrial activities, motorized traffic, and agricultural activities, especially over the last century, has resulted in a strong increase of emissions of many species, such as sulfur dioxide (SO_2), NO_x and VOCs including carbon monoxide (CO) and methane (CH_4). Except for SO_2, these species are involved in the chemical production of O_3 in the troposphere. There is increasing evidence for the emergence of long-term trends in tropospheric O_3. Early satellite measurements indicating a hemispheric rise in tropospheric O_3 are now supported by more recent studies, which suggest a rising trend in surface O_3 in areas of North America and Europe (Lin et al., 2000).

A large number of studies have been conducted to investigate the long-term variations in ground-level O_3 concentrations around the world (Vingarzan and Taylor,

2003; Vingarzan, 2004; Oltmans et al., 2006; Jenkin, 2008; Tanimoto, 2009; Tarasova et al., 2009; Wang et al., 2009; Gilge et al., 2010). Vingarzan (2004) characterized the background levels and trends of O_3 by reviewing the historical and current surface O_3 data from 30 background stations in Canada, the United States and other locations around the world, reporting that background O_3 levels over the midlatitudes of the Northern Hemisphere have continued to rise over the past three decades, with an increase of 0.5 – 2% per year. In addition, it was indicated by model projections using Intergovernmental Panel on Climate Chang (IPCC) emission scenarios for the 21st century that background O_3 may rise to levels that would exceed internationally accepted environmental criteria for human health and the environment.

In Europe, surface O_3 concentration is highly variable in both space and time on long scale. For instance, Simmonds et al. (2004) showed that background O_3 in the clean oceanic sector measured at Mace Head, Ireland, increased by about 8 ppb for the period 1987 – 2003. Oltmans et al. (2006) reported a significant increase in O_3 concentration with an overall increase of 12.6 (± 0.8) % /decade from 1978 to 2004 at Zugspitze, Germany. Similarly, a gradual increase, resulting from global scale effects, was also found in the north-hemispheric baseline O_3 concentrations by investigating the average trends of O_3 concentrations at 13 rural sites in 1990 – 2006 and at 5 urban sites in 1993 – 2006 in the UK.

Tarasova et al. (2009) investigated the historical O_3 trends based on long-term O_3 measurements at two background mountain sites, namely the Kislovodsk High Mountain Station in Caucasus, Russia (KHMS) and the Jungfraujoch in Switzerland (JFJ), reporting that O_3 mixing ratio increased at JFJ (0.73 ± 0.20 ppb/year in 1991 – 2001 and 0.04 ± 0.21 ppb/year in 2001 – 2006) and decreased at KHMS (-0.91 ± 0.17 ppb/year in 1991 – 2001 and -0.37 ± 0.14 ppb/year in 2001 – 2006) due to the

different influence of topographic features and emission sources. Consistent with Oltmans et al., 2006 and Tarasova et al., 2009, Gilge et al. (2010) also reported that the O_3 mixing ratios have slightly increased at three Global Atmosphere Watch (GAW) program mountain stations: Hohenpeissenberg, Sonnblick and Jungfraujoch. This feature was observed independent of wind sector and for most seasons, with a tendency to higher positive trends in winter and lower, partly negative trends in summer.

In North America, an increasing O_3 trend has often been found in the past two decades. Lin et al. (2000) examined the long-term trend of background O_3 in surface air over the United States using the hourly O_3 data at EPA monitoring stations from 1980 – 1998. A feature of increase in the highest percentile concentrations and decrease in the lowest percentile concentrations was extracted from the analysis of monthly probability distributions. They reported that the increase was significant in spring and fall with a range of 3 – 5 ppbv, probably attributed to the increase in the O_3 background transported from outside of the United States, which was demonstrated by a recent study by Oltmans et al. (2008). Similarly, Jaffe et al. (2003) presented that O_3 concentration in spring had increased by approximately 10 ppbv from the mid-1980s to 1995 by using a 15-year record of O_3 at a rural elevated site, Lassen Volcanic National Park in North California. They explained that the increased spring O_3 was due to the increase in global NO_x emissions, which was further evidenced by Parrish et al. (2004). In addition, an increasing O_3 trend was also identified in the western US by the analysis of O_3 data for the period 1987 – 2004 (Jaffe and Ray, 2007). Interestingly, Parrish et al. (2009) pointed out that the background boundary layer O_3 mixing ratios over the 130 years covered by available data had increased substantially (by a factor of two to three). They held the opinion that the increase continues at

present, at least in the marine boundary layer of the Pacific coast region of North America. In Canada, a decreasing and an increasing trend for annual O_3 was found between 1985 and 2000 in the eastern and western portion of southern British Columbia, respectively (Vingarzan and Taylor, 2003).

In Asia, most of the studies about long-term variations of O_3 were concentrated in Japan, Mainland China, Hong Kong and Taiwan. Lee et al. (1998) presented an evaluation trend of O_3 in Northeast Asia based on 8 year-long O_3 sounding data obtained between 1989 and 1997 at Naha in Japan. They reported an O_3 increase of 2.5%/year in Asian continental air during the winter – spring period, relating to the increasing emission of NO_x from the Northeast Asia region. Compared to the O_3 concentration in 1999 – 2002, an increasing trend was observed during springtime in 2003 – 2006 (Tanimoto, 2009) at a mountainous site in Japan. In Taiwan, Chou et al. (2006) reported that the annual average concentration of O_3 increased by 58% from 1994 – 2003 in Taipei, while the emissions of O_3 precursors, i.e. NO_x and VOCs decreased significantly in the same period. They explained that the increasing trend of O_3 in Taipei was due to the reduced titration by NO.

In Mainland China, Xu et al. (2008) reported that the average O_3 concentrations have increased by 2.0%/year, 2.7%/year, 2.4%/year and 2.0%/year for spring, summer, fall and winter, respectively, based on the data collected during 6 periods between August 1991 and July 2006 at Lin'an in eastern China. They pointed out that the increase of O_3 was likely attributed to the increase of NO_x concentration. In Beijing, O_3 concentrations increased at a rate of 1.1 ± 0.5 ppb/year during 2001 – 2006 based on the analysis of data collected at six urban sites between the months of July and September. This surface O_3 variability was accentuated primarily by a decrease in

NO_x emissions and an increase in non-methane hydrocarbon compounds (NMHCs) emissions.

Wang et al. (2009) presented a continuous record of surface O_3 in a background air monitoring station at Hok Tsui, Hong Kong from 1994 to 2007. The O_3 mixing ratio was found to be increased by 0.58 ppbv/year based on a linear fit to the 14-year record. They explained that the increasing background O_3 in the South China coastal region was associated with the increasing NO_2 column concentration in upwind Eastern China.

2.2.3 Temporal variations of ozone concentrations

The following section will be reviewed the studies of temporal variations of O_3, such as seasonal variations and diurnal variations around the world.

2.2.3.1 Seasonal variations of ozone concentrations

Extensive measurements have shown that O_3 concentration exhibits pronounced seasonal cycles that may have different shapes at different latitudes and altitudes (Monks, 2000). The seasonal cycle of O_3 in the troposphere is controlled by a number of processes such as proximity to large sources areas of O_3 precursors, geographical location and meteorological factors (Vingarzan and Taylor, 2003).

Over the last couple of decades typical seasonal variations were found for the annual cycle of O_3 over the mid-latitudes with a broad summer maximum typical of populated and industrialized areas and a spring maximum typical of remote regions under the influence of background conditions (Ancellet and Beekmann, 1997; Monks, 2000; Tanimoto et al., 2002; Carnero et al., 2010). For example, Tiwari et al. (2008) stated that daytime 12-hourly mean O_3 mixing ratios varied from 45.18 to 62.35 ppbv during summer and from 28.55 to 44.25 ppbv during winter in Varanasi, India, during

2002 – 2006. Elevated O_3 levels during the summer months can be attributed to high temperature, favoring photochemical production of O_3, while relatively lower levels of O_3 during the winter might be due to greater atmospheric stability and an increased incidence of nocturnal inversions, which might enhance the chemical scavenging of O_3 and dry deposition. Carnero et al. (2010) also reported that O_3 concentrations in Spain presented a seasonal variability, with higher values in summer and, lower concentrations in winter. The high levels in summer could be due to the photochemical production in-situ and/or the influence of horizontal or vertical O_3 transport. It could be concluded that the relatively higher O_3 concentrations in summer are mostly associated with the in-situ photochemical O_3 formation, relating to the stronger solar radiation. On the other hand, the primary reason for the origin of the spring maximum O_3 concentrations was the accumulations of its precursors, i.e. VOCs and NO_x during winter (Simpson et al., 1995).

2.2.3.2 Diurnal variations of ozone concentrations

In general, O_3 variation over the diurnal scale can provide insight to the interplay of emissions, chemical and physical processes that operate on a diurnal cycle.

Previous studies have shown that O_3 levels tend to follow the solar radiation intensity, resulting in higher O_3 concentrations during the daylight period (Wang et al., 2006a; Guo et al., 2009). For instance, maximum O_3 mixing ratio was frequently observed in the afternoon, which was primarily due to the higher solar radiation, temperature, and the active in-situ photochemical formation. On the other hand, the destruction of O_3 by primary pollutants and different deposition mechanisms resulted in the minimum levels observed at night (Chan et al., 1998a; Wang et al., 2001; Cheng et al., 2010a). Though the typical diurnal behavior was observed at different locations, different characteristics are also existed due to the different conditions of air

pollutants, deposition and air masses transport. For example, relatively higher O_3 mixing ratios were observed at the suburban site in Hong Kong (Tung Chung, TC) than at a rural site in the inland Pearl River Delta (PRD) region at night, which may be due to the import of O_3 from the ocean in Hong Kong (Guo et al., 2009). On the other hand, the diurnal variation of O_3 exhibited a broad daytime peak at a relatively remote coastal site (Cape D'Aguilar, i.e., Hok Tsui), while the peak of O_3 was much narrower at a downwind suburban site (Sha Lo Wan) in Hong Kong (Wang et al., 2001a).

2.2.4 O_3 studies in the mountainous areas

Unlike from surface measurements and aircraft observations, studies conducted in mountain areas often provide information on the regional background concentrations of air pollutants, the influence of regional transport and mesoscale circulations, the photochemistry of biogenic volatile organic compounds (BVOCs), and the influence of meteorological factors on O_3 chemistry (Pochanart et al., 2003; Zellweger et al., 2003; Gao et al., 2005; Wang et al., 2006b; Fu et al., 2010). The characteristics of O_3 in mountainous areas have been investigated in various locations in recent years (e.g. Evtyugina et al., 2009; Scott and Ahmet, 2009; Crowley et al., 2010). For example, Burley and Bytnerowicz (2011) investigated the O_3 distribution at White Mountains (1237 ~ 4342 m) in California and concluded that high O_3 concentrations were correlated with slow-moving back-trajectories which had spent more time inland and less time offshore. Monteiro et al. (2012) analyzed a high O_3 episode by employing a statistical technique and a modeling approach at a mountain site (1086 m) in the Mediterranean region, and reported that transport of O_3 and its precursors by local mountain breezes and sea-breeze circulation was mainly responsible for the high O_3 concentrations. Turnipseed et al. (2004) simulated the

mesoscale atmospheric flow conditions influenced by regional topography in the Niwot Ridge Ameriflux site within the Rocky Mountains (3050 m), and significant influence of mesoscale winds was found under the strong synoptic westerly winds. Ou Yang et al. (2012) investigated the seasonal and diurnal variations of O_3 at a high-altitude mountain site (2862 m) in central Taiwan and concluded that the springtime maximum O_3 concentration was most likely caused by the long-range transport of air masses from Southeast Asia.

In Mainland China, limited studies have been undertaken to investigate the characteristics of O_3 pollution in mountainous areas (e.g. Gao et al., 2005; Wang et al., 2006b; Li et al., 2008; Xue et al., 2011). Gao et al. (2005) reported measurements of O_3 and CO at the summit of Mt. Tai (1534 m) and suggested that air masses from the North China Plains or the re-circulation over the Shandong Peninsula had significant influence on air pollutants. Li et al. (2008) investigated the impact of chemical production and transport on summer diurnal O_3 behavior at a mountainous site on the North China Plain. They suggested that in-situ chemistry accounted for most of the O_3 increment from morning to mid-afternoon. Wang et al. (2006) and Xue et al. (2011) studied the origin of surface O_3 and reactive nitrogen speciation at Mt. Waliguan (3816 m) in western China, and indicated that high O_3 events were mostly derived from the downward transport of the upper tropospheric air rather than anthropogenic pollution. It should be noted that all of these studies were carried out only at mountain sites in northern/western China.

2.3 Characteristics of O_3 and VOCs in the Pearl River Delta (PRD)

In recent years, the local governments in the Pearl River Delta (PRD) have taken measures to control O_3 pollution in the region (http://www.epd.gov.hk/epd/english/environmentinhk/air/air_maincontent.html) with the increasing recognization of

detrimental health effects of O_3. Many local and international research teams have undertaken studies on O_3 pollution (e.g. Wang and Kwok, 2003; Wang et al., 2003, 2005; Zhang et al., 2008; Guo et al., 2009; Shao et al., 2009b; Zheng et al., 2010a) as well as the O_3 precursors (VOCs) (e.g. So and Wang, 2004; Wang et al., 2005; Simpson et al., 2006; Chan et al., 2006; Guo et al., 2004a, b, 2006, 2007, 2009; Jiang et al., 2010; Cheng et al., 2010a, b). Elevated ground O_3 concentrations are still being reported in the PRD region. For instance, Zheng et al. (2010a) demonstrated that there were 3 – 5 ppbv increases in 1 h-average O_3 levels and 8 – 11 ppbv increases in 1 h-max O_3 levels in 2007 compared to the values in 2006 across the PRD region. Moreover, a 14-year continuous study provides clear evidence that O_3 levels in the background atmosphere of South China have exhibited a slow rising trend since 1994 (Wang et al., 2009).

2.3.1 Photochemical ozone pollution in the PRD

The PRD region is situated on the coast of South China (21°17′-23°56′N and 111°59′-115°25′E) and has an area of 41,700 km^2. This region is one of the most populated city clusters in China, where major cities include Hong Kong, Shenzhen, Guangzhou, Dongguan, and Huizhou. With its astonishing economic growth, rapid industrialization and urbanization, the PRD region is facing increasing serious photochemical O_3 pollution. Research into O_3 pollution has been conducted in the PRD region since the 1990s. Apart from the 14 air quality monitoring stations established by the Hong Kong Environmental Protection Department (HKEPD), the Hong Kong Polytechnic University set up the Atmospheric Chemistry Research Laboratory at Cape D'Aguilar, Hong Kong in 1993. Wang et al. (1998) reported that four O_3 episodes were observed at Cape D'Aguilar in 1994, and the hourly averaged O_3 concentrations exceeded 100 ppbv and in one case reached 162 ppbv. They found

that recirculation of urban air caused by the reversal of surface winds was an important mechanism for transporting the "aged" urban plumes to the monitoring sites.

In Hong Kong, seasonal variations were obvious, with relatively higher O_3 concentrations often observed in fall and lower levels in summer. Chan et al. (1998a) analyzed the surface O_3 through the study of the temporal and spatial variations of the rural and urban O_3 levels in Hong Kong. A seasonal pattern of O_3 with a major peak in autumn and a trough in summer was found. They concluded that the alternation of the prevailing oceanic and continental air masses, plus the climate system associated with the Asian monsoon had significant influences on the seasonal variations of O_3 in Hong Kong. Similarly, Lam (2001) evaluated the seasonal behavior of the surface O_3 at Cape D'Aguilar station. The result indicated that the average O_3 levels were high in fall with maximum of 41 ppbv and low in summer with a minimum of 16 ppbv. For diurnal variation, the O_3 mixing ratio typically reaches a maximum value in the afternoon due to active in-situ photochemical production, and has a minimum level at night because of the surface deposition and nighttime reaction with primary pollutants (Wang et al., 2006a; Guo et al., 2009).

It was well documented that meteorological conditions have significant influence on O_3 formation in the PRD (e.g. Lee et al., 2002a; Wang and Kwok, 2003; Ding et al., 2004; Lam et al., 2005; Wang et al., 2006a; Huang et al., 2005; Huang et al., 2006; Jiang et al., 2008, 2010). Guo et al. (2009) and Cheng et al. (2010a) compared the meteorological conditions between the O_3 and non-O_3 episode days based on field measurement in the PRD in 2007. They pointed out that high temperature, intense solar radiation, low winds, and low relative humidity were favorable for photochemical O_3 formation. In addition to the above meteorological parameters,

tropical cyclone was found to be mostly conducive to the occurrence of high O_3 mixing ratios in the PRD (Lam et al., 2004, Huang et al., 2005, Jiang et al., 2008). Huang et al. (2005) counted that about 62% of O_3 episodes from 1999 to 2003 resulted from cyclonic weather patterns. Jiang et al. (2008) used regional air quality modeling to evaluate a continuous O_3 episode that occurred when Typhoon Nari was located northeast of Hong Kong during the period September 14 – 19, 2001. When a tropical cyclone was formed and its center was over the East and the South China Sea, it intensified the inflow in the lower atmospheric layer and the outflow in the upper atmosphere, which caused stagnation and subsidence air over Hong Kong, forming an inversion layer. Such an inversion layer was not favorable for the dispersion of air pollutants, resulting in the high O_3 mixing ratios. Besides the tropical cyclone system, an anticyclone appearing over Mainland China to the north and a trough situated to the east over the South China Sea were also found to be the optimal weather conditions for the occurrence of O_3 episodes in Hong Kong (Huang et al., 2006).

Whereas O_3 production is associated with specific weather conditions, i.e. high temperature, strong solar radiation, low relative humidity and calm winds, many previous studies pointed out that the O_3 episodes were also influenced by different flow patterns, i.e., regional transport and/or mesoscale circulations. Most studies showed that elevated O_3 concentrations in the PRD were influenced by local photochemical production and regional transport from the outside of PRD region (related to Hong Kong) (e.g. Lee and Hills, 2003; So and Wang, 2003; Ding et al., 2004; Huang et al., 2006; Lam et al., 2005; Zhang et al., 2007; Zhang et al., 2008; Cheng et al., 2010a, b). A few studies indicated the association of super-regional transport from the East China coastline with O_3 pollution in the PRD (Wang et al., 2009; Guo et al., 2009; Jiang et al., 2010; Zheng et al., 2010a; Zhao et al., 2011). For

example, Guo et al. (2009) investigated the O_3 characteristic at a suburban site in the PRD and found that the high O_3 mixing ratios there were associated with air masses from eastern China. Based on the data simulated by WRF-Chem model, Jiang et al. (2010) reported that the weather conditions induced regional transport of O_3 pollution occurred in the fall of 2007. However, all these studies were constrained within the PRD region and could not provide a detailed mechanism on how super-regional transport from eastern China and/or other areas affects the air quality in the PRD. The relative contributions of local photochemical production and super-regional transport to O_3 pollution in the PRD are not fully understood.

It has been well known that mesoscale circulations, like mountain-valley/sea-land breezes, play important roles in redistributing air pollution in mountainous/coastal regions. Although Hong Kong has an area of only about 1000 km^2, its topography and physical features are complex. About 75% of the land area is hilly and the highest peak rises to 957 m (Mt. Tai Mo Shan). The coastline and the mountains combine to give a terrain with many complex physical features, not to mention the influence of the city itself (i.e. skyscrapers) on the local meteorology. The role of sea-land breezes in air pollution transport has been well studied in the PRD (Zhang and Zhang, 1997; Liu et al., 2000; Ding et al., 2004). For example, Wang et al. (1998) investigated four O_3 episodes using observation O_3 data from a coastal location in Hong Kong. Reversal of surface winds, which transported the "aged" plumes from urban area to the monitoring site, resulted in the high O_3 concentrations. Liu and Chan (2002) applied a 3-D atmospheric model with the local wind fields to investigate the local boundary-layer dynamics on a high O_3 episode observed in Hong Kong in 2000. They found that the calm winds and the delicate interaction between the synoptic forcings and the local circulations, and between the different sea-breeze circulations

were the dominant factors responsible for the severe air-pollution episode in Hong Kong. In addition, Ding et al. (2004) studied the impact of sea-land breeze on transporting air pollutants during an O_3 episode in the PRD region and concluded that cross-border transport and sea-land breeze did play a critical role in air-quality deterioration in the PRD region.

2.3.2 VOC studies in the Pearl River Delta region

2.3.2.1 Levels of VOCs in the PRD region

Volatile organic compounds (VOCs), emitted from anthropogenic and biogenic sources, are one of the most important groups of air pollutants in the atmosphere. In addition to their important roles in tropospheric photochemistry, some VOCs, i.e., benzene, toluene, ethylbenzene and xylenes, are hazardous air pollutants. Therefore, VOCs have been studied extensively in the PRD region in recent years (Sin et al., 2000; Lee et al., 2002a; Ho et al., 2004; So and Wang et al., 2004; Guo et al., 2004a, 2006; Cheng et al., 2010a, b; Wang et al., 2005; Zhang et al., 2012; Tang et al., 2007a, b; Zhang et al., 2007). In general, previous studies have found that VOCs levels in Hong Kong were generally lower or comparable to those of overseas cities (Derwent et al., 2000; Borbon et al., 2002), but much lower than those found in Asia and South America (Grosjean et al., 1998; Morikawa et al., 1998; Barletta et al., 2002). Sin et al. (2000) reported the annual average concentrations of VOCs based on the measurement conducted from July 1997 to June 1998 at two sites, central/western (C/W) and Tsuen Wan (TW) in Hong Kong. The annual average concentration of the measurable VOCs was comparable to that observed in American and European cities, with a range of 0.20 ~ 5.0 ppbv. Among all the VOCs, toluene had the highest mixing ratio, which occasionally exceeded 20 ppbv.

In addition to Sin et al. (2000), other previous studies reported that toluene was the most abundant VOC species in Hong Kong. For example, Guo et al. (2004a) analyzed the VOC samples collected at C/W and TW from January 10 to December 30, 2001 and reported that toluene was the most abundant VOCs in all the samples, with the maximum daily value up to 53 μg/m^3. In addition, Ho et al. (2004) reported the VOCs levels at PolyU campus (PU), Kwun Tong (KT), and Hok Tsui (HT). Toluene was the most abundant hydrocarbon, followed by benzene in all the stations. The concentrations of toluene at PU ranged from 14.4 to 54.3 μg /m^3 in winter and from 11.6 to 39.2 μg /m^3 in summer, while toluene at KT had an average concentration of 26.42 μg /m^3 in winter and 64.34 μg /m^3 in summer. In addition, So and Wang (2004) analyzed the annual VOCs data from four sites: Tsuen Wan, Mong Kok, Central/Western, and Hok Tsui in Hong Kong. Alkanes contributed the most to the ambient VOCs in Hong Kong, followed by aromatics and alkenes. Toluene had the highest level at the road site, Mong Kok, with the average concentration of 8.24 ppbv. At Tai O, a rural/coastal site in Hong Kong, large variations were observed in the measured NMHCs from August 2001 to December 2002. Alkanes had the highest contribution to the ambient VOCs, followed by aromatics, alkynes and alkenes, which accounted for 40%, 35%, 11%, and 10%, respectively. The top 10 most abundant compounds, toluene, ethyne, ethane, propane, ethene, *n*-butane, CH_3Cl, ethylbenzene, benzene, and *i*-pentane, contributed 76% to total measured VOCs. In particular, toluene contributed 22% to the total measured VOCs. Recently, Guo et al. (2009) reported that alkanes accounted for most of the NMHCs abundance at Tung Chung (TC) (63%) in Hong Kong during the fall of 2007, while akenes, aromatics and biogenic VOCs accounted for 16%, 19% and 2%, respectively. They concluded that

the high contribution of alkanes at TC may be due to widespread use of liquefied petroleum gas (LPG).

Many studies have been conducted in the inland PRD, especially in the major cities, i.e., Guangzhou, Dongguan, Foshan, Jiangmen and Zhongshan (Wang et al., 2002; Barletta et al., 2005; Chan et al., 2006; Tang et al., 2007a, b; Barletta et al., 2008; Liu et al., 2008b; Tang et al., 2008; Zhang et al., 2012). Chan et al. (2006) investigated the VOC levels in the PRD region by collecting 78 ambient air samples throughout Dongguan, Foshan, Guangzhou, Jianmen, and Zhongshan in late summer 2000. The samples were classified into three categories: industrial, industrial-urban and industrial-suburban. Influenced by the emissions from industrial solvent use and vehicular emissions, toluene was the most abundant VOC quantified, followed by ethane, ethene, ethyne, propane, *n*-butane, *i*-pentane, benzene, and *m*-xylene. Tang et al. (2007b) investigated the VOC levels at three sites in Guangzhou in April 2005, reporting that toluene was the most important VOC species in Guangzhou, with the average concentration ranging from 3.09 to 10.02 ppbv. However, in September 2005, Barletta et al. (2008) collected a total of 96 VOC samples in two important urban centers of the PRD region, Guangzhou and Dongguan. The most abundant VOCs in Guangzhou and Dongguan were propane and toluene, with an average mixing ratio of 6.7 ppbv and 6.1 ppbv, respectively. Liu et al. (2008b) measured levels of ambient VOCs at seven sites in the PRD region during the Air Quality Monitoring Campaign spanning 4 October to 3 November 2004. Alkanes constituted the largest percentage (> 40%) in the mixing ratios of the quantified VOCs at six urban and rural sites, while the exception was one major industrial site (Dongguan) was dominated by aromatics (about 52%).

Recently, Zhang et al. (2012) investigated the levels of ambient VOCs before and after outbreak of the 2008 financial crisis at a small town, Wanqingsha (WQS) in the PRD region. Toluene was still the most important VOC though the influence of financial crisis. However, the composition of total VOCs was different before and after the financial crisis. Before the financial crisis, aromatics were the most important VOC group (44.2%), followed by alkanes (34.8%), alkenes and alkynes (21%). After the financial crisis in 2008, alkanes contributed the most to the total VOCs, accounting for 50.8%, followed by alkenes and alkynes (27.1%) and aromatics (22.1%).

To extend the investigation of VOCs levels in the PRD region and provide representative VOC measurements over the entire study area, a two-year grid study, with sampling sites covering a total area of 40,000 km^2, was performed by Louie et al. (2012) in summer and winter of 2008 and 2009. The largest contributing VOCs, accounting over 80% of the total VOCs mixing ratio, were toluene, ethane, ethyne, propane, ethene, butane, benzene, pentane, ethylbenzene, and xylenes. Among them, toluene had the highest level, with the mixing ratio of 4.18 ppbv.

2.3.2.2 Spatial variations of VOCs

VOCs levels in the PRD region present remarkable spatial variations. In general, the VOC levels were higher in the urban sites than the suburban and the rural sites. Guo et al. (2004a) compared the VOC levels at two different sites in Hong Kong, Tsuen Wan (TW) and Central/Western (CW). It was found that the levels of all the alkanes and alkenes, like propane, butane, *i*-butane, and propene, were higher at TW than at CW. The higher concentrations at TW may be due to the presence of more industrial combustion sources and busier traffic, which was attributed to the fact that

the TW station is located in a mixed of industrial, residential and commercial area whereas the CW station is in an urban residential area.

So and Wang (2004) investigated the spatial variations of VOCs at four different sites in Hong Kong: Tsuen Wan (industrial), Mong Kok (roadside), Central/Western (residential) and Hok Tsui (rural). In general, the average concentrations of hydrocarbons were, in descending order: roadside > industrial > residential > rural. The highest level of VOCs at roadside was attributed to the heavy vehicular emissions and the presence of surrounding buildings, which could prevent the vehicular emission from dispersing effectively. Due to fewer industrial activities and a lower volume of traffic, the residential site (C/W) presented relatively lower levels of VOCs.

Based on a two-year grid study in the summer and winter of 2008 and 2009 in the PRD region, Yuan et al. (2012) identified three hotspot areas with significant VOC contributions: 1) the Pearl River Estuary; 2) an area from Central Dongguan to North Shenzhen; and 3) the Zhuhai-Zhongshan-Jiangmen area. Zhang et al. (2013) compared the composition and levels of aromatic hydrocarbons (AHs) at urban (Guangzhou Environmental Monitoring Center, GEMC), suburban (Guangzhou Higher Education Mega Center, HEMC), upwind rural (Zencheng College of South China Normal University, ZC) and downwind rural (Wanqingsha, WQS) sites in Guangzhou. The total mixing ratios of aromatic hydrocarbons at GEMC, HEMC, ZC and WQS averaged 9.26 ± 1.04, 6.40 ± 1.63, 2.50 ± 0.71 and 10.4 ± 1.33 ppbv, accounting for 12%, 14%, 11%, and 28% to the total NMHCs, respectively. Toluene was the most abundant compound among the AHs at all sampling sites except ZC, where benzene exhibited the highest mixing ratio. In addition, the levels of benzene, toluene, C_8 – and C_9 – aromatics at urban GEMC, suburban HEMC, and downwind

rural WQS were all significantly higher than those at upwind rural ZC. In particular, benzene showed significantly higher levels at the urban site GMEC than the suburban site HEMC or rural sites ZC and WQS. However, the highest mixing ratios of toluene and C_8 – aromatics were observed at WQS.

2.3.2.3 Temporal variations of VOCs

It is well documented in previous studies that the diurnal variations of VOCs in the PRD are generally controlled by three factors: meteorology, emissions, and chemical reactions (Ho et al., 2004; So and Wang, 2004; Tang et al., 2007b; Liu et al., 2008b; Wang et al., 2008). Ho et al. (2004) investigated the diurnal variations of benzene, toluene, ethylbenzene and xylene at the PolyU station in Hong Kong. The concentrations of toluene, ethylbenzene, *m,p*-xylene, and *o*-xylene followed the same pattern: they increased at 09:00 – 12:00, then decreased at 12:00 – 15:00, then peaked at 15:00-18:00, and finally decreased slightly at 18:00 – 21:00. Ho et al. (2004) pointed out that the decrease of VOCs at noon may be due to the decrease of traffic volume and the dilution effects caused by an increase of the mixing depth, while the increased level of VOCs in the afternoon was because of the increased traffic volume and other evaporative emissions.

Tang et al. (2007b) performed a study on diurnal variations of non-methane hydrocarbons (NMHCs) in the PRD region in 2005. The diurnal patterns of hydrocarbons and total NMHCs were quite different for the urban (Guangzhou, GZ), suburban (Panyu, PY), and rural sites (Dinghu Mountain, DM). In GZ, NMHCs showed high mixing ratios in the morning (08:00 – 09:00, local time), decreased to the lowest at the afternoon (14:00 – 15:00) and then increased gradually to the highest value in the evening (20:00 – 21:00). This feature was corresponded to the traffic volumes in GZ, indicating that traffic emissions were the major sources of the

NMHCs. The lowest levels observed at noon were likely due to the increased mixing height of the planetary boundary layer and the intensive reaction with OH radical. However, in PY, a higher total NMHC mixing ratio was observed at 11:00 – 12:00, indicating that hydrocarbons in PY were more influenced by aged air masses from the urban areas than from fresh local vehicular emission. In addition, Liu et al. (2008b) investigated the diurnal variations of VOCs in Guangzhou (GZ, urban site) and Xinken (XK, rural site) in the PRD region, confirming that fresh emissions, OH reactions and the variations of mixing height had a significant influence on the diurnal variations of VOCs. Guo et al. (2009) analyzed VOC samples collected at Wanqingsha (WQS) in Guangzhou and Tung Chung (TC) in Hong Kong in the autumn of 2007. They found that the total NMHCs at WQS showed two major peaks, one in the early morning and the other in the late afternoon, but the peaks were much weaker and were not statistically different from the troughs at TC.

The total NMHC levels at urban sites in the PRD region presented significant seasonal patterns. In Hong Kong, high levels in winter and low levels in summer were often observed (Lee et al., 2002b; Ho et al., 2004; So and Wang, 2004; Guo et al., 2007; Tang et al., 2007b; Wang et al., 2008). The seasonal variations of VOCs in Hong Kong are greatly influenced by the Asian monsoons. In winter, the weaker vertical mixing, slower photochemical reaction, and regional/super-regional transport could result in the higher VOCs levels. However, in summer, due to the influence of Asian monsoon circulations, the oceanic air frequently influenced Hong Kong, bringing in clean marine air, which could dilute the air pollutants. In addition, the rainy weather in the summertime causes a wet deposition of pollutants, and results in lower concentration than in winter. On the other hand, Zheng et al. (2009a) reported that in the inland PRD, relatively higher levels of VOCs were observed during

July-November, while relatively lower levels of VOCs were observed from December to February in 2006. The higher levels from July to November were due to the large emissions from different industries, i.e., alcoholic beverage production, electronic manufacture, heavy-manufacture, and pulp and paper industries. The lowest VOC emissions were found in February because of Chinese New Year occurred in this month.

2.3.3 Roles of VOCs in photochemical O_3 formation

Volatile organic compounds are composed of hundreds, if not thousands, of organic compounds. Each species varies distinctly from others in its abundance and reactivity, and together they determine their roles in photochemical O_3 formation. VOC photochemical reactivity is a measure of how much a VOC species reacts in the atmosphere and contributes to the formation of O_3, which is an important consideration when policy makers think about controlling VOC emission sources to prevent O_3 or photochemical smog formation. In this section, studies of photochemical reactivity of VOC and Oxygenated VOC (OVOC) in Hong Kong and the rest of PRD region are reviewed.

2.3.3.1 Overview of VOC photochemical reactivity

There are some frequently used scales with regards to the VOC photochemical reactivity. The first and oldest method is to compare the rate constant of the reaction between a VOC and the OH radical, which is known as k_{OH} value with the unit of cm^3 $molecule^{-1}$ s^{-1} (Atkinson et al., 1994, 1998a, b, 2003; Warneke et al., 2004). To compare the OH reactivity of VOC species, the Propene-Equivalent concentration of species (j) (Prop-Equiv(j)) (Chameides et al., 1992) was further developed by Equation (2-1):

$$\text{Prop} - Equiv(j) = Conc.(j) \times \frac{k_{OH}(j)}{k_{OH}(C_3H_6)} \quad (2\text{-}1)$$

The second method is to compare the maximum incremental reactivity (MIR) of a VOC, which reflects the greatest effect of a VOC on O_3 formation when an amount of VOC is added to the mixture atmosphere, with units of grams of O_3 formed per gram of organic compound reacting (Carter, 1994, 1995, 2008). The MIR method is thought to be more robust since it takes into account the real world atmospheric conditions where the reaction takes place rather than just the chemical structure of the molecule represented by k_{OH} value. The MIR scales of hundreds of VOC compounds were published by Carter (2000, 2008). Based on MIR, the ozone formation potential (OFP) of a VOC (j) can be calculated by multiplying its mixing ratio with the corresponding MIR value (Carter, 1994):

$$\text{OFP}(j) = \text{Conc.}(j) \times \text{MIR}(j) \quad (2\text{-}2)$$

The third method is called the photochemical ozone creation potential (POCP), which aims to provide a VOC ranking under conditions leading to elevated O_3. The POCP of a given VOC specie (j) is defined as:

$$\text{POCP}(j) = \frac{\text{O}_3 \text{ increment with the } j\text{th VOC}}{\text{O}_3 \text{ increment with ethene}} \times 100 \quad (2\text{-}3)$$

OH loss rate (L_{OH}) is another frequently used scale to measure the initial peroxy radical (RO_2) formation rate, which might be the rate-limiting step of O_3 formation in polluted atmospheric environment (Carter, 1994). L_{OH} of a given species (j) can be calculated by its ambient concentration ($[VOC]_j$) and the OH reaction rate coefficient (k_j^{OH}).

$$L_{OH} = [VOC]_j \times k_j^{OH} \quad (2\text{-}4)$$

OVOC is an important fraction of VOC species and has attracted growing interest in recent years. Earlier studies suggested the important role of OVOC in the

process of atmospheric O_3 formation (Loyd, 1979; Singh et al., 1995; Wennberg et al., 1998). Relatively high MIR scales of some OVOC were also reported by Carter (2000). However, due to the analytical difficulties in OVOC sampling and analysis, OVOC abundances in the atmosphere remained uncharacterized. In recent years, technological improvement such as proton transfer reaction-mass spectrometry (PTR-MS) has facilitated the quantification of OVOC and new data are appearing continuously. The total OVOC abundance was found much higher than C_2 – C_8 NMHCs in the Pacific troposphere (Singh et al., 2001, 2004). High abundances and OFP contributions of OVOC were also found recently in the PRD (Louie et al., 2012).

2.3.3.2 VOC and OVOC photochemical reactivity in Hong Kong and the PRD region

In Hong Kong, photochemical reactivity was found to be dominated by a few highly reactive VOC species, among which isoprene was the major contributor in rural sites and toluene, propene, xylene and formaldehyde were found to be the leading contributors in urban sites (Guo et al., 2004a; So and Wang ,2004; Zhang et al., 2007). Based on the C_3 – C_{12} NMHC annual data of four sites in HK from 2000 to 2001, So and Wang (2004) evaluated the reactivity of OH radicals and OFP of NMHCs. Isoprene was found to have the highest OH-reactivity and O_3 formation potential at the rural site, while toluene was the most important contributor at the roadside sites. Guo et al. (2004a) collected ambient measurements of 156 VOC species (39 alkanes, 32 alkenes, 2 alkynes, 24 aromatics, 43 halocarbons, and 16 carbonyls) in Central/West (CW) and Tsuen Wan (TW) in 2001. Analysis revealed that formaldehyde, toluene, propene, *m,p*-xylene, acetaldehyde, 1-butene/*i*-butene, isoprene, and *n*-butane were major contributors to O_3 formation. Examination of C_1 to C_{10} hydrocarbons and 2 halocarbons measured in 2002 showed that the reactivity of

VOCs was dominated by anthropogenic VOC, especially the reactive aromatics (e.g. toluene and xylene) (Zhang et al., 2007).

In the rest of the PRD region, earlier observations of hydrocarbons did not include OVOC and photochemical reactivity analysis revealed that toluene, ethene, propene and xylene were the leading contributors to the photochemical reactivity in urban areas while isoprene dominated in rural areas (Tang et a., 2007b; Barletta et al., 2008; Liu et al., 2008b; Lai et al., 2009; Tan et al., 2012). Tang et al. (2007b) found that isoprene from biogenic emission contributed largely to the OFP at the remote site, while ethene, toluene and *m,p*-xylene were the main contributors to the OFP at the urban and suburban sites of GZ. Barletta et al. (2008) reported that ethene and toluene were among the top compounds in terms of O_3 formation in urban centers in the PRD, due to their high mixing ratios and MIR (3.97 for toluene; 9.07 for ethene). Liu et al. (2008b) calculated the OH loss rate to estimate the chemical reactivities of 38 alkanes, 37 alkenes, 17 aromatics and 1 halocarbon. It showed that of the anthropogenic VOCs, alkenes played a predominant role in VOC reactivity at an urban area whereas the contributions of reactive aromatics were more important at a rural site. However, the contributions of isoprene to the OH loss rate were very low at both urban and rural sites. Lai et al. (2009) reported that although LPG alkanes account for 24% of the total VOC (TVOC), their contribution to the total OFP was only about 7%. In contrast, ethene and propene accounted for about 16% of the TVOC, but contributed about 26% to the total OFP in Guangzhou. Tan et al. (2012) also reported the leading contributors to OFP and Prop-Equiv in Foshan were ethene, toluene, propene, *i*-pentane, and *m/p*-xylene.

Based on the speciated VOC emission inventory, the top 10 VOC species contributing to OFP in the inland PRD region were isoprene, *m,p*-xylene, toluene,

ethene, propene, *o*-xylene, 1,2,4-trimethylbenzene, 2-methyl-2-butene, 1-butene, and α-pinene. With 35.9% contributions to total VOC emissions, they accounted for 64.1% of the OFP in the region (Zheng et al., 2009b). One OVOC (methanol) contributed 5.3% to the VOC emissions but accounted for just 0.8% of the OFP. The OFP of all 7 OVOC species estimated in this inventory contributed 2.42% of the total OFP. The relatively low contribution was mainly due to the fact that the source profiles (Liu et al., 2008a) adopted in this study did not include quantification of OVOC. For the biogenic emission inventories (Tsui et al., 2009; Zheng et al., 2010b), isoprene and monoterpenes together contributed 70% and 59% of the total biogenic VOC in HK and the inland PRD region, respectively. Though O_3 formation was not calculated in these study (Tsui et al., 2009; Zheng et al., 2010b), based on the large emission of these two species and their high reactivities, they dominated the OFP of biogenic emissions.

For OVOCs, they were silted into the category of "other VOC" and no significant contributions of any OVOC to OFP were reported. Recently, continuous new data regarding OVOC in Hong Kong and the inland PRD have appeared. In addition to the significant contributions of alkenes and aromatics to O_3 formation revealed by the above studies, recent studies suggested that the contributions of OVOC were also important in this region. Lü et al. (2010) investigated the seasonal and diurnal variations of carbonyl compounds in Guangzhou. Formaldehyde, acetaldehyde and acetone were the most abundant carbonyl compounds, accounting for more than 60% of the total concentrations of carbonyls. Formaldehyde, acetaldehyde, valeraldehyde, butyraldehyde, and propionaldehyde contributed 89 – 96% of the total OFP of carbonyls while acetaldehyde, butyraldehyde, formaldehyde, and valeraldehyde account for 75 – 90% to the total Prop-Equiv concentrations. During

the PRIDE PRD2006 Campaign, Lou et al. (2010) directly measured the OH reactivities (k_{OH}) and found that k_{OH} in PRD was dominated by organic compounds. The comparison between calculated reactivities from measured CO, NO_x and hydrocarbons and measured k_{OH} revealed a missing reactivity of unmeasured species, which box model calculations revealed was related to OVOCs.

Yuan et al. (2012) measured 47 hydrocarbons and 3 carbonyls at six sites in the PRD. The contributions of anthropogenic alkenes and isoprene to OH loss rates (L_{OH}) were dominant. Alkane contributions to total L_{OH} were minor due to their low k_{OH} value. The calculated L_{OH} from VOCs at the urban sites in the PRD was comparable to that of studies in Beijing (Shao et al., 2009a) and Houston (Gilman et al., 2009), but lower than the average urban values of heavily polluted Mexico (Ape et al., 2010). Carbonyls contributed 19.1% – 50.5% of the total L_{OH} at suburban/rural sites. The significant contributions of carbonyls to L_{OH} further confirmed the box model results of Lou et al. (2010). Moreover, observation-based model (OBM) showed that a large increment in both simulated HO_2 and O_3 concentrations was achieved with additional input of hourly carbonyl data, suggesting that apart from hydrocarbons, carbonyls might significantly contribute to the O_3 production in the PRD region (Cheng et al., 2010a).

Another photochemical trajectory modeling study calculated the photochemical ozone creation potential (POCP) of 139 VOC species including 19 OVOCs (Cheng et al., 2010b). Alkenes and aromatics had relatively high POCP values. OVOC had lower POCP values than the above two groups but was higher than alkanes. Among OVOC, aldehydes showed the highest mean POCP values, ranging from 30 to 116. Ethers and glycol ethers had lower mean POCP values (16 – 77), followed by alcohols and glycols (9 – 65) and ketones (8 – 65). Considering both the POCP and the

emission amount, isoprene, ethene, α-pinene, *m*-xylene, propene, formaldehyde, toluene, and 1, 2, 4-trimethylbenzene were the key emitted precursors to O_3 formation in the PRD. More recently, a large spatial-temporal scale of VOC and OVOC sampling campaign was conducted throughout the PRD region (HKEPD, 2010). Compared to toluene, the mixing ratios for the most abundant OVOC species, i.e., formaldehyde, actone, acetaldehyde and 2-butanone, were lower, which were about 0.6, 0.6, 0.26, and 0.19 times the mixing ratio of toluene. Altogether, OFP from OVOC was more than 1/3 of that from VOC alone, demonstrating the important roles of OVOC in O_3 formation in the PRD region (Louie et al., 2012).

2.3.4 Sources of VOCs in the PRD region

Source-receptor relationships revealed by the chemical and physical characteristics of hydrocarbons measured at source and receptor can be used to identify and quantify the VOC emission sources based on receptor concentrations. Usually, they start with the measurements of VOC species in the atmosphere. Then diagnostic ratios and correlation analysis between different species or receptor models are applied to identify and quantify the VOC contributing sources. Receptor models can be grouped into two groups: multivariate analysis, including principal components analysis (PCA) and positive matrix factorization (PMF), and chemical mass balance (CMB) receptor model, which requires detailed VOC source speciation information. In this section, observation-based VOC source characterization studies in Hong Kong and the inland PRD are reviewed.

2.3.4.1. Observation-based VOC source characterization studies in Hong Kong

A number of field measurements of VOCs have been conducted in the last decade to characterize the sources of ambient VOCs in Hong Kong.

Earlier studies presented VOC ambient measurements and characterized VOCs contributing sources by diagnostic ratios and correlation analysis (Sin et al., 2000; Lee et al., 2002b; Ho et al., 2004; Guo et al., 2004a; So and Wang, 2004; Zhang et al., 2008). Generally, vehicles were the most identified source, followed by fuel evaporations and industrial emissions. For example, Lee et al. (2002a) detected 12 VOCs at five roadside sites, 60% of which consisted of toluene, benzene, ethylbenzene and xylenes. High toluene to benzene ratios (T/B ratio) were found as in other cities in Asia. As toluene and benzene were the major pollutants from vehicle exhausts, Lee et al. (2002a) recommended the necessity to control automobile emissions. Ho et al. (2004) collected ambient VOCs at three locations and the Cross Harbor tunnel. Toluene was found to be the most abundant VOC detected in Hong Kong. High toluene/benzene ratios were also found in this study, suggesting large industrial emissions (additional sources of toluene beside vehicles) in these areas. Vehicular emissions were found to be one of the most important pollutant sources in Hong Kong, making an important contribution to the aromatic compounds in the atmosphere. Evaporative emission of gasoline was found to be another important VOC source.

Guo et al. (2004a) measured 156 VOC species at two urban sites. Strong correlation of most hydrocarbons with propene and *n*-butane were found, indicating vehicular emissions were primary contributions to levels of hydrocarbons in Hong Kong. In addition, gasoline evaporation, use of solvents, leakage of liquefied petroleum gas (LPG), natural gas leakage, and other industrial emissions, as well as biogenic emissions affected the ambient levels of hydrocarbons. So and Wang et al. (2004) applied principal component analysis to a subset of NMHCs and suggested that while isoprene at the rural site mainly came from biogenic emissions, vehicular

emissions were the major source in the urban areas, especially at roadsides. Zhang et al. (2008) analyzed the ratios of xylenes-to-ethylbenzene, C_6H_{14}-to-toluene and *p*-xylene-to-total xylenes for diagnostic analyses and found that sources of reactive aromatics did not appear to be dominated by mobile emission but rather were related to industrial, waterfront, and fuel-storage activities.

The application of receptor models provided more comprehensive understanding of VOC source characteristics in Hong Kong (Guo et al., 2004b, 2006, 2007, 2011a; Cheng et al., 2010a; Lau et al., 2010; Feng et al., 2012; Yuan et al., 2012a). In the earlier studies, VOC source apportionments in Hong Kong were firstly estimated using PCA/APCS receptor model by Guo et al. (2004b, 2006, 2007) and Cheng et al. (2010a), which does not require prior knowledge of source compositions. Later on, CMB (Feng et al., 2012), UNMIX (Feng et al., 2012), and PMF (Lau et al., 2010; Guo et al., 2011a; Yuan et al., 2012a) models were also used in source apportionment studies, among which, PMF was believed to generate more reliable results (Miller et al., 2002; Yuan et al., 2012a; HKEPD, 2012b). Vehicle exhaust (11.5 – 48%), LPG/natural gas usage (11 – 40.8%) and solvent usage (14.6 – 36.4%) were the major contributing sources in urban areas in Hong Kong, followed by industrial emissions (3.1 – 9%) and gasoline evaporation (unidentified to 4.7%). Biogenic emissions were relatively low at urban areas, with contributions between 0.1 – 2%. For sub-urban sites, solvent (11.3 – 55.8%), vehicle exhaust (16.8 – 53%) and LPG/natural gas usage (unidentified to 41.3%) were the large contributors. Gasoline evaporation (2 – 17.4%), industrial emissions (unidentified to 5.7%), biomass burning (unidentified to 4%) and biogenic emissions (unidentified to 3.3%) were also identified. At the rural sites, vehicle exhausts were identified as the major contributor (15.2 – 48%). The contributions from gasoline evaporation varied from 6.5% to 21% and LPG/natural

gas usage varied from unidentified to 15.6%. Industrial emissions contributions varied from 3% to 35%, of which the highest values observed in Tai O (adjacent to Shenzhen), were believed to be related to regional transport from the inland PRD. Large contributions of aged VOC were also found at the rural site.

2.3.4.2 Observation-based VOC source characterization studies in the inland PRD

Early in 2005, a study reported that vehicular emissions, combustion, natural gas leakage or other methane/ethane sources might be the important contributors to the urban atmosphere in China, based on cross-correlations of VOC measurements in 43 Chinese cities (Barbara et al., 2005). Further efforts have been made to study the VOC source characteristics in the inland PRD based on ambient measurements with diagnostic ratios and correlation analysis (Chan et al., 2006; Tang et al., 2007b; Barletta et al., 2008; Liu et al., 2008b; Wang et al., 2008; Tan et al., 2012; Yuan et al., 2012b) and receptor models (Guo et al., 2006, 2011a; Liu et al., 2008a,b,c; Cheng et al., 2010a; Tan et al., 2012; Yuan et al., 2012a).

According to the diagnostic and correlation studies, vehicular exhausts were the most often identified contributors in urban areas and were major contributors to ambient NMHC (excluding aromatic hydrocarbons) (Chan et al., 2006; Tang et al., 2007b; Barletta et al., 2008; Wang et al., 2008; Liu et al., 2008b; Tan et al., 2012; Yuan et al., 2012b). Industrial emissions and solvent evaporation had widespread effects in the inland PRD region (Chan et al., 2006; Tang et al., 2007b; Barletta et al., 2008; Yuan et al., 2012b) and were found to be the major contributions to aromatic hydrocarbons (Tang et al., 2007b; Yuan et al., 2012b), especially in industrial areas or cities with prosperous solvent-related industries, such as Dongguan and Foshan. More aged VOCs transported from upwind sites were found in non-urban sites, with mixed

contributions from vehicular exhausts, industrial emissions and others (Liu et al., 2008b; Wang et al., 2008; Yuan et al., 2012b).

Emissions from industrial activities were found to greatly impact the air quality in the inland PRD. Tang et al. (2007b) collected NMHC samples at three sites in the inland PRD. Vehicular exhaust and industrial emissions were found to be the major sources. Barletta et al. (2008) measured NMHC at Guangzhou and Dongguan, where propane and toluene were found to be the most abundant species respectively. Based on correlation analysis, vehicular emission appeared to be the dominant source in Guangzhou, while industrial activities may be the major contributor of selected species (including toluene) in Dongguan. Wang et al. (2008) continuously observed 50 NMHC at an urban site in Guangzhou and a rural site in Xinken. High correlations between NO_x, CO and VOC in the urban site suggested the dominant contribution from motor vehicles. Propane, *i*-butane and *n*-butane accounted for nearly 40% of NMHCs in the urban site, indicating the impact of LPG usage. In comparison, VOCs were found to be more aged in the rural sites due to the transport from the upwind urban centers. Liu et al. (2008b) studied the VOCs correlations in Guangzhou and Xinken and results suggested that VOCs in Guangzhou came directly from local sources, such as automobiles, while VOCs at Xinken were influenced by both local emissions and transport of air mass from upwind areas.

Yuan et al. (2012b) studies the correlations between VOC species in Guangzhou. Vehicular emissions and LPG usage were found to be the dominant sources of $C_4 - C_5$ alkenes (except isoprene), whereas industrial and/or solvent use accounted for a significant fraction of aromatic concentrations. Tan et al. (2012) measured 40 hydrocarbons and calculated their OFP in Foshan. According to the temporal patterns and VOC species correlations, vehicular emissions were a major source for NMHCs

except for aromatics. Solvent evaporation was the major contributor of aromatics, due to the prosperous solvent-related industries in Foshan. Recently, Zheng et al. (2013) investigated industrial sector-based VOC source profiles based on source samples collected from sources operating under normal conditions. The industrial sectors included printing, wood furniture coating, shoemaking, paint manufacturing and metal surface coating. Benzene, toluene, ethyl acetate and isopropyl alcohol were the major species related to the printing industry, while acetone and 2-butanone were the major species observed in the shoemaking sector. In addition, aromatics formed the most important group in the paint manufacturing, wood furniture coating and metal surface coating industries.

For the source apportionment studies using receptor models, Guo et al. (2006) applied the PCA/APCS model to apportion the source contributions of air masses originating in the inland PRD. Based on the experimentally determined local VOC source profiles (Liu et al., 2008a), Liu et al. (2008c) applied the CMB model in the inland PRD. In addition, the PMF model has been extensively used for the source apportionments of VOCs in the inland PRD. For example, Guo et al. (2011a) and Ling et al. (2011) investigated the souce apportionemts of VOCs at a suburban site in the inland PRD region. Solvent- and vehicular-related emissions were the major contributors to ambient VOCs. Based on the VOC measurements of the PRD grid study, Yuan et al. (2012a) conducted VOC source apportionment with PMF model for 84 sites across the PRD. Zhang et al. (2012) used PMF to study the contributing sources of aromatic hydrocarbons in urban, sub-urban, downwind rural and upwind rural sites in the inland PRD. Vehicular exhausts were important contributors of ambient VOC to the entire region, with contributions of about 30%. The contributions were higher in urban areas (44 – 52.6%) compared to non-urban and rural areas (19 –

31.2%). Solvent usage was also an important contributor but displays different spatial patterns from vehicular exhausts. Compared to urban areas (16.2 – 38%), contributions of solvent usage were higher in non-urban, industrial and rural sites (23 – 51%). Industrial emissions account for 12.9% of ambient VOC for the entire region. Much higher contributions of industrial emissions were found by Guo et al. (2006), which may be a mixed source including solvent evaporation from related industries. LPG usage and gasoline evaporation are identified at the urban and non-urban sites, with a contribution of 13% and 8.7% in the entire region, respectively.

In summary, the above literature review indicates that although many studies have investigated the characterization of O_3 and its precursors in the PRD region, such as the temporal and spatial variations, the O_3-precursors relationships, the influence of meteorological conditions on O_3 pollution and the source apportionments of O_3 precursors, there are still scientific gaps that need to be filled. For example, most of the previous studies were undertaken at the low-elevation urban, suburban and rural sites. There is little knowledge about the mechanisms of the variations of O_3 at different elevations in the mountainous areas in this region, where topography and physical features are complex. Though previous studies have investigated the photochemical reactivity in this region, most of these studies were conducted at specific sites in the inland PRD region with relatively simple data and chemical mechanisms. Compared to previous studies, our group is the only one who conducted concurrent field measurement in Hong Kong and inland PRD, and used photochemical box models and chemical transport models to explore the O_3 formation mechanisms. In this study, concurrent measurements were conducted at the mountain site and at the foot of the mountain for the first time to investigate the characteristics of photochemical air pollutants and the impact factors for the O_3 variations at different

elevations in mountainous areas in Hong Kong. In addition, a photochemical box model couple with master chemical mechanism (PBM-MCM) was developed for the first time to understand the detailed chemistry involved in O_3 formation under the influence of different levels of O_3 and precursors at the two sites.

Furthermore, although different methods have identified the main VOC emissions in the PRD region and evaluated the O_3-precursors relationships, the roles of specific VOC sources and species of individual sources in the formation of O_3 in this region, where O_3 formation is generally VOC-limited, are still unclear. In addition, though different measures have been conducted to control VOCs in the PRD region, most of the measures are mass-based, which focus on the control of the weight of total VOC emitted and do not consider the O_3 formation potentials of VOCs, which photochemical O_3 formation is more correlated with. Therefore, to effectively control VOCs, reactivity-based approaches are urgently needed. In this study, a new reactivity-based method, combining the PMF and an observation-based model (OBM), was firstly developed to investigate the roles of VOC sources in the O_3 formation in Hong Kong and the inland PRD region.

In addition, to understand the factors that influence photochemical O_3 pollution, conceptual models of O_3 have been developed in recent years for different regions. However, there is no conceptual model for the O_3 pollution in Hong Kong and the inland PRD region. In this study, in order to obtain a full picture of O_3 pollution and to formulate and implement effective control strategies for O_3 pollution in Hong Kong, a conceptual model based on the 6-year monitoring data at Tung Chung (TC) was firstly developed.

Chapter 3 Methodology

3.1 Sampling sites

Hong Kong (22°6′-22°36′ N, 113°48′-114°30′ E) is situated on the coast of South China and enclosed by the Pearl River Delta (PRD) with a total area of 1,104 km^2 and a population of seven million People (HKCSD, 2012). The climate in the Hong Kong is dominated by the Asian monsoons. One year can be divided into two distinct seasons – wet season and dry season – with the alternation of summer monsoon and winter monsoon. The wet season lasts from around April to October when the summer monsoon is prevailing, including spring and summer seasons. The prevailing wind is from the southeast, south and southwest. It is hot, humid and rainy, with about 90% of the rain falling. The dry season lasts from late October to March when the Asian winter monsoon is dominant, including autumn, winter and early spring. The prevailing wind is from the northeast and north.

In this study, field measurements were simultaneously carried out at two sites. One was the Hong Kong EPD air quality monitoring station at Tsuen Wan (TW), and the other site was set on the Mt. Tai Mo Shan (TMS) in Hong Kong. The sampling period was from 06 September to 29 November, 2010 (Figure 3.1).

Tsuen Wan (TW) (22.373 ^{o}N, 114.112 ^{o}E), located at the foot of Mt. Tai Mo Shan and an urban area, is a mixed residential, commercial and light industrial area in the New Territories in Hong Kong. The monitoring site was located on the rooftop of a building approximately 15 – 20 m above the ground level, which is adjacent to the main traffic road-Castle Peak Road and surrounded by residential and industrial blocks. This site can be represented as mixed urban residential, commercial and industrial area.

Mt. Tai Mo Shan (TMS) is the highest mountain in Hong Kong. Enveloping this massif is 1440 hectares of natural territory, which borders Tai Po Kau nature Reserve in the east and Shing Mun Country Park in the south. To the west is Route Twisk highway and Tai Lam Country Park. To the north is the old valley of the Lam Tsuen (AFCD, 2008). There are forest plantations in the southeastern part of the mountain. Limited by climatic and geographic factors, these plantations end at the 550 m contour, above which shrubs and grasses dominate (AFCD, 2008). Farther to the south are the urban centers of the partial New Territory, Kowloon peninsula and Hong Kong Island. To the southwest is the newly-developed residential area of Tung Chung, the international airport and the South China Sea. To the west are the Tuen Mun residential areas. Because of its unique topography, mountain-valley breezes and sea-land breezes are often observed at Mt. Tai Mo Shan. These mesoscale circulations enhance the interaction of polluted urban air and the mountain air. The sampling site was set on the rooftop of the building in the Youth Hostel Association at the mountain waist of Mt. Tai Mo Shan (22.405^{o} N, 114.118^{o} E, and 640 a.s.l.), about 500 meters away from the Tai Mo Shan Road, which provides access to the summit. In addition, TW and TMS sites are suitable for assessing the influence of mesoscale circulations on redistributing air pollutants.

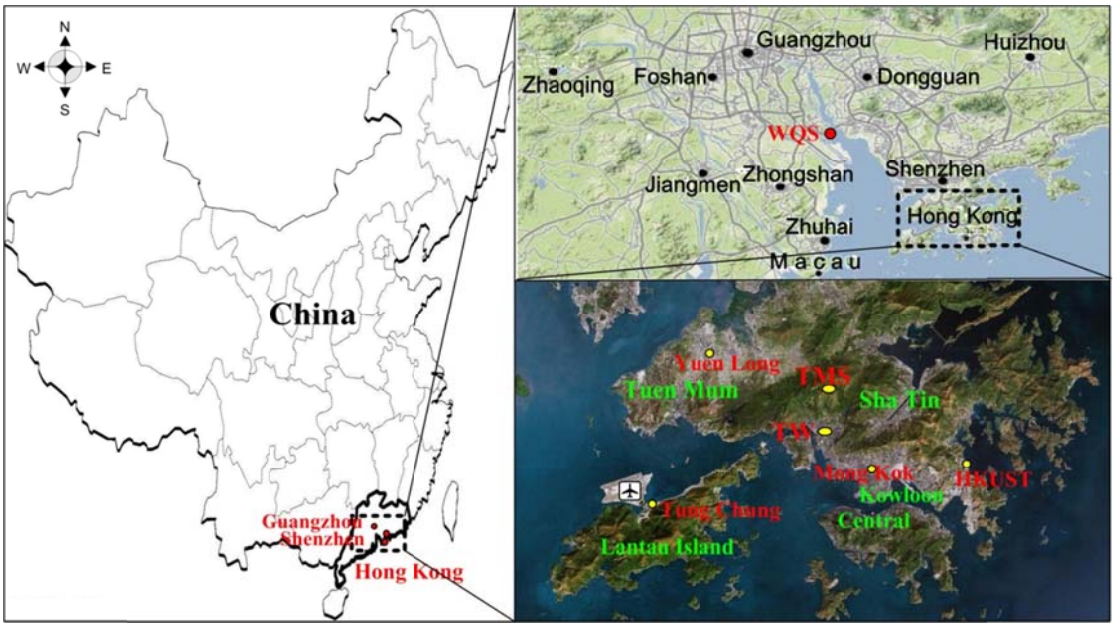

Figure 3.1 The sampling sites and the surrounding environment

In addition to the measurements conducted at TMS and TW, data from another sampling campaign undertaken at a suburban site (i.e Wanqingsha, WQS) near the center of inland PRD region was used to develop a new method combining the Positive Matrix Factorization (PMF) and the Observation-based model (OBM) to investigate the contributions of VOC sources to O_3 formation. Detailed description of the sampling campaign can be found in Guo et al. (2009). In Brief, WQS (22.711^{o} N, 113.549^{o} E) was a suburban site surrounding by farmlands located near the center of the PRD, with Guangzhou urban center 50 km to the northwest, Dongguan city 40 km to the northeast, Shenzhen city 50 km to the southeast, and Zhongshan city 25 km to the southwest. VOCs from local anthropogenic sources at WQS were not significant because of sparse population, light traffic and few industries, while the influence from emissions of surrounding cities was remarkable. The samples were collected on the rooftop of a 15 m high building in a secondary school.

Finally, to develop a conceptual model for the identification of high O_3 episodes in Hong Kong, a sampling campaign lasting 6 years (from 2005 to 2010) was conducted at Tung Chung (TC). Tung Chung (TC, 22.301 ^{o}N, 113.931 ^{o}E, Fig. 1) is a

newly-developed residential town located on northern Lantau Island, about 3 km south of the Hong Kong International Airport at Chek Lap Kok with Hong Kong urban center 20 km to the southwest and Macau 38 km to the northeast. The TC site was adjacent to highway and railway lines that connect the airport with other islands of Hong Kong. The potential impact of the airport, highway and railway lines on VOC and NO_x levels at the sampling site was demonstrated to be insignificant (AOAQS, 2011; Guo et al., 2007; So and Wang, 2004). In addition to the influence of local emission sources, TC is also affected by polluted continental air masses from the highly industrialized PRD region, South China. As such, the TC site is an ideal location to assess the O_3 pollution in Hong Kong.

3.2 Measurement techniques

3.2.1 Continuous measurements of O_3, CO, SO_2 and NO

At TW, O_3, CO, SO_2, NO-NO_2-NO_x and meteorological parameters were measured at a monitoring station operated by the HKEPD. This station used similar instruments and quality assurance and control protocols to those in the US air-quality monitoring program (http://epic.epd.gov.hk/ca/uid/airdata). At TMS, measurement instruments were installed in a room of the building, beneath the rooftop. Ambient air samples were drawn through a 5m long perfluoroalkoxy (PFA) Teflon tube (OD: 12.7 mm; ID: 9.6 mm). The inlet of the sampling tube was located 2 m above the rooftop of the building. The other end of the sampling tube was connected to a PFA manifold with a bypass pump drawing air at a rate of 5 L min^{-1}. The intake of the analyzers for O_3, CO, SO_2 and NO-NO_2-NO_x was connected to the manifold.

A detailed description of the in-situ measurements of O_3, CO, SO_2, and NO-NO_2-NO_x is given below:

Ozone (O_3) was measured using a commercial UV photometric instrument (Advanced Pollution Instrumentation (API), model 400E) that had a detection limit of 0.6 ppbv. The analyzer was calibrated by a transfer standard (TEI 49PS) prior to the field studies.

Sulfur dioxide (SO_2) was measured by a pulsed UV fluorescence (API, model 100E), with a detection limit of 0.4 ppbv and 2-σ precision of 0.5% for ambient levels of 50 ppbv (2-min average). Carbon monoxide was measured with a gas filter correlation, nondispersive infrared analyzer (API, Model 300E) with a heated catalytic scrubber (as purchased) to convert CO to carbon dioxide (CO_2) for baseline determination. Zeroing was conducted every 2 h, each lasting 12 min. The 2-min data at the end of each zeroing were taken as the baseline. The detection limit was 30 ppbv for a 2-min average. The 2s precision was about 1% for a level of 500 ppbv (2- min average) and the overall uncertainty was estimated to be 10%. Nitric oxide and NO_x were detected with a chemiluminescence NO-NO_2-NO_x analyzer (API, Model 200E). The analyzer had a detection limit of 0.4 ppbv. The Model 200E is a single chamber, single photomultiplier tube design which cycles between the NO, NO_x, and zero modes. The addition of the zero mode provides excellent long term stability and extremely low minimum detectable limits. All the SO_2, CO, and NO-NO_x-NO_2 analyzers were calibrated daily by injecting scrubbed ambient air (TEI, Model 111) and a span gas mixture. A NIST-traceable standard (Scott-Marrin, Inc.) containing 156.5 ppmv CO (± 2%), 15.64 ppmv SO_2 (± 2%), and 15.55 ppmv NO (± 2%) was diluted using a dynamic calibrator (Environics, Inc., Model 6100), according to the calibration protocol in HKEPD (2012c). For the O_3, SO_2, NO and NO_x analyzers, a data logger (Environmental Systems Corporation, Model 8816) was used to control the calibrations and to collect data, which were averaged to 1-min values.

In addition to the above chemical measurements, several meteorological parameters were monitored by an integrated sensor suite (Vantage Pro^{TM} & Vantage Pro 2 Plus TM Weather Stations, Davis Instruments). The weather station has two components: the sleekly designed integrated sensor suite, also known as the ISS, and the data-receiving console. The ISS collects weather data such as outdoor temperature, solar radiation, relative humidity, wind speed and direction, and wirelessly transmits its data to the console, which displays the data. To make viewing the data easier, the console is designed with an easy-to-read (7.6 cm × 8.5 cm) screen and a glow-in-the-dark keypad for night viewing.

3.2.2 Sampling and analysis of VOCs by canister

Concurrent VOC samples were collected on selected non-O_3 episode (i.e. 28 September, 02, 08, 14, 18 – 19, 27 – 28 October, and 20 – 21 November) and O_3 episode days (i.e. 23 – 24, 29 – 31 October, 01 – 03, 09 and 19 November) at TMS and TW. The potential high O_3 episode days were selected based on weather prediction and meteorological data analysis, and were generally related to stronger solar radiation, lower wind speeds, and less vertical dilution of air pollution compared to non-O_3 episode days. These O_3 episode and non-O_3 episode days were later on confirmed by the observed O_3 mixing ratios. In this study, an O_3 episode day was defined when the peak one-hour average O_3 mixing ratio exceeded 100 ppbv (i.e. China's Grade II Standard). Ambient VOC samples were collected using cleaned and evacuated 2-L electro-polished stainless steel canisters. The canisters were prepared and delivered to Hong Kong by the Rowland/Blake group at University of California, Irvine (UCI). A flow-controlling device was used to collect 1-h integrated samples. During non-O_3 episode days, hourly VOC samples were collected at 2-h intervals from 7 a.m. to 7 p.m. per day at both sites. For O_3 episode days, hourly samples were

consecutively collected from 9 a.m. to 4 p.m., with additional samples collected at 6 p.m., 9 p.m., midnight, 3 a.m. and 7 a.m.. Due to logistic issues, 19 additional samples were collected at TMS, and one additional sample was taken at TW. Totally, 201 and 183 VOC samples were collected at TMS and TW, respectively.

After sampling, the whole air samples were returned to the laboratory at UCI for chemical analysis. The analytical systems are described as below (Colman et al., 2001). The whole system included multicolumn gas chromatography. The first HP-6890 (GC-1) in a system contained two columns. The first column was a J&W DB-5 (30 m; i.d., 0.25 mm; film ,1 μm) connected in series to a RESTEK 1701 (5 m; i.d., 0.25 mm; film, 0.5 μm), which was output to an ECD detector. The DB-5/RESTEK 1701 union helped to resolve halocarbon and organic nitrate species that have similar polarity through higher retention of the nitrate species. The second column was a DB-5ms (60 m; i.d., 0.25 mm; film, 0.5 μm), which was output to an MSD detector (HP-5973). The DB-5/RESTEK 1701 received 6.84% of the total carrier flow, and the DB-5ms received 10.1%. The second HP-6890 (GC-2) contained a J&W DB-1 column (60 m; i.d., 0.32 mm; film, 1 μm) output to an FID detector. This column received 15.1% of the flow. The third HP-6890 (GC-3) contained a J&W GS-Alumina PLOT column (30 m,; i.d., 0.53 mm) connected in series to a DB-1 (5 m; i.d., 0.53 mm; film, 1 μm), which was output to a FID detector, and a RESTEK 1701 (60 m; i.d., 0.25 mm; film, 0.50 μm), which was output to an ECD detector. The PLOT/DB-1 union helped to reduce signal spikes from PLOT column bleed and tightened up the CO_2 peak width. The GS-Alumina PLOT column received 60.8% of the flow, and the RESTEK 1701 received the remaining 7.16%. The oven parameters employed for each GC can be found in Colman et al. (2001) and Simpson et al. (2010). Liquid nitrogen was used to achieve subambient initial temperatures.

3.2.3 Sampling and analysis of carbonyls

Carbonyl samples were collected simultaneously at TMS and TW on the same sampling days as for the NMHC samples. Silica cartridges impregnated with acidified 2,4-dinitrophenylhydrazine (DNPH) were used for sampling. Air samples were drawn through the cartridge at a flow rate of 0.8 L min^{-1} for 2 hours; the flow rate through the cartridges was monitored with a rotameter which was calibrated before and after each sampling. An O_3 scrubber was connected to the inlet of the DNPH–silica cartridge to prevent interference from O_3. During non-O_3 episode days, carbonyl samples were simultaneously collected from 7 a.m. to 7 p.m. every two hours at both sites. For O_3 episode days, carbonyls were consecutively collected every two hours from 7 a.m. to 7 p.m., with additional samples collected at midnight and 3 a.m. Totally 172 and 157 carbonyl samples were collected during O_3 and non-O_3 episode days, respectively. The unequal sample size is because some samples at the two sites were contaminated.

All cartridges were stored in a refrigerator at 4°C after sampling. The sampled carbonyl cartridges were eluted slowly with 2 ml of acetonitrile into a 2-mL volumetric flask. A 20-µl aliquot was injected into the high performance liquid chromatography (HPLC) system through an auto-sampler. The operating conditions of the HPLC are shown in Table 3.1. Typically, $C_1 - C_8$ carbonyl compounds can be measured effectively by this technique with a detection limit of ~0.2 ppbv.

Since the sampling periods were 2 hours, cubic spine interpolation was used to derive hourly carbonyl concentrations for modeling purpose. Cubic spine interpolation is a useful technique to interpolate between known data points due to its stable and smooth characteristics. As an interpolation method, this method tends to

derive the unknown values with the help of the known ones and tries to interpolate the values as closer to the original ones as possible.

Table 3.1 Gradient separation of $C_1 - C_8$ aldehyde and ketone derivatives

Column	Nava-Pak C18 3.9 ×150 mm
Moblie phase	A: Water/Acetonitrile/ Tetrahydrofuran 60/30/10
Gradient	B: Water/Acetonitrile 40/60
Flow rate	100% A for 2 min then a linear gradient from 100% A to 100% B in 18 min, 100% B for 4min
Injection volume	20μL
Detection	Absorbance at 360 nm

3.2.4 Quality control and quality assurance for VOC and carbonyl analyses

Before sampling, all canisters were cleaned at least five times by repeatedly filling and evacuating humidified pure nitrogen gas. In order to check whether there was any contamination in the canister, we filled the evacuated canisters with pure N_2 and stored them in the laboratory for at least 24 hours. These canisters were then checked by the same VOC analytical method to ensure that all the target compounds were not found or were under the method detection limit (MDL). In addition, duplicate samples were regularly collected to check the precision and reliability of the sampling and analytical methods.

NMHCs were identified by their retention times and their mass spectra. The quantification of target VOCs was accomplished using multi-point external calibration curves, which was employed by a combination of National Bureau of Standards, Scott Specialty Gases (absolute accuracy estimated to be within ± 5%) and UCI-made standards. The measurement precision, accuracy and detection limits of NMHCs varied compound by compound and were periodically quantified for each species during the sampling period. Detailed procedures are described in Simpson et al. (2010) and Colman et al. (2001). Briefly, the measurement precision for NMHCs is 1% or 1.5 pptv (whichever is larger) for the alkanes and alkynes, and 3% or 3 pptv

(whichever is larger) for the alkenes, and 5% for aromatics. The limit of detection is 3 pptv for the NMHCs.

Identification and quantification of carbonyl compounds were based on retention times and peak areas of the corresponding calibration standards, respectively. The instrument was calibrated using five standard concentrations covering the concentrations of interest for ambient air. There were good linear relationships ($R^2 >$ 0.998) between the concentrations and responses for all carbonyls identified. Cartridge collection efficiency was determined with two cartridges in series; over 98% of carbonyl compounds were found in the first cartridge. Relative percent differences for duplicate analysis were within 10%.

3.2.5 Sampling on-line VOCs at Tung Chung

For online VOCs data, it was collected and analyzed by the online VOC analyzers (Syntech Spectras GC 955, Series 600/800, the Netherlands) from 2005 to 2010 in TCAQMS. This instrument is a separating and analytical system which consists of two sampling systems and two column separating systems: one for the C_2 – C_5 hydrocarbons (GC1) and the other for the C_6 – C_{10} (GC2) hydrocarbons. The target C_2 – C_{10} hydrocarbons included ethane, ethene, ethyne, propane, propene, *n*-butane, *i*-butane, 1-butene, *trans*-2-butene, *cis*-2-butene, 1,3-butadiene, *n*-pentane, *i*-pentane, 1-pentene, *trans*-2-pentene, isoprene, *n*-hexane, *i*-hexane, *n*-heptane, *n*-octane, *i*-octane, benzene, toluene, ethylbenzene, *m*-xylene, *p*-xylene, *o*-xylene, 1,2,3-trimethylbenzene, 1,2,4-trimethylbenzene, and 1,3,5-trimethylbenzene. In this study, the GC system operated continuously and collected as well as analyzed the ambient sample every 30 minutes, 24 hours every day. For example, the time stamp 00:30 indicated the end of the sampling period, i.e. from 00:00 until 00:30 and the

start of the analysis period, i.e. from 00:30 until 01:00. Furthermore, the half-hourly data was averaged into hourly values and used in this study.

For these analyzers, built-in computerized programmes of quality control systems, i.e. auto-linearization and auto-calibration, and calibration with span gas were used. Before sampling, the analyzers were calibrated weekly by injecting certified calibration gas (NPL span gas, National Physical Laboratory). In addition, the quality of the real-time data was assured by comparison with the canister samples which were analyzed at UC-Irvine. The measurement precision, accuracy and detection limits of the above VOCs varied compound by compound. Briefly, the detection limit was 0.002 – 0.787 ppbv. The accuracy of the measurements was 1% – 10% for the above VOCs, whereas the measurement precision was 2.5 – 20%.

3.3 Models used in this study

3.3.1 The description of PMF model

USEPAPMF 3.0 model (EPA, 2008a) was utilized for the source apportionment of the 183 VOC samples. Detailed description of this model can be found in Ling et al. (2011). In general, the budget of ambient VOCs is determined by the emissions from different sources, the deposition of chemical and physical processes. Based on the fundamental assumption of mass conservation of species from the emissions sources to the receptor site, the concentration of one specific VOC could be proportional to its emission amounts from different sources in the certain atmospheric volume. According to the above assumption, a speciated data set in the PMF model is represented as a data matrix X of *i* by *j* dimensions, where *i* number of samples and *j* chemical species (VOCs) were measured (Eq. 3-1, Paatero, 2000). The function of the PMF model is to identify the number of emission sources and the species profile of each source, and to attribute the amount of mass from each source to each species in

each individual sample by an analyst based on the measured data at the receptor site, which could presented by equation 1. Therefore, two metrics, i.e., factor contributions and factor profiles, were included and exported in the PMF results.

$$x_{ij} = \sum_{k=1}^{p} g_{ik} f_{kj} + e_{ij} \qquad (3\text{-}1)$$

where x_{ij} is the j^{th} species concentration measured in the i^{th} sample, g_{ik} is the species contribution of the k^{th} source to the ith sample, f_{kj} is the j^{th} species fraction from the k^{th} source, e_{ij} is the residual for each sample/species, and p is the total number of independent sources (Paatero, 2000).

In this study, although 41 species were identified and quantified, it is not necessary to use all of them for the PMF model due to the fundamental assumption of non-reactivity or mass conservation of the PMF model. The selection of the VOC species for the input of the PMF model was based on the following principles: 1) Species at low concentrations with high uncertainty due to their relatively low abundance and/or high reactivity, i.e. β-pinene, camphene and myrcene, were excluded (Guo et al., 2011a; Lau et al., 2010; EPA, 2008; Paatero, 2000; Huang et al., 1999). More than 25% of the samples for these species were below the detection limit; 2) Species that are highly reactive (i.e. butenes, pentene and 1,3-butadiene with lifetime of a few hours) were excluded, since they were rapidly consumed in the atmosphere and affected the apportionment results (Zhang et al., 2013; Guo et al., 2011a; Lau et al., 2010; Brown et al., 2007). An exception to this principle was the inclusion of unique species that are important tracers of sources, for example, isoprene is an important biogenic VOC; 3) Species at low concentrations that are not typically tracers of sources were excluded, i.e. ethyltoluenes. In total, 25 major VOCs together with CO were input into the PMF model to explore the sources of observed

VOCs. These 25 selected VOCs accounted for 96% (ppbv/ppbv) of the total concentrations of the 41 VOC species. The uncertainties for each species were determined as the sum of 5% of VOC concentration and two times the method detection limit of the species, as suggested by Paatero (2000). For values below the detection limit, they were replaced by half of the detection limit values and their overall uncertainties were set at 5/6 of the detection limit values. In addition, due to the complex speciation of VOCs, one VOC may be a tracer of several sources. For instance, benzene, xylenes, hexane and its isomer, C_9-C_{10} alkane species could be emitted not only from vehicular emissions/fuel evaporation, but also from solvent emissions. Another example, though propane and *n/i*-butanes are typical components of LPG, they are also emitted from vehicles. In this analysis, different numbers of factors were tested, and an optimum solution was determined based on both a good fit to the observed data and the most meaningful results by comparing with previous studies (Guo et al., 2011a; Lau et al., 2010). It is noteworthy that the number and profile of factors (sources) in this study were determined based on the results from previous receptor-modeling studies (Guo et al., 2011a, 2007; Ling et al., 2011; Lau et al., 2010) and VOCs source emission studies (Guo et al., 2011b; Ho et al., 2009; Liu et al., 2008; Tang et al., 2008, 2007; Borbon, et al., 2002; Blake and Rowland, 1995). Good correlations were found between the observed and predicted VOC concentrations at TW (R^2 = 0.98) after PMF implementation. Moreover, all the selected species had scale residuals normally distributed between -3 and 3, confirming that the measured data were well modeled (EPA, 2008).

Furthermore, to estimate the sensitivity of the whole analysis to the selection of 25 species, the results for these two scenarios were compared. The general characteristics for the source profiles on the basis of 41 input VOC species were

almost the same as those by using the 25 selected VOC species as input except for the attributions of some VOC species, i.e., α/β-pinene, camphene, limonene, ρ-cymene and 1-pentene. Two additional source profiles were found for the result of 41 species (data not shown). One is the profile with relatively high contributions of α/β-pinene, camphene, limonene and *ρ*-cymene (additional source 1), in addition to the significant contributions of these species in the source of biogenic emissions, while the other is solely dominated by 1-pentene, with some contribution of butenes (additional source 2). It is well documented that butenes and 1-pentene were mainly from vehicular emissions in Hong Kong and the rest of PRD region (Guo et al., 2011; Ho et al., 2009; Liu et al., 2008). The variations for these sources indicated that the source profiles may be biased due to the large uncertainty of these species caused by their low abundance and/or high reactivity (Table 2). In addition, ethyltoluenes showed high correlations with paint and sealant solvent tracers, i.e., ethylbenzene and xylenes, indicating that paint and sealant was the main contributor to these species. Furthermore, butenes and 1,3-butadiene correlated well with the tracers of LPG usage, i.e., propane, butanes, ethene and propene, indicating that these species would emit from LPG vehicles (Guo et al., 2011b; Liu et al., 2008). It should be noted that, though there were some variations for the results of the addition input VOCs, the contributions of these species/sources were small due to their low abundance. Therefore, based on the above discussion, we believe that the selection of 25 species for the PMF simulation is reasonable and valid in this study.

3.3.2 The description of Observation-Based Model (OBM)

The observation-based model (OBM) developed by Cardelino and Chameides (1995) uses the measured ambient mixing ratios of O_3 and its precursors (i.e. VOCs, CO, NO), as well as meteorological data as a function of time at given sites input as

for the photochemical box model to simulate the total amount of photochemical O_3 production and to explore O_3-precursors relationships at these locations based on the carbon bond IV mechanism. This mechanism categorizes each VOC species into different groups according to their functional bonds. Therefore, this model could only be used to calculate the O_3 production, the O_3-precursors relationships in a given area. It can't be used to investigate the detailed chemistry of photochemical pollution in the atmosphere. On the other hand, due to the fact that measured meteorological data, including the temperature, relative humidity and boundary layer depth should be input into the model for simulation, the OBM model could only reflect the influence of above parameters on O_3 formation in a given area.

OBM model includes two base simulations for calculating total photochemical O_3 production. The first simulation uses the concentrations of specified species such as O_3, NO, CO and the primary VOC functional groups based on carbon IV mechanism to calculate the concentrations of the unspecified species and the integrated source functions by the following equation (Equation 3-2):

$$\frac{\partial C_j}{\partial t} = P_j - L_j - D(t)(C_j - C_j^{FT}), \quad (3\text{-}2)$$

where C_j is the concentration of the j^{th} specified species, and $[\partial C_j/\partial t]_{obs}$ is the observed local time derivative in C_j. This source function, $\Sigma j\ (t)$ (in unit of ppb hr^{-1}) represents the combined effects of emissions at the site, including horizontal transport to the measurement site and the horizontal transport away from the measurement site.

In addition, based on the first simulation results, the second base case simulation can give an internal check on the accuracy of the source function calculated in the first simulation and determine the O_3 formation potential at the given sites (i.e., $P^s_{O3\text{-}NO}$, which is the integration of model-calculated rates of the net O_3 production, including

total O_3 production and NO destruction). The second base case simulation is conducted by the following equation (Equation 3-3):

$$\frac{\partial C_j}{\partial t} = P_j - L_j + \sum_j - D(t)(C_j - C_j^{FT}), \quad (3\text{-}3)$$

With the source function, Σ_j is given by the solutions obtained from the first simulation (Equation 3-3).

Based on the integrated results of the above two base case simulations, the model can be used to evaluate the sensitivity of O_3 photochemical production to the changes in the concentration of its individual precursors at the given locations by the relative incremental reactivity (RIR) method which is developed by Carter and Atkinson (1989) and defined as the percent change in O_3 production per percent change in precursor sources. Equation (3-4) illustrates the RIR of precursor *X* at a site "*S*".

$$RIR^S(X) = \frac{(P^S_{O_3-NO}(X) - P^S_{O_3-NO}(X-\Delta X))/P^S_{O_3-NO}(X)}{\frac{\Delta S(X)}{S(X)}}, \quad (3\text{-}4)$$

Where superscript "*S*" is the specific measurement site; *X* represents a specific precursor; *S(X)* means the integrated amount of species *X* (in ppbv) emitted or transported to the measurement site that results in the concentration of *X* at the site; Δ *X* is the change in the concentration of *X* caused by a hypothetical change Δ *S(X)*; $P^s_{O3\text{-}NO}$ represents the ozone formation potential, which is the net O_3 formation and NO consumed during the evaluation period. The RIR functions, thus calculated, giving a relative measure of the effectiveness of reducing the emissions of one compound or group of compounds over that of another compound or group of compounds represent a series of sensitivity factors that can be used to directly infer the basic ozone-precursor relationships within given locations (Cardelino and Chameides, 1995).

In addition, to calculate the RIR function for a specific precursor or class of compounds over multiple sampling days, an area-averaged RIR function is used as follows, which defines the average RIR function for source X on the S^{th} sampling day

$$\overline{RIR(X)} = \frac{\sum_{S}^{NS}[RIR^{S}(X)P^{S}_{O_3-NO}(X)]}{\sum_{S}^{NS}P^{S}_{O_3-NO}(X)}, \quad (3\text{-}5)$$

Furthermore, the standard deviation and standard error for this area-averaged RIR function is defined by equations 3-6, 3-78 and 3-8:

$$\sigma^{2}_{\overline{RIR(X)}} = \frac{\sum_{S}^{NS}[(RIR^{S}(X)^{2} - \overline{RIR(X)}^{2})P^{S}_{O_3-NO}(HC_i, NO, O_3, CO)]}{(NS)(\sum_{S}^{NS}P^{S}_{O_3-NO}(HC_i, NO, O_3, CO))}, \quad (3\text{-}6)$$

$$\sigma = \frac{\sqrt{\sigma^{2}_{\overline{RIR(X)}}}}{\sqrt{NS}}, \quad (3\text{-}7)$$

$$\sigma\% = \frac{\sigma}{\overline{RIR}} \times 100\%, \quad (3\text{-}8)$$

This standard error can be used to determine whether an application of the OBM to a given dataset is appropriate or not. If the standard error of the mean for the time-averaged RIRs defined in the OBM is relatively small, the calculated RIRs will be more likely to be robust (Cardelino and Chameides, 1995). Since the data used in the OBM are the concentrations of precursors at a site, which is related to its emission rate, RIRs can be used to determine the sensitivity of O_3 photochemical production to precursor emissions in the area of the original measurements without a detailed or accurate knowledge of these emissions (Cardelino and Chameides, 1995).

3.3.3 WRF simulation

The Weather Research and Forecasting (WRF) model is a next-generation mesoscale numerical weather prediction system designed to serve both operational

forecasting and atmospheric research needs (Skamarock and Klemp, 2008). It is suitable for use in a broad spectrum of applications across scales ranging from meters to thousands of kilometres (http://wrf-model.org/index.php). Simulations and real-time forecasting tests have indicated that the WRF model has a good performance for weather forecasts, and has broad application prospects (Steven et al., 2004; Done et al., 2004).

As mountain-valley breezes are small scale weather phenomena caused by thermal forcing, and there is a complex terrain in Hong Kong (AFCD, 2008), considerably high model resolution is needed to capture these breezes. In this study, the mountain-valley breezes were simulated using a domain system of five nested grids (36, 12, 4, 1.333, and 0.444 km). The domain with finest resolution (0.444 km grid) covered the Hong Kong region. In the vertical scale, there were 31 sigma levels for all five domains, with the model top fixed at 100 hPa. For physical processes, the WRF single-moment 3-class microphysics scheme (Hong et al., 2004), RRTM long wave radiation scheme (Mlawer et al., 1997), Goddard short wave radiation scheme (Chou and Suarez, 1994), MM5 similarity surface layer (Zhang and Anthes, 1982), Noah land surface model coupled with urban canopy model (Chen and Dudhia, 2001), and Yonsei planetary boundary layer scheme (Hong et al., 2006) were applied for all domains. The Grell-Devenyi ensembled cumulus parameterization scheme (Grell and Dévényi, 2002) was applied for the outer three domains, while there was no cumulus parameterization scheme in the inner two domains. In addition, the distribution of urban land cover was replaced using the latest data downloaded from http://webmap.ornl.gov. To assess the simulation of the WRF model, simulated hourly mean meteorological parameters were compared with observation data at TMS and TW site, together with the measured meteorological data from 22 surface weather

stations and 2 sounding stations in the PRD region. The respective correlation coefficients of 2 m temperature and relative humidity, 10 wind directions and wind speed ranged from 0.50-0.80, reflecting that the simulation could provide a reasonable description for the variations of temperature, relative humidity, wind speed and wind direction in the PRD region. It should be noted that the WRF simulation was conducted with the helpof Dr. Jiang Fei from Nanjing University.

3.3.4 Photochemical box model (PBM) implementing the most up-to-date version of near-explicit photochemical mechanism (PBM-MCM)

A simple box-model coupled with the MCMv3.2 was used to describe the chemical development of the photooxidants in an air parcel with its base on the ground, its upper lid set as top of the boundary layer. The boundary layer mixing height gradually increased during the morning from 300 m to 1400 m and collapsed back to 300 m at night, representative of the autumn conditions in the region (Fan et al. 2008). The grid of the model was set as 7 km × 7 km. As the simple box model includes no treatment of vertical or horizontal dispersion, the VOCs are assumed to be well mixed throughout the model atmospheric boundary layer. The box-model follows a similar format to that described previously (Carslaw et al, 1999, 2001) for constraining with observational data. Here the extensive field measurements at TMS and TW provide input data. As well as the photochemical processes, the model also includes the physical processes of dry deposition and exchanges with the aloft layer at night for the long-lived peroxides, carbonyls, and PAN-type species, as well as heterogeneous losses for N_2O_5, HO_2, CH_3O_2, OH, HNO_3, and NO_3 as given in previous modeling studies (e.g. Carslaw et al. 1999, Derwent et al. 1998, Cheng at al. 2010b). The modelling results were then used to provide insight into the complex chemical processing in the region. The model represents an idealised situation of

worst-case scenario for the photochemical O_3 development by investigating the targeted species photo-oxidant concentrations. The simulated concentrations of the targeted species and intermediates might not reflect the actual values as the observation data may be influenced by short-term increases or reductions from local sources that are not represented on the scale of the well-mixed box.

All the input data were averaged over one-hour time intervals for the purpose of data evaluation. The base model was constrained with relative humidity, pressure, temperature, NO, NO_2, SO_2, CO and 55 VOCs over the period of the episode days. It should be noted that that this PBM-MCM model was developed by Sean Lam and Sam Saunders from the University of Western Australia with financial support of Dr. Hai Guo's projects.

For the photochemical box model, several measures were adopted to control the accuracy for the model simulation. Firstly, the model used was the latest version of master chemical mechanism (MCM v3.2). The parameters used in this mechanism were mostly based on experimental data. For the photolysis rate, the up to date NCAR TUV model was used to generate site specific photolysis rate for the study area according to the measured meteorological conditions. All the available species in the MCM scheme were constrained with direct measurement data from the field campaign. Finally, the model simulation results were compared with the observed data at the two sampling sites. The results indicated that the model predicted well for peak O_3 during the study period (Lam et al., 2013), further suggesting that photochemical box model used in this study could provide a reasonable description of O_3 formation at the sampling sites.

3.3.4.1 Photolysis rates

The photolysis rates for particular VOCs vary with solar zenith angle, which can be calculated for different locations and times of the year. Hence a set of photolysis rates specific for the 2010 measurement campaign period and Hong Kong domain were tailored for this work. Detail calculation of the photolysis rates could be found in Lam et al. (2013). In brief, initially the photolysis rates from the original MCM two-stream isotropic scattering model (Hough, 1988), set for the location of Hong Kong and solar zenith angle were calculated for the period of the field measurements in 2010. To assess the influence this may have on the model output, an alternative calculation of photolysis rates was conducted. Adopting a similar approach to that developed by Pinho et al. (2009) for Portugal in Europe, photolysis coefficients were calculated using the photon flux determined from the Tropospheric Ultraviolet and Visible Radiation (TUVv5) Model (Madronich, 2013). To reduce the calculation time, a scaling factor was then applied to the original MCM two-stream isotropic scattering model in order to fit the photolysis rates calculated by the TUV model (Table 3.2).

Table 3.2 Modelled photolysis rate parameterization in PRD

Reactions	MCMv3.2 photolysis designation	Ratio
$O_3 \rightarrow O_2 + O(1D)$	J<1>	1.708
$O_3 \rightarrow O_2 + O(3P)$	J<2>	1.223
$H_2O_2 \rightarrow 2OH$	J<3>	1.265
$NO_2 \rightarrow NO + O(3P)$	J<4>	1.381
$NO_3 \rightarrow NO + O_2$	J<5>	1.167
$NO_3 \rightarrow NO_2 + O(3P)$	J<6>	1.341
$HNO_2 \rightarrow OH + NO$	J<7>	1.270
$HNO_3 \rightarrow OH + NO_2$	J<8>	1.489
$CH_2O \rightarrow H + HCO$	J<11>	1.366
$CH_2O \rightarrow H_2 + CO$	J<12>	1.249
$CH_3CHO \rightarrow CH_3 + HCO$	J<13>	1.850
$C_2H_5CHO \rightarrow C_2H_5 + HCO$	J<14>	1.450
$C_3H_7CHO \rightarrow n\text{-}C_3H_7 + HCO$	J<15>	1.000
$C_3H_7CHO \rightarrow C_2H_4 + CH_3CHO$	J<16>	1.000
$i\text{-}C_3H_7CHO \rightarrow n\text{-}C_4H_9 + HCO$	J<17>	1.000
$CH_2=C(CH_3)CHO \rightarrow$ Products	J<18><19>	0.833
$CH_3COCH_3 \rightarrow CH_3CO + CH_3$	J<21>	1.216
$CH_3COCH_2CH_3 \rightarrow CH_3CO + CH_2CH_3$	J<22>	2.774
$CH_3COCHCH_2 \rightarrow$ Products	J<23><24>	0.407
$CHOCHO \rightarrow CO + CO + H_2$	J<31>	0.092

$CHOCHO \rightarrow$ Products	J<32>	9.183
$CH_3COCHO \rightarrow CH_3CO + HCO$	J<34>	1.179
$CH_3COCOCH_3 \rightarrow$ Products	J<35>	1.366
$CH_3OOH \rightarrow CH_3O + OH$	J<41>	1.313
$CH_3ONO_2 \rightarrow CH_3O + NO_2$	J<51>	1.230
$CH_3CH_2ONO_2 \rightarrow CH_3CH_2O + NO_2$	J<52>	1.737
$CH_3CHONO_2CH_3 \rightarrow CH_3CHOCH_3 + NO_2$	J<54>	1.299
$C(CH_3)_3(ONO_2) \rightarrow C(CH_3)_3(O.) + NO_2$	J<55>	1.266
$CH_3COCH_2(ONO_2) \rightarrow CH_3COCH_2(O.) + NO_2$	J<56>	8.458
$CH_3COCH_2(ONO_2) \rightarrow CH_3CO + HCHO + NO_2$	J<57>	1.000

3.3.4.2 Model scenarios

Three model scenarios were considered in this study: 1) Stationary photochemical box in TW: in this scenario, the monitoring station at TW was assumed to be the centre of the box model and the concentrations of the targeted species were homogenous throughout the box. Hence, the model in scenario 1 was constrained with TW data only; 2) Stationary photochemical box in TMS: similar to scenario 1, monitoring station at TMS was assumed to be the centre of the box model and the model was constrained only with TMS data; 3) Moving box (Mbox): this scenario was an over simplified mountain-valley breezes phenomenon with the grid sitting between TW and TMS monitoring stations and an air parcel moving on an idealized trajectory. During daytime hours (18:00 – 07:00, local time (LT)), the monitoring station at TW was assumed to be the centre of the box model and the concentrations of the targeted species were homogenous throughout the box. The air parcel from TW followed the valley breezes entering the grid simultaneously, which brought trace gases emitted from TW to the top of the mountain. Photochemical reaction occurred under abundant sunlight at the top of the mountain (TMS). At this scenario, the model was constrained with TW data only. If mesoscale circulations were dominated, the modeled O_3 levels compared well with the observations at TMS during daytime hours. When at dusk, the air parcel was carried back down by the mountain breezes into the grid until the next

morning (18:00 – 07:00 LT). At this scenario, TMS was assumed to be the centre of the box model and the model was constrained with TMS data only.

Chapter 4 Characterization of photochemical pollution at different elevations in mountainous areas in Hong Kong

4.1 Introduction

Distinguished from surface measurements and aircraft observations, studies conducted in mountain areas often provide information on the regional background concentrations of air pollutants, the influence of regional transport and mesoscale circulations, the photochemistry of biogenic volatile organic compounds (BVOCs), and the influence of meteorological factors on ozone (O_3) chemistry (Pochanart et al., 2003; Zellweger et al., 2003; Gao et al., 2005; Wang et al., 2006b; Fu et al., 2010). The characteristics of O_3 in mountainous areas have been investigated in different locations in recent years (e.g. Evtyugina et al., 2009; Scott and Ahmet, 2009; Crowley et al., 2010). For example, Burley and Bytnerowicz (2011) investigated the O_3 distribution at White Mountains (1237 – 4342 m) in California and concluded that high O_3 concentrations were correlated with slow-moving back-trajectories which had spent more time inland and less time offshore. Monteiro et al. (2012) analyzed a high O_3 episode by a statistical technique and a modeling approach at a mountain site (1086 m) in the Mediterranean region, and reported that transport of O_3 and its precursors by local mountain breezes and sea-breeze circulation was mainly responsible for the high O_3 concentrations. Turnipseed et al. (2004) simulated the mesoscale atmospheric flow conditions influenced by regional topography in the Niwot Ridge Ameriflux site within the Rocky Mountains (3050 m), and significant influence of mesoscale winds was found under the strong synoptic westerly winds. Ou Yang et al. (2012) investigated the seasonal and diurnal variations of O_3 at a high-altitude mountain site (2862 m) in central Taiwan and concluded that the

springtime maximum O_3 concentration was most likely caused by the long-range transport of air masses from Southeast Asia.

In mainland China, limited studies have been undertaken to investigate the characteristics of O_3 pollution in mountainous areas (e.g. Gao et al., 2005; Wang et al., 2006b; Li et al., 2008; Xue et al., 2011). Gao et al. (2005) reported measurements of O_3 and CO at the summit of Mt. Tai (1534 m) and suggested that air masses from the North China Plains or the re-circulation over the Shandong Peninsula had significant influence on air pollutants. Li et al. (2008) investigated the impact of chemical production and transport on summer diurnal O_3 behavior at a mountainous site in North China Plain. They suggested that in-situ chemistry accounted for most of the O_3 increment from morning to mid-afternoon. Wang et al. (2006) and Xue et al. (2011) studied the origin of surface O_3 and reactive nitrogen speciation at Mt. Waliguan (3816 m) in western China, and indicated that high O_3 events were mostly derived from the downward transport of the upper tropospheric air rather than anthropogenic pollution. Nonetheless, all of these studies were carried out only at mountain sites in northern/western China.

Hong Kong and the rest of Pearl River Delta (PRD) region are situated along the coast of southern China. The rapid economic development has caused elevated levels of air pollution in this region (Huang et al., 2006; Guo et al., 2009). Owning to its critical role in the atmospheric oxidizing capacity, human health and vegetation (NRC, 1991; PORG, 1997; IPCC, 2007), photochemical O_3 has been studied in Hong Kong and the PRD region for the past two decades (Chan et al., 1998a, b; Wang et al., 2003; Ding et al., 2004; Zhang et al., 2007; Guo et al., 2009). Though these studies help us better understand the O_3 pollution in the PRD region, they were conducted at low-elevation urban and rural sites (< 50 m).

Many studies showed that mesoscale circulations like sea-land breezes and/or mountain-valley breezes play important roles in air pollution transport in such a region with complex topography and land-use/land cover. The role of sea-land breezes in air pollution transport has been well-studied previously (Zhang and Zhang, 1997; Liu et al., 2000; Ding et al., 2004). For mountain-valley breezes, there were relatively few Hong Kong studies focusing on this topic, even though it is almost certainly very important to air pollution transport in Hong Kong, where topography and physical features are complex and where about 75% of the land area is hilly (AFCD, 2008). In addition, there were very few works conducting field measurements at mountain site, especially the concurrent measurements at the foot and summit of the mountain in this region.

In this chapter, we investigated the characteristics of air pollutants and the causes of variations of air pollutants at the mountain site (TMS) and the low-elevation urban site (TW), the relationship between the two sites and the influence of mesoscale circulations were explored by integrated data analysis and different models. In addition, the relationships of O_3-precursors at the two different sites were further evaluated.

4.2 Overall observation results

4.2.1 Levels of trace gases and O_3 episodes

Table 4.1 summarizes the statistics of trace gases during the sampling period. In general, the mixing ratios of air pollutants were greater at TW than TMS, whereas the secondary pollutant O_3 was greater at TMS than TW. The average concentrations of NO_x, CO and SO_2 at TMS were 10.7 ± 0.3 ppbv, 436 ± 7 ppbv and 4.1 ± 0.1 ppbv, which were 0.19, 0.85 and 0.67 times those measured at TW, respectively. On the other hand, the mean O_3 concentration was 55 ± 1 ppbv at TMS, 2.5 times that at TW.

To gain further information on the O_3 pollution at the two sites, the frequency of O_3 episode days was investigated. At the urban TW site, only one O_3 episode day (19 September, concentration = 116 ppbv) and three near-O_3 episode days (i.e. the peak hourly O_3 mixing ratio between 80 – 100 ppbv, or China's Grade I Standard) were observed. At the TMS site, the maximum hourly average O_3 mixing ratio reached 163 ppbv. Twenty-one O_3 episode days (i.e. 8, 19 – 20 September, 23 – 24, 29 – 31 October, 1 – 3, 8 – 9, 11, 17 – 19, 22 – 23, 26 – 27 November) were found during the sampling period.

Table 4.1 Statistics of trace gases at the TMS and TW sites

Species	**TMS**		**TW**	
	Mean±95% CI*	Max Value	Mean±95% CI*	Max value
O_3 (ppbv)	55 ± 1	163	22 ± 1	116
O_x(ppbv)[1]	58 ± 1	178	47 ± 1	157
NO_x (ppbv)[2]	10.7 ± 0.3	75	55 ± 1	262
CO (ppbv)	436 ± 7	842	517 ± 8	1150
SO_2 (ppbv)	4.1 ± 0.1	28	6.1 ± 0.2	31

* Mean ± 95% confidence intervals.
[1] $O_x = NO_2 + O_3$
[2] $NO_x = NO + NO_2$

4.2.2 Diurnal variation

Figures 4.1a and b show the diurnal variations of mean O_3, NO_x, CO, SO_2 and surface winds at TMS and TW, respectively. TMS and TW had similar diurnal patterns of O_3, experiencing O_3 maxima in the afternoon and minimum at night and in the morning. However, the maximum O_3 at TMS showed a delay, when compared with that at TW. The average daily maximum O_3 mixing ratio at TMS (76 ± 6 ppbv, 15:00 LT) appeared 1 h later ($p < 0.05$) than that observed at TW (35 ± 4 ppbv, 14:00 LT). The delayed daily maximum O_3 at TMS was due to the fact that the air mass arriving at TMS was generally more aged than that at TW, which may be attributed to regional transport (section 4.3.4.1) and/or mesoscale circulations (section 4.3.4.2). At TMS, O_3 exhibited relatively stable concentrations from midnight to the early

morning, a decrease at sunrise, a minimum at about 10:00 LT, a daytime buildup to a broad maximum value at about 15:00 LT, and a slow decrease until midnight, with an average diurnal difference of 16 ppbv. The slow nighttime decay of O_3 at TMS might be attributed to the limited NO titration and the reduced boundary layer mixing height. Indeed, the boundary layer height was approximately 2 km in the daytime and reduced to about 1 km at night in Hong Kong (Guo et al., 2012).

The diurnal variations of O_3 at TW had one peak at about 03:00 and another at 14:00 LT with a trough at about 07:00 LT (Figure 4.1b). The peaks and the trough of O_3 were corresponding to NO minimum and maximum, consistent with previous studies (Chan et al., 1998a; So and Wang, 2003). The combination of photochemical formation and downward mixing from the overlying air masses could result in the O_3 daily peak in the afternoon (So and Wang, 2003; Guo et al., 2009). After reaching the daily peak (14:00 LT), O_3 gradually decreased and approached to the normal background level at night due to the fact that NO emitted during the rush hours could titrate some O_3 and the photochemical production of O_3 ceased at night (Chan et al., 1998a; So and Wang, 2003) and to a lesser extent, the dry deposition process could also cause the drop of O_3 concentration (Zanis et al., 2007; Xue et al., 2011). Then, O_3 started to buildup slowly and presented a peak in the early morning, which was more obvious when a trough was generated at 07:00 LT. This trough was caused by the NO from the fresh vehicular emission which titrated part of the O_3 (Chan et al., 1998a; So and Wang et al., 2003). On the other hand, the small O_3 peak in the early morning may be caused by the decreased titration of NO. While NO started to decrease at 00:00 LT and reached its lowest level at about 04:00 LT (data not shown), O_3 increased gradually and formed a peak at 00:00 – 05:00 LT. In addition, the small O_3 peak in the early morning might be also attributed to the constant transport of O_3 to

TW by southeasterly flows from the South China Sea where O_3 was less consumed (So and Wang et al., 2003; Guo et al., 2009). This speculation was based on the fact that the winds changed from easterly to southeasterly from midnight until dawn. The imposed O_3 from the South China Sea and the minimum traffic activities caused higher O_3 concentrations in the early morning than the normal background level at night (So and Wang, 2003; Guo et al., 2009). The speculation was further evidenced by the diurnal variations of dimethyl sulfide (DMS), an ocean tracer. DMS had a small peak observed from 00:00 to 03:00 LT (data not shown), corresponding to the small O_3 peak observed between midnight and dawn. Previous studies indeed reported that southeasterly winds from South China Sea could result in higher O_3 levels at night (So and Wang, 2003; Guo et al., 2009).

The diurnal variation of NO_x at the TW site showed a typical urban profile, i.e. bimodal structure. The first peak appeared in the early morning (07:00 – 09:00 LT) while the second peak was at about 18:00 – 19:00 LT, coincident with the traffic pattern of Hong Kong. On the other hand, a broad NO_x peak with a delay (compared to TW) was observed at TMS. The peak NO_x value (15.3 ± 2.2 ppbv) at TMS was much lower ($p < 0.01$) than that at TW (84.5 ± 8.1 ppbv). In addition, the diurnal profiles of SO_2 and CO were similar at TMS, with a small and broad peak in the afternoon, which might be indicative of the influence of regional transport (Guo et al., 2009; Jiang et al., 2010) and/or mesoscale circulations (Parrish et al., 1993; Gao et al., 2005; Wang et al., 2006b).

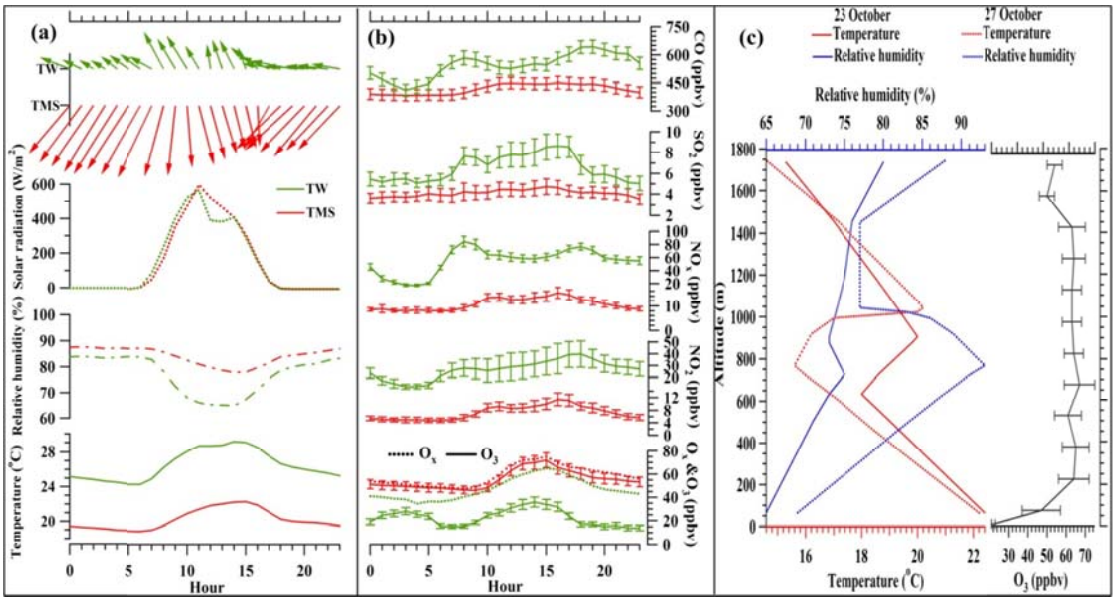

Figure 4.1 (a) Surface meteorological conditions and (b) average diurnal patterns of trace gases at TMS and TW and (c) vertical profiles of meteorological condition and O_3 in Hong Kong

4.3 Which factors are responsible for the discrepancy of O_3 pollution observed at TMS and TW?

While comparable solar radiation was found at the two sites ($p > 0.1$, with the average values of 275 ± 114 and 270 ± 105 W/m^2 at TMS and TW, respectively), higher temperature, lower relative humidity and wind speed, which are conducive for photochemical O_3 formation (Wang et al., 2003; Jiang et al., 2008; Guo et al., 2009), were found at the urban TW site (Figures 4.1a, b). Nonetheless, the O_3 concentrations at TW were much lower than TMS. The difference of the mean O_3 levels between the two sites during the sampling period was 33 ppbv (Table 4.1), while hourly differences reached up to 122 ppbv. As the two sites are separated by a distance of about 7 km and an elevation of 630 m, the factors that could cause the discrepancy of O_3 levels observed at the two sites are discussed in the following sections.

4.3.1 Degree of photochemical reactions

Comparing the levels of precursors is a useful tool to investigate the degree of photochemical reactions at two different sites (Sillman, 1999; Jenkin and Clemitshaw, 2000). Figure 4.2a shows the mean mixing ratios of different VOC groups at the two sites. The VOC species were classified into six functional types, i.e., R-AROM group (reactive aromatics; including xylenes, toluene, trimethylbenzenes and ethylbenzene), R-OLE (reactive olefins; comprising all olefins except ethene), C ≥ 4 (including alkanes with four or more carbons), LRHC (low reactive hydrocarbon carbons; comprising ethane, propane, ethyne and benzene), ETHE (ethene) and BVOC (including isoprene, α-pinene and limonene). During the sampling period, the VOC levels were considerably lower at TMS than TW ($p < 0.01$), which is consistent with other O_3 precursors, i.e., NO_x and CO (Table 4.1).

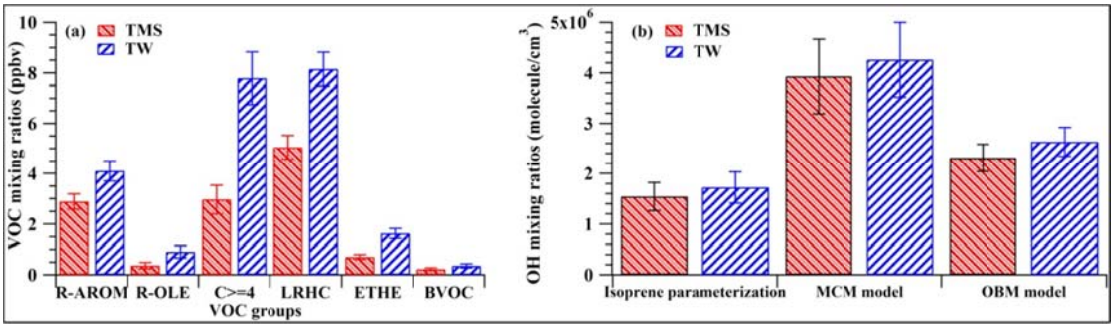

Figure 4.2 The mean mixing ratios of (a) different VOC species and (b) OH radical at TMS and TW during the sampling period. Vertical bars are 95% confidence intervals

On the other hand, the levels of hydroxyl radical (OH radical) were further compared at the two sites. As we did not measure OH radical in situ, its mixing ratio during daytime hours (07:00 – 19:00 LT) was calculated using two models, i.e., an observation based model (OBM) and a Master Chemical Mechanism (MCM) model. The detailed description of the OBM model can be found elsewhere (Zhang et al., 2007, 2008; Cheng et al., 2010a). Besides simulation results, the concentration of OH radical was also estimated from the parameterization method through the empirical relationship between isoprene (ISOP) and its oxidation products i.e. methacrolein

(MAC) and methyl vinyl ketone (MVK), based on the assumption that the processing time of the air mass was identical for MAC and MVK and there were no additional sources of MAC and MVK apart from the oxidation of isoprene (equations 4-1 – 4-5 as follows),

ISOP + OH → 0.63 HCHO + 0.32 MVK + 0.23 MAC $k_1 = 1.0 \times 10^{-10}$ cm^{-3} s^{-1} (4-1)

MAC + OH → products $k_2 = 3.3 \times 10^{-11}$ cm^{-3} s^{-1} (4-2)

MVK + OH → products $k_3 = 1.9 \times 10^{-11}$ cm^{-3} s^{-1} (4-3)

$$\frac{[MAC]}{[ISOP]} = \frac{0.23k_1}{(k_2 - k_1)}(1 - e^{(k_1 - k_2)[OH]_{avg}t}) \quad (4\text{-}4)$$

$$\frac{[MVK]}{[ISOP]} = \frac{0.32k_1}{(k_3 - k_1)}(1 - e^{(k_1 - k_3)[OH]_{avg}t}) \quad (4\text{-}5)$$

where [MAC], [ISOP] and [MVK] were the measured values for MAC, isoprene and MVK, respectively, and t is the processing time. Details of this method can be found in Liu et al. (2009) and Yuan et al. (2012). Figure 4.2b presents the calculated and simulated OH radical concentrations at TMS and TW during daytime hours. At TMS, the average mixing ratios of OH radical simulated by OBM and MCM models were (2.31 ± 0.27) × 10^6 and (3.93 ± 0.74) × 10^6 molecule cm^{-3}, respectively, and (2.03 ± 0.28) × 10^6 molecule cm^{-3} from the calculations of the parameterization method. On the other hand, the average concentrations of OH at TW calculated by the corresponding three methods were (2.63 ± 0.29) × 10^6, (4.26 ± 0.74) × 10^6 and (2.27 ± 0.31) × 10^6 molecule cm^{-3}, respectively. Though variations were found for the results of different methods, the average mixing ratios of OH radical at the two sites were comparable ($p > 0.05$). In addition, by considering the factor of fractional conversion which represented the relative importance of photolysis reactions on OH radical formation in the atmosphere (Jenkin et al., 2000; Atkinson et al., 1997), the mean fraction conversion index at TMS (0.17 ± 0.03) was lower than that at TW (0.23 ±

0.04, $p < 0.05$). Based on the aforementioned analyses, it could be concluded that photochemical reactions at TMS were not stronger than at TW. Hence, the higher O_3 levels observed at TMS than those at TW were not induced by the different degrees of photochemical reactions.

4.3.2 Influence of NO titration

The feature of higher O_3 at the higher elevation site (TMS) than at the ground-level site (TW) is somewhat in line with the vertical profiles of O_3 observed in Hong Kong and other locations (e.g. Wang et al., 2001; Chen et al., 2002; Tseng et al., 2009; Ma et al., 2011). Wang et al. (2001) showed that O_3 generally increased with elevation above surface and had a modest peak between 550 and 650 m at the subtropical Cape D' Aguilar site in Hong Kong in October and November, 2001. In addition, Chen et al. (2002) and Tseng et al. (2009) reported that high O_3 concentrations appeared at the height of 500 – 600 m and decreased rapidly towards the ground during daytime in central Taiwan. Both studies suggested that high O_3 concentrations at higher elevations were partially attributed to the limited NO titrations, due to the lower levels of NO at higher elevations. In this study, the average NO mixing ratio at the mountain site (TMS) was 3.5 ± 0.1 ppbv, compared to 28 ± 1 ppbv at TW, indicating that the higher O_3 mixing ratios at TMS were likely attributed to the limited NO titration ($O_3 + NO = NO_2 + O_2$). The NO titration is a main process of loss for O_3, which can convert NO to NO_2 rapidly (Tang et al., 2012). In order to investigate the titration effect, the concentrations of "oxidant" O_x (the sum concentration of $O_3 + NO_2$) were calculated at the two sites (Jenkin et al., 2000; Chen et al., 2002; Jiang et al., 2010). The mean O_x mixing ratio was 47 ± 1 ppbv at TW, close to the value (58 ± 1 ppbv) found at TMS (Table 4.1), confirming lower degree of NO titration at the TMS site.

4.3.3 Influence of vertical meteorological conditions

Besides NO titration, vertical structure of meteorological variables is an important factor that could influence the O_3 levels at different elevations (Lin et al., 2007; Ma et al., 2011). Therefore, we investigated the vertical profiles of meteorological conditions, such as temperature and relative humidity in Hong Kong on the selected 40 days, including twenty-one (21) O_3 episode days and selected nineteen (19) non-O_3 episode days before/after the O_3 episode days. Two cases (23 and 27 October) were presented here as examples (Figure 4.1c). The vertical profile of meteorological data for Hong Kong was downloaded from the Department of Atmospheric Science, College of Engineering, University of Wyoming (http://weather.uwyo.edu/upperair/sounding.html). In addition, the vertical profile of O_3 was the average pattern of the data in 2005 – 2010, which were obtained from the Measurement of Ozone by Airbus In-Service Aircraft project (MOZAIC, http://mozaic.aero.obs-mip.fr/web/). Detailed description for this dataset could be found in Ding et al. (2008). It should be noted that the vertical meteorological data presented here were obtained from the King's Park station (site 45004, 22.32 ^{o} N, 114.17 ^{o} E, with straight distances of 12 km and 7 km to TMS and TW, respectively), at 08:00 LT. Inspection of the figure suggested that fluctuation in relative humidity and potential temperature caused by inversion layers was found at the altitudes of 600 – 900 m on 23 October and 720 – 1000 m on 27 October. Furthermore, the modified bulk Richarson number (R_i) (Doran et al., 2003) was calculated, and the R_i values were 4.6 and 1.0 at the altitudes from 600 to 900 m on 23 October and from 720 to 1000 m on 27 October, respectively, indicating that the atmosphere was stable and no wind-shear turbulence existed at those elevations (Lin et al., 2007). These inversion layers suppressed dispersion of air pollutants and gave rise to high O_3 levels at high

altitudes, consistent with previous studies (Lin et al., 2007; Ma et al., 2011). Indeed, the inversion layer was often (24 days of the selected 40 days) observed at the range of altitudes of 500 to 1000 m, which may be a factor that resulted in the high O_3 levels at the TMS site located at the elevation of 640 m.

4.3.4 Influence of atmospheric processes

Figure 4.3 presents the scatter plots of (a) *m,p*-xylene to ethylbenzene and (b) *i*-butane to propane at TMS and TW. Since *m,p*-xylene and *i*-butane are more reactive than ethylbenzene and propane, respectively, the ratios of *m,p*-xylene/ethylbenzene and *i*-butane/propane will decrease when photochemical reaction occurs during the air mass transport. These two pairs of ratios were much lower at TMS ($p < 0.05$), with the *m,p*-xylene/ethylbenzene ratio of 0.74 ± 0.04 pptv/pptv (1.66 ± 0.05 at TW) and the *i*-butane/propane ratio of 0.62 ± 0.06 pptv/pptv (0.78 ± 0.02 at TW). In addition, the ratio of alkyl nitrates to their parent hydrocarbons was also investigated. Since the lifetime of ethyl nitrate is shorter than ethane, and the lifetime of 2-butyl nitrate is longer than *n*-butane, the more aged air mass will have smaller ratio of ethyl nitrate/ethane vs. 2-butyl nitrate/*n*-butane (Roberts et al., 1998; Reeves et al., 2007). The ratio of ethyl nitrate/ethane vs. 2-butyl nitrate/*n*-butane was 0.17 ± 0.01 at TMS, while it was 0.91 ± 0.10 at TW. The results suggested that the air mass arriving at TMS was generally more aged than that at TW, which may be attributed to regional transport (Guo et al., 2009; Cheng et al., 2010a) and/or mesoscale circulations, i.e., mountain-valley breezes.

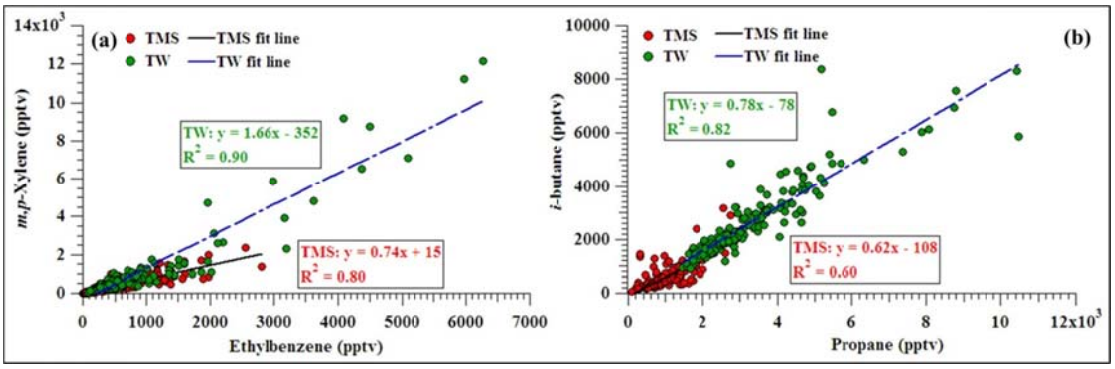

Figure 4.3 The scatter plots of (a) *m,p*-xylene vs ethylbenzene and (b) *i*-butane vs propane at TMS and TW

4.3.4.1 Regional transport

Different wind fields were observed at TMS and TW, indicating the influence of different air masses. The combined wind roses (Figure 4.4) during the sampling period clearly demonstrated that the dominated surface winds at TMS were generally from north with the dominant wind speeds between 0.02 and 4 m/s, whereas the prevailing winds were generally from southeast with dominant wind speeds of 1 – 3 m/s at TW. Moreover, the diurnal wind patterns showed a clear diurnal shift in wind direction at TW, from easterly winds at night and early morning to stronger southerly winds in the afternoon (Figures 4.1a, b). On the other hand, the winds at TMS were generally from the north, with increased speeds at night and in the early morning, and decreased speeds during daytime hours. The two different wind patterns indicated that O_3 mixing ratios at TMS and TW may be influenced by different air flows. Previous studies (So and Wang, 2003; Wang and Kwok, 2003; Guo et al., 2009) have reported that ratios of SO_2/NO_x and CO/NO_x were lower in Hong Kong than in PRD due to the use of low sulfur-containing fuel and more efficient combustion technology in Hong Kong. In this study, the ratios of SO_2/NO_x and CO/NO_x were 0.13 ± 0.04 and 12.85 ± 0.37 ppbv/ppbv at TW, within the ranges of 0.02 – 0.19 and 5.21 – 19.25 ppbv/ppbv from September to November 2010 observed in Hong Kong urban air (data from

HKEPD, http://www.epd.gov.hk), respectively. This suggested that air masses at TW were mainly influenced by Hong Kong local emissions. On the other hand, the ratios of SO_2/NO_x and CO/NO_x were much higher at TMS, with the values of 0.40 ± 0.01 and 46.38 ± 0.71 ppbv/ppbv, respectively, which were within the values reported in the PRD region (0.40 – 1.26 and 11.9 – 52.0 ppbv/ppbv, respectively) (Wang et al., 2005; Guo et al., 2009; Zhao et al., 2011). Hence, the relatively higher ratios of SO_2/NO_x and CO/NO_x at TMS indicated the possible influence of PRD emissions.

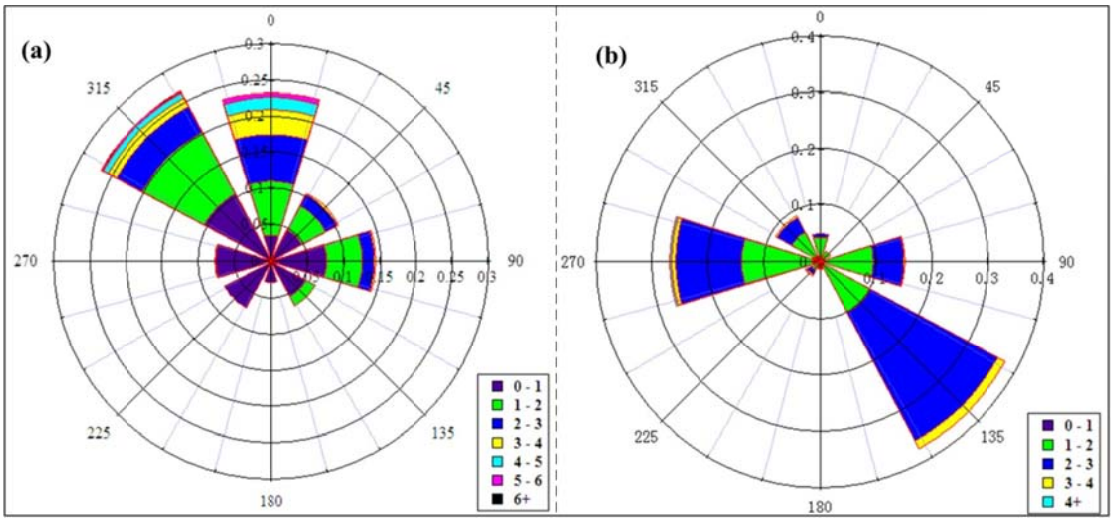

Figure 4.4 Combined wind rose maps at daytime hours during the sampling period at (a) TMS and (b) TW

The urban centers in the PRD region of China, located at straight line distances of 15 – 184 km north of the TMS site, are sources of air pollutants, including O_3 and its precursors (Chan and Chan, 2000; Huang et al., 2006; Guo et al., 2009). At high wind speed (> 2m/s), interregional transport of air pollutants generated from the PRD region could arrive in Hong Kong in several hours, thereby increasing the levels of O_3 and its precursors (Wang et al., 2005, 2009; Huang et al., 2006; Zhang et al., 2007; HKEPD, 2012b). To investigate the effect of regional transport from the PRD region on the air pollutants at the TMS site, we first examined the levels of air pollutants under the influence of regional transport (scenario 1), i.e. northerly winds ($270^o <$ wind direction $\leq 360^o$ and $0^o \leq$ wind direction $< 90^o$) with high speeds (> 2m/s) and

local emissions (scenario 2), i.e. southerly and easterly winds ($90^o \leq$ wind direction $\leq 270^o$) and northerly winds with low speeds (< 2m/s). O_3, CO, SO_2 and TVOCs showed higher mixing ratios ($p < 0.05$) in scenario 1, with average values of 57 ± 2 ppbv, 495 ± 9 ppbv, 4.6 ± 0.2 ppbv and 47 ± 7 ppbC, respectively, while the respective average concentrations were 48 ± 2 ppbv, 370 ± 11 ppbv, 3.6 ± 0.2 ppbv and 33 ± 7 ppbC for scenario 2. This feature was consistent with previous studies (Chan and Chan, 2000; Guo et al., 2009). In addition, the relationship between VOC variability and the atmospheric lifetime was analyzed to estimate the distance of the sources of air pollutants with/without the influence of regional transport (Jobson et al., 1998; Warneke and de Gouw, 2001; Wang et al., 2005). This relationship is expressed as follows (equation 4 – 6):

$$S_{lnx} = A\tau^{-b} \qquad (4 - 6)$$

where S_{lnx} is the standard deviation of the natural logarithm of the mixing ratio X, τ is the atmospheric lifetime, and *A* and *b* are fit parameters. The detailed description for this function can be referred to Wang et al. (2005). In brief, the constant *b* is related to the source-receptor distances and lies between 0 and 1. The closer the sampling site is from the air pollutant sources, the smaller the exponent *b* (Ehhalt et al., 1998; Wang et al., 2005). Figure 4.5 presents the relationship of variability with lifetime for different VOC species under the influence of scenarios 1 and 2. It can be found that the *b* exponent was higher in scenario 1 than in scenario 2 ($p < 0.05$), indicating that air masses at TMS were more frequently impacted by regional transport, particularly under prevailing northerly winds with high speeds (Wang et al., 2005).

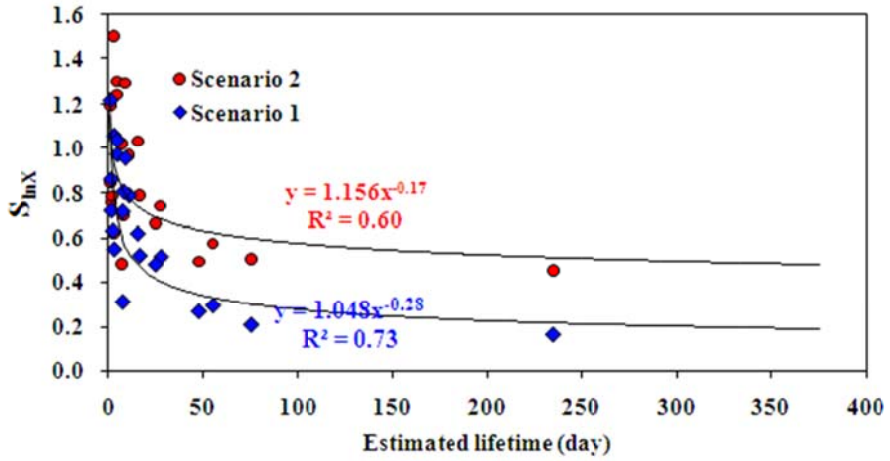

Figure 4.5 The correlation of variability with lifetime for different VOC species with/without the influence of regional transport

Therefore, to further assess the possible influence of PRD air masses on the air quality at TMS, ambient concentration ratios of VOCs i.e., ethyne/propane, benzene/propane, toluene/benzene and *n*-butane/propane were compared among the TMS samples affected by regional transport, the Hong Kong urban air samples and samples collected in the PRD region (Table 4.2). Compared to those in Hong Kong urban areas, higher ratios of ethyne/propane and benzene/propane were found in the PRD region due to the high combustion emissions and solvent usage (Barletta et al., 2008; HKEPD, 2010; Zhang et al., 2012). On the other hand, *n*-butane and propane are generally Liquefied Petroleum Gas (LPG) tracers. The ratio of *n*-butane/propane was lower in the PRD than that in Hong Kong urban areas because of the high percentage of *n*-butane in the composition of LPG used in Hong Kong (Tsai et al., 2006; Tang et al., 2008; Ho et al., 2009; Zhang et al., 2012). Moreover, higher ratio of toluene/benzene was found in Hong Kong urban air as toluene was a distinct emission from Hong Kong due to the high toluene content in unleaded gasoline (So and Wang et al., 2003; Ho et al., 2004, 2009). In this study, for the TMS samples affected by regional air masses, the above four pair ratios were between the values observed in Hong Kong urban air and the PRD region. These results confirmed that the air

pollutants at TMS were somewhat influenced by air masses from the highly polluted PRD region, apart from the influence of Hong Kong urban air by mesoscale circulations (discussed in section 4.3.4.2).

Table 4.2 Comparison of VOC ratios for TMS regional air, urban Hong Kong and PRD region

Site	TMS regional air[a]	TW urban air[a]	Other Hong Kong Urban air[b]	PRD region[c]
Ethyne/propane	1.46	0.89	0.99	0.73 – 1.89
Benzene/propane	0.57	0.25	0.29	0.35 – 0.70
Toluene/benzene	3.14	5.13	4.11	1.75 – 5.40
n-Butane/propane	0.62	1.22	0.93	0.47 – 0.52

[a]This study; [b]HKEPD, 2010; [c]data from Barletta et al. (2008) and Zhang et al. (2012)

4.3.4.2 Mesoscale circulations

To investigate the influence of mountain-valley breezes on air mass transport during this study, correlations of SO_2 and CO at the TMS and TW sites were analyzed. Figures 4.6a and b show correlations of daytime and nighttime averages of CO and SO_2 for TMS vs. TW. In general, good to moderate correlations were found for both CO (R^2 = 0.73 and 0.63 for daytime and nighttime hours, respectively) and SO_2 (R^2 = 0.62 and 0.69 for daytime and nighttime hours, respectively) between the two sites, suggesting some interplays of air masses. The slopes, which were less than one, implied the dilution of air masses during their transport from TW to TMS. Note that the prevailing winds at the mountain site were mainly from the north while those at TW were mostly from southeast (Figure 4.1a). It is unlikely that the correlations for TMS versus TW were caused by the same regional air mass. Therefore, it suggested that the interplays of air masses and the moderate to good correlations between the two sites were likely caused by the influence of mesoscale circulations, i.e. mountain-valley breezes. The lower correlation for CO observed during the nighttime hours was likely due to the fact that the observed CO concentrations at TW were

higher because of the local urban emissions. The lower correlation for SO_2 during daytime hours was driven by a few data points with higher observed than predicted SO_2 levels at TMS. This was mostly attributed to the influence of regional transport (section 4.3.4.1) which could bring the air pollutants from the PRD region to TMS (Figure 4.6b).

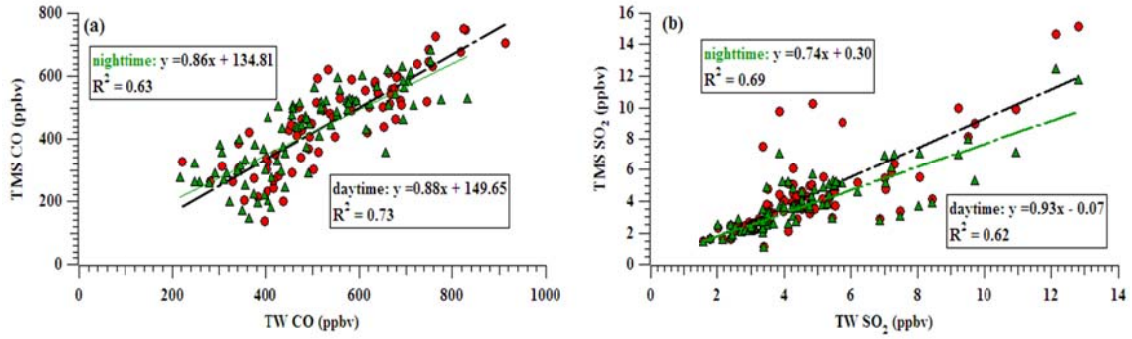

Figure 4.6 Scatter plots of (a) CO and (b) SO_2 during daytime and nighttime hours between TMS and TW

The correlation between the observation and the results of moving box (Mbox) model developed by the PBM-MCM for TMS and TW was also explored to evaluate the influence of mesoscale circulation. Since photochemical O_3 formation occurs during daytime hours, the photochemical processes between 08:00 and 17:00 LT were simulated using Mbox model on the selected VOC sampling days, i.e., 24, 29 – 31 October, 1 – 3, 9 and 19 November, 2010, when the potential influence of mesoscale circulations was dominant (Figure 4.8). In addition, to determine whether regional transport had influence on the air pollutants for the modeling periods as stated above, wind speeds, ratios of SO_2/NO_x, CO/NO_x and toluene/benzene during daytime hours (08:00 – 17:00 LT) at TMS were compared with those influenced by the regional transport (in section 4.3.4.1). If the mesoscale circulations were dominant during the Mbox modeling periods, lower wind speeds, lower ratios of SO_2/NO_x and CO/NO_x and higher ratio of toluene/benzene would be observed, when compared to those observed for the period influenced by regional transport (section 4.3.4.1). Indeed, the

wind speed, ratios of SO_2/NO_x, CO/NO_x during the mesoscale modeling periods were 1.57 ± 0.16 m/s, 0.37 ± 0.02 and 42.01 ± 1.08 ppbv/ppbv, respectively, which were much lower ($p < 0.05$) than those observed in the period influenced by regional transport at TMS, with values of 2.93 ± 0.07 m/s, 0.45 ± 0.02 and 51.01 ± 1.28 ppbv/ppbv, respectively. Moreover, the ratio of toluene/benzene (4.01 ± 0.28 pptv/pptv) was much higher ($p < 0.05$) during the selected days for Mbox modeling than that (3.14 ± 0.38) in the period affected by regional transport, confirming mesoscale circulations were dominant for the modeling periods. Figure 4.7 shows the correlation between observed and modeled O_3 during daytime hours. The time lag between the two sites was evaluated from dividing the distance between TMS and TW by the average value of the observed wind speed during daytime hours. The value of time lag was factored in for pairs of data points used for correlation analysis, i.e. a sample collected at 09:00 LT at TW corresponding to a sample at 10:00 LT at TMS for a valley breeze during daytime hours if the time difference was one hour. Good correlation ($R^2 = 0.70$) between Mbox modeled O_3 and observed O_3 was found during daytime hours (Figure 4.7), suggesting that O_3 at TMS was related to the air pollutants at TW. This further indicated the influence of mesoscale circulations.

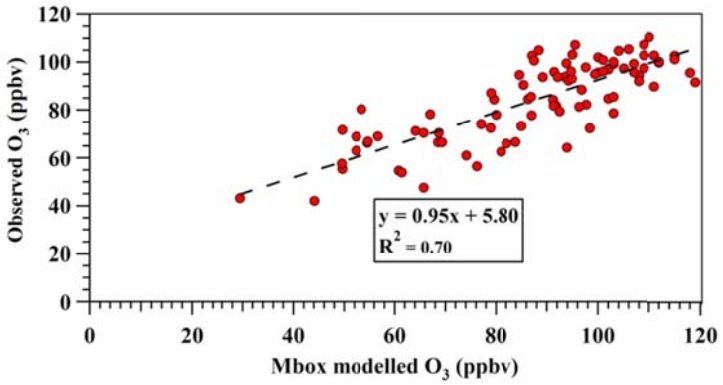

Figure 4.7 The correlation between the observed data and the MCM modeled results during daytime hours

In addition to the above analysis, mountain-valley breezes were simulated using a domain system of five nested grids (Chapter 3). The modeling focused on 16 – 18,

23 September, 23 – 24, 29 – 31 October, 1 – 3, 9, 12, and 19 November, 2010, when evidence for the mesoscale circulation was clear based on the meteorological data and the levels of air pollutants. Here, the simulation results for 9 November are presented as an example (Figure 4.8).

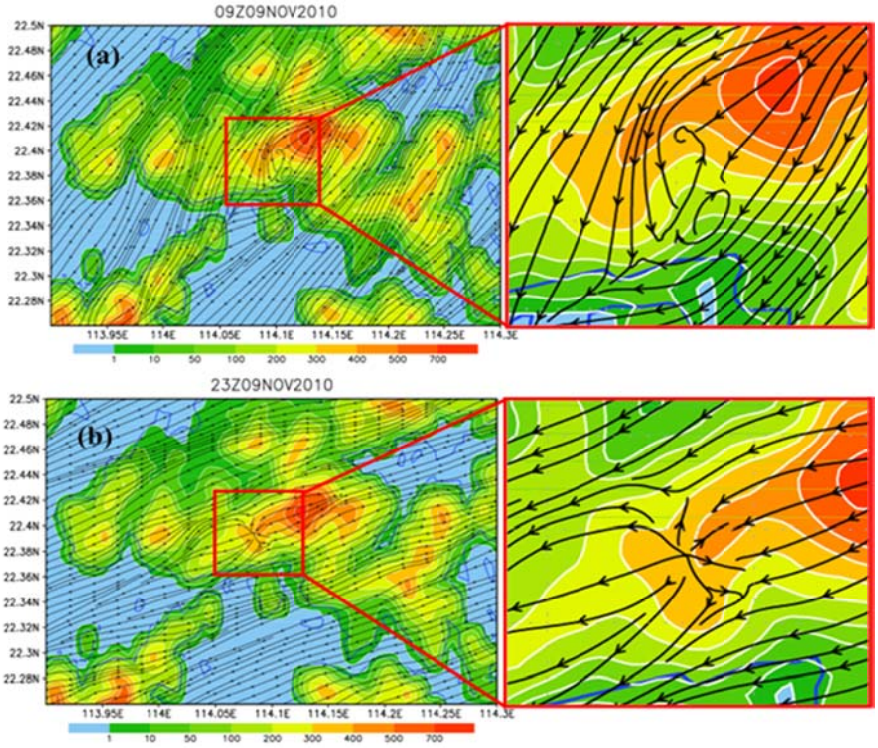

Figure 4.8 Simulation of mountain-valley breezes on 9 November 2010: (a) valley breezes at daytime; (b) mountain breezes at nighttime

The outer four nested domains were simulated using a two-way interactive method from 00:00 UTC (08:00 LT) on 8 November, which was initialized using NCEP (National Centers for Environmental Prediction) FNL (Final Analysis Data) Operational Model Global Tropospheric Analyses data (1° × 1°, http://rda.ucar.edu/datasets/ds083.2/), while the inner domain was simulated using a one-way nested method from 12:00 UTC (20:00 LT) on 8 November, with initial and boundary fields provided by the fourth domain (1.333 km grid). The model results showed that, although the dominant synoptic wind direction was from the north during daytime and nighttime hours, weak mesoscale flows was observed. The model simulation showed a valley breeze in daytime (09:00 LT) on 9 November and a

mountain breeze during nighttime (23:00 LT) hours. Therefore, the model simulation results further confirmed the influence of mountain-valley breezes on the redistribution of air pollutants between TW and TMS. Since O_3 is a secondary pollution, as the air masses aged, secondary reactions occurred and the accumulated O_3 pollution increased (Jiang et al., 2010). Mesoscale circulations, i.e. mountain-valley breezes, can bring freshly-emitted precursors such as VOCs and newly-formed O_3 including that formed during the transit from the urban areas at the foot of the mountain (i.e. TW) to the summit (i.e. TMS) during daytime hours, which induced higher O_3 levels at TMS.

In summary, based on the above discussion, it could be concluded that the higher O_3 mixing ratios at TMS was attributed to the combination influence of NO titration, vertical meteorological conditions, and different atmospheric processes including mesoscale circulations and regional transport.

4.4 The relationships between O_3 and its precursors

Different variations of O_3 and other trace gases at the two sites indicated that relationships between O_3 and its precursors may be different at the two sites. Correlations between O_3 and reactive nitrogen (NO_y) can provide useful information on the chemistry of photochemical O_3 formation in a given location (Sillman et al., 1998 and references therein). It is reported that positive correlations between O_3 and NO_y indicated that O_3 formation was mainly controlled by NO_x, while negative correlations between O_3 and NO_x suggested a VOC-sensitive regime and positive correlations indicated a NO_x-sensitive regime (Sillman et al., 1998 and references therein, Wang et al., 2006). In this study, NO was detected with a chemiluminescence analyzer (API, Model 200E), while NO_2 was converted to NO by a hot molybdenum oxide (MoO) convertor and measured by the chemiluminescene detector. This

analysis technique converts not only NO_2 but also other reactive nitrogen species, including peroxyacetyl nitrate anhydride (PAN), organic nitrates and nitric acid to NO (Wang et al., 2001; Steinbacher et al., 2007; Xu et al., 2013). The "NO_x" measured, defined as "NO_x^*", is thus the sum of NO, NO_2 and other reactive nitrogen species described above, which approximates to NO_y levels in the atmosphere (Wang et al., 2001; Steinbacher et al., 2007; Xu et al., 2012). As such, the measured NO_x^* was taken as a surrogate of NO_y in this study.

Since the range of peak O_3 levels was large at TMS, correlations between O_3 and NO_x^* were investigated for six scenarios, which were divided according to different ranges of the peak 1 h average O_3 mixing ratio. Figure 4.9 presents the correlations of O_3 with NO_x^* for the 10 min average data during the photochemical active hours (10:00 – 18:00, LT) in different O_3 scenarios. Negative correlations between O_3 and NO_x^* were found at TMS in the scenarios with lower O_3 levels (the highest hourly average of 20 ~ 80 ppbv, $p < 0.05$). These features suggested a VOC-sensitive regime, where the photochemical O_3 formation was suppressed as NO_x mixing ratios increased (with average NO_x^* levels changing from 7.8 ± 0.4 to 13.4 ± 0.8 ppbv) in the corresponding scenarios. However, correlations deteriorated ($p > 0.3$) when O_3 levels were higher (the highest hourly average of 80 – 140 ppbv), indicating that the suppression of NO_x^* was reduced and photochemical O_3 formation had changed from VOC-sensitive to both VOC- and NO_x-sensitive as O_3 levels increased (Sillman et al., 2003). However, it should be noted that the correlations could only provide a rough evaluation for the O_3-precursor relationships at the two sites.

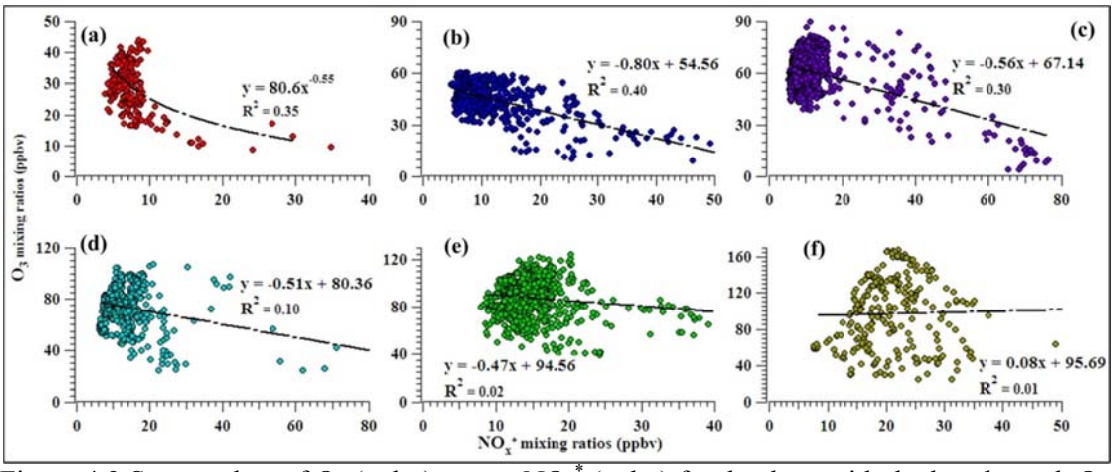

Figure 4.9 Scatter plots of O_3 (ppbv) versus NO_x^* (ppbv) for the days with the hourly peak O_3 of (a) $20 \leq O_3 \leq 40$; (b) $40 < O_3 \leq 60$; (c) $60 < O_3 \leq 80$; (d) $80 < O_3 \leq 100$; (e) $100 < O_3 \leq 120$; (f) $O_3 > 120$ at TMS during sampling period

Figure 4.10 shows the scatter plots of O_3 and NO_x^* during the photochemical active hours (10:00 – 18:00 LT) at TW. The results indicated that O_3 concentrations were negatively correlated with NO_x^*, implying that O_3 formation was primarily VOC-sensitive at TW (Sillman et al., 2003).

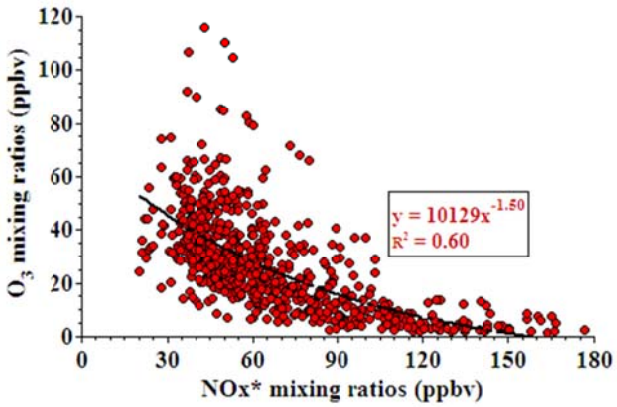

Figure 4.10 Scatter plot of O_3 (ppbv) versus NO_x* (ppbv) at TW during the sampling period

The ratio of VOCs/NO_x (NO + NO_2) is an important parameter to evaluate the relationships between O_3 and its precursors (Sillman, 1999; Jenkin et al., 2000). Previous studies (Dodge, 1977; Finlayson-Pitts and Pitts, 1993; NESCAUM, 1995; Jenkin et al., 2000) found that the VOCs/NO_x (ppmC/ppm) ratio of 8 was an approximate reference point for evaluating relative benefits of NO_x and VOC controls. O_3 could be effectively reduced by a decrease of VOC under VOC-limited conditions,

with the ratio of VOCs/NO_x < 4/1; and by a reduction of NO_x concentration under NO_x-limited conditions, with the ratio of VOCs/NO_x > 15/1. In the transition area, when the ratios range from 4/1 to 15/1, a combination of VOCs and NO_x controls was needed. Figure 4.11 shows the range of measured VOCs vs. NO_x during daytime hours at TW and TMS. At TW, about 82% of data points had VOC/NO_x ratio within the range of 1 to 4, while the ratio for 17% of data points was ranging from 4 to 8. This result indicated that photochemical O_3 formation was mainly VOC-limited at TW; therefore, VOC reduction was most effective in reducing O_3. On the other hand, different characteristics were observed at TMS. Most of the data points (about 60 %) had the ratios in the transition area, with values of 4 to 15, while the rest 40 % of data points had values ranging from 1 to 4. Additionally, about 96% of those data points with ratios ranging from 4 to 15 were found to range from 4 to 8. The relatively higher ratios of VOCs/NO_x at TMS indicated that though VOCs were the most important compounds in the production of O_3 at TMS, the contribution of NO_x was also significant and a combination of VOC and NO_x reductions may be warranted. However, it should be noted that the VOCs observed at TMS may be residues left from the VOCs in the upwind source areas due to photochemical reactions during transport. In addition, different VOC species react at different rates and with different reaction mechanisms, which induce the nonlinear dependency of O_3 formation on NO_x and VOCs. Furthermore, the ratios of VOCs/NO_x used in this study to separate the VOCs/NO_x-sensitive regimes were based on the results of previous studies (Sillman, 1999; Jenkin and Clemitshaw, 2000), which may not be representative of the actual conditions in Hong Kong and/or the inland PRD region. The above limitation could cause uncertainties for the analysis of the ratios of VOCs/NO_x at TMS.

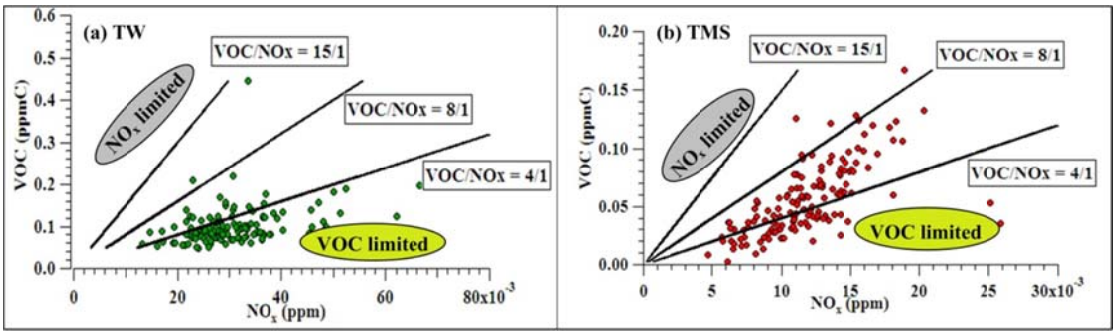

Figure 4.11 Scatter plots of VOCs versus NO_x at daytime hours (07:00 – 18:00 LT) during sampling period at (a) TW and (b) TMS

Therefore, in order to investigate the O_3-precursors relationships in more details, an observation-based model (OBM) was applied in this study. In this study, measured data at 10:00 – 18:00 LT on the selected O_3 episode days at TMS and TW were input into the OBM model to calculate the sensitivity of O_3 production to its precursors, i.e., RIR. Figure 4.12 presents the RIRs for O_3 precursors at TMS and TW. It was found that VOC showed the highest RIR values at the both sites, meaning that VOC was the most important group in O_3 production. In addition, relatively higher RIRs were found for CO at TMS, indicating that CO could have a significant impact on the O_3 formation when it transported from the upwind areas (Ling et al., 2011). Interestingly, the RIRs of NO at TMS were positive but small, indicating that NO also had some influence on O_3 production. On the other hand, the RIRs of NO were negative at TW, indicating a strong VOC-limited regime. Based on the VOCs/NO_x ratio analysis and OBM results, it was concluded that photochemical O_3 formation at TMS was mostly influenced by VOCs, with measurable influence of NO, while O_3 production at TW was generally limited by the concentrations of VOCs.

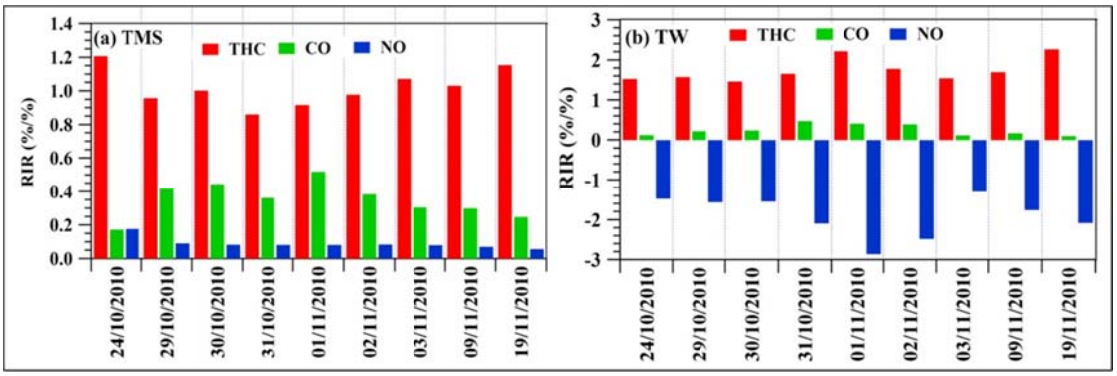

Figure 4.12 RIR values of O_3 precursors, i.e., THC (total hydrocarbons, consist of the VOCs described in section 4.3.1), NO and CO at (a) TMS and (b) TW

4.5 Summary

This chapter investigated the characteristics of O_3 pollution and the factors influenced the variations of photochemical pollution based on the simultaneous systematic measurements of air pollutants conducted at the foot and near the summit of a mountain in Hong Kong from September to November 2010. The levels of primary air pollutants (i.e., CO, SO_2, NO_x and VOCs) were lower at TMS than at TW, while O_3 was greater at TMS than at TW. Only one O_3 episode day and three near-O_3 episode days were observed at TW, while a total twenty one (21) O_3 episode days were found at TMS. The relatively higher levels of O_3 at TMS were attributed to the combination effects of NO titration, vertical meteorological conditions, regional transport and mesoscale circulations. On the other hand, the correlations over the entire ranges of observed O_3 with NO_x, the ratio of VOCs/NO_x and the OBM modeling results implied that photochemical O_3 formation at TMS was mostly influenced by VOCs, with a measurable effect of NO_x, while O_3 production at TW was generally limited by the concentrations of VOCs.

Chapter 5 Sources of ambient volatile organic compounds and their contributions to photochemical ozone formation at a site in the Pearl River Delta

5.1 Introduction

Volatile organic compounds (VOCs) in the atmosphere have received much attention for decades due to the fact that they are important precursors to photochemical smog and their possibilities of causing adverse health effects (Singh et al., 1981; Edgerton et al., 1989; Carter, 1994; Cardelino and Chameides, 1995; Eric et al., 1998; Sillman, 1999). The main anthropogenic sources of VOCs are vehicular emissions, solvent usage, consumer products, biomass/biofuel combustion and fossil fuel combustion, whereas the natural sources are mainly emissions of vegetation. Previous studies have found that the increasing trend of ground-level ozone (O_3) was related to high anthropogenic VOC emissions (So and Wang, 2004; Chang et al., 2005; Shiu et al., 2007; Zhang et al., 2007, 2008; Wang et al., 2009; Cheng et al., 2010a). Studies on the relationships between O_3 and its precursors also show that O_3 production was VOC-limited in the urban areas in Hong Kong and the inland PRD region (So and Wang, 2004; Huang et al., 2005; Zhang et al., 2007, 2008; Cheng et al., 2010a, b; Zheng et al., 2010a). Therefore, an effective strategy for controlling photochemical air pollution could be formulated and implemented through identification and quantification of emission sources of VOC and their relationships with O_3 production.

Positive matrix factorization (PMF) is a receptor-oriented source apportionment model that has been applied in identifying and quantifying the source profiles of VOCs in different locations in the world (Jorquera and Rappengluck, 2004; Latella et

al., 2005; Xie and Berkowitz, 2006; Song et al., 2007; Sauvage et al., 2009). For example, Brown et al. (2007) studied VOC source apportionment by PMF in Los Angeles area in the USA. Yuan et al. (2009) estimated VOC source apportionment in Beijing using PMF. Guo et al. (2011a) conducted source apportionment by PMF in the PRD region, identifying 5 and 6 emission sources of VOCs in Hong Kong and inland PRD, respectively.

It is well documented that VOCs can react with the hydroxyl radical (OH) and nitrogen oxides (NO_x) and result in photochemical O_3 production in the atmosphere (Chameides et al., 1992; Cardelino and Chameides, 1995; Sillman, 1999; Poisson et al., 2000). As such, effort has been made to investigate the relationship between VOCs and O_3 with different methods, including emission-base models (EBMs) and an observation-base model (OBM) (Cardelino and Chameides, 1995; Russell and Dennis, 2000). Compared with EBMs, OBMs simulate O_3 photochemical production and destruction based on measured ambient concentrations of O_3 and its precursors, which can avoid the uncertainties caused by emission inventories and the simulated boundary layer dynamics (Russell and Dennis, 2000).

In recent years, though studies had been conducted for the VOC source apportionments and/or the ozone precursor relationships in different locations in the world (Cardelino and Chameides, 1995; Latella et al., 2005; Xie and Berkowitz, 2006; Zhang et al., 2007, 2008; Song et al., 2007; Liu et al., 2008a; Sauvage et al., 2009; Yuan et al., 2009; Zheng et al., 2009a, b; Cheng et al., 2010a, b), there is little knowledge about the roles of specific VOC sources and species of individual sources in the formation of O_3 in these locations, especially Hong Kong and the inland PRD region, which is the dynamic region on the southern coast of China with astonishing economic growth, rapid industrialization and urbanization.

In this chapter, in order to understand the contributions of different VOC sources and their species to photochemical O_3 production in Hong Kong and the inland PRD region, a new method combining the PMF model and the OBM model was firstly developed based on the data collected at a suburban site (i.e., WQS) of the PRD region. Our objectives are: i) to use the PMF model to identify the source profiles of VOC in PRD; and ii) to use the OBM model to analyze the contributions of these sources to the O_3 formation in the inland PRD; 3) compared the results with previous studies and conducted sensitivity analysis to assess the application for the above new method.

5.2 The source profiles and apportionments of VOCs at WQS

In this chapter, 22 main VOC species were selected for the analysis, as these species are the most abundant species and/or are typical tracers of various anthropogenic emission sources (Table 5.1). Species that are highly reactive (i.e. with lifetime of a few hours) or with high uncertainty were excluded, since they react away quickly in the atmosphere and including them may bias the modeled source profiles (Brown et al., 2007). Correlation between two VOC species can be used to determine whether the two VOCs originate from the same source, and/or participate in photochemical reactions. If two VOCs from the same source are involved in photochemical reactions, their correlation will weaken due to different reactivity. As an example, Figure 5.1 illustrates the scatter plots of ethylbenzene versus *o*-xylene, and propane versus *i*-butane at WQS. These pairs had good correlations (R^2 = 0.96 and 0.63, respectively), showing clear source signatures. This confirms that the VOC species selected are appropriate for source apportionment in this study.

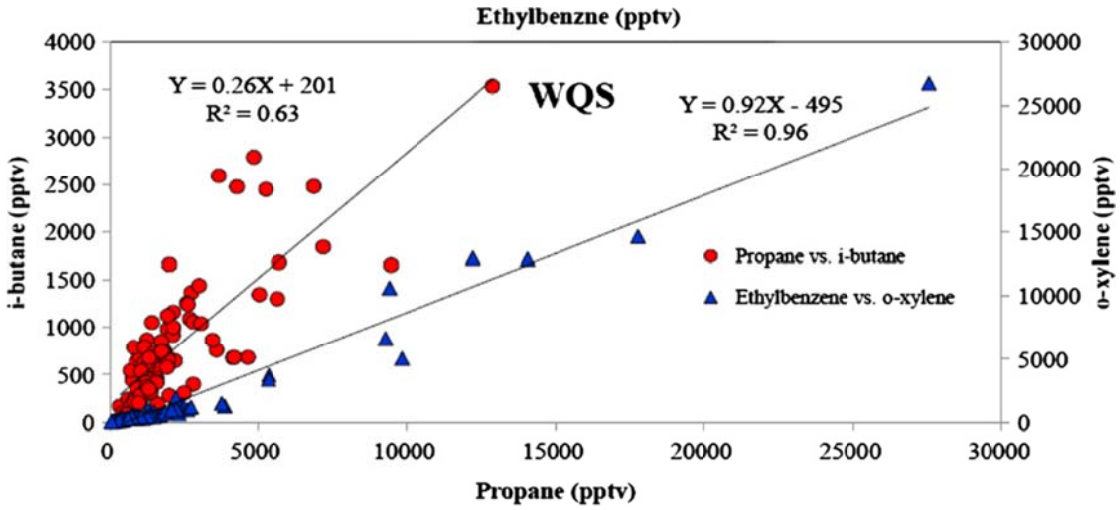

Figure 5.1 Scatter plots of VOC species at WQS

The PMF model was performed on the collected 102 samples and 22 main VOCs. After running the PMF model, 10 factors were resolved at WQS. Factor profiles are shown in Figure 5.2 and the error bars in the figure are the standard errors. The factors were identified as paint and varnish, LPG usage, solvent usage 1, gasoline evaporation, adhesives and sealants, gasoline vehicular emissions, solvent usage 2, biomass/biofuel burning, solvent usage 3, diesel vehicular emissions.

Source 1 was characterized by a high percentage of trimethylbenzenes, accounting for 60% of the total VOCs in the source, with a considerable presence of ethylbenzene (6%) and xylenes (18%). Similarly, a high percentage of aromatics (11% – 45%) was also identified in Source 5. However, the dominant species of VOCs and their mixing ratios were different between source 1 and source 5. In source 5, xylenes were the dominant species, accounting for 45% of VOCs in this source profile, while the percentages of trimethylbenzenes, ethylbenzene and toluene were also remarkable. It is well known that these aromatics can be emitted from either vehicular exhaust or solvent use such as paint, varnish and thinner for decoration (Borbon et al., 2002). In these two sources, these aromatics had poor correlations with ethyne and ethene which are tracers of vehicular emissions, suggesting that these sources represented emissions related to textiles, furniture manufacturing, shoemaking, printing and

plastics (Seila et al., 2001). Hence, high levels of trimethylbenzenes observed in source 1 represented paint and varnish, mainly used in coating and furniture manufacturing that is abundant in Dongguan and Foshan cities (Liu et al., 2008b; http://www1.dg.gov.cn/, http://www.foshan.gov.cn/). On the other hand, source 5 is identified as adhesive and sealants due to high levels of xylenes, which are frequently used in shoemaking, printing, packaging, toy and textiles industries in Dongguan and Shenzhen (http://www1.dg.gov.cn/, http://www.sz.gov.cn). As Dongguan and Shenzhen are upwind of the WQS site, VOCs at WQS are often influenced by these two cities (Chan et al., 2006; Guo et al, 2009, 2011a; Cheng et al., 2010a).

Table 5.1 General characteristics of VOCs selected for model simulation

VOC species	Precision (%)	Accuracy (%)	Reactivity [a]	Concentration (μg/m^3)				Lifetime [c]
				Max	Min	Mean	95%C.I [b]	
Ethane	0.5	5	0.27	16.36	0.32	3.25	0.49	47day
Propane	0.7	5	1.15	23.15	0.60	3.83	0.69	11day
n-Butane	0.6	5	2.54	7.85	0.42	2.49	0.34	4.9day
i-Butane	1	5	2.34	8.38	0.19	1.72	0.28	5.5day
n-Pentane	2	5	3.94	3.71	0.25	1.21	0.14	3.0day
3-Methylpentane	2	5	5.7	21.26	0.41	3.36	0.66	2.2day
i-Pentane	2	5	3.90	24.17	0.73	5.08	0.89	3.2day
n-Hexane	2	5	5.61	45.71	0.03	4.45	1.59	2.2day
n-Heptane	2	5	7.15	12.03	0.08	1.35	0.31	1.7day
n-Octane	2	5	8.68	8.19	0.09	1.10	0.22	1.4day
Ethene	0.7	5	8.52	11.82	0.64	4.35	0.53	1.4day
Propene	16	5	26.3	3.40	0.26	0.64	0.08	11h
1,3-Butadiene	2	5	66.6	0.67	0.01	0.09	0.02	4.2h
Ethyne	0.5	5	0.8	10.72	0.76	4.56	0.40	12-17day
Benzene	2	5	1.23	9.32	0.70	2.50	0.29	9.5day
Toluene	3	5	6.0	116.13	0.44	18.04	3.69	2.1day
o-Xylene	5	5	13.7	115.90	0.14	3.45	2.41	20h
m,p-Xylene	5	5	14.3-23.6	365.54	0.25	9.47	7.71	12-19h
Ethylbenzene	5	5	7.1	119.46	0.20	6.17	2.61	1.7day
1,3,5-Trimethylbenzene	5	5	57.5	5.62	0.05	0.41	0.14	4.9h
1,2,4-Trimethylbenzene	5	5	32.5	98.88	0.20	2.88	2.11	8.5h
1,2,3-Trimethylbenzene	5	5	32.5	22.48	0.05	0.61	0.46	8.5h

[a] unit in $\times 10^{12}$ cm^{-3} molecule^{-1} s^{-1}

[b] 95% confidence interval

[c] Simpson et al., 2010

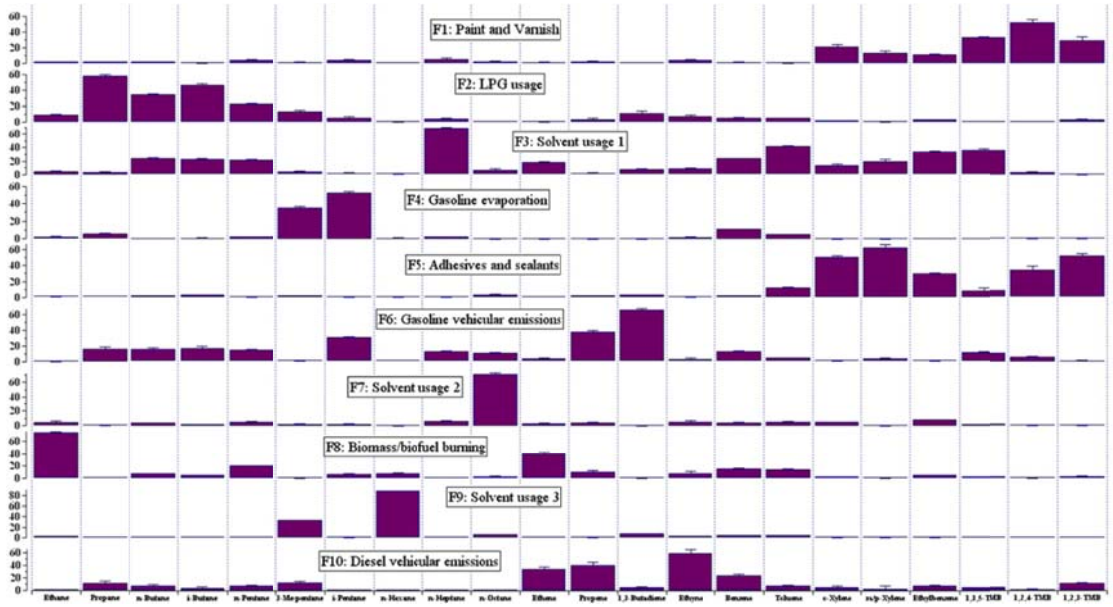

Figure 5.2 Source profiles (percentage of species total) resolved from PMF at WQS

Source 2 was dominated by propane and n/i-butanes that are main constituents and typical tracers for LPG. Therefore, source 2 is identified as LPG usage (Blake and Rowland, 1995). LPG has been used as fuel for buses and taxis in Hong Kong and Guangzhou. Previous VOC studies at roadside sites have found that LPG-fuelled vehicular emissions were a main source of propane and *n/i*-butanes in the PRD region (Tang et al., 2007b; Liu et al., 2008a).

Source 3 was characterized by large amount of *n*-heptane and toluene. *n*-Heptane is widely used as a non-polar solvent (Kwon et al., 2007), while toluene is applied frequently as a solvent in shoemaking, furniture, adhesives, printing and other industries (He et al., 2002; Chan et al., 2006; Liu et al., 2008a). Therefore, source 3 is assigned to solvent usage 1.

Source 4 was dominated by a high percentage of *i*- and *n*-pentanes which are main constituents of gasoline (Morikawa et al., 1998; Tsai et al., 2006). Thus, source 4 is identified as gasoline evaporation.

C_3 – C_4 alkanes, *i*-pentane, propene, 1,3-butadiene, benzene and 1,3,5-trimethylbenzene had a high percentage in source 6. These species are all

associated with vehicular emissions, likely from gasoline-fuelled vehicles as the contributions of 1,3-butadiene, propene and *i*-pentane were usually high when the vehicular speed was over 50 km/h (Mugica et al., 2001;Watson et al., 2001; HKEPD, 2005; Liu et al., 2008a; Guo et al., 2011b).

Source 7 can be characterized as solvent usage 2 as the tracer *n*-octane solely had a high percentage in this source. It is reported that *n*-octane is widely used as a solvent in paint, adhesives and liquid process photocopiers (Health Canada, 1993).

Source 8 was distinguished by high percentages of ethane and ethene (33% and 18%, respectively), which could be emitted from incomplete combustion and/or natural gas usage (Barletta et al., 2005; Durana et al., 2006; Guo et al., 2011b). To ensure that this source profile is correctly interpreted, we added the biomass/biofuel burning tracer i.e. methyl chloride (CH_3Cl) and the combustion tracer i.e. CO into the dataset for the PMF modeling. The rerunning modeling results showed that ethane, ethene, CH_3Cl and CO correlated well with the source 8, suggesting that this source was biomass/biofuel burning (data not shown here). Indeed, our previous source apportionment study found that the contribution of natural gas usage to ambient VOCs in the study region was negligible (Guo et al., 2011a), so did the emission inventory study (Zheng et al., 2009a, b).

Source 9 was characterized by high levels of *n*-hexane. *n*-Hexane is often used as a solvent in shoemaking, furniture and textile industries (ATSDR, 1999). Thus, source 9 is assigned to solvent usage 3.

Source 10 was identified by high percentages of ethyne, ethene, propene and benzene, and low levels of some aromatics and alkanes. These species are all associated with vehicular emissions, especially diesel vehicular emissions as diesel engine combustion generated much higher percentages of ethene and ethyne than

gasoline vehicles (Mugica et al., 2001; HKEPD, 2005; Liu et al., 2008a; Guo et al., 2011b; unpublished data).

Figure 5.3 shows the source apportionment of VOCs extracted from PMF. Solvent usage made the largest contribution to ambient VOCs, about 51 ± 10% (5 ± 2 % for paint and varnish; 24 ± 8 % for solvent 1; 7 ± 4 % for adhesive and sealants; 6 ± 2 % for solvent 2 and 9 ± 4 % for solvent 3), and the contribution of vehicular emissions accounted for 19 ± 2 % (8 ± 2 % and 11 ± 2 % for gasoline and diesel vehicular emissions, respectively) of the total VOCs. The contribution of biomass/biofuel burning was 12 ± 2 %. Additionally, the contribution of LPG usage was 10 ± 3% and gasoline evaporation accounted for 7 ± 2 %.

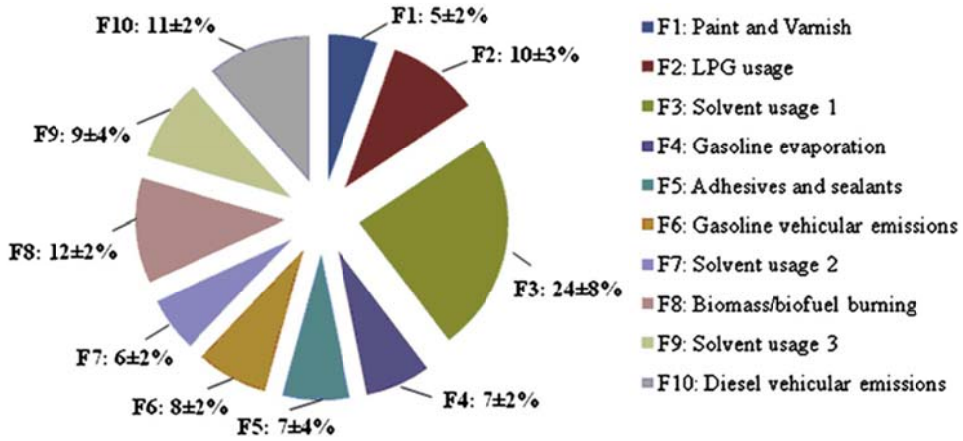

Figure 5.3 Source contributions to ambient VOCs at WQS

5.3 Contributions of VOC sources to O_3 formation

As illustrated previously, the RIR functions represent the percent change in O_3 production per percent change in precursor sources at different sampling sites. Thus, a larger RIR value of a given precursor means a greater probability that reducing emissions of this precursor will reduce O_3 concentrations effectively.

Figure 5.4 shows the RIR values of different sources of VOCs on the sampling days. Although significant variability of RIR values was observed for different sources from day to day, it is apparent that O_3 production was generally VOC-limited

at WQS. Except for the sources of LPG usage, gasoline evaporation, solvent usage 2 and solvent usage 3 on 13 November, 2007, the RIR values of the ten VOC sources were all positive with negative RIR value for NO, indicating that reducing VOCs would actually cause a reduction in O_3 production. In contrast, the negative RIR values of the sources of LPG usage, gasoline evaporation, solvent usage 2 and solvent usage 3 found on 13 November, 2007 suggest that reducing VOC emissions from these sources would lead to an increase in O_3 production on that day. It is well known that O_3 formation is a complex process which is not only closely associated with VOC and NO levels, but also related to VOC/NO_x ratios. The negative RIR values of the above four sources on 13 November 2007 might indicate that the VOC/NO_x ratios in these sources were not favorable to the O_3 formation. Indeed, Evtyugina et al. (2007) found that the VOC/NO_x ratio had a close association with O_3 formation. The result also suggests that whether O_3 formation is increased or decreased depends on not only location and time period, but also emission sources. In addition, the RIR values of the same source varied on different days. This temporal variation may be caused by different emission patterns of the source and the meteorological conditions.

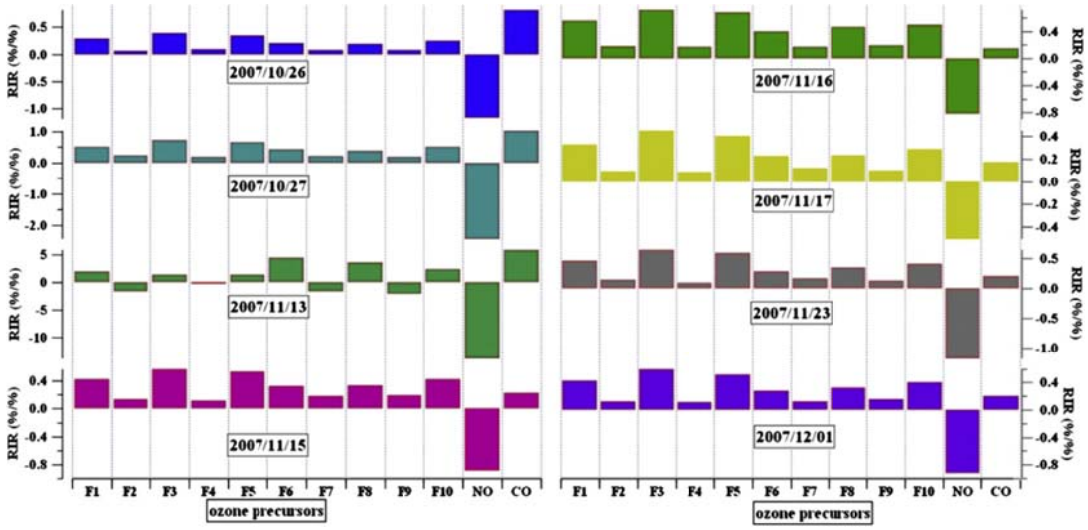

Figure 5.4 The RIR values of different VOC sources on different sampling days at WQS

Figure 5.5 presents the average RIR values for different sources during the sampling period. Among all the sources, the highest RIR value was found for solvent usage 1, which was characterized by high percentages of *n*-heptane and toluene. Besides, the sources of paint and varnish (source 1) and adhesives and sealants (source 5) had higher RIR values. Furthermore, high RIR values were found for vehicular emissions. In total, the RIR value of solvent usage (including paint and varnish, solvent usages 1, 2 and 3, adhesives and sealants) and vehicular emissions (including gasoline and diesel vehicular emissions and gasoline evaporation) accounted for 51% and 28% of the total RIR values (VOCs), respectively. The high RIR value for solvent usage is consistent with a previous study conducted at Xinken of Guangzhou, a location near WQS site (Zhang et al., 2008).

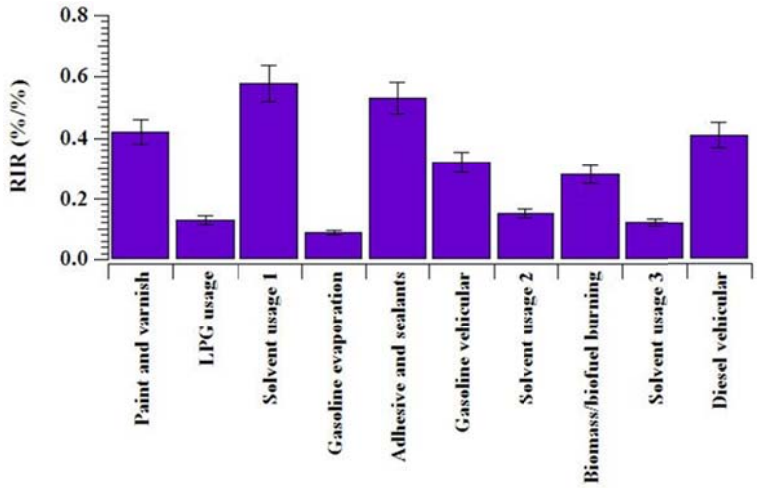

Figure 5.5 The average RIR values of VOC sources at WQS during the sampling period

Figure 5.6 shows the relative contributions of different VOC sources to photochemical O_3 production. It was found that though a total of 10 VOC sources were identified at WQS, the sources of solvent usage 1, diesel vehicular emissions and biomass/biofuel burning accounted for 69% of total contributions at WQS, indicating that local photochemical O_3 production can be mainly attributed to a small number of VOC sources. At WQS, solvent usage 1 made the most contribution to the

photochemical O_3 production among all the VOC sources (34 ± 7 %), whereas diesel vehicular emissions and biomass/biofuel burning contributed 19 ± 7 % and 16 ± 6 % to the O3 formation, respectively. The results suggested that local photochemical O_3 pollution could be effectively reduced by controlling the VOC emissions from these three sources.

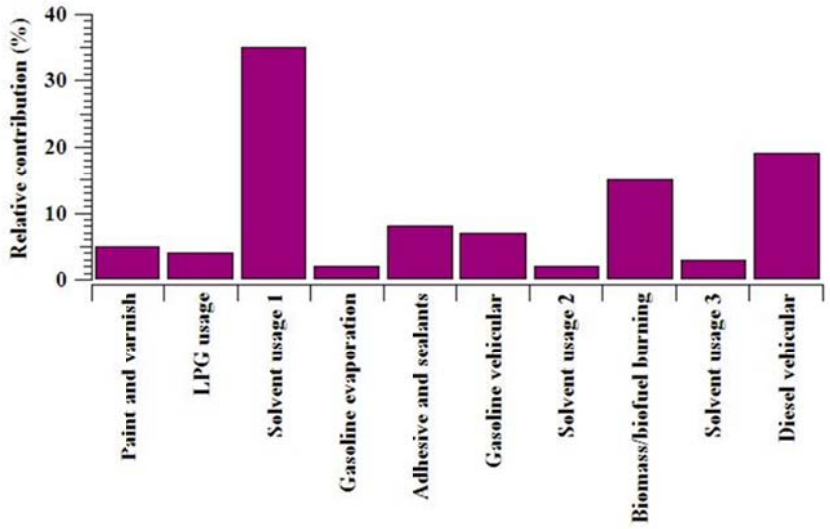

Figure 5.6 The relative contributions of VOC sources to photochemical O_3 production

5.4 Contributions of major VOC species in different sources to ozone production

As described above, solvent usage 1, diesel vehicles and biomass/biofuel burning were the top three VOC sources that mainly contributed to the local photochemical O3 formation at WQS. To investigate the relative contribution of individual VOC species in each source to O_3 formation at WQS, a method using three parameters (i.e. RIR, RIR-weighted and contributions) was adopted, in which the importance of each major VOC species to O_3 production was ranked by RIR-weighted concentrations and contribution. At first, we used this method to investigate the contribution of each VOC species in the diesel vehicular emissions and found that the contributions of the major species identified by PMF accounted for 71% of total contributions for that source (data not shown). Therefore, we used the PMF-extracted concentrations and the OBM-extracted RIR values of the major species in each source to calculate their

RIR-weighted values. The results are shown in Table 5.2. Among all the major species in these three dominant sources, alkenes and most aromatic species generally had the high RIR-weighted values, whereas ethyne and benzene showed different patterns in different sources. Benzene had negative RIR-weighted values in solvent usage 1 and biomass/biofuel burning (-0.06 and -0.34, respectively), but a small positive value in the diesel vehicular emissions (0.24). Generally, the contributions of benzene to O_3 formation in the three sources were very small (-3.1% – 0.5%). The negligible contributions of benzene to O_3 formation were attributed to its low reactivity, similar to the findings of other studies (Derwent et al., 1998; Cheng et al., 2010b). It is noteworthy that though benzene had a low impact on the O_3 formation on local scale, it might have a large impact on the O_3 formation on regional scale when it transported to the downwind areas. On the other hand, the RIR-weighted value of ethyne in the source of biomass/biofuel burning was negative, but it was highly positive in the source of diesel vehicular emissions caused by its high concentration in this source. Similarly, it was found that the contribution of ethyne to the O_3 formation was negligible in the source of biomass/biofuel burning (-0.97%). However, its contribution was moderate in the source of diesel vehicular emissions though its RIR-weighted value was high. This may be due to the fact that though ethyne had low reactivity, it can still contribute to the photochemical O_3 formation when its concentration was high (Du et al., 2007). Overall, these results are consistent with previous studies which found that aromatics and alkenes made significant contributions to photochemical O_3 production in the PRD region and in southern Taiwan, based on either MIR or RIR evaluations (Chang et al., 2005; Zhang et al., 2007, 2008; Cheng et al., 2010a).

On the other hand, alkanes had low RIR-weighted values, which were due to their low RIR values, though some of them had high concentrations in some sources (i.e. *n/i*-butane and *n*-heptane in solvent usage 1; ethane in biomass/biofuel burning; propane and 3-methylpentane in diesel vehicular emissions) (Table 5.2). For solvent usage 1, the dominant VOC species were toluene, *m/p*-xylene and ethene,while ethene, toluene and ethyne dominated the contribution to O_3 formation in diesel vehicular emissions (Table 5.2). And for biomass/biofuel burning, ethene showed the highest contribution. The results suggest that a relatively small number of VOC species in a small number of VOC sources were responsible for the photochemical O_3 formation at the site.

Table 5.2 Contribution of major VOC species in different sources to the O_3 production

VOC sources	Major species	Mean Con	RIR ($\times 10^{-2}$, %/%)	RIR-weighted[a]($\times 10^{-2}$)	Contribution[b](%)
Solvent usage 1	*n*-Butane	0.57	0.5	0.29	0.21
	i-Butane	0.37	0.7	0.26	0.21
	n-Pentane	0.24	0.1	0.02	0.03
	n-Heptane	0.92	0.8	0.72	0.55
	Ethene	0.75	8.8	6.29	5.09
	Benzene	0.56	-0.1	-0.06	-0.06
	Toluene	7.61	9.4	71.57	55.35
	o-Xylene	0.43	5.9	2.53	1.94
	m/p-Xylene	1.82	26.1	47.54	36.68
	1,3,5-Trimethylbenzene	0.14	1.9	0.27	0.21
Biomass/biofuel burning	Ethane	0.15	0.3	0.04	1.86
	n-Butane	0.11	0.2	0.02	0.09
	n-Pentane	0.07	0.4	0.03	0.21
	Ethene	0.12	21.1	2.63	84.27
	Propene	0.02	8.2	0.20	1.12
	Ethyne	0.26	-3.8	-0.97	-2.99
	Benzene	0.09	-3.6	-0.34	-3.11
	Toluene	1.05	3.2	3.36	18.54
Diesel vehicular emissions	Propane	0.42	0.7	0.31	0.63
	n-Butane	0.20	0.8	0.16	0.31
	n-Pentane	0.09	0.5	0.05	0.09
	3-Methylpentane	0.41	1.0	0.41	0.83
	Ethene	1.51	17.2	26.01	52.15
	Propene	0.25	8.6	2.18	4.38
	Ethyne	2.69	4.1	10.92	21.89
	Benzene	0.60	0.4	0.24	0.53
	Toluene	1.42	6.8	9.73	19.50
	1,2,3-Trimethylbenzene	0.07	2.3	0.16	0.33

[a] RIR-weight = RIR(X) × concentration (X), X represents the specific VOC species
[b] contribution = [RIR(X) × concentration(X)]/∑[RIR(X) × concentration(X)]

5.5 Sensitivity analysis

In order to evaluate the importance of the input parameters in the OBM model, an uncertainty assessment on the contributions of VOC sources to the O_3 formation was conducted. The PMF-extracted concentrations of VOC species for each of the ten VOC sources were input into the OBM model. The "basic RIR value" of each source that corresponded to the mean PMF-extracted concentrations of VOC species in this source was obtained. As there were standard deviations for the PMF-extracted concentrations of individual VOC species for each source, we defined the "mean concentration + standard deviation" as the upper range, and the "mean contribution – standard deviation" as the lower range, and the upper range and lower range data were input into the OBM for model simulation. By comparing the RIR values obtained from the upper and lower range data simulation with the "basic RIR values", the uncertainties of the OBM-extracted RIR values were estimated.

As such, the uncertainty of the modeling results was calculated using Equation 5-1:

$$V_{\pm} = \frac{RIR_{upper/lower} - RIR_{mean}}{RIR_{mean}} \times 100\% \quad (5\text{-}1)$$

where $V_{\pm}$ is the percentage of uncertainty of the modeling results.

Table 5.3 shows the uncertainty assessment results based on the source categories identified by the PMF model. As shown in Table 5.3, various uncertainties in the RIR values were identified for each source. In general, when the mass contribution of a VOC source to the total ambient VOCs increased, the RIR value of the source was higher than the basic RIR value. In the present study, the contribution of diesel vehicular emissions showed the lowest uncertainty, whichwas from -11% to 7%, followed by the biomass/biofuel burning (-16% – 7%). The lower uncertainties may be attributed to the relatively stable emissions of VOC species from these sources, though the dominant species in these sources were highly reactive. In contrast, the

contribution of gasoline evaporation presented the highest uncertainty, ranging from -44% to 67%. The highest uncertainty of gasoline evaporation may be due to the large variations of the tracers (i.e. *n/i*-pentane) in this source during the entire sampling period, and the uncertainty caused by the PMF model.

Table 5.3 Sensitivity analysis of the concentrations of VOC sources identified by the PMF model to the O_3 formation

Sources	Mean Con.(%)[a]	S.D.(%)[b]	Basic RIR(%/%)[c]	Uncertainty of RIR(%)
Paint and varnish	5	±2	0.43	-30 – 31
LPG usage	10	±3	0.14	-18 – 46
Solvent usage 1	24	±8	0.59	-21 – 19
Gasoline evaporation	7	±2	0.12	-44 – 67
Adhesives and sealants	7	±4	0.53	-38 – 29
Gasoline vehicular emissions	8	±2	0.30	-22 – 12
Solvent usage 2	6	±2	0.13	-8 – 39
Biomass/biofuel burning	12	±2	0.33	-16 – 7
Solvent usage 3	9	±4	0.15	-38 – 30
Diesel vehicular emissions	11	±2	0.39	-11 – 7

[a] The mean mass contribution extracted by PMF modeling.
[b] Standard deviation derived from PMF modeling.
[c] The value corresponded to the mean mass contributions of VOC species extracted by PMF modeling

5.6 Summary

In this chapter, a new method combining positive matrix factorization (PMF) model and observation-base model (OBM) were first developed to investigate the contributions of VOC sources and species to local photochemical O_3 formation in the Pearl River Delta region. The 10 VOC sources identified at WQS by the PMF model were solvent usage 1, biomass/biofuel burning, diesel vehicular emissions, LPG usage, solvent usage 3, gasoline vehicular emissions, gasoline evaporation, adhesives and sealants, solvent usage 2 and paint and varnish. Solvent usage and vehicular emissions (including gasoline, diesel vehicular emissions and gasoline evaporation) were two major contributors to local VOCs. The photochemical O_3 production at WQS was VOC-limited with positive RIR values for VOCs and a negative RIR value for NO. Solvent usage 1, diesel vehicular emissions and biomass/biofuel burning were the top

three VOC sources that made significant contributions to the photochemical O_3 formation at WQS. Furthermore, the summed RIR values of solvent usage (including paint and varnish, solvent usages 1, 2 and 3, adhesives and sealants) and vehicular emissions (including gasoline, diesel vehicular emissions and gasoline evaporation) accounted for 51% and 28% of the total RIR (VOCs), respectively. Alkenes and most aromatics, especially ethene, toluene and *m/p*-xylene, had high RIR-weighted values, indicating that these species were significant contributors to the O_3 formation. The findings suggest that photochemical O_3 pollution in the PRD region could be efficiently controlled by reducing specific VOC species in specific VOC sources (i.e. toluene, m/p-xylene and ethene in solvent usage 1; ethene in biomass/biofuel burning and in diesel vehicular emissions). Sensitivity analysis revealed that the sources of diesel vehicular emissions, solvent usage 1 and biomass/biofuel burning had low uncertainties while the gasoline evaporation showed the highest uncertainty.

Chapter 6 Contribution of VOC sources to photochemical ozone formation and its control policy implication in Hong Kong

6.1 Introduction

With rapid urbanization and industrialization in the past two decades, surface ozone (O_3) pollution, which determines the oxidative capacity of the atmosphere, reduces visibility and affects human and vegetation health, has been frequently observed in Hong Kong and the rest of Pearl River Delta (PRD) region (HKEPD, 2012a; Wang et al., 2009; Guo et al., 2009). As key O_3 precursors, volatile organic compounds (VOCs) are the most important chemicals contributing to high O_3 production rates in the PRD region, where O_3 formation is sensitive to VOCs in urban areas (Ling et al., 2011; Cheng et al., 2010a,b; Zhang Y.H. et al., 2008; Zhang J. et al., 2007). Therefore, identification of VOC sources and quantification of source contributions are fundamental for the formulation and implementation of O_3 pollution control measures.

In recent years, with increasing recognition of adverse impact of VOCs on photochemical smog and human health, a series of control measures to reduce VOCs emissions have been implemented in Hong Kong and the rest of PRD region (GDEMC and HKEPD, 2005 – 2012; Cheng et al., 2010a, b; Zheng et al., 2010a). Most of the control strategies implemented were mass-based approach, focusing on the control of the weight of total VOC emitted. Though measurability and practicality are the major advantage of the mass-based approach, it does not consider the O_3 formation potentials of VOCs (Avery et al., 2006). The O_3 pollution would be worse by replacing heavier VOCs with lower photochemical reactivity by lighter VOCs with higher photochemical reactivity, as the more reactive VOCs would increase the photochemical O_3 formation (HKEPD, 2010; Derwent et al., 2007a). Reactivity-based

methods using MIR (maximum incremental reactivity) and OFP (O_3 formation potential) can overcome the limitation by considering the contributions of VOC species to photochemical O_3 (Chang et al., 2005; Derwent et al., 1998; Carter, 1994; Chameides et al., 1992); but the two methods just simply estimate O_3 formation under optimum or ideal conditions. As a matter of fact, there is no unique relationship between the competitive reaction rates of a set of organic compounds with hydroxyl radical (OH) and their ability to produce O_3 in the atmosphere because the latter depends on the subsequent reaction mechanisms of the products of the OH radical attack. Therefore, a newly reactivity-based method, combining the positive matrix factorization (PMF) model with an observation-based model (OBM), was firstly developed by Ling et al. (2011), which was only applied at a non-urban site in the inland PRD region. The relative contributions of the sources of O_3 precursors and the species in these sources to O_3 production remain unclear in Hong Kong, where severe O_3 pollution exists and control strategies should be different (GDEMC and HKEPD, 2005 – 2012).

The PMF model is a receptor-oriented source apportionment model, which constrains all the elements in the factor score (source profiles) and the factor loading (source contributions) matrix to be positive. Through identifying the intrinsic characteristics of the data, the model can apportion the ambient concentration data into different sources (Yuan et al., 2009; EPA, 2008). Although the fundamental assumption of mass conservation may cause uncertainty in the PMF simulation (Hopke, 2003), Na and Kim (2007) have concluded that the reaction loss does not significantly influence the quantification of source contributions by incorporating the reaction loss of the ambient VOCs in a receptor model. To date, PMF model has been applied extensively and provided robust results in identifying and quantifying the

sources of VOCs in different areas in the world, including urban, suburban, rural and background locations (Guo et al., 2011a; Ling et al., 2011; Lauz et al., 2008, 2009; Song et al., 2007;Xie and Berkowitz, 2006). In Hong Kong, Guo et al. (2011a) reported that vehicular emissions and solvent use contributed 48% and 43% to ambient VOCs, respectively, at a suburban site in 2007. Lau et al. (2010) identified 9 sources of VOCs at four sites in Hong Kong in 2002 – 2003 and 2006 – 2007 by the same approach, concluding that vehicle and marine vessel related sources and liquefied petroleum gas (LPG) were the most significant local sources. However, most previous studies of the source identification and evaluation regarded each individual VOC as equally important to the O_3 formation, without considering actual difference in O_3 formation potentials of individual compounds. Hence, the relative importance of potential VOC sources to the O_3 formation could be misled.

In this chapter, the method combining the PMF and OBM model developed in Chapter 5 was used to identify the major VOC sources and assess the contributions of these sources to photochemical O_3 formation by analyzing the VOC data collected at the urban site in Hong Kong. The following questions were targeted: 1) the major sources of VOCs in urban areas of Hong Kong? 2) the contributions of the VOC sources and the major species in these sources to photochemical O_3 formation? 3) the reduction degree of VOC sources for the highest reduction efficiency of O_3 pollution? The findings in this study are expected to provide valuable information to relevant parties for the formulation and implementation of VOCs and O_3 control strategies in Hong Kong. To our best knowledge, this study is the first of its kind in Hong Kong.

6.2 Source profile and source apportionment

Figure 6.1 presents the explained variations (EVs) of individual apportioned sources and the corresponding major tracers, explaining the contributions of each

source to the specific VOCs at TW. Seven sources were identified, including gasoline exhaust, gasoline evaporation, paint and sealant solvent, LPG usage, diesel exhaust, consumer and household products and biogenic emissions.

Source 1 was characterized by high percentages of *n/i*-pentanes, *n*-heptane, benzene and toluene, with considerable presence of 2-methylpentane and CO, indicating that it is related to vehicular emissions, likely from gasoline-fuelled vehicles as *n/i*-pentane, 2-methylpentane, benzene and toluene were demonstrated good tracers for gasoline exhaust in Hong Kong (Guo et al., 2011a; Ho et al., 2009; Tsai et al., 2006). Similarly, source 2 showed a dominance of *n/i*-pentanes, accounting for 40% of the total VOCs in the source profile, with certain amounts of 2-methylpentane, *n*-heptane and toluene. This source is believed to be gasoline evaporation due the fact that the contributions of other combustion and/or vehicular tracers, i.e., ethane, ethene, benzene and CO were negligible while *n/i*-pentane levels were relatively high.

Source 3 was dominated by high percentages of ethylbenzenes, xylenes and trimethylbenzenes, with aromatics accounting for 70% of the VOC source profile. In addition to vehicular emissions, these species could be from the solvent emissions of paints, inks, sealant, varnish and thinner for architecture and decoration (Liu et al., 2008c; Borbon et al., 2002; Seila et al., 2001). The poor correlation among the above aromatics and other combustion tracers, i.e., ethyne, ethene, and CO in this source suggested that combustion and/or vehicular emissions were not the major contributors of ethylbenzenes, xylenes and trimethylbenzens in Hong Kong. Hence, this source can be identified as paint and sealant solvents.

Source 4 was distinguished by high percentages of propane and *i/n*-butanes, which were typical tracers for LPG (Liu et al., 2008c; Blake and Rowland, 1995). In

addition, ethene and propene showed high levels in the source profile, indicating that this source could be also related to combustion emissions. Indeed, previous studies on roadside and exhaust samples have demonstrated that LPG fuelled vehicular could emit significant amount of ethene and propene (Tang et al., 2007b, 2008). In Hong Kong, LPG was used as fuel for taxis and public and private light bus. For example, about 99.9% of the registered taxi, 51.1% of the register public and private buses were powered by LPG by December 2010 in Hong Kong (HKCSD, 2010). Furthermore, consumer products may also contribute to this source as some of them use LPG as propellant (Lau et al., 2010). Therefore, this source could be assigned as LPG usage.

Ethane, ethene, ethyne, benzene, *n*-decane and CO had a high percentage in source 5, with certain contributions of C_3 – C_4 alkanes and *n*-nonane. These species are all associated with vehicular emissions, likely from diesel-fuelled vehicles as the percentage of C_2 species, benzene and *n*-decane were usually high in the diesel exhaust (Ho et al., 2009; Liu et al., 2008c).

Source 6 was associated with high percentage of *n*-hexane and its isomer 2-methylpentane, accounting for 62% and 40% of those VOCs measured concentrations. In addition to the possible emissions from combustion processes, these two species could be used in the solvents for household products and consumer products (Guo et al., 2011a; Lau et al., 2010; Kwon et al., 2007). The negligible amount of combustion tracers, i.e., CO, C_2 species, in the source profile confirmed that the source could be assigned to consumer and household products.

Source 7 was solely dominated by isoprene, which is the indicator of biogenic emissions (BVOCs) (Tsui et al., 2009; Song et al., 2008).

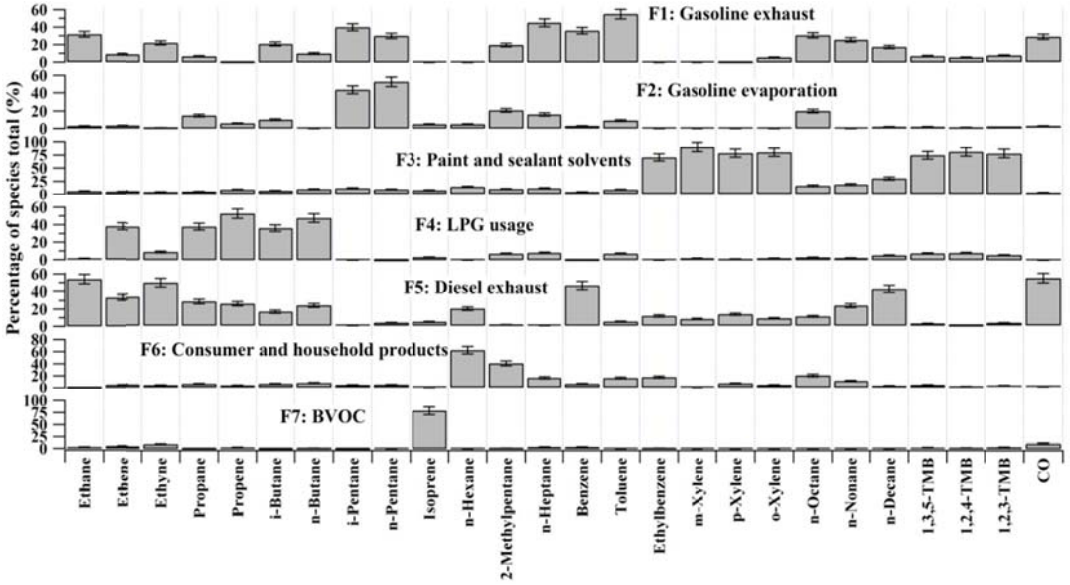

Figure 6.1 Explained variations of seven identified sources at TW

Figure 6.2 illustrates the relative contributions of each source to ambient VOCs at TW. Vehicle exhaust made the largest contributions, responsible for about 42% of the ambient VOCs, followed by solvent-related sources (~ 25%), LPG usage (~ 21%), gasoline evaporation (~ 8%) and BVOCs (~ 4%). To understand variations in VOC sources, we compared the contributions of the identified sources obtained in this work to those from other sites that were previously studied by PMF model in Hong Kong (Table 6.1). It should be noted that some disagreement may be found for the source apportionment results due to different tracers, sampling locations and sampling time. The contribution of vehicular emissions in this study (42 ± 3%) was comparable to those obtained in 2007 at Tung Chung (TC, 48 ± 4%), a suburban site, while it was about twice that estimated at the other four sites in 2002 – 2003 and 2006 – 2007 in Hong Kong (Lau et al., 2010). The difference between this study and the study in 2002 – 2003 and 2006 – 2007 was caused by the identification of source profiles. It was well documented that vehicular emissions could contribute significantly to the ambient levels of some specific VOCs, i.e., benzene, ethane and ethyne (Guo et al., 2011a; Ho et al., 2009; Liu 2008). However, in the study of 2002 – 2003 and 2006 –

2007, these species were categorized as aged VOCs due to their low photochemical reactivity, resulting in the lower contributions of vehicle exhaust. For LPG usage, its contribution in this study was close to that obtained in 2002 – 2003 and 2006 – 2007, indicating that LPG usage has become a remarkable contributor to the ambient VOC loading in Hong Kong. Since 1999, the diesel-fuelled taxis and public and private buses were replaced by LPG. These LPG-fuelled vehicles would run long hours on roads and generate high mileage, resulting in high emissions of LPG usage (Lau et al., 2010). In addition, the high contribution of LPG usage could be related to the increasing LPG consumption, i.e. from 230,000tons in 2001 to 400,000tons in 2010 (HKCSD, 2010). This could be further confirmed by the average concentrations of major tracers of LPG, i.e., propane, *n/i*-buane at TW, which increased from 4.87, 3.63 and 8.83 in 2001 (Guo et al., 2004b) to 6.39, 6.71 and 10.12 μg/m^3 in 2010, respectively. For solvent-related sources, its contribution was comparable to that observed in 2002 – 2003 and 2006 – 2007 (Lau et al., 2010), while it was much lower than that in fall 2007 (Guo et al., 2011a). Although samples in this study and the study by Guo et al. (2011) were both collected in fall, the variations of the contribution of solvent-related sources might be attributed to the sampling site difference. Compared to TW, TC is a relatively new town, still under rapid development. Materials for decoration, i.e. paint and varnish, are being applied to residences in each new apartment block, resulting in higher contributions of solvent-related sources (Lam et al., 2013).

It is interesting to compare the results of this study (top-down approach) with the current VOC emission inventory (bottom-up approach) in Hong Kong. The contributions of vehicle exhaust and solvent-related emissions were different from those of the emission inventory, which reported that about 24% and 60% of VOCs

were from road transport and non-combustion solvent related sources in 2010. The difference between the results of the above two approaches was consistent with previous studies (Lau et al., 2010; Lanz et al., 2008). The discrepancy may be related to the different mechanisms and performance in the two approaches. For example, the PMF model investigated the source characteristics of VOCs based on the concentrations of VOCs measured at the receptor location, while the emission inventory estimated the strength of individual source emissions based on bottom-up survey. On the other hand, different estimation methods were adopted for different emission activities, which could induce significant uncertainties on the VOC emission strengths in the emission inventory (HKEPD, 2005; EPA, 2004). In summary, the comparison suggests a general characteristic of source apportionments of VOCs in Hong Kong, where vehicle exhaust, LPG usage and solvent-related emissions are the major contributors to ambient VOCs.

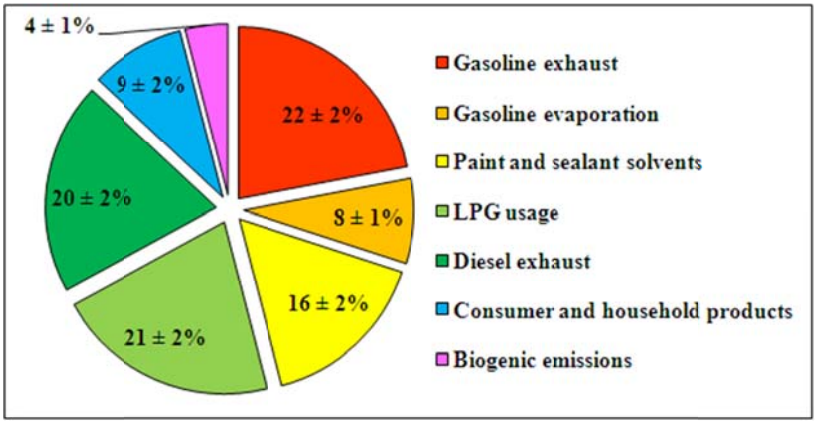

Figure 6.2 Source apportionments of VOCs at TW

Table 6.1 Comparison of source apportionments at TW with those from other areas in Hong Kong by PMF

Factor	Fall, 2010[a]	Fall, 2007[b]	2002–2003[c]	2006–2007[c]	2010[d]
Site	TW	TC	CW, TC, TM, YL	CW, TC, TM, YL	
Vehicle exhaust	42±3%	48±4%	16~27%	12~22%	24%
Diesel	20±2%	21±2%	--	--	
Gasoline	22±2%	27±3%	--	--	
LPG usage	21±2%	--	15-30%	16-41%	
Gasoline evaporation	8±1%	--	4-8%	5-8%	
Solvent related sources	25±3%	43±2%	12-19%	11-15%	60%
Biogenic	4±1%	--	2-6%	1-4%	
Remarks	PMF	PMF	PMF	PMF	EI[e]

[a]This study; [b]Guo et al., 2011a; [c]Lau et al. (2010)
[d]HKEPD, http://www.epd.gov.hk/epd/english/environmentinhk/air/data/emission inve.html.
[e]EI-Emission inventory
TC-Tung Chung, CW-Central/Western, TM-Tap Mum, YL-Yuen Long

6.3 Roles of VOC sources in photochemical O_3 formation

The PMF model could provide the concentration of each VOC in each source directly, defined as PMF extracted concentration. The OBM model was driven on the 20 VOC sampling days by the PMF extracted concentrations. Figure 6.3a presents the average RIR values of different VOC sources, while Figure 6.3b gives the relative contribution of each VOC source to O_3 by considering the reactivity and abundance of VOCs in the function of RIR-weighted value. It can be found that paint and sealant solvents had the highest RIR value, followed by BVOCs, diesel exhaust, LPG usage, gasoline exhaust, consumer and household products and gasoline evaporation. The relatively higher RIR values for paint and sealant and BVOCs were mostly attributed to the high reactivity of the major VOCs in those sources, i.e., ethylbenzene, trimethylbenzenes, xylenes and isoprene (Simpson et al., 2010). However, after taking into account both RIRs and the emission amount of each VOC source, paint and sealant solvents, diesel exhaust and LPG usage were the main contributors at TW, with about 78% to the total RIR-weighted value (VOC sources). The result suggested that controlling vehicular- and solvent-related VOCs is essential for effective control

of O_3 production in Hong Kong. In addition, this result confirmed that an optimum O_3 control strategy should consider both the reactivity and emission quantity of VOCs.

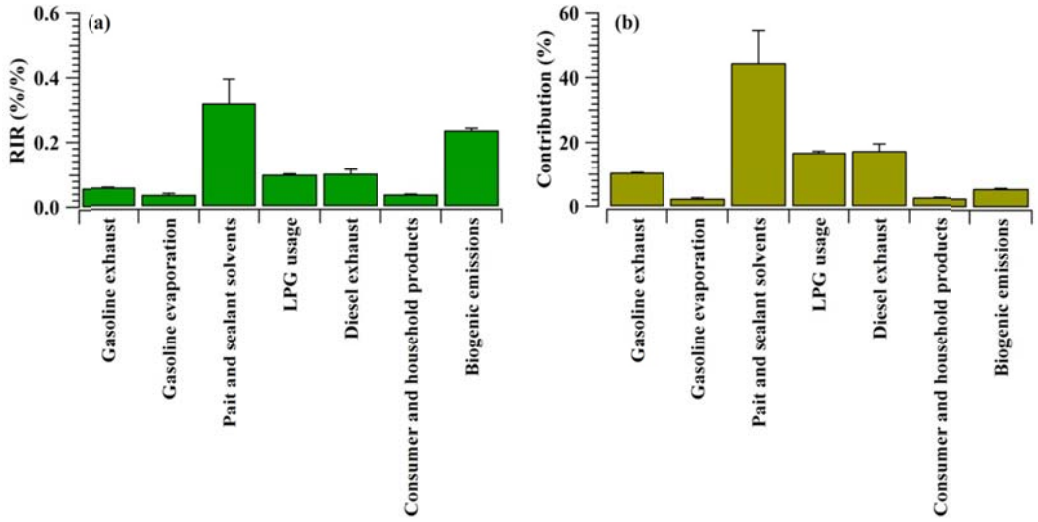

Figure 6.3 The average RIR values of VOC sources (a) and their relative contributions (b) to photochemical O_3 formation

6.4 Contribution of major VOC species in different sources to O_3 production

To further investigate the relative importance of VOC species in different sources, contributions of individual VOCs were calculated using the RIR-weighted values. Figure 6.4 shows the top 15 VOC species with high (a) RIR and (b) RIR-weighted values at TW. After taking into account the mass emissions of VOCs in each source, xylenes and ethylbenzene in paint and sealant solvents, toluene in gasoline exhaust, *n*/*i*-butane, ethene, propane and propene in LPG usage, toluene in diesel exhaust, toluene in consumer and household product and *n*-pentane in gasoline evaporation had high RIR-weighted values at TW. It is worthy to note that though the reactivity of *n*/*i*-butane and propane may not be as high as that of some aromatics, i.e., toluene and xylenes, their RIR-weighted values were relatively higher, indicating that a VOC with relatively lower reactivity could also have significant impact on O_3 production when its concentration was high. In addition, isoprene contributed significantly to local O_3 formation in Hong Kong with relatively higher RIR-weighted values, consistent with

previous studies using different methods (Cheng et al., 2010a, b). This indicated that further reduction of anthropogenic VOCs (AVOCs) may be less effective due to the significant contribution of BVOCs as most of the practical strategies for controlling O_3 pollution in Hong Kong are to effectively reduce AVOCs (HKEPD, 2012b). On the other hand, the results in this work were somewhat different from those observed in the inland PRD, where *m/p*-xylenes and toluene in solvent usage, ethene in biomass/biofuel burning and diesel vehicular emissions contributed significantly to O_3 formation. The variations may be attributed to the different industrial and energy structures between Hong Kong and the inland PRD region (HKEPD, 2012a, b). These findings further confirmed that the current policies on controlling vehicular emission and solvent usage should be prioritized to alleviate photochemical O_3 production in regional perspective and suggested that different strategies should be implemented in such two close areas (Louie et al., 2012; Zhong et al., 2013).

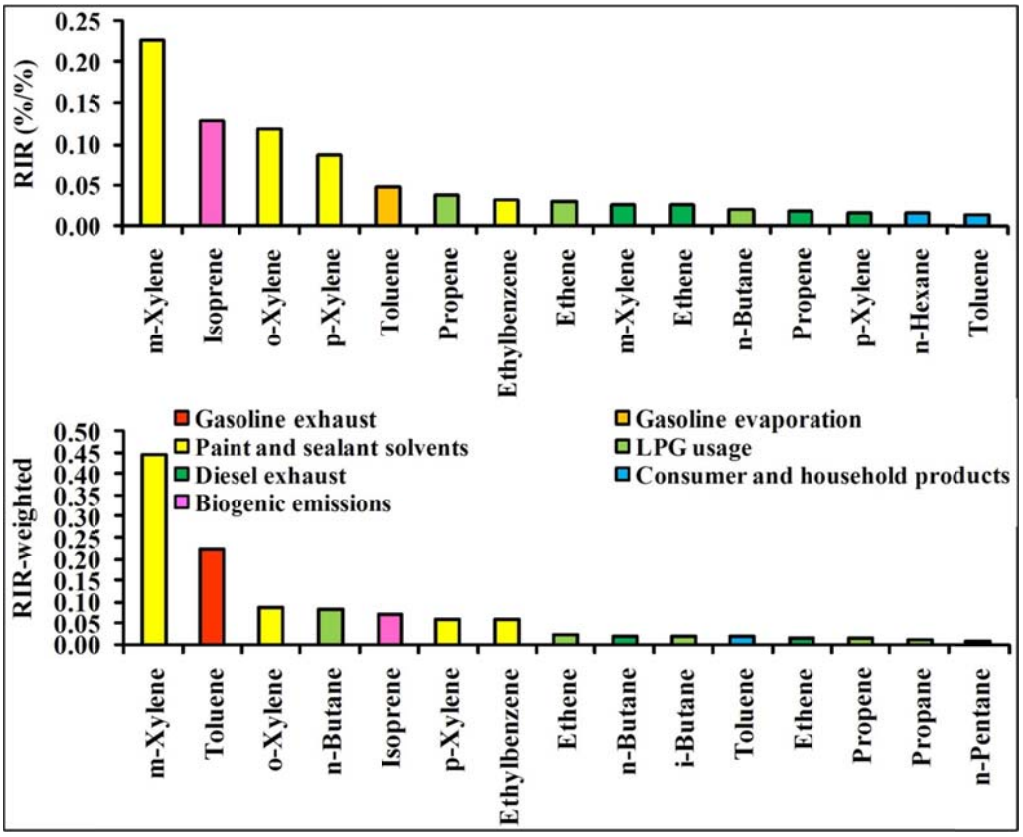

Figure 6.4 Contribution of major VOC species in different sources to the O_3 production at TW

6.5 O_3 reduction efficiency

From section 6.3, paint and sealant solvents, diesel exhaust and LPG usage were found to be the major contributors to the O_3 formation. Hence, cutting their emissions would be the most effective for the remediation of O_3 production. One question is that how much VOC source cut would have the highest O_3 reduction efficiency. Here, a new parameter, namely relative O_3 reduction efficiency (RORE), was adopted to evaluate the sensitivity of O_3 reduction under different scenarios of VOC cut. Additional simulations were run by reducing the original amounts of measured VOCs by 10%, 20%, 30%, 40%, 50%, 60%, 70%, 80% and 90%, while the other measured parameters were unchanged. The RORE was calculated as the relative difference in O_3 formation potential ($\Delta P_{O3\text{-}NO}$) between the base case with original VOCs and the above VOC reduction scenarios divided by the corresponding reduction percentage of VOCs. Figure 6.5 presents the average RORE values of each VOC source under different VOC-cut scenarios. It can be seen that paint and sealant solvents (F3) and BVOCs (F7) presented higher RORE values followed by diesel exhaust (F5) and LPG usage (F4), because of the high reactivity of the major VOCs in those sources as described in subsection 3.2. It is interesting to note that BVOC source (F7) had relatively higher RORE values (~0.20 – 0.35), implying the high reactivity of its VOC component. Indeed, as its major substituent, isoprene has rather high reactivity with OH radical. Nevertheless, the concentration of the BVOC source was relatively low. In contrast, the source of paint and sealant solvents (F3) also had higher RORE values (~0.28 – 0.44), and remarkably its concentration was higher, suggesting that the most cost-effective approach for O_3 reduction was to cut the sources with higher RORE values and higher concentrations. Further inspection found that the RORE value of each source differed under different VOC reduction scenarios, and the scenario with

the highest RORE value varied for each source, suggesting that each source had its own VOC cut percentage which would be the most efficient for O_3 reduction. For example, the RORE was the highest when 40% of VOCs in paint and sealant solvents were cut, indicating that controlling O_3 would be the most effective when the VOC emissions from paint and sealant solvents were reduced by 40%. Similarly, the highest RORE values for the other sources, i.e., gasoline exhaust, gasoline evaporation, LPG usage, diesel exhaust, consumer and household products and BVOCs were presented in the scenarios of 50%, 40%, 80%, 40%, 10% and 50%, respectively. One of the reasons why each source had its own highest RORE was probably the differences of the VOC composition and their photochemical reactivity among the sources. Different reactivity of VOC sources, caused by the different composition, would lead to different capacities for the O_3 formation (Gilman et al., 2009; Zheng et al., 2009b). Hence, the prefect cutting percentage of each VOC source would be subsequently changed. Moreover, it was well recognized that photochemical O_3 production is related to the relative concentrations of its precursors, i.e., VOCs and NO_x, with a non-linear relationship (Thornton et al., 2002; Jenkin and Clemitshaw, 2000; Sillman et al., 1999). The reduction of VOCs changed the ratios of VOCs/NO_x, resulting in variations of RORE values under different VOC-cutting scenarios. However, the above simulation results were based on the simplified carbon bond IV mechanism which does not look into the chemical reactions of each VOC species in a source. As such, further simulations by a photochemical box model coupled with more explicit mechanisms, i.e., master chemical mechanisms, are needed to better understand detailed processes and pathways of the O_3 formation under different VOC-cutting scenarios (Derwent et al., 2007a; Jenkin and Clemitshaw, 2000). It shoud be noted that the highest of RORE value in each reduction scenario in VOC emission

represented the most optimized results in the resolution of 10% extracted from the OBM model. To further investigate the cutting estimate of VOC to O_3 reduction in higher resolution, additional studies with other models with higher resolutions, i.e., Empirical Kinetic Modelling Approach (EKMA) and Air Quality model systems (AQMS), are needed.

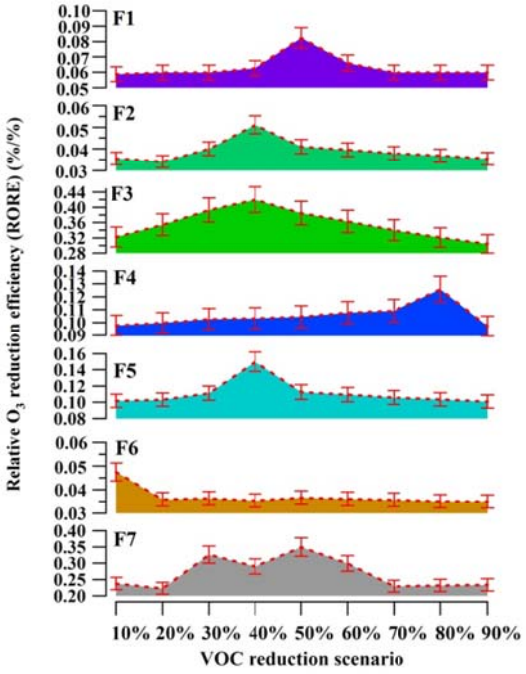

Figure 6.5 ROREs of VOC sources under different VOC-cutting scenarios (the ROREs in the Y axis were set between minimum and maximum values for different scenarios in order to present the variations clearly)

In order to further evaluate the RORE corresponding to the reduction of major VOC species in each source, additional OBM simulation was conducted with the input of 10 ~ 90% of the top 15 VOC species that had relatively higher RIR-weighted values (Figure 6.4). Table 6.2 presents the average RORE values of the top 15 VOC species under different cutting scenarios. It can be found that the cutting percentage for the highest RORE value of the specific species in the sources varied. For example, ethylbenzene, *m/o*-xylene had the highest RORE values when they were reduced by 10% in the emission of paint and sealant solvents, while the maximum RORE value of *p*-xylene in the same source was by cutting 40%. Furthermore, *n/i*-butane, propane

and propene in LPG usage, *n*-butane in diesel exhaust and toluene in consumer and household product displayed the highest RORE values in the scenario with 10% reduction, while toluene in the gasoline exhaust, *n*-pentane in gasoline evaporation and ethene in diesel exhaust showed maximum RORE value in the scenario of 30%, 30% and 50% reduction, respectively. Interestingly, the RORE values of isoprene in BVOC source (i.e. F7) were relatively higher than those of major VOC species in other sources and reached the maximum in the scenario of 50%, suggesting that reducing BVOC emissions may be more efficient in O_3 reduction in terms of single VOC species. Previous studies suggested that the measures in the newly-developed urban green areas and roadside vegetation seemed more practical by planting low isoprene emitting trees and canopy size of trees during the implementation of urban planning, when compared to forest, shrubland and grassland (Leung et al., 2010; Tsui et al., 2009).

Table 6.2 Average RORE values for the main VOC species in each source under different scenarios

Source	Species	RORE ($\times 10^{-2}$) (%/%)								
		10%	20%	30%	40%	50%	60%	70%	80%	90%
F1*	Toluene	2.83	3.25	3.83	3.68	3.66	3.64	3.68	3.62	3.67
F2	*n*-Pentane	0.10	0.48	0.57	0.30	0.45	0.33	0.32	0.39	0.40
F3	Ethylbenzene	3.41	2.77	2.28	2.71	2.81	2.65	2.77	2.42	2.71
	m-Xylene	22.66	20.59	7.85	9.28	18.22	16.55	15.82	14.35	9.01
	o-Xylene	12.14	11.47	11.33	11.01	11.07	11.41	10.63	10.82	10.59
	p-Xylene	8.68	9.32	9.29	9.77	8.96	9.13	8.92	8.74	8.67
F4	Ethene	2.89	2.93	2.97	2.97	3.18	2.78	2.90	2.64	2.85
	i-Butane	0.92	0.75	0.77	0.77	0.76	0.75	0.73	0.75	0.76
	n-Butane	2.01	1.87	1.80	1.90	1.91	1.88	1.90	1.82	1.82
	Propane	0.61	0.38	0.33	0.34	0.33	0.32	0.32	0.29	0.33
	Propene	3.83	3.60	3.49	3.24	3.51	3.47	3.33	3.29	3.23
F5	*n*-Butane	0.94	0.76	0.82	0.78	0.77	0.77	0.74	0.77	0.77
	Ethene	2.55	2.59	2.62	2.64	2.73	2.45	2.56	2.33	2.52
F6	Toluene	1.36	1.07	1.07	1.05	1.00	1.05	1.03	1.04	1.04
F7	Isoprene	12.97	12.83	12.72	16.60	19.36	16.04	18.06	12.35	13.16

*F1 ~ F7 corresponded to the identified sources in Figure 6.2

6.6 Summary

The method combining positive matrix factorization (PMF) model with observation-base model (OBM) developed in Chapter 5, was applied for the first time

to better understand the VOC sources and their contributions to O_3 formation in Hong Kong. Totally, 7 sources including gasoline exhaust, gasoline evaporation, paint and sealant solvents, LPG usage, diesel exhaust, consumer and household products and BVOCs were identified at TW. Subsequently RIR-weighted values, considering both RIRs and the concentrations of each VOC source, showed that paint and sealant solvents, diesel exhaust and LPG usage were the key contributors to O_3 formation at TW, suggesting controlling solvent- and vehicular-related emissions should be the most effective strategy to reduce photochemical O_3 formation in Hong Kong. In addition, the RIR-weighted method indicated that *m/o/p*-xylene and ethylbenzene in paint and sealant solvents, toluene in gasoline exhaust, *n/i*-butane, ethene, propene and propane in LPG usage and *n*-butane and ethene in diesel exhaust were the significant contributors to the O_3 formation at TW. Analysis on the RORE values under varied VOC cutting scenarios of the sources and the major species in these sources indicated that the cutting percentages of the VOC sources and the major species from these sources were different for the most effective O_3 reduction in Hong Kong. For instance, by cutting 40% of the dominant VOC source i.e. paint and sealant solvents, the efficiency of O_3 reduction would be the highest for this source.

Chapter 7 Atmospheric photochemical reactivity and ozone production at two sites in Hong Kong: Application of a photochemical box model with master chemical mechanism (PBM-MCM)

7.1 Introduction

It has been well recognized that high concentrations of O_3 have detrimental effects on human health, crops, and vegetation, in addition to its central roles in photochemistry and oxidizing capacity in the lower atmosphere. The abundance of O_3 in the atmosphere is determined by downward transport from the stratosphere, the dry deposition to Earth's surface and the in-situ photochemical formation through reactions involving anthropogenic emitted VOCs and NO_x in the presence of sunlight.

The mechanisms of photochemical reactions resulting in O_3 formation have been studied for decades. The OH radical, formed primarily via the photolysis of O_3, initiates the reaction sequence. The OH radical reacts with both saturated and unsaturated hydrocarbons to produce alkyl proxy radicals (RO_2) and hydroperoxyl radical (HO_2), which convert NO to NO_2 efficiently. Among these reactions, the formation of RO_2 is the rate-controlling step (Gilman, et al., 2009). Finally, NO_2 is converted back to NO by photolysis, resulting in the regeneration of O_3. The photochemical O_3 formation has a non-linear relationship with its precursors, i.e., VOC- or NO_x-sensitive chemistry, which is dependent on the relative concentrations of NO_x and VOCs (Sillman, 1999; Jenkin et al., 2000; Lu et al., 2010; Liu et al., 2012). At low [VOC]/NO_x conditions (VOC-sensitive regime), the reaction between OH and NO_2 is the dominant chain terminating reaction, competing with chain propagating reactions of OH and hydrocarbons. Therefore, reducing the concentration of

hydrocarbons by VOC emission controls would lead to a decrease in O_3 formation. On the other hand, at high [VOC]/NO_x ratios (NO_x-sensitive regime), the peroxy-peroxy reactions are the dominant chain-terminating reactions, while the oxidation of NO to NO_2 by hydroperoxy and alkyl peroxy radicals is the key propagating reactions, which forms O_3 consequently. Hence, any reduction in NO_x would decrease the photochemical O_3 formation.

Hong Kong and the rest of the PRD, one of the most urbanized and industrial regions in southern China, is experiencing severe O_3 pollution with hourly mixing ratio frequently exceeding 100 ppbv in recent years due to large emissions of its precursors (Wang et al., 2009; Zheng et al., 2010a; HKEPD, 2012b; Ling et al., 2013). Though previous studies have been conducted to investigate the O_3 pollution in this region in recent years, most of these studies only focused on the temporal and spatial variations, influence of meteorological conditions, and NO_x- and/or VOC-limited regime for the photochemical O_3 formation (Zhang J. et al., 2007; Zhang Y.H. et al., 2008; Jiang et al., 2008, 2010; Cheng et al., 2010a; Ling et al., 2011; Guo et al., 2009, 2013a). For example, Chan et al. (1998a, b) investigated the seasonal variations of O_3 in Hong Kong, reporting that the outflow of polluted continental air and the inflow of maritime air helped shape the seasonal patterns of O_3 in Hong Kong. Guo et al. (2009) investigated the variations of O_3 and its precursors at a suburban site in the inland PRD and a suburban site in Hong Kong, stating that regional transport had significant influence on the redistributions of air pollutants between inland PRD and Hong Kong based on the results of ratio analyses and Lagrangian trajectories and dispersion simulation. On the basis of the same data set, Cheng et al. (2010a) compared the meteorological conditions during O_3 and non-O_3 episode days, further confirming that higher temperature, stronger solar radiation, lower relative humidity, lower wind

speed and northerly wind could induce high O_3 levels observed in the PRD region. By using an observation-based model, Zhang et al. (2007) and Cheng et al. (2010a) reported that 50 – 100% of the observed O_3 enhancements in Hong Kong during O_3 episodes were attributed to local photochemical generation and that the O_3 formation was VOC-limited.

The photochemical reactivity of O_3, its precursors, free radicals and intermediate products, which could provide valuable insights into the formation and abatement of O_3 pollution, were poorly understood in this region. In addition, the photochemical reactivity may be different due to the variations of O_3, its precursors, meteorological conditions in different areas, and especially the topography and physical features that are complex in this region (AFCD, 2008). As such, for further policy implementation of alleviating photochemical O_3 problem in regional perspective, it is necessary to understand the photochemistry of O_3 and its precursors at different areas. In the present study, simultaneous field measurements were conducted in a rural site (Mt. Tai Mo Shan, TMS) and an urban site (Tsuen Wan, TW) in Hong Kong. An overview of the project was presented in Chapter 4, while this chapter mainly focuses on a period, when the variations of O_3 and its precursors were large at the two sites and the field measurements were intensive. The goal of this chapter is to investigate the difference of O_3 photochemistry under different relative concentrations of O_3 and its precursors at two sites. The output could provide valuable information on how to alleviate the O_3 pollution in the PRD region. We first investigate the variations of O_3 and its precursors at the two sites in a selected period, i.e., from October 27 to November 03, 2010, when large variations of O_3 were found. Then we evaluate the difference of photochemical reactivity at the two sites under the conditions of different levels of O_3 and its precursors by using a newly developed photochemical box model coupled with

Master Chemical Mechanisms (PBM-MCM) on the basis of a full suite of measurement data of different parameters, i.e., meteorological conditions, VOCs, and trace gases, i.e., SO_2, CO and NO_x. Detailed description for the development of the PBM-MCM model could be found in Lam et al. (2013). Briefly, the chemical mechanisms for the input reactants, the boundary layer conditions, abundance and the photolysis rates of particular VOCs were revised according to the actual conditions in the PRD region. It is noteworthy that this is the first study on the investigation of photochemical reactivity in subtropical Hong Kong and southern China with the application of PBM-MCM model. The target issues are: 1) what is the difference of photochemical oxidations between the two sites? And 2) what are the roles of photochemical oxidations in in-situ photochemical O_3 formation at the two sites?

7.2 Characteristics of air pollutants during the episode event

7.2.1 Overview of O_3 and its precursors

The variations of O_3 have been overviewed in Chapter 4. In general, the mixing ratios of O_3 were higher at TMS than at TW, which might be related to the combined effects of NO titration, vertical meteorological conditions, regional transport and mesoscale circulations (Chapter 4). In the chapter, the analysis focused on a selected period from October 27 to November 03, 2010, when larger variations of O_3 were found at the two sites. For instance, the average mixing ratios of O_3 were 35 ± 2 and 73 ± 3 ppbv for TW and TMS, respectively. In addition, six days, i.e., from October 29 to November 03, were classified as O_3 episode days at TMS with daytime maximum values higher than 100 ppbv (i.e. China's Grade II Standard), while the daytime maximum O_3 levels at TW were within the range of 48 ~ 66 ppbv. Apart from O_3, Table 7.1 presents the median, average and maximum mixing ratios of 55 VOCs together with CO and NO_2 at TMS and TW during the O_3 episode event. It should be

noted that most of the compounds in this table were primarily categorized by chemical class, while some species were grouped by their sources e.g. isoprene and terpenes classified as biogenic VOCs (BVOCs). In general, the mixing ratios of VOCs were higher at TW than at TMS due to the difference of sampling locations, with the mean total VOCs concentrations of 42 ± 2 (mean ±95% confidence interval) and 25 ± 1 ppbv, respectively. As mentioned previously, the TW sampling site is located in an urban environment surrounded by major roadways as well as residential and industrial blocks, while TMS is a mountain site. At TMS, oxygenated VOCs (OVOCs) dominated the total VOC composition (48 ± 2%), followed by alkanes (22 ± 1%), aromatics (12 ± 1%), alkenes (11 ± 1%), other VOCs (i.e. Cl- and Br-contained halocarbons and dimethyl sulfur (DMS)) (7 ± 0.2%) and BVOCs (1 ± 0.1%). In particular, the most abundant VOC species at TMS were methanol (4023 pptv), acetone (3707), formaldehyde (3315), ethane (2015), toluene (1729) and ethyne (1621). At TW, though OVOCs had the highest contribution to the total VOCs, its percentage was lower than that observed at TMS ($p < 0.05$), with average value of 38 ± 2%, followed by alkanes (31 ± 2%), alkenes (12 ± 1%), aromatics (12 ± 1%), other VOCs (6 ± 0.5%) and BVOCs (1 ± 0.1%). Methanol (4805 pptv), acetone (3976), *n*-butane (3834), formaldehyde (3702), propane (3027) and toluene (2187) were the most abundant VOCs measured at TW. The similar VOC composition at TMS and TW suggested comparable VOC source influences at these two sites, reflecting the possible linkage between the mountain summit and its foot. Indeed, the results in Chapter 4 have concluded that mesoscale circulations, i.e., mountain-valley breezes, could influence the redistribution of air pollutants between the two sites.

For non-methane hydrocarbons (NMHCs), though alkanes made the highest contribution, the abundance of individual species was different at the two sites. At

TMS, ethane and ethyne were the two major species of NMHCs. Such long lifetime species, together with the relatively higher percentage of OVOCs mentioned above indicated that the air masses at TMS were aged, which may be transported from the urban centers in Hong Kong and the inland PRD region under the influence of mesoscale circulations and regional transport (Chapter 4). On the other hand, the composition of NMHCs at TW was consistent with the findings of an intergrated analysis on NMHCs data collected at urban and suburban sites, i.e., Yuen Long, Central/Western and Tung Chung in Hong Kong, which reported that alkanes were the most important group for ambient NMHCs (44 – 63%) (Guo et al., 2009; HKEPD, 2010). Among alkanes, propane and butanes had relatively higher mixing ratios ($p < 0.05$) than other species, suggesting widespread use of the liquefied petroleum gas (LPG) at urban areas in Hong Kong because C_3-C_4 alkanes are mainly emitted from leakage of LPG (Guo et al., 2009, 2013b; Ho et al., 2009; Ling et al., 2013). In Hong Kong, LPG was used as fuel for 99.9% of the registered taxis and 51.1% of the public and private light bus by December 2010 (HKCSD2010). The higher emissions of propane and butanes from LPG usage could be further confirmed by comparing the levels of propane and butanes at TW in this study with those obtained in 2001 at TW. The average concentrations of major tracers of LPG, i.e., propane, *n/i*-buane at TW have increased from 4.87, 3.63 and 8.83 in 2001 (Guo et al., 2004b) to 6.39, 6.71 and 10.12 μg/m^3 in 2010, respectively. Correspondingly, the LPG consumption has increased from 230,000 tons in 2001 to 400,000 tons in 2010 in Hong Kong (HKCSD, 2010).

Table 7.1 Statistics of the observed mixing ratios, OH reaction rate coefficients for O_3 precursors at TMS and TW

Compound	TMS			TW			k_{OH}[b]
	Median[a]	Average	Maximum	Median	Average	Maximum	
Alkanes							
Ethane	1971	2015	2590	2250	2299	3446	0.25
Propane	1022	1037	2560	2598	3027	10427	1.1
n-Butane	626	672	2983	3065	3834	16121	2.4
i-Butane	473	540	3174	1887	2327	8279	2.1
n-Pentane	221	403	4507	340	408	2056	3.8
i-Pentane	319	430	2886	489	627	4942	3.6
n-Hexane	157	190	756	211	308	1457	5.2
2-methylpentane	129	157	667	194	228	2045	5.6
3-methylpentane	90	108	361	124	145	1136	5.2
n-Heptane	81	95	290	134	168	1335	6.8
n-Octane	25	29	84	42	52	751	8.1
n-Nonane	23	29	81	52	57	413	9.7
n-Decane	26	31	107	58	62	133	11
Alkenes							
Ethene	675	715	1816	1526	1715	5936	8.5
Propene	92	120	510	387	464	2555	26.3
1-Butene	27	33	122	64	72	216	31.4
i-Butene	84	221	3591	175	285	1465	51.4
trans-2-Butene	3	6	40	22	28	242	64
cis-2-Butene	4	5	26	17	22	204	56.4
1,3-Butadiene	2	4	54	39	43	157	66.6
1-pentene	13	17	97	24	34	279	31.4
Ethyne	1638	1621	2541	2557	2552	4366	0.9
Aromatics							
Benzene	614	640	1022	752	739	1195	1.2
Toluene	1428	1729	6079	2187	2830	23919	5.6
Ethylbenzene	307	439	1591	459	585	2201	7.0
m-Xylene	137	210	1058	263	372	1955	23.1
p-Xylene	91	126	513	161	223	1271	14.3
o-Xylene	91	115	452	150	204	776	13.6
3-Ethyltoluene	13	18	93	36	52	651	17
4-Ethyltoluene	8	11	51	21	27	322	18
2-Ethyltoluene	7	9	36	16	21	181	13
1,3,5-Trimethylbenzene	6	10	77	16	29	317	56.7
1,2,4-Trimethylbenzene	13	21	160	45	70	955	32.5
1,2,3-Trimethylbenzene	4	7	43	15	21	169	32.7
BVOCs and its related oxidants							
Isoprene	50	51	143	146	141	303	100
α-Pinene	6	7	84	14	19	132	52.3
β-Pinene	2	3	19	4	4	15	74.3
Limonene	8	32	329	10	21	326	164
Methacrolein (MAC)	39	48	271	61	74	319	29
Methyl vinyl ketone (MVK)	104	135	747	129	148	408	20
Oxygenated VOCs (OVOCs)							
Formaldehyde	3271	3315	8093	3241	3702	9017	9.4
Acetaldehyde	1107	1243	3921	1452	1774	9096	15
Acetone	3537	3707	8243	3555	3976	9404	0.17
Methanol	3895	4023	10184	4259	4850	16690	0.9
Ethanol	518	670	5576	1271	2809	25209	3.2
n-Hexanal	22	36	331	23	34	432	30
Other VOCs							
$CHCl_3$	72	72	121	97	99	166	0.1

CH_3CCl_3	8	9	11	9	9	28	2.5e-7
CH_2Cl_2	482	551	1410	806	1078	4396	6.1e-7
C_2HCl_3	42	55	190	46	61	263	2.2
C_2Cl_4	64	77	243	99	130	639	0.17
CH_3Cl	1008	1014	1566	1037	1055	1770	7.4e-7
CH_3Br	14	15	42	15	16	40	0.74
DMS	3	4	10	5	7	33	5.4
Non-VOCs							
CO	516	506	660	598	586	858	0.2
NO_2	7	8	29	27	27	62	8.7
CH_4	2	2	2	2	2	2	6e-3

[a] Median, average and maximum mixing ratios are presented in pptv, except CH_4 (in ppmv)
[b] OH reaction rate coefficients (in 10^{-12} cm^3 $molecule^{-1}$ s^{-1}) at 298 K and 1013 mbar

7.2.2 The OH reactivity at the two sites

In addition to the levels of O_3 precursors, the OH reactivity of these species could provide more relevant information on the formation processes of ground level O_3. By investigating the total OH reactivity, the roles of VOCs and NO_x in the balance between perpetuation and termination of O_3 formation reaction sequences could be determined (Gilman et al., 2009; Mao et al., 2010). Here, we compared the total OH reactivity for better understanding of the descrepancy of O_3 and its precursors at TMS and TW. The total OH reactivity, i.e., $R_{OH,TOTAL}$, which is the inverse of the OH lifetime, is defined as sum of the OH reactivities of all the measured reactants. It could be calculated as the sum of the reaction rate coefficients multiplied by the concentrations of all reactants with OH using the following equation (Equation 7-1):

$$\begin{aligned} R_{OH,TOTAL} &= k_{OH+CH_4}[CH_4] + k_{OH+CO}[CO] + \sum(k_{OH+VOC}[VOC]) + k_{OH+NO_2}[NO_2] \\ &= R_{OH,CH_4} + R_{OH,CO} + R_{OH,VOC} + R_{OH,NO_2} \end{aligned} \quad (7\text{-}1)$$

The reaction rate coefficients here were obtained from Sander et al. (2006), Atkinson and Arey (2003), Atkinson et al. (2006) and Master Chemical Mechanism (http://mcm.leeds.ac.uk/mcm). It should be noted that the calculation of OH reactivities in this study represented the minimum values due to the fact that it only included the identified VOCs and excluded the undetectable VOCs in the atmosphere. However, previous studies have demonstrated that these values are expected to

adequately represent the ambient OH reactivity (Di Carlo et al., 2004; Yoshino et al., 2006; Gillman et al., 2009).

In general, higher OH reactivities were found at TW as a result of larger emissions of VOCs and NO_2 in the urban environment. The average values of OH reactivity for VOCs, NO_2, CO and CH_4 at TW were 5.34 ± 0.38 (average ± 95% confidence interval), 6.08 ± 0.45, 2.91 ± 0.12, 0.29 ± 0.01 s^{-1}, which were 1.73, 3.44, 1.16 and 1.02 times those measured at TMS, respectively. Figure 7.1 presents the relative contribution of different atmospheric constituents to total OH reactivity at the two sites. At TMS, though VOCs dominated the OH reactivity, CO had a remarkable contribution, indicating that CO could react with OH effectively and lead to a significant contribution to O_3 formation, consistent with previous studies conducted in other locations where air masses were aged (Zhang et al., 2008; Gilman et al., 2009). On the other hand, NO_2 and VOCs had comparable contribution to the OH reactivity at TW, in line with earlier studies undertaken in other urban environments (Gilmant et al., 2009; Mao et al., 2010). The remarkable contributions of NO_2 and VOCs to OH reactivity at TW were due to the high emissions of these reactive compounds in the urban environments (Gilman et al., 2009; Mao et al., 2010). Figures 7.1c and d give the contribution of each VOC group to the total OH reactivity of VOCs at the two sites. Among the VOCs, OVOCs was the biggest contributor to the total OH reactivity, followed by alkenes and aromatics, suggesting the importance of OVOCs in O_3 formation (Cheng et al., 2010a). OVOCs could be both secondarily formed by the oxidation of hydrocarbons and emitted from primary sources. For further evaluation of the specific roles of primary and secondary OVOCs in the photochemistry of O_3, combinations of different models, i.e., source apportionment model and photochemical box model are needed. In addition, anlkenes and alkanes made higher

contributions at TW than that at TMS, while the contributions of BVOCs and aromatics were comparable and the contributions of other VOCs were negligible at the two sites.

In summary, in addition to the mixing ratios of O_3, the levels and reactivity of O_3 precursors were different at TMS from those at TW. The discrepancy may be the causes of different photochemical reactivity at the two sites. One question is that how these differences influenced the photochemical reactivity at the two sites. In the following section, the photochemical reactivity at the two sites, i.e., the HO_x budget, the OH chain length, the chemical O_3 budget and O_3 formation, would be explored by the PBM-MCM model.

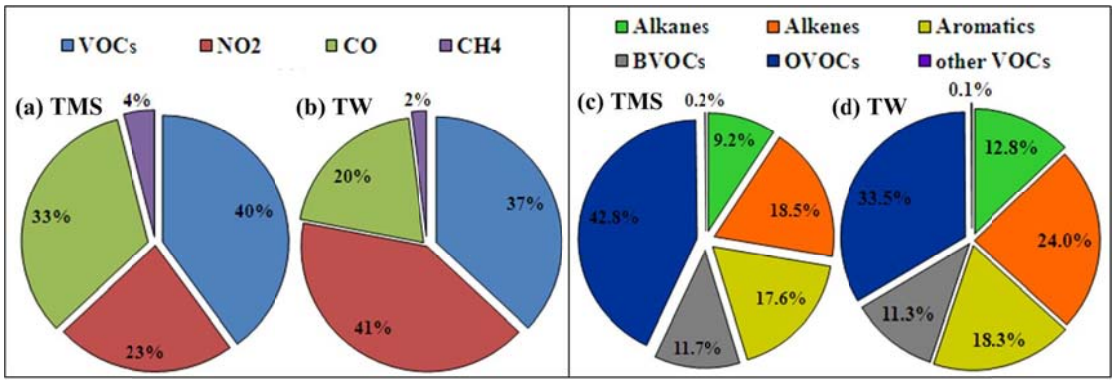

Figure 7.1 The average contribution of different groups to total OH reactivity at TMS and TW

7.3 The photochemical reactivity at the two sites

7.3.1 The HO_x budget

Figure 7.2 shows the diurnal variations of OH and HO_2 simulated by the model at the two sites. As expected, peak values of OH and HO_2 were found during the midday at the two sites, consistent with previous study conducted in the PRD region, in which maximum OH and HO_2 were observed around noon (Hofzumahaus, et al., 2009). The average HO_2 mixing ratio (17.7 ± 2.7 pptv) was slightly higher (p = 0.05) at TMS than that at TW (14.2 ± 2.3 pptv) during daytime hours (07:00 – 19:00, LT), whereas the average OH value at TW (0.14 ± 0.02 pptv) was higher ($p < 0.05$), about

1.7 times those at TMS (0.09 ± 0.01 pptv), suggesting that the cycling between OH and HO_2 was different at the two sites. Note that the calculated OH mixing ratios in here were slightly different from those in Chapter 4, because the mixing ratios in chapter were the average values for the period from October 27 to November 03, while the results in Chapter 4 were the average mixing ratios for the total 20 non-O_3 and O_3 episode days during the sampling campaign at the two sites. The relatively higher OH at TW was primarily attributed to the high levels of NO at this urban site, which shifted the balance of HO_x toward OH by the propagation of HO_2 and RO_2 with NO (Mao et al., 2010). Since the levels of NMHCs were higher at TW, in theory, more RO_2 should be produced accordingly via the reaction of NMHCs and OH. However, lower RO_2 mixing ratios were found at that site by model simulation (TW: 9.6 ± 1.3 pptv, TMS: 16.3 ± 2.4 pptv, $p < 0.01$). This was likely due to the fact that there was higher NO levels at TW and NO can react with RO_2 to form RO, resulting in more RO_2 was consumed at TW. On the other hand, the formed RO radical could further react with O_2 to form HO_2, which finally turned to OH by the reaction with NO. This further confirmed that the higher levels of NO shifted the balance of HO_x to OH at TW.

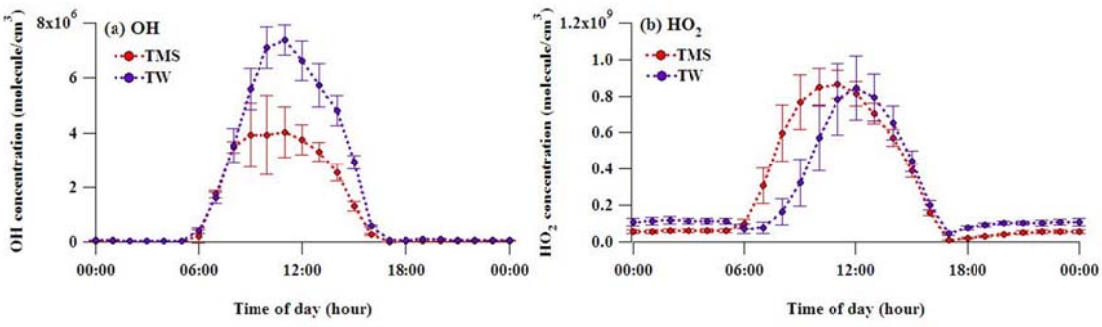

Figure 7.2 Diurnal variations of (a) OH and (b) HO_2 at TMS and TW

To further characterize the photochemical reactivity of HO_x, it is of interest to investigate the pathway of HO_x sources and sinks at the two sites. The sources of HO_x in this study included the photolysis of O_3 ($O(^1D) + H_2O$), HONO, HCHO and other

OVOCs, peroxides and the ozonolysis of alkenes, while the HO_x sinks were radical-radical reactions, i.e., $HO_2 + HO_2 \rightarrow HOOH + O_2$, $HO_2 + RO_2 \rightarrow ROOH + O_2$ and $HO_2 + OH \rightarrow H_2O + O_2$, and the reactions between OH and NO_2, i.e., $OH + NO_2 + M \rightarrow HNO_3 + M$. These reactions have been extensively studied (Mao et al., 2010; Jenkin et al., 2000). Figure 7.3 illustrates the average diurnal variations for different pathways of HO_x sources and sinks at TMS and TW. Due to the fact that the photolysis of peroxides, i.e., H_2O_2 and CH_3OOH was much less significant compared to the reaction shown in the figure, it was excluded in the present study (Sommariva et al., 2004; Jackson and Hewitt, 1999). It can be seen that the contributions of pathways to the sources and sinks of HO_x were different at TMS and TW. This is not surprising because of the difference in atmospheric constituents. During daytime hours, the photolysis of O_3 (with the average contribution of 58%) dominated the HO_x production at TMS, where the O_3 levels were higher, similar to the results obtained in other rural areas (Jenkin et al., 2000; Ren et al., 2008; Kim et al., 2013). At TW, the major contributors to free radicals were the photolysis of O_3 and HCHO, with the average contributions of 35% and 40% to the total HO_x production, respectively, suggesting that the photolysis of HCHO was an important source of HO_x production, consistent with other studies in urban and suburban environments (Liu et al., 2012; Volkamer et al., 2010). This is different from the results obtained by Jenkin et al. (2000) and Mao et al. (2010), who claimed that the photolysis of HCHO dominated the HO_x production at the urban sites in Europe and Mexico City, respectively. The discrepancy was dependent on the differences in O_3 and HCHO levels in Europe cities and the Mexico City (Jenkin et al., 2000; Shirley et al., 2006; Lei et al., 2009). For instance, the average levels of HCHO were much higher in European cities (~ 10 ppbv) and Mexico City (~ 7.4 ppbv), compared to that observed at TW (~ 4.1 ppbv).

It is also noteworthy that the photolysis of HONO acted as another very important source to HO_x production (with the contribution of 17%), especially in the morning rush hour at TW, while its contribution was negligible at TMS. The higher contribution of HONO at TW might be owing to the higher levels of NO during morning rush hours, resulting in higher levels of HONO through reaction of OH and NO (Kurtenbach, et al., 2001). Indeed, measurement data indicated that diurnal variation of HONO at the urban sites in Hong Kong presented a peak during morning rush hours (Prof. T. Wang's group, personal communication, 2013). Similar results were also found in some recent urban and suburban studies, in which about 20 – 35% of HO_x were produced from the photolysis of HONO in urban areas in Berlin, Houston and Mexico City (Alicke et al., 2003; Dusanter et al., 2009; Ren et al., 2013). In addition, though the reactions between O_3 and alkenes could produce OH, their contributions were only significant during nighttime hours when HO_x production from photolytic processes was negligible.

On the other hand, the radical-radical reactions, i.e., $HO_2 + HO_2$ and $HO_2 + RO_2$, were the major contributors to the HO_x sinks at TMS, while the reaction of $OH + NO_2$ was less significant. However, the relative importance of different pathways to HO_x sinks was different at TW due to the discrepancy of ambient conditions (Jenkin et al., 2000). For example, $OH + NO_2$ dominated HO_x sinks in the morning rush hours when the NO_x levels were high (Chapter 4), while the radical-radical reactions, i.e., $HO_2 + HO_2$ and $HO_2 + RO_2$ dominated the HO_x sinks with similar rates to those at TMS at noon (~ 5×10^6 molecule cm^{-3} s^{-1}). The results are consistent with the observations in other urban locations with similar NO_x concentrations, i.e., New York City, Houston and Mexico City (Mao et al., 2010; Shirley et al., 2006).

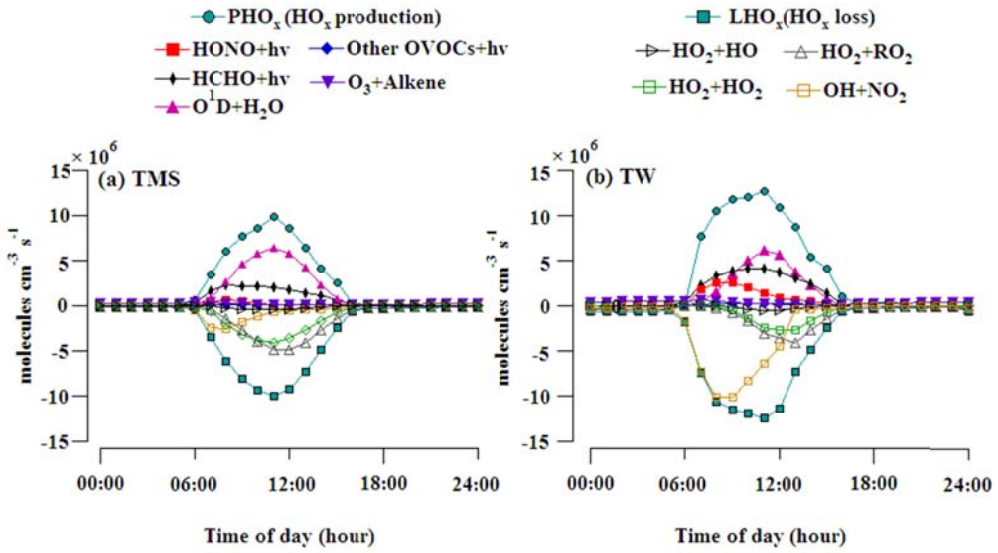

Figure 7.3 The average diurnal profiles of HO_x sources and sinks at (a) TMS and (b) TW

7.3.2 Calculated O_3 production

During daytime hours, the O_3 production rate can be determined by the conversion of NO to NO_2 by HO_2 and RO_2 and the subsequent photolysis of NO_2 as these reactions do not consume O_3. As such, the O_3 production rate can be expressed as follows (Equation 7-2):

$$P(O_3) = k_{HO_2+NO}[HO_2][NO] + \sum k_{RO_{2i}+NO}[RO_{2i}][NO] \quad (7\text{-}2)$$

On the other hand, in addition to its production, O_3 can be consumed through different mechanisms at daytime hours, i.e., the reactions with HO_2, OH and unsaturated VOCs, the O_3 photolysis and reactions that consume NO_x as described in Ren et al. (2013), i.e., the reactions between OH and NO_2 and the formation of $RONO_2$. Thus, the ozone destruction rate can be described as the following equation (Equation 7-3):

$$D(O_3) = k_{HO_2+O_3}[HO_2][O_3] + k_{OH+O_3}[OH][O_3] + k_{o(^1D)+H_2O}[O(^1D)][H_2O] + \sum k_{O_3+alkenes}[alkenes][O_3] + k_{OH+NO_2}[OH][NO_2] + P(RONO_2) \quad (7\text{-}3)$$

the k terms in the above two equations mean the reaction rate coefficients of the corresponding reactions. The difference between the O_3 production rate and the O_3

destruction rate represents the net instantaneous O_3 production rate. Figure 7.4 depicts the modeled average diurnal variations of O_3 production, destruction and net O_3 production rates at TMS and TW. It was found that the O_3 production was significantly greater than the O_3 destruction during daytime hours with peak values at around noon, indicating the net O_3 production from in-situ photochemistry at the two sites. At TMS, the daytime (07:00 – 19:00 LT) average net O_3 production rate was estimated to be 2.9 ppbv h^{-1}, corresponding to ~ 36 ppbv O_3 formed from the in-situ photochemistry. The amount is coincident with the average increment of O_3 observed from early morning to late afternoon at TMS (~ 40 ppb), suggesting that in-situ photochemical formation significantly contributed to the O_3 increment at TMS, in addition to other factors such as mesoscale circulations and regional transport that shaped the diurnal variations of O_3 (Chapter 4). On the other hand, the daytime average net O_3 production rate at TW was higher, with a value of 8.1 ppb h^{-1}, indicating that 97 ppb of O_3 could be formed from in-situ photochemistry, which was much higher than the observed O_3 increment (~ 52 ppb). The lower observed O_3 levels were likely caused by the impact of the in-situ emissions of NO_x from nearby emission sources, i.e., vehicular emissions, which titrated part of the O_3 at this urban site (HKTD, 2011; Lam et al., 2013). This effect can not be determined in the model because the model results only represented averaged boundary layer values in a well mixed box (Lam et al., 2013). Analysis of the individual reaction pathways for O_3 production rates found that the reactions between HO_2 and NO dominated the convection from NO to NO_2 at the both sites, with the average daytime contribution of 68% and 67% at TMS and TW, respectively, while the reactions of RO_2 + NO composed the remainder, about 37% and 33% to the O_3 production at TMS and TW, respectively. It shoul be noted that the reaction rates among HO_2, RO_2 and NO were

much higher at TW ($p < 0.05$), with the average value of 4.8×10^7 and 2.4×10^7 molecule cm^{-3} s^{-1}, respectively, 2.6 and 2.5 times those calculated at TMS during daytime hours. Among all the RO_2 + NO reactions, CH_3O_2 + NO had the highest O_3 production rate, with a considerable contribution of 8% and 9% at TMS and TW, respectively. In contrast, the reaction of OH + NO_2 was the major mechanism for O_3 destruction at TW, with an average contribution of 41%, while the other reactions composed the remainder. On the other hand, O_3 photolysis and the reaction of O_3 + HO_2 were the two major mechanisms for O_3 destruction at TMS, with average contributions of 28% and 34%, respectively, followed by ozonolysis of alkenes (17%), the reactions of OH + NO_2 (16%) and O_3 + OH (5%).

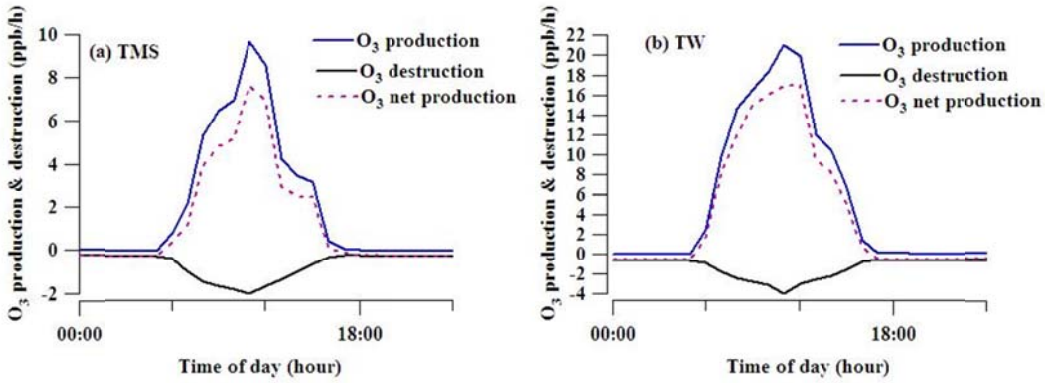

Figure 7.4 The average diurnal profiles of O_3 production, destruction and net production at (a) TMS and (b) TW

7.3.3 The relationship between O_3 production efficiency and OH chain length

The O_3 production efficiency is closely related to the OH chain length as it is an indicator of HO_x cycling. The OH chain length, defined as the ratio of OH cycling to OH terminal loss, can be calculated using the following equation (Equation 7-4):

$$\text{OH Chain Length} = \frac{k_{OH} \times [OH] - k_{OH+NO_2+M}[OH] \times [NO_2]}{k_{OH+NO_2+M}[OH] \times [NO_2]} \quad (7\text{-}4)$$

where OH reactivity k_{OH} is calculated in section 7.2.1, while mixing ratio of OH, i.e., [OH] and the terminal loss of OH by the reaction with NO_2 are from the simulation of

PBM-MCM model. The longer chain length means that more OH can be regenerated from free radical propagation cycles, and subsequently that more O_3 can be produced before termination occurs (Jenkin et al., 2000; Mao et al., 2010). Figure 7.5 presents the average diurnal variation of OH chain length at TMS and TW. The OH chain lengths started to increase in the morning and reached its maximum value at noon, consistent with previous studies, in which minimum and maximum values were observed in the morning and at noon, respectively (Martinez et al., 2003; Emmerson et al., 2007; Mao et al., 2010). The results indicated that the O_3 formation efficiency through the free radical propagation cycles was the highest at noon. The OH chain lengths at TW were between 2 and 25, similar to the results observed at Houston (6 – 28), but higher than those (3 – 12) at other US urban cities (Mao et al., 2010). In contrast, the OH chain lengths at TMS were much higher, with a range of 4 ~ 65. This might be caused by the relatively smaller sinks of OH + NO_2 due to the lower concentrations of NO_x. Nonetheless, the longer chain length at TMS suggested that the O_3 production at TMS was more efficient than at TW though the concentrations of precursors, OH and the O_3 production rate were lower.

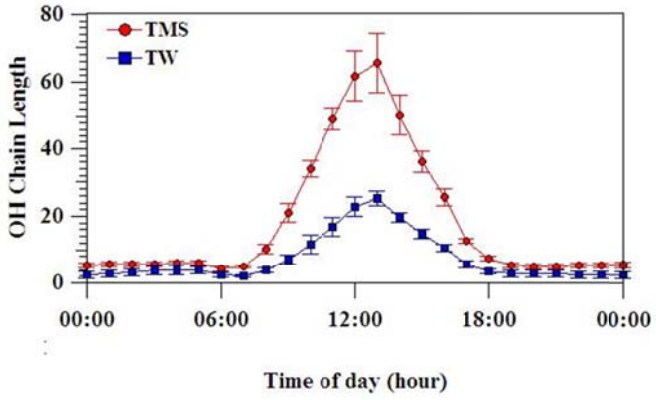

Figure 7.5 The average diurnal variations of OH chain length at TMS and TW

7.4 Summary

Both similarities and differences of photochemical reactivity at a rural site and an

urban site in Hong Kong were analyzed during an O_3 episode event from October to November in 2010. Much higher O_3 values were observed at TMS, while the levels of O_3 precursors, i.e., VOCs and NO_x were higher at TW. In addition, the compositions of VOCs indicated the influence of aged air masses and secondary formation at TMS and the wide spread of LPG usage at TW. VOCs and CO were two major contributors to OH reactivity at TMS, while NO_2 and VOCs had comparable contribution to the OH reactivity at TW. Overall, the mixing ratios of O_3 and its precursors, together with the magnitudes of OH reactivity of O_3 precursors suggested significant difference of photochemical reactivity at the two sites. Furthermore, a PBM-MCM model was applied to and constrained by a full suite of measurement data to probe the photochemical reactivity at the two sites, including HO_x budget, calculated O_3 production, OH chain length and O_3 sensitivity. Slightly higher HO_2 concentrations were found at TMS, while much higher OH concentrations were estimated at TW, suggesting that the HO_x cycling processes were different at the two sites, perhaps caused by the differences of precursors. The O_3 formation was dominated by the reaction of HO_2 + NO at the two sites. On the other hand, O_3 was mainly destroyed by the reactions of OH + NO_2 at TW and by the O_3 photolysis and the reaction of O_3 + HO_2 at TMS. Furthermore, the OH chain length was used to investigate the O_3 production efficiency to the OH generation at the two sites. Longer OH chain length was found at TMS, indicating that more O_3 could be produced for each radical that was generated at that site. On the other hand, the model revealed that intermediate oxidants played important roles on the propagation and initiations of photochemical reactions. However, these intermediate oxidants, i.e., HONO, H_2O_2 and PAN were not measured in this study. It is suggested that measurement of measurements of these intermediate oxidants should be conducted in the future studies for improvement of

the photochemical models and more thorough investigation of the mechanisms of photochemical reactions in Hong Kong.

Chapter 8 Establishing a conceptual model for photochemical ozone pollution in subtropical Hong Kong

8.1 Introduction

In most urban areas, ambient concentrations of photochemically formed O_3 are related to its precursors, while favorable meteorological conditions are required for the occurrence of high O_3 concentrations (Ding et al., 2004; Seinfeld and Pandis, 2006; Guo et al., 2009; Zheng et al., 2010a). In Hong Kong, high O_3 concentrations or "O_3 episodes" are commonly observed in late summer and autumn, and are closely associated with local photochemical production and long-range transport (Guo et al., 2009; Wang et al., 2009).

In order to understand the factors that influence photochemical O_3 formation, conceptual models of O_3 air pollution have been developed in recent years for different regions. A conceptual model is a qualitative explanation of the formation and accumulation of O_3 in a given area based on the chemical characteristics of the ambient atmosphere, as well as the physical transport and removal process observed in given locations (Tom et al., 2006; Pun et al., 1998). Pun et al. (1998) developed a conceptual model to investigate the O_3 formation in San Joaquin Valley in the USA and found that the high O_3 concentrations observed resulted from both the transport of O_3 and precursors from upwind locations, and the local production of O_3 in urban areas within the valley. Tom et al. (2006) developed a conceptual description of the nature of the O_3 air quality problem in the O_3 transport region (OTR), including Connecticut, Delaware, the District of Columbia, Maine, Maryland, Massachusetts, New Hampshire, New Jersey, New York, Pennsylvania, Rhode Island, Vermont and north Virginia in USA and concluded that a severe O_3 episode in the OTR can contain elements of long range air pollution transport from outside the OTR, regional scale

transport within the OTR from channeled flows in nocturnal low level jets, and local transport along coastal shores due to bay, lake, and sea breezes.

To formulate and implement effective control strategies for O_3 pollution, the major objective of this chapter is to develop a conceptual model for the first time for the formation, transport and accumulation of O_3 in subtropical Hong Kong by integrated data analysis at Tung Chung (TC) between 2005 and 2010. We chose the TC site because only at this site the most comprehensive dataset including real-time O_3, CO, NO_x, SO_2, VOCs and meteorological parameters has been systematically collected so far. In addition to the influence of local emission sources, the sampling site is also affected by polluted continental air masses from the highly industrialized PRD region of mainland China (Guo et al., 2009; Zhang et al., 2007). Thus, this site is capable of monitoring air pollutants transported from the inland PRD region and is suitable for assessing their impact on local air quality. A variety of aspects, including meteorological conditions, source apportionments of O_3 precursors, O_3-precursors relationships, and the characteristics of air masses in Hong Kong are evaluated. The conceptual model in this study tries to answer the following questions: 1) what meteorological conditions are favorable to photochemical O_3 formation? 2) does regional transport have an important influence on high O_3 levels? 3) Is the O_3 formation limited by VOCs, or NO_x, or both, and therefore what are the main sources of them and which ones should be the most prioritized to be controlled?

8.2 Procedures for developing a conceptual ozone model

Figure 8.1 illustrates three steps for developing a conceptual ozone model. The first step is to generalize the meteorological conditions, air mass transport characteristics, and precursor levels on O_3 episode days by analyzing the measurement data: first, we identified the O_3 episodes, especially multi-day O_3

episodes from 2005 to 2010; second, we analyzed and compared the meteorological conditions on O_3 and non-O_3 episode days; third, we investigated the characteristics of air masses on O_3 and non-O_3 episode days; fourth, we analyzed the source contributions of VOCs and investigated the O_3-precursors relationships. Based on the generalized requirements for an O_3 episode day in step 1, we proposed a conceptual model for O_3 pollution which considers atmospheric chemical and physical processes, emission sources of O_3 precursors and meteorological parameters during O_3 episode events (step 2). Once the conceptual model is established, O_3 episode events will be forecast by looking into the meteorological conditions, air mass transport and abundance and sources of precursors (step 3). The proposed conceptual model will be evaluated by case studies.

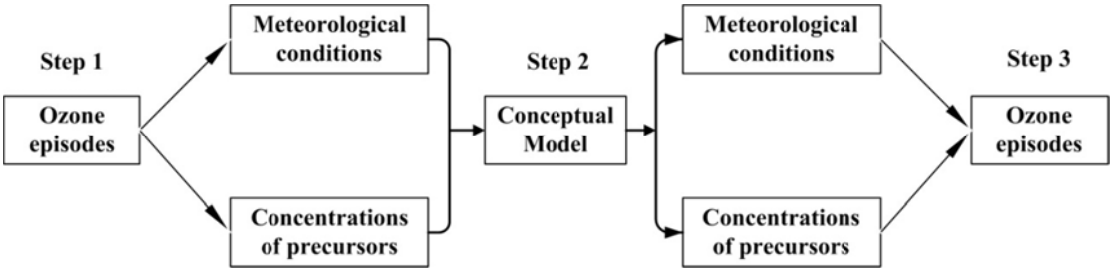

Figure 8.1 Procedure for developing the O_3 conceptual model in Hong Kong

8.3 Conceptual model development for the O_3 pollution

8.3.1 What meteorological conditions are favorable to photochemical O_3 formation?

8.3.1.1 General characteristics of meteorological conditions conducive to O_3 formation

In this study, an O_3 episode day was defined when the highest hourly O_3 concentration of a given day exceeded 200 μg/m^3 (~102 ppbv) based on the Ambient Air Quality Standard in China (China's Grade II standard, http://english.mep.gov.cn/standards_reports/standards/). In addition, a multi-day O_3

episode referred to a period of at least 3 consecutive O_3 episode days. Table 8.1 identifies multi-day O_3 episodes and selected non-O_3 episodes at TC from 2005 to 2010. A total of 10 multi-day O_3 episodes were observed from 2005 – 2010 at TC. The non-O_3 episodes were selected as the days with the hourly maximum O_3 concentration lower than 102 ppbv in the same month as that for multi-O_3 episodes. To provide the representative characteristics of non-O_3 episode days, investigate the influence of different factors and improve the statistical significance, non-O_3 episode days were selected as many as possible for comparison.

Table 8.1 Ozone episode and non-ozone episode days in 2005-2010

Ozone episode	**Period**	**Non- ozone episode[1)]**	**Period[2)]**
2005 episode 1	18/19/20 Jul 2005	2005 non-episode 1	Jul 2005
2005 episode 2	2/3/4 Oct 2005	2005 non-episode 2	1~15 Oct 2005
2006 episode 1	3/4/5 Nov 2006	2006 non-episode 1	1~15 Nov 2006
2007 episode 1	15~21 Sep 2007	2007 non-episode 1	Sep 2007
2007 episode 2	5/6/7 Oct 2007	2007 non-episode 2	Oct 2007
2007 episode 3	24/25/26 Oct 2007		
2008 episode 1	10~16 Sep 2008	2008 non-episode 1	Sep 2008
2009 episode 1	6~9 Oct 2009	2009 non-episode 1	Oct 2009
2009 episode 2	22~24 Oct 2009		
2010 episode 1	28~ 31 Aug 2010	2010 non-episode 1	Aug 2010

1) Days with low ozone concentration (<200 μg/m^3), used for comparison with ozone episode day (>200 μg/m^3)
2) Ozone episode days excluded if applicable

Table 8.2 shows statistical descriptions of air pollutants together with meteorological parameters for O_3 and non-O_3 episode days. Figure 8.2 illustrates the mean diurnal variations of O_3 and meteorological parameters, including solar radiation, temperature, relative humidity, wind speed, and wind direction at TC on O_3 and non-O_3 episode days from 2005 to 2010. Much higher concentrations ($p < 0.01$) of O_3 and some primary pollutants, i.e. SO_2 and CO, were observed on the O_3 episode days. However, NO level was comparable on both O_3 episode and non-O_3 episode days ($p > 0.05$), while higher NO_2 ($p < 0.01$) was observed on O_3 episode days. In

addition, temperature and solar radiation were higher on the O_3 episode days than non-O_3 episode days ($p < 0.01$), while the relative humidity and wind speed were lower ($p < 0.01$), indicating that meteorological parameters had significant impact on O_3 levels. Indeed, inspection of all the 10 multi-day O_3 episodes found that high O_3 levels were closely associated with high temperature (> 28 ^oC at daytime), strong solar radiation (> 700 W/m^2 at daytime), low wind speed (< 2 m/s at daytime) and relative humidity (< 70% at daytime).

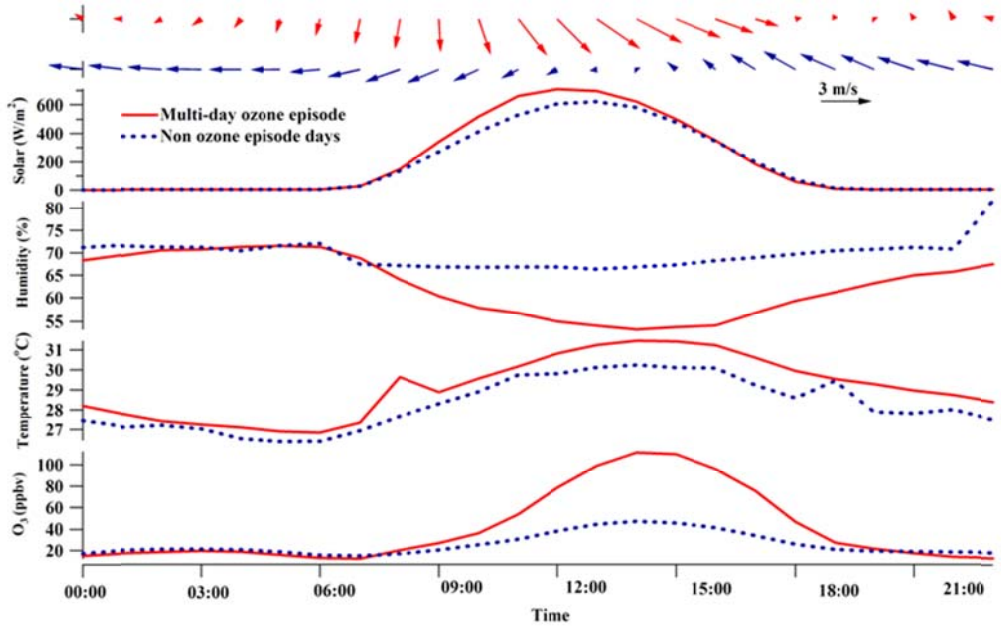

Figure 8.2 Mean diurnal variations of wind speed and wind direction, solar radiation, relative humidity, temperature and O_3 on the O_3 and non-O_3 episode days

Table 8.2 Statistical description of air pollutants and meteorological parameters during the O_3 episode events and the selected non-O_3 episode days* (Mean ± 95% confidence interval)

	O_3 (ppbv)	NO (ppbv)	SO_2 (ppbv)	CO (ppbv)	Temperature (^oC)[a]	NO_2 (ppbv)	Wind speed (m/s)[a]	Solar radiation (W/m^2)[a]	Humidity (%)[a]
O_3 episodes	40.4 ± 2.4	11.5 ± 0.9	13.6 ± 0.7	793.1 ± 0.1	34.1 ± 2.6	37.9 ± 1.1	3.7 ± 0.2	764 ± 32	77.1 ± 1.9
Non-O_3 episodes	25.6 ± 0.6	12.5 ± 0.6	7.7 ± 0.4	570.1 ± 5.6	31.2 ± 1.1	21.5 ± 0.4	4.7 ± 0.2	705 ± 29	81.1 ± 1.1

[a] Daily average maximum value
*The selected non-O_3 episode days were presented in Table 1

On a regional scale, a high pressure system over China may transport polluted continental air masses to Hong Kong, resulting in high O_3 concentrations. Guo et al. (2009) investigated the relationship between meteorological conditions and O_3

concentrations from October to December 2007. It was found that when there was an intensive high-pressure system over northern China, Hong Kong was in the front of the high pressure ridge. Due to the influence of the high-pressure system, the prevailing synoptic winds in Hong Kong were from the northeast, which might lead to high O_3 levels. Indeed, on 24 − 26 October, an O_3 episode event was found at TC. Furthermore, the diurnal patterns on the O_3 episode days observed in 2005 − 2010 (Figure 8.2) showed a clear diurnal shift in wind speed and direction at TC − southeasterly/northeasterly at lower speeds at night and northerly/northwesterly at higher speeds during daytime when the O_3 levels were usually high, confirming that synoptic winds were associated with high O_3 concentrations. Previous studies demonstrated that the prevailing north and northeast winds brought VOC-laden air and O_3 from inland PRD region to Hong Kong (Guo et al., 2009; Wang et al., 2009).

8.3.1.2 Impact of tropical cyclones

Figure 8.3 presents the mean sea level pressure and wind field for O_3 and non-O_3 episodes in Hong Kong between 2005 and 2009. Figure 8.4 shows the typical synoptic charts on the nine O_3 episode days. It is remarkable that the nine severe O_3 episode days from 2005 to 2009 were all influenced by tropical cyclones over the East and South China Sea. The tropical cyclones were also found to be most conducive to the occurrence of high O_3 episodes from 1994 to 2003 (Lee et al, 2002; Huang et al., 2005). When a tropical cyclone was formed and its center was over the East and the South China Sea, it intensified the inflow in the lower atmospheric layer and the outflow in the upper atmosphere, which caused stagnation and subsidence air over Hong Kong, forming an inversion layer. Such an inversion layer is not favorable to the dispersion of air pollutants. Nevertheless, it should be noted that though all tropical cyclones over the East and the South China Sea caused high O_3 levels, it does

not mean that all the O_3 episode days in Hong Kong were induced by tropical cyclones. Under stable meteorological conditions which include high temperature, strong solar radiation, and calm winds, high O_3 levels could also be observed. Huang et al. (2005) counted that about 62% of O_3 episodes from 1999 to 2003 resulted from cyclonic weather patterns.

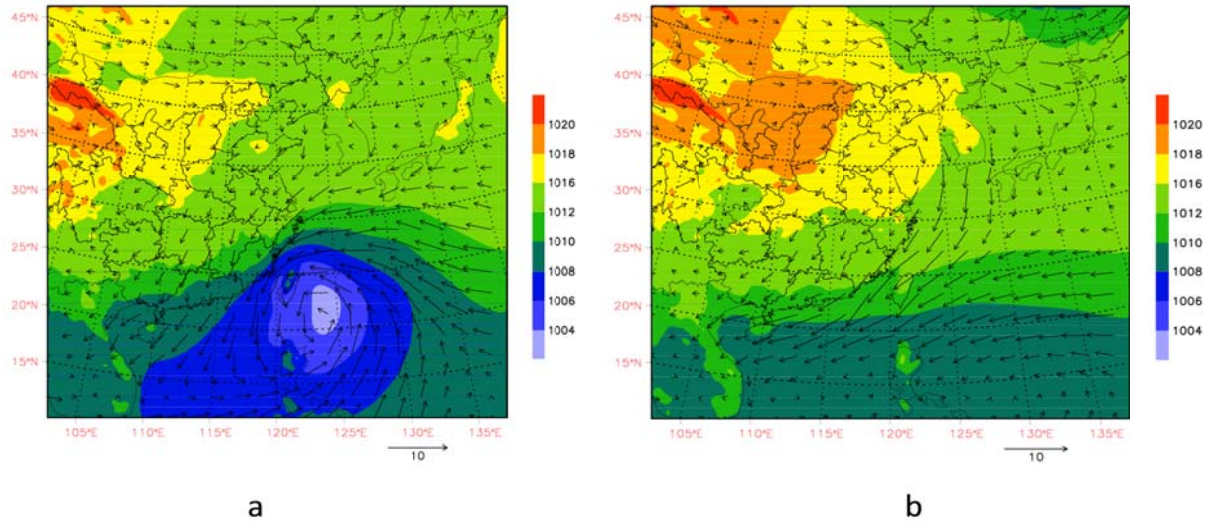

Figure 8.3 Mean weather conditions for multi-day ozone episodes (a), and non-ozone episodes (b) (shaded: sea level pressure, hpa; vector: wind, m/s; meteorological data was output from WRF simulation in three-hour intervals)

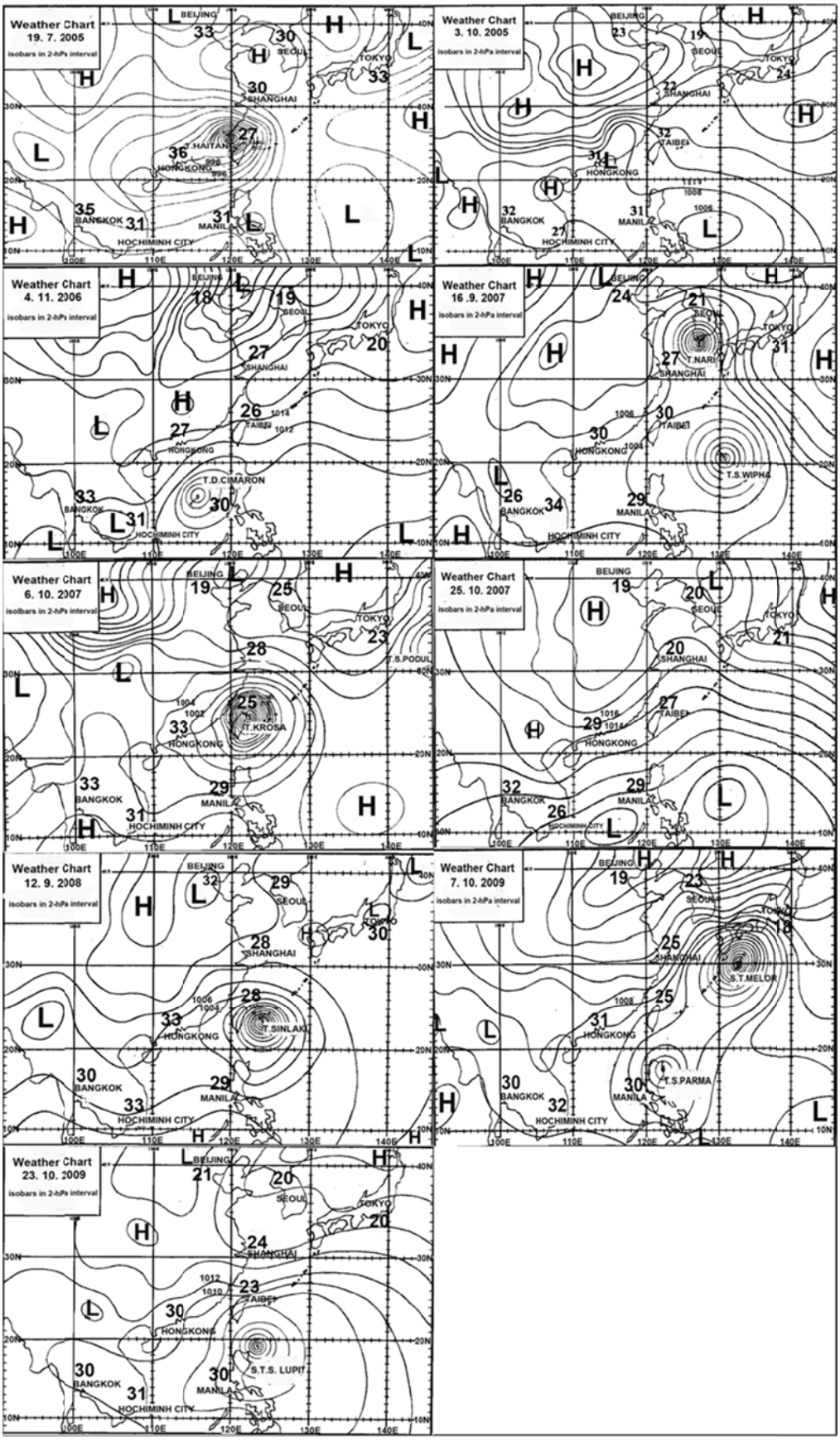

Figure 8.4 Synoptic charts for the nine O_3 episode events (Source: http://envf.ust.hk/dataview/hko_wc/current/)

8.3.2 Does regional transport have an important influence on high O_3 levels?

Analysis of synoptic wind patterns above suggested the influence of regional transport of air pollutants at TC. In order to determine whether the air masses originated from local, regional and super-regional sources, 24-h backward trajectories were developed using the NOAA-HYSPLIT 4.9 model with the Global Data Assimilation System (GDAS) meteorological data for 3-h intervals at the ending point of 200 m above sea level. These air masses were classified into local, regional (from PRD region), oceanic and super-regional air masses according to their source origins (i.e. longitude and latitude). In addition, cluster analysis was applied to segregate the calculated trajectories into a number of groups for each month from 2005 to 2010 using the hierarchical Ward's method with a square Euclidean measure (Ward 1963). In total, 55 cluster groups were obtained. Based on their pathways, air masses arriving at TC were classified into four categories for each month from 2005 – 2010. In order to characterize the four types of air masses, two cases are presented here. Taking September 2005 and June 2010 as examples (Figure 8.5), in September 2005, four categories were described: i) air masses originating from inland China, passing over Guangdong province and finally arrived at TC (track 1); ii) air masses originating in the Hong Kong area (track 2); iii) air mass originating in the South China Sea (track 3) with fast movement; and iv) air masses originating from the eastern China coast, passing over the coast of eastern Guangdong with very slow movement (track 4). Hence, tracks 1 and 4 were identified as super-regional transport; track 2 was identified as local transport while track 3 originated from the South China Sea. In June 2010, four categories were obtained as well: i) air masses originating from eastern China coast, passing over the coast of eastern Guangdong with very slow movement (track 1); ii) air masses originating from the PRD region (track 2) with

slow movement; iii) air mass originating from South China Sea (tracks 3 and 4) with fast movement. Track 1 was identified as super-regional transport, while track 2 was classified as regional transport. The trajectory results confirmed that the air masses were of different origins during different periods.

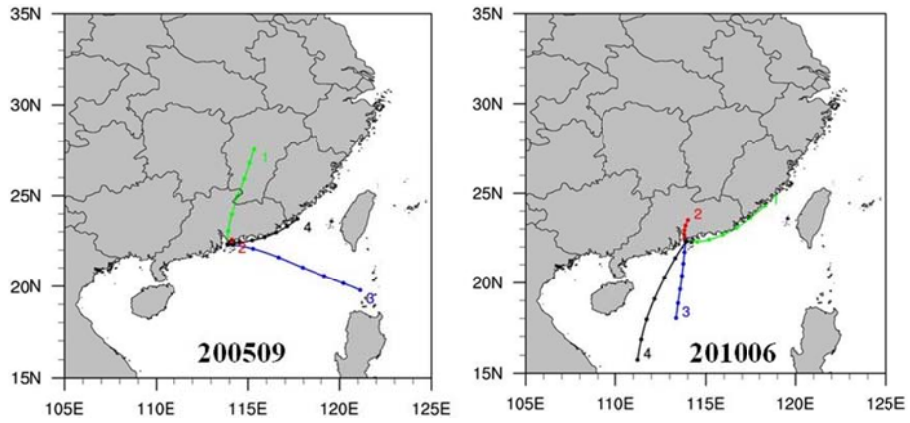

Figure 8.5 Backward trajectories for September 2005 and June 2010

Table 8.3 presents the average values of different pollutants of the four types of air masses from 2005 to 2010. SO_2, NO and TVOCs showed higher concentrations in the local and regional air masses, and lower concentrations in the oceanic air masses, most likely due to the dilution of cleaner air from the ocean. However, O_3 had the highest concentration in the super-regional air masses, followed by regional, oceanic and local air masses. The relatively higher O_3 levels in super-regional and regional air masses indicated that long-range transport contributed significantly to the increase of background O_3 levels in Hong Kong. Indeed, Wang et al. (2009) found that long-range transport made a significant contribution to the increase in "total ozone" in urban Hong Kong, and about 81% of the O_3 increase in Hong Kong was due to the O_3 increase in the background air. On the other hand, the lower O_3 level ($p < 0.01$) in the local air masses was due to the titration of NO at TC. To better understand the NO titration for local air masses, the "total ozone" O_x (i.e. O_3 + NO_2) was further examined. The mean concentration of O_x was 49.5 ± 2.4 ppbv (mean ± 95% confidence interval) for local air masses, while it was 44.5 ± 0.5 ppbv and 54.7 ± 0.5

ppbv for regional and super-regional air masses, respectively. This confirmed that lower O_3 concentration in local air masses was attributed to high emissions of NO in urban Hong Kong (Guo et al., 2009; Wang et al., 2009). Further inspection found that over the six years, the transport regime at TC was dominated by the air originating from super-regional transport (about 65% to the total air masses), followed by oceanic air (29%), regional transport (5%) and local emissions (1%). Due to the influence of Asian monsoon circulations, most of the oceanic air arrived at TC in summer, bringing in clean marine air, while super-regional and regional transport were often observed in autumn and winter, leading to the movement of precursor-laden air from the Asian continent to Hong Kong. The high frequency of air masses from super-regional and regional transport is another factor that contributes to high O_3 levels in autumn in Hong Kong, confirmed by the highest O_3 mixing ratio in the super-regional air masses (Table 8.3). Indeed, a study conducted at TC in October − December 2007 also found that high O_3 levels were attributed to regional and super-regional transport (Guo et al., 2009; Cheng et al., 2010a, b).

Table 8.3 Average values of SO_2, NO, O_3, CO and TVOCs in the four major types of air masses at TC from 2005 to 2010

		2005	2006	2007	2008	2009	2010
SO_2 (ppbv)	L[a]	3.6(21)[b]	23.5(48)		6.9(45)	10.1(36)	8.2(24)
	R[a]	12.2(321)	16.6(474)	14.5(22)	9.4(690)	9.5(513)	8.1(497)
	S[a]	6.1(4242)	10.9(3855)	10.4(1665)	8.7(5310)	5.8(5160)	4.6(5208)
	O[a]	4.3(2740)	4.4(2520)		3.4(1977)	2.5(1599)	2.4(2181)
NO (ppbv)	L	26.4	61.3		33.2	25.3	78.3
	R	24.9	29.8	25.2	26.3	24.7	37.2
	S	11.6	13.6	13.2	14.1	11.2	14.7
	O	15.4	10.3		8.5	12.0	8.0
O_3 (ppbv)	L	9.0	3.1		9.6	16.7	11.3
	R	19.8	11.0	11.0	14.6	21.7	9.5
	S	25.2	23.3	27.7	25.9	28.0	22.6
	O	15.7	15.7		18.6	16.8	20.4
CO (ppbv)	L	499.3	948.0		704.3	584.9	918.3
	R	813.6	786.7	529.8	845.8	732.0	866.6
	S	769.9	640.4	739.7	809.4	589.2	677.6
	O	650.7	512.3		564.3	440.0	498.6
TVOCs ($\mu g/m^3$)	L	24.8	38.6		37.8	48.5	72.0
	R	33.5	56.0	15.7	40.7	48.6	75.8
	S	14.5	14.4	18.4	26.8	27.4	29.1
	O	7.8	8.8		5.7	11.8	6.3

[a] L, R, S, O stand for air masses from local, regional, super-regional and oceanic transport
[b] Data in the bracket means the total number of air masses observed

Figure 8.6 shows a conceptualization of the influence of different air masses on O_3 levels at TC. The figure was generated based on the following steps. First, the transport history of air masses was investigated and the air masses were classified for the sampling period. In this study, 24-h backward trajectories were carried out using the HYSPLIT model with the GDAS meteorological data. For each day in the sampling period, eight trajectories were generated corresponding to arrival times at TC of 00:00, 03:00, 06:00, 09:00, 12:00, 15:00, 18:00, and 21:00 LT at the ending point of 20 m above sea level. These air masses were classified into local, regional, super-regional and oceanic air masses according to their original positions (i.e., latitude and longitude). In addition, the air masses for other hours during the day were classified using the following method: if an air mass at 03:00 was identified as regional transport, the air masses at 02:00 and 04:00 were also considered as regional transport; Secondly, the dominant surface winds of different air masses on high O_3

days and non-O_3 episode days in summer and autumn were identified; Finally, the relative O_3 concentrations in different air masses (i.e. local, regional, super-regional and oceanic) with different dominant surface winds were determined. It should be noted that due to the consideration of the statistical power of the trajectory results, a high O_3 day is defined as the day with the highest hourly average O_3 mixing ratio exceeding 80 ppbv in the figure. In addition, only O_3 mixing ratios during daytime (08:00 – 18:00, LT) were considered due to the fact that O_3 is formed by VOCs and NO_x reacting in the presence of sunlight. It is noteworthy that O_3 episode days usually occur in summer and autumn in Hong Kong. Inspection of the figure found that the dominant surface wind was generally from the northwest during high O_3 days, whereas the prevailing winds were generally from the southwest and northeast during summer (May − August) and autumn non-O_3 episode days (September − November), respectively. Moreover, the contributions of super-regional, regional, oceanic and local air masses to the average O_3 levels were 31 − 49%, 20 − 31%, 18 − 29 % and 0 − 27%, respectively, during summer non-O_3 episode days, while they were 29 − 56%, 19 − 37%, 15 − 24% and 0 − 31%, respectively, on autumn non-O_3 episode days. The relatively low contribution of oceanic air may be attributed to the fact that the south/southeast winds from the South China Sea brought in clean oceanic air with less primary pollutants and thus led to lower O_3 concentrations (Zheng et al., 2010a). On the other hand, during high O_3 days, super-regional, regional, and local air masses contributed 28 − 100%, 0 − 61% and 0 − 42% respectively to the O_3 mixing ratios in summer, while the respective contributions were 33 − 100%, 0 − 56% and 0 − 39% in autumn. However, no contribution of oceanic air masses was found on high O_3 days in summer and autumn. Overall, regional and super-regional air masses made the most significant contributions to the average O_3 mixing ratio, followed by local and oceanic

air masses, consistent with previous studies (Wang et al., 2009; Zheng et al., 2010a). The results further demonstrated that regional and super-regional air pollution had notable influence on the O_3 pollution in Hong Kong. However, it should be noted that the backward analysis was based on the HYSPLIT model results with the input of GDAS meteorological data, which had a relatively low resolution and could cause uncertainties in the identification of air masses and subsequently their influence on O_3 levels at TC.

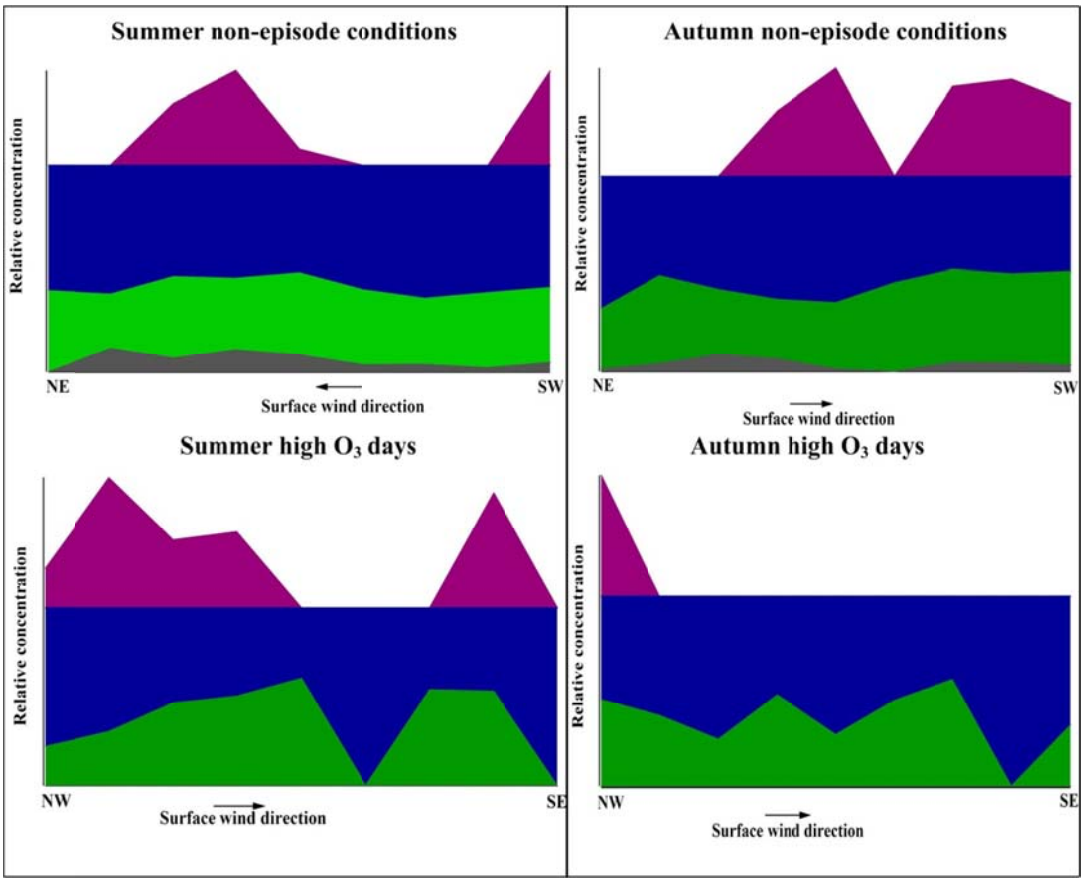

Figure 8.6 Graphical illustration of O_3 pollution in Hong Kong. The gray, green, blue and red areas represent the relative concentration of O_3 from oceanic, regional, super-regional and local emissions, respectively

8.3.3 Is photochemical O_3 formation limited by VOCs, or NO_x or both?

Due to the complex O_3 chemistry, photochemical O_3 formation could be dominated by either VOCs or NO_x or both. As such, it is important to understand the mechanisms of O_3 formation in a location. Moreover, since O_3 is a secondary

pollutant, the regional influence should therefore be considered. On a regional scale, Zheng et al. (2010) reported that the O_3 production was controlled by VOCs in urban areas and possibly controlled by NO_x in the northern/northeastern rural areas in the PRD region. Locally, Zhang et al. (2007) and Cheng et al. (2010b) found that the O_3 formation throughout Hong Kong was limited by VOCs, especially by reactive aromatics and some carbonyl compounds, and high NO concentrations suppressed O_3 production. In this section, measurement data for a total of 115 days (i.e. 17, 15, 13, 27, 23 and 20 days in years 2005 − 2010, respectively) with the maximum hourly O_3 mixing ratios above 80 ppbv were input into the OBM model to investigate the O_3-precursors relationships at TC. Figure 8.7 presents the average RIR values for different precursors on those 115 high O_3 days. It is apparent that O_3 production was generally VOC-limited at TC, indicating that reducing VOCs decreased the O_3 formation and reducing NO could increase O_3 levels. The anthropogenic volatile organic compounds (AVOCs) made the most significant contributions to the O_3 formation, except for 2007 and 2009 when biogenic volatile organic compounds (BVOCs) had the highest contributions due to the high isoprene emissions in these two years. Among the top 10 VOC species, the average RIR value of isoprene was the highest, followed by aromatic compounds i.e. toluene and *o*-xylene, and alkenes i.e. propene and *tran*-2-butene (Figure 8.8), revealing that the O_3 formation in Hong Kong was controlled by a small number of VOC species.

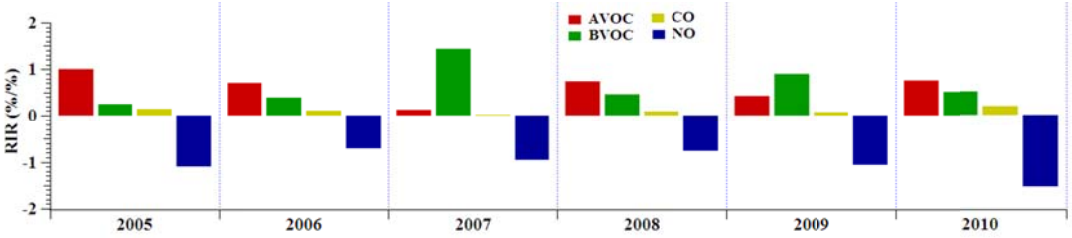

Figure 8.7 Average RIR (Relative Incremental Reactivity) values for O_3 precursors at TC

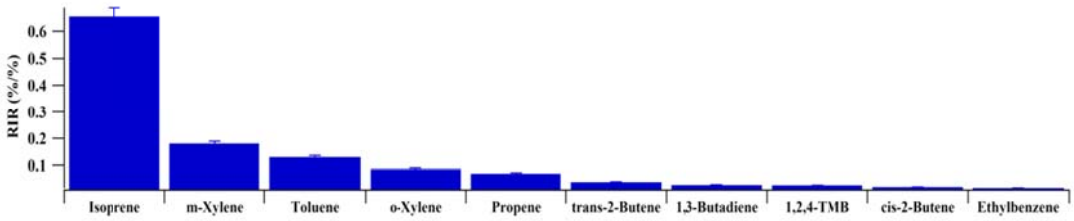

Figure 8.8 Average RIR values for individual VOC species at TC

In the PTM-MCM model, another method was applied to evaluate the relative contribution of each VOC to O_3 formation, in which the importance of each VOC to O_3 production was ranked by POCP-weighted values (Cheng et al., 2010a). The POCP values were calculated by the PTM-MCM model, while the POCP-weighted values were calculated by combining the POCP value and emissions of each VOC (i.e. the emission rate of the VOC in Hong Kong (tonne yr^{-1}) multiplies by its POCP value). The 15 most abundant VOC species accounted for 51.7% of the total VOC emission rates in the PRD region (Cheng et al., 2013). Among these species, isoprene, *cis*-2-pentene, 1,3,5-trimethylbenzene, acetaldehyde, 1,2,4-trimethylbenzene, 1,2,3-trimethylbenzene and propene had high POCP values, while toluene, benzene, ethene, isoprene had high emission rates, which are accounted for 6.2%, 5.8%, 5.5%, and 5.3% of the total emission rates, respectively.

After taking account into both the POCP and the emission amount of each VOC (POCP-weighted values), isoprene, ethene, toluene, formaldehyde, *m*-xylene, propene, acetaldehyde, 1,2,4-trimethylbenzene, *o*-xylene, 1-butene and ethylbenzene became the key precursors to photochemical O_3 formation in Hong Kong (Cheng et al., 2013). However, some highly reactive species, such as *cis*-2-pentene, 1,3,5-trimethylbenzene and 1,2,3-trimethylbenzene, had relatively lower contributions to the O_3 formation. This may be due to their low emissions, accounting for 0.1%, 0.5% and 0.4% of the total emission rates, respectively. In contrast, benzene and ethyne accounted for a relatively high percentage of the total VOC emissions (5.8% and 3.3%). Yet they had

negligible contribution to the O_3 formation because of their low reactivity. This feature suggests that the contribution of a VOC to the O_3 formation is determined by the combination of its reactivity and emission.

Despite some variations, the results of both OBM and PTM-MCM models showed that some reactive VOCs including BVOCs i.e. isoprene, and AVOCs i.e. toluene, *o*-xylene and propene had the highest contributions to the O_3 formation. Given that it is difficult to control BVOC emissions, the practical strategy to control O_3 pollution is to effectively reduce AVOC emissions. In addition, POCP-weighted values calculated by PTM-MCM model suggest that the optimal strategy should also consider the emission quantity together with reactivity of individual VOCs when it is formulated and implemented.

8.3.4 Which emission sources are responsible for the volatile organic compounds in the atmosphere of Hong Kong?

Since photochemical O_3 formation at TC was mostly VOC-limited, investigation of the characteristics of VOC source profiles and apportionments is the prerequisite for the formulation and implementation of O_3 control strategies at TC in Hong Kong. Table 8.4 illustrates the source apportionment of VOCs at TC using the PMF model. It can be seen that the main VOC sources were solvent use (e.g. paint and varnish, adhesives and sealants), and household products, gasoline and diesel vehicular emissions, gasoline evaporation, liquefied petroleum gas (LPG) usage, biomass burning, biogenic emissions, and the petrochemical industry. Solvent usage made the greatest contribution to ambient VOCs at TC (41 ± 6 %, mean ± 95% confidence interval), followed by gasoline and diesel vehicular emissions (31 ± 8%) and a mixed source of gasoline evaporation and LPG usage (22 ± 3%). The results are in line with previous studies (Table 8.4). For instance, the contributions of vehicular emissions in

this study (21 – 43%) were similar to previous studies (20 – 48%), except the study conducted by Lau et al. (2010) who reported the vehicular emissions of -70% in Hong Kong. In contrast, the percentage contribution of vehicular emissions in 2008 – 2010 obtained in this study was half that quantified in 2001-2003 (Guo et al., 2006, 2007), perhaps suggesting effective VOC control strategies such as utilizing cleaner diesel for buses in Hong Kong (http://www.epd.gov.hk/epd/english/environmentinhk/air/air_maincontent.html). On the other hand, the contribution of solvent usage in this study (about 30% – 56%) was consistent with the results found in previous studies (32% – 45%), and about twice of the study conducted in 2002 – 2003 (14 – 24%). The lower contribution of solvent usage to VOC emissions in 2002 – 2003 may be attributable to lower usage because of much fewer household, commercial and industrial activities caused by the severe acute respiratory syndrome (SARS) events in 2002 – 2003 in Hong Kong (Guo et al., 2011a). Furthermore, results of this study and HKEPD emission inventory (EI) indicated that solvent usage in Hong Kong was still the major contributor to ambient VOCs. In this study, gasoline evaporation and LPG usage were sometimes identified as a mixed source. This mixed source contributed 20.4 – 27%, similar to the results found in 2001 – 2003 and 2006 – 2008 (Guo et al., 2006; Lau et al., 2010), suggesting the emission from LPG usage and gasoline evaporation had less change in recent years. Therefore, these results point out the importance of effectively controlling solvent usage and vehicular emissions in Hong Kong.

Table 8.4 Comparison of results with previous studies and emission inventories

Factor	2005	2006	2007	2008	2009	2010	Sep2002-Aug2003	Sep2006-Aug2007	Fall 2007	2001	2001-2002	2002-2003	2007
Vehicle exhaust	43%	33.60 %	32%	20.50 %	25.30 %	36.90 %	69.8±0.7 %	69.5±0.9%	48±4%	39-48 %	39%	48-65%	20%
Gasoline	21.50 %	20.30 %	21.50 %	11.50 %	13.30 %	20.80 %			21±2%				
Diesel	21.50 %	13.30 %	10.50 %	9%	12%	16.10 %			27±3%				
Gasoline evaporation	17.40 %	*23.8 %	7.80%	*20.4 %	*27%	*20.5 %	4.4±0.2%	5.4±0.2%			14%	21-26%	
LPG/natural gas usage							18.1±0.6 %	27.6±0.8%		11-19 %	12%	15%	
Paint/varnish/solvents	29.50 %	41.30 %	41.20 %	55.80 %	33.20 %	48.20 %	33.8±0.3 %	41.1±0.1%	43%±2 %	32-36 %	35%	14-24%	75%
Industrial						4.40%	2.8±0.1%	2+0.1%		5-9%		8-15%	
Biomass/Combustion	5.60%	1.32 %			14.70 %				9±2%				
Biogenic	0.10%	0.10%	19.10 %	3.30%			2.20%	2.50%					0.2-2%
Aged VOC							27.6±0.5 %	23.8±0.5%					
Remarks	PMF	PMF	PMF	PMF	PMF	PMF	PMF	PMF	PMF	PCA /APCS	PCA /APCS	PCA /APCS	EI**
References	This Study	This Study	This Study	This Study	This Study	This Study	Lau et al., 2010	Lau et al., 2010	Guo et al., 2011a	Guo et al., 2004b	Guo et al., 2006	Guo et al., 2007	HKEPD, 2011***

* Mixed source of gasoline evaporation and LPG usage

** EI=Emission Inventory

*** HKEPD, 2011 http://www.epd.gov.hk/epd/english/environmentinhk/air/data/emission inve.html

8.3.5 Application of the conceptual model – model verification

In the sections described above, a conceptual description for O_3 pollution in Hong Kong was developed. During O_3 episodes, the most frequent weather systems affecting Hong Kong were tropical cyclones over the East and the South China Sea (Scenario 1), followed by regional high-pressure systems (anticyclones) to the north over mainland China (Scenario 2), and low-pressure system (trough) to the south and east over the South China Sea (Scenario 3) (Figure 8.9 a-c) (Huang et al., 2006; Guo et al., 2009). In this section, we conducted the model verification for four cases, i.e. 26 October 2007, 15 November 2008 and 04 June 2010 as examples for the high O_3 episode scenarios, and 29 July 2010 as an example for non-O_3 episode case.

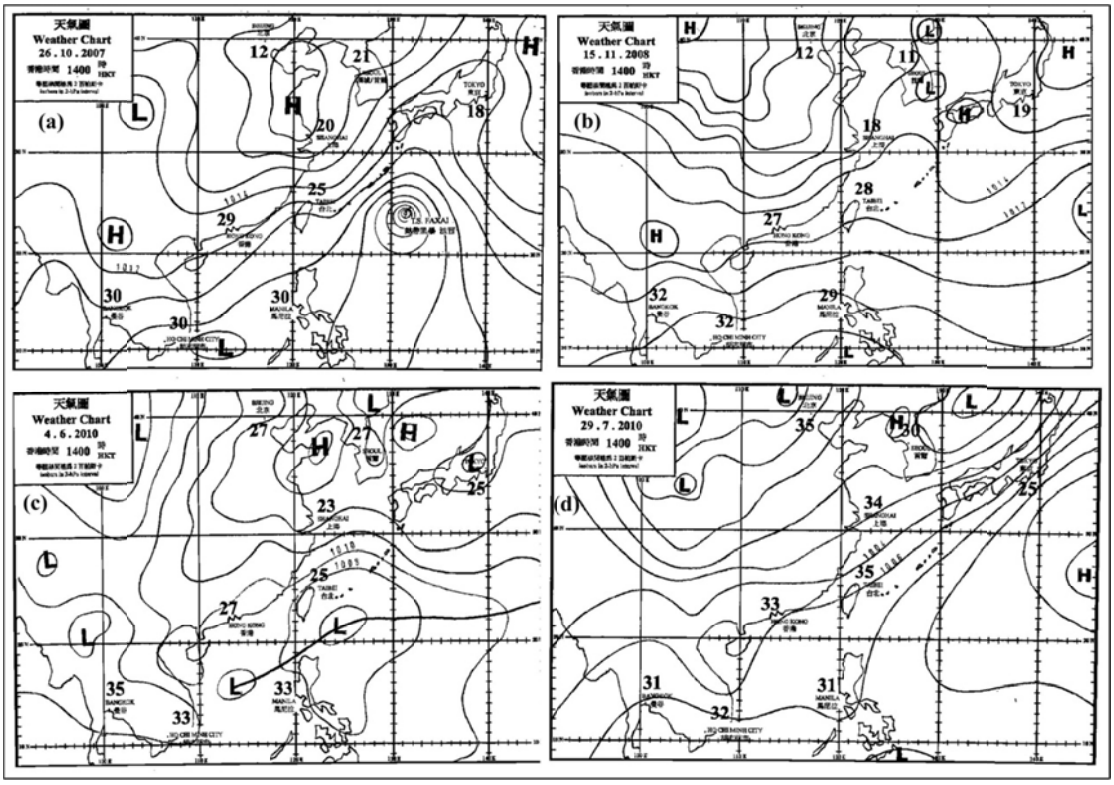

Figure 8.9 Weather Charts on (a) 26 October 2007, (b) 15 November 2008, (c) 04 June 2010 and (d) 29 July 2010

Figure 8.10 presents the diurnal variations of meteorological parameters for the four cases. It was found that there were some similarities in weather conditions at TC on the days of 26 October 2007, 04 June and 29 July 2010. First, the temperature and

solar radiation were relatively high on these three days, which had daily maximum temperature of 30 ^{o}C with solar radiation of 806 W/m^2, 29 ^{o}C with solar radiation of 805 W/m^2, and 33 ^{o}C with solar radiation of 888 W/m^2, respectively. Second, the relative humidity on these three days was comparable ($p > 0.05$). However, some differences were also found on these days. Firstly, a tropical cyclone was found over the East China Sea on 26 October 2007 (Figure 8.9a). On 04 June 2010, a low-pressure system (trough) to the south and east was over the South China Sea (Figure 8.9c), while an intense low-pressure system was found over Northern China and Hong Kong was in the front of the low pressure ridge on 29 July 2010 (Figure 8.9d). Secondly, the wind patterns were different on these three days. On 26 October 2007, the prevailing winds were southeasterly and northeasterly at night and northwesterly during daytime hours, while the dominant winds were southerly on 29 July 2010 with high wind speeds. However, the winds were calm (0.5 – 2 m/s) on 04 June 2010 with northerly and westerly winds during daytime hours and easterly winds at night. Thirdly, the backward trajectories analysis revealed that air masses arriving at TC were caused by super-regional transport on 26 October 2007, while the air masses were mainly from the ocean on 29 July 2010 (data not shown), indicating that high O_3 levels on 26 October 2007 (hourly peak value: 139 ppbv) and low O_3 level (~ 20 ppbv) on 29 July 2010 were attributed to the influence of different air masses. Indeed, the OBM modeling results suggested that super-regional transport contributed as high as 50% to the O_3 pollution at TC on 26 October 2007. On the other hand, the conditions of high temperature, strong solar radiation, and the low wind speeds on 04 June 2010 created a relatively stable lower tropospheric layer, which was favorable to the O_3 formation and accumulation at TC. This was confirmed by the OBM modeling results,

which revealed that high O_3 levels (i.e. peak value: 132 ppbv) on 04 June 2010 were mainly (90%) controlled by local formation.

On 15 November 2008, there was an intensive high-pressure system over northern China, while Hong Kong was in the front of the high pressure ridge. Due to the influence of this high-pressure system, more frequent northerly winds with higher speeds (maximum value: 6 m/s) were observed on 15 November 2008. In addition, the temperature and solar radiation (daily maximum value: 730 W/m^2) on 15 November 2008 were lower ($p < 0.05$) and the relative humidity was comparable to those on 29 July 2010. This implied that the O_3 levels could be lower on 15 November 2008 than on 29 July 2010. However, the O_3 mixing ratio was actually higher on 15 November 2008 (hourly peak value: 123 ppbv). Further inspection showed that the discrepancy between O_3 levels on 15 November 2008 and 29 July 2010 was also attributed to the influence of different air masses. The higher O_3 levels on 15 November 2008 were caused by the regional and super-regional transport. Backward trajectory analysis demonstrated that regional and super-regional air masses were frequently observed on 15 November 2008, and the OBM modeling simulations further confirmed that 90% of O_3 was caused by regional/super-regional transport on that day.

In summary, the above discussion indicated that tropical cyclone was mostly conducive to the occurrence of high O_3 mixing ratios. In addition, meteorological conditions such as high temperature, intense solar radiation, low relative humidity and wind speed were favorable to photochemical O_3 formation. Furthermore, polluted continental air masses brought by the northerly winds facilitated the O_3 production in Hong Kong. Nevertheless, it should be noted that these conditions were necessary but insufficient for the occurrence of O_3 episodes.

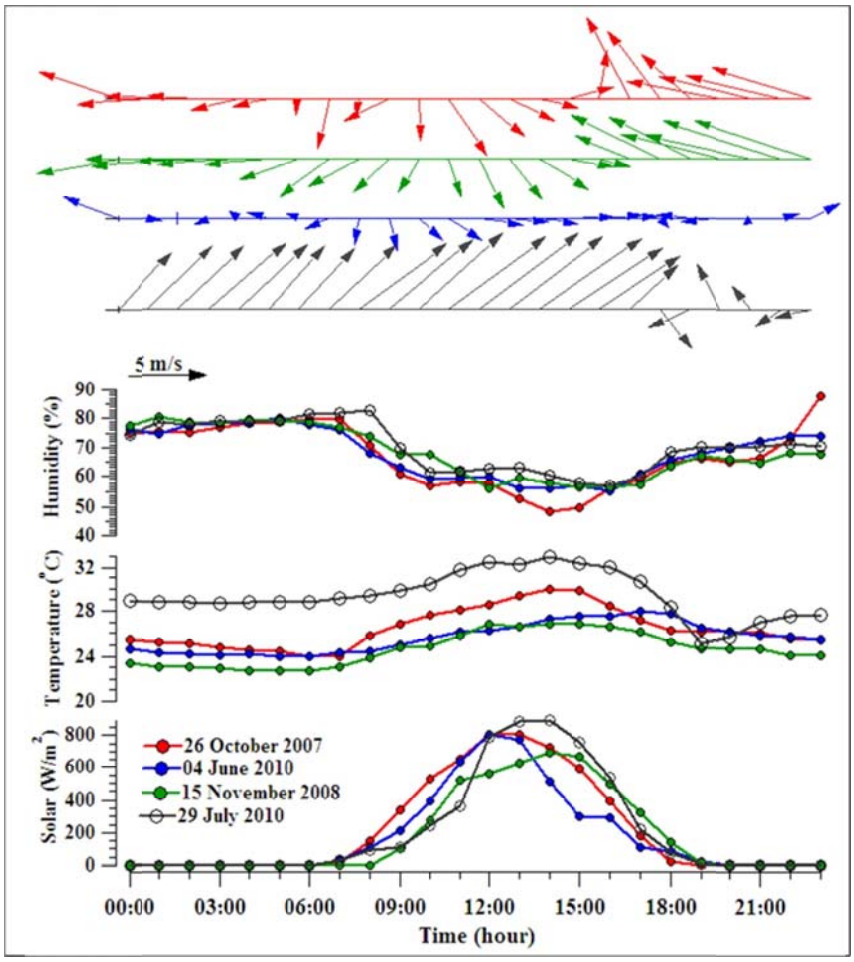

Figure 8.10 Diurnal variations of meteorological parameters on 26 October 2007, 04 June 2010, 15 November 2008 and 29 July 2010

8.4 Summary

A conceptual model of O_3 pollution in Hong Kong was developed in this study. Results suggested that tropical cyclone was mostly conducive to the occurrence of high O_3 mixing ratios, while conditions such as high temperature, intense solar radiation, low relative humidity and wind speeds and northeasterly and/or northwesterly prevailing winds were favorable to photochemical O_3 formation. In addition, super-regional and regional transport had significant influence on high O_3 levels in Hong Kong. The simulation of OBM and PTM-MCM models revealed that photochemical O_3 formation was generally VOC-limited in Hong Kong, and solvent usage and vehicular emissions made the most significant contributions to ambient VOCs. It should be noted that the relative contributions of local, regional and

super-regional air masses to the O_3 formation on O_3 episode days were extracted from the back trajectory analyses, even when the air movement was stagnant on some O_3 episode days, which could lead to uncertainties on the relative contributions.

8.5 Implications for ozone control measures

By considering the meteorological conditions, atmospheric chemistry and physics, and source apportionment of O_3 precursors, a conceptual description of O_3 pollution problem at TC in Hong Kong was presented above. However, some details remain to be thoroughly understood.

1) A key factor for the occurrence of O_3 episodes in Hong Kong is the influence of tropical cyclones which cause subsidence, stagnation air and inversion layer. However, the mechanisms of such influence are not fully understood.

2) Photochemical O_3 formation was generally VOC-limited and related to a small number of VOC species in Hong Kong, and solvent usage and vehicular emissions are the two major VOC sources. It appears that an effective control measure on the emissions of solvent usage and vehicles is an optimal strategy for controlling O_3 pollution in Hong Kong. In addition, the optimal strategy should also consider the emission quantity together with reactivity of individual VOCs when it is formulated and implemented.

3) Many VOC sources are located in the PRD region and regional transport from the inland PRD region has significant influence on the amount of air pollutants in Hong Kong (Tang et al., 2007a; Guo et al., 2009). As such, more concurrent field measurements should be conducted in these two closely interactive areas. In addition, air quality control strategies formulated in Hong Kong should consider the emissions from distant sources together with local sources.

4) In Hong Kong, the combination of the coastline and the mountains gives a terrain with many complex physical features. The role of sea-land breezes in air pollution transport has been well-studied previously (Ding et al., 2004). However, there are relatively few studies on mountain-valley breezes in Hong Kong, though it is very important to air pollution transport in Hong Kong.

5) Although remarkable improvements in the VOC emission inventory and VOC measurements have been made in Hong Kong, significant uncertainties still exist in the source profiles and apportionments of VOC data. Hence, further survey on the VOC emission sources and accurate VOC source profile measurements and analyses are essential to better understand the VOC emissions from different sources in Hong Kong and its surrounding areas i.e. inland PRD region, to provide more reliable results on VOC sources and species which contribute the most to photochemical O_3 formation in Hong Kong.

6) Though photochemical O_3 formation is generally VOC-limited in Hong Kong, the influence of other highly reactive chemicals such as HONO, PAN, H_2O_2 and other reactive oxidants on the O_3 formation should not be ignored. Besides VOCs, the characteristics of other precursors, i.e. NO_x and products, i.e. particles, are required in order to better understand the specific atmospheric chemistry. Flux measurements of O_3 and its precursors over different areas, i.e. Hong Kong and inland PRD, under different meteorological conditions, i.e. anticyclones and cyclones, mixing heights and transport processes are also necessary.

7) Since the conceptual model was developed based on the data collected at one site i.e. TC, it is suggested that this model should be further confirmed and improved by using data from other sites in Hong Kong.

Chapter 9 Conclusions

In this study, in-depth data analysis and model simulations were conducted based on the data collected in a number of field campaigns. The variations of air pollutants at different elevations and their impact factors were investigated based on the concurrent measurements conducted at TMS and TW. The mixing ratios of air pollutants were greater at TW than at TMS, except for O_3, which was attributed to the mixed effects of NO titration, vertical meteorological conditions and different flow patterns. The variations of NO and "oxidant" O_x (O_3 + NO_2) between the two sites indicated that the discrepancy of O_3 was partially related to the different degree of NO titration. In addition, the inversion layer formed at altitudes of 500 ~ 1000 m might caused higher O_3 levels at TMS. Furthermore, analysis of the wind fields and various ratios of air pollutants indicated that high O_3 concentrations at TMS were somewhat influenced by regional air masses from the highly polluted PRD region. In particular, the diurnal profiles and correlations of gaseous pollutants suggested influence of mesoscale circulations, which was confirmed using an Mbox model and a WRF model. The photochemical O_3 formation at TMS was mostly influenced by VOCs, with measurable influence of NO_x, while O_3 production at TW was generally limited by the concentrations of VOCs.

Furthermore, the photochemistry at the two sites was firstly investigated by a PBM-MCM model. Slightly higher HO_2 concentrations were found at TMS, while much higher OH concentrations were estimated at TW, suggesting that the HO_x cycling processes were different at the two sites, likely due to the different levels of O_3 and its precursors. The O_3 formation was dominated by the reaction of HO_2 + NO at the two sites, while O_3 was mainly destroyed by the reactions of OH + NO_2 at TW, and by the O_3 photolysis and the reaction of O_3 + HO_2 at TMS. Furthermore, longer

OH chain length was found at TMS, indicating that more O_3 could be produced for each radical that was produced.

To provide additional support to reduce VOCs in order to reduce O_3 pollution in Hong Kong and the inland PRD region, where O_3 formation was generally VOC-limited, a newly developed reactivity-based approach was developed in this study. Ten VOC sources were identified in the inland PRD region. Solvent usage, diesel vehicular emissions, and biomass/biofuel burning were the major VOC sources to O_3 formation. Among these sources, ethene, toluene and *m/p*-xylene were mainly responsible for local O_3 formation.

In Hong Kong, seven sources were identified. Paint and sealant solvents, diesel exhaust and LPG usage were the key contributors to O_3 formation. For the major species in the above three sources, *m/o/p*-xylene and ethylbenzene in paint and sealant solvents, toluene in gasoline exhaust, *n/i*-butane, ethene, propene and propane in LPG usage, and *n*-butane and ethene in diesel exhaust were the significant contributors to the O_3 formation. The relative O_3 reduction efficiency values indicated that the cutting percentages of the VOC sources and the major species from these sources were different for the most effective O_3 reduction in Hong Kong.

Finally, a conceptual model was developed based on a 6-year sampling campaign at Tung Chung to provide a general description of the influence factors of O_3 pollution in Hong Kong. It was found that high temperature, strong solar radiation, low wind speed and northerly winds, and regional and/or super regional transport are favorable for high O_3 levels, while the tropical cyclones were mostly conducive to the occurrence of high O_3 mixing ratios.

Overall, through the first concurrent measurements at the mountain site and the urban site at the foot of the mountain in Hong Kong, the variations of photochemical

pollutants, impact factors and photochemical reactivity at different areas were investigated. It could be concluded that O_3 formation was associated with the related concentrations of its precursors and meteorological conditions, which could influence the photochemical reactivity of O_3 formation in Hong Kong. Tropical cyclones were mostly conducive to the occurrence of high O_3 mixing ratios. On the other hand, analysis on chemical mechanisms of O_3 formation indicated that the cycling processes among radicals were different at the mountain and urban sites due to the different levels of O_3 and its precursors. O_3 production in Hong Kong was controlled by the pathway of HO_2 and NO, while the mechanism for O_3 destruction was different at the two sites. It is suggested that controlling solvent- and vehicular-related VOCs should be the most effective strategy to reduce photochemical O_3 formation in Hong Kong. Among these sources, *m/o/p*-xylene and ethylbenzene in paint and sealant solvents, toluene in gasoline exhaust, *n/i*-butane, ethene, propene and propane in LPG usage and *n*-butane and ethene in diesel exhaust should be prioritized to alleviate O_3 production in Hong Kong. In other words, O_3 formation could be effectively alleviated by controlling a small number of VOCs from specific sources, and the relatively O_3 reduction efficiency could be the highest when the VOC emissions were reduced by certain percentages.

References

AFCD (Agriculture, Fisheries and conservation Department), 2008. Available at website: http://www.afcd.gov.hk/.

Alicke, B., Geyer, A., Hofzumahaus, A., Holland, F., Knonard, S., Patz, H.W., Schafer, J., Stutz, J., Volz-Thomas, A., Platt, U., 2003. OH formation by HONO photolysis during the BERLIOZ experiment. Journal of Geophysical Research 108(D4), 8247, doi:10.1029/2001JD000579.

Ancellet, G., Beekmann, M., 1997. Evidence for changes in the ozone concentrations in the free troposphere over Southern France from 1976 to 1995. Atmospheric Environment 31, 2835-2851.

AOAQS (Airport Operational Air Quality Study), 2011. Final Report prepared by Institute for the Environment. The Hong Kong University of Science and Technology.

Apel, E.C., Emmons, L.K., Karl, T., Flocke, F., Hills, A.J., Madronich, S., Lee-Taylor, J., Fried, A., Weibring, P., Walega, J., Richter, D., Tie, X., et al., 2010. Chemical evolution of volatile organic compounds in the outflow of the Mexico City Metropolitan area. Atmospheric Chemistry and Physics, 10, 2353–2375.

Atkinson, R., 1994. Gas-phase tropospheric chemistry of organic compounds. Journal of Physical Chemistry Reference Data. Monograph 2, 1-216.

Atkinson, R., 1998a. Gasphase degradation of organic compounds in the troposphere. Pure and Applied Chemistry, 70(7), 1327-1334.

Atkinson, R., 1998b. Product studies of gas-phase reactions of organic compounds. Pure and Applied Chemistry, 70 (7), 1335-1343.

Atkinson, R., 2007. Gas-phase tropospheric chemistry of organic compounds: a review. Atmospheric Environment 41, S200-S240.

Atkinson, R. and Arey, J., 2003. Atmospheric degradation of volatile organic compounds. Chemical Review 103, 4605-4658.

Atkinson, R., Baulch, D.L., Cox, R.A., Crowley, J.N., Hampson, R.F., 2003. Summary of evaluated kinetic and photochemical data for atmospheric chemistry, IUPAC Subcommittee for Gas Kinetic Data Evaluation for Atmospheric Chemistry, Web version, available at http://www.iupac-kinetic.ch.cam.ac.uk/.

Atkinson, R., Baulch, D.L., Cox, R.A., Crowley, J.N., Hampson, R.F., Hynes, R.G., Jenkin, M.E., Rossi, M.J., Troe, J., 2006. Evaluated kinetic and photochemical

data for atmospheric chemistry: volume II – gas phase reactions of organic species. Atmospheric Chemistry and Physics 6, 3625-4055.

Atkinson, R., 2000. Atmospheric chemistry of VOCs and NOx, Atmos. Environ., 34, 2063-3101.

Atkinson, R., 1997. Gas-phase tropospheric chemistry of volatile organic compounds: 1. Alkanes and alkenes, J. Phys. Chem. Ref. Data 26 (2), 215.

ATSDR (Agency for Toxic Substances and Disease Registry), 1999. Toxicological Profile for N-Hexane. U.S. Department of Health and Human Services, Public Health Service, Atlanta, GA.

Avery, R.J., 2006. Reactivity-Based VOC control for solvent products: more efficient ozone reduction strategies. Environmental Science and Technology 40, 4845-4850.

Barletta, B., et al., 2009.Characterization of volatile organic compounds (VOCs) in Asian and North American pollution plumes during INTEX-B: identification of specific Chinese air mass tracers. Atmospheric Chemistry and Physics 9, 5371–5388.

Barletta, B., Meianrdi, S., Rowland, F. S., Chan, C. Y., Wang, X. M, Zou, S. C., Chan, L. Y., Blake, D. R., 2005. Volatile organic compounds in 43 Chinese cities. Atmospheric Environment, 39, 5979–5990.

Barletta, B., Meinardi, S., Simpon, I. J., Zou, S. C., Rowland, F. S., Blake, D. R., 2008. Ambient mixing ratios of nonmethane hydrocarbons (NMHCs) in two major urban centers of the Pearl River Delta (PRD) region: Guangzhou and Dongguan. Atmospheric Environment, 42, 4393-4408.

Barletta, B., Meinardi, S., Simpson, I. J., Khwaja, H. A., Blake, D. R., Rowland, F. S., 2002. Mixing ratios of volatile organic compounds (VOCs) in the atmosphere of Karachi, Pakistan. Atmospheric Environment, 36, 3429-3443.

Barletta, B., Meinardi, S., Simpson, I.J., Zou, S.C., Rowland, F.S., Blake, D.R., 2008. Ambient mixing ratios of nonmethane hydrocarbons (NMHCs) in two major urban centers of the Pearl River Delta (PRD) region: Guangzhou and Dongguan, Atmospheric Environment 42, 4393-4408.

Bell, M.L., McDermott, A., Zeger, S.L., Samet, J.M., Dominici, F., 2004. Ozone and short-term mortality in 95 US urban communities, 1987-2000. JAMA , 292, 2372-2378.

Blake, D.R., Rowland, F.S., 1995. Urban leakage of liquefied petroleum gas and its impact on Mexico City air quality. Science 269, 953-956.

Blake, N.J., Penkett, S.A., Clemitshaw, K.C., 1993. Estimates of atmospheric hydroxyl radical concentrations from the observed decay of many reactive hydrocarbons in well-defined urban plumes. Journal of Geophysical Research 98 (D2), 2851–2864, 1993.

Bloss, C., Wagner, V, Jenkin, M.E., Volkamer, R., Bloss, W.J., Lee, J.D., Heard, D.E., Wirtz, K., Martin-Reviejo, M., Rea, G., Wenger, J.C., and Pilling, M.J.:, 2005. Development of a detailed chemical mechanism (MCMv3.1) for the atmospheric oxidation of aromatic hydrocarbons, Atmospheric Chemistry and Physics 5, 641-664.

Borbon, A., Locoge, N., Veilerot, M., et al., 2002. Characterization of NMHCs in a French urban atmospheric: overview of the main sources. Science of the Total Environment 292, 177-191.

Brodin, M., Helmig, D., and Oltmans, S., 2010. Seasonal ozone behavior along an elevation gradient in the Colorado Front Range Mountains, Atmospheric Environment 44, 5305-5315, 2010.

Brown, S.G., Frankel, A., Hafner, H.R., 2007. Source apportionment of VOCs in the LosAngeles area using positive matrix factorization. Atmospheric Environment 41, 227-237.

Burley, J.D. and Bytnerowicz, A.: Surface ozone in the white mountains of California, Atmospheric Environment, 45, 4591-4602, 2011.

Cardelino, C.A. and Chameides, W.L., 1995. An observation-based model for analyzing ozone precursor relationships in the urban atmosphere. Journal of Air and Waste Management Association 45 (3), 161-180.

Carnero, J.A.A., Bolivar, J.P., de la Morena, B.A., 2010. Surface ozone measurements in the southwest of the Iberian Peninsula (Huelva, Spain). Environmental Science and Pollution Research 17, 355-368.

Carslaw, N, Creasey, D.J., Heard, D.E., Lewis, A.C., McQuaid, J.B., Pilling, M.J., Monks, P.S., Bandy, B.J., Penkett, S.A., 1999. Modeling OH, HO_2 and RO_2 radicals in marine boundary layer – 1. Model construction and comparison with field measurements. Journal of Geophysical Research 104, 30241-30255.

Carslaw, N., Creasey, D.J., Harrison, D., Heard, D.E., Hunte, M.C., Jacobs, P.J., Jenkin, M.C., Lee, J.D., Lewis, A.C., Pilling, M.J., Saunders, S.M., Seakins, P.,

2001. “OH and HO_2 radical chemistry in a forested region of north-western Green Source”. Atmospheric Environment 35, 4725-4737.

Carter, W. P. L. and Atkinson, R., 1996. Development and evaluation of a detailed mechanism for the atmospheric reactions of isoprene and NOx, International Journal of Chemical Kinetics 28, 497-530.

Carter, W. P. L., 2000. "Documentation of the SAPRC-99 Chemical Mechanism for VOC Reactivity Assessment," Report to the California Air Resources Board, Contracts 92-329 and 95-308, May 8.

Carter, W.L. and Atkinson, R., 1989. Computer modeling study of incremental hydrocarbon reactivity. Environmental Science and Technology 23, 864-880.

Carter, W.P.L., 1994. Development of ozone reactivity scales for volatile organic compounds. Journal of Air and Waste Management Association 44 (7), 881-899.

Carter, W.P.L., 1995. Computer modeling of environmental chamber measurements of maximum incremental relativities of volatile organic compounds. Statewide Air Pollution Research Center, University of California, U.S.A.

Carter, W.P.L., 2008. Reactivity estimates for selected consumer product compounds. Air Resources Board, California. Contract No. 06-408.

Chameides W.L. and Demerjian K.L.: An Assessment of Tropospheric Ozone Pollution: a North America Perspective, Palo Alto, California, USA, 2000.

Chameides, W.L., Fehsenfeld, F., Rodgers, M.O., Cardelino, C., Martinez, J., Parrish, D., Lonneman, W., Lawson, D.R., Rasmussen, R.A., Zimmerman, P., Greenberg. J., Middleton, P., Wang, T., 1992. Ozone precursor relationships in the ambient atmosphere. Journal of Geophysical Research, 97, 6037 –6055.

Chan, C.Y. and Chan, L.Y., 2000. Effect of meteorology and air pollutant transport on ozone episodes at a subtropical coastal Asian city, Hong Kong, Journal of Geophysical Research 105, 20707-20724.

Chan, L.Y., Chan, C.Y., Qin, Y., 1998a. Surface ozone pattern in Hong Kong. Journal of applied meteorology 37, 1153-1165.

Chan, L. Y., Liu, H. Y., and Lam, K. S.: Analysis of the seasonal behavior of tropospheric ozone at Hong Kong, Atmos. Environ., 32(2), 159–168, 1998b.

Chan, L.Y., Chu, K.W., Zou, S.C., Chan, C.Y., Wang, X.M., Barletta, B., Blake, D.R., Guo, H., Tsai, W.Y., 2006. Characteristics of nonmethane hydrocarbons (NMHCs) in industrial, industrial-urban, and industrial-suburban atmospheres of the Pearl

River Delta (PRD) region of south China. Journal of Geophysical Research, 111, D11, doi: 10.1029/2005JD006481.

Chang, C.C., Chen, T.Y., Lin, C.Y., Yuan, C.S., Liu, S.C., 2005. Effects of reactive hydrocarbons on ozone formation in southern Taiwan. Atmospheric Environment 39, 2867-2878.

Chen, C.L., Tsuang, B.J., Tu, C.Y., Cheng, W.L., and Lin, W.D., 2002. Wintertime vertical profiles of air pollutants over a suburban area in central Taiwan, Atmospheric Environment 36, 2049-2059.

Chen, F., and Dudhia, J., 2001. Coupling an Advanced Land Surface-Hydrology Model with the Penn State–NCAR MM5 Modeling System. Part I: Model implementation and sensitivity. Monthly Weather Review 129, 569–585.

Cheng, H.R., Guo, H., Saunders, S.M., Lam, S.H.M., Jiang, F., Wang, X.M., Simpson, I.J., Blake, D.R., Louie, P.K.K. and Wang, T.J., 2010b. Assessing photochemical ozone formation in the Pearl River Delta with a photochemical trajectory model, Atmospheric Environment 44 (34), 4199-4208.

Cheng, H.R., Guo, H., Wang, X.M., Saunders, S.M., Lam, S.H.M., Jiang, F., Wang, T., Ding, A., Lee, S. and Ho, K.F., 2010a. On the relationship between ozone and its precursors in the Pearl River Delta: application of an observation-based model (OBM), Environmental Science and Pollution Research 17, 547-560, 2010a.

Cheng, H.R., Saunders, S.M., Guo, H., Louie, P.K.K., Jiang, F., 2013. Photochemical trajectory modeling of ozone concentrations in Hong Kong, Environmental Pollution, doi: 10.1016/j.envpol.2013.04.039.

Chou, C.C.K., Liu, S.C., Lin, C.Y., Shiu, C.J., Chang, K.H., 2006. The trend of surface ozone in Taipei, Taiwan, and its causes: Implications for ozone control strategies. Atmospheric Environment 40, 3898-3908.

Chou, M.D., Suarez, M.J., 1994. An efficient thermal infrared radiation parameterization for use in general circulation models. NASA Tech. Memo. 104606, 3, 85.

Colman, J. J., Swanson, A. L., Meinardi, S., Sive, B. C., Blake, D. R., Rowland, F. S., 2001. Description of the analysis of a wide range of volatile organic compounds in whole air samples collected during PEM-Tropics A and B, Analytical Chemistry 73, 3723 – 3731.

Crowley, J. N., Schuster, G., Pouvesle, N., Parchatka, U., Fischer, H., Bonn, B., Bingemer, H., and Lelieveld, J., 2010 Nocturnal nitrogen oxides at a rural mountain-site in south-western Germany. Atmospheric Chemistry and Physics, 10, 2795-2812.

Derwent, R. G., Davies, T. J., Delaney, M., Dollard, G. J., Field, R. A., Dumitrean, P., Nason, P. D., Jones, B. M. R., Pepler, S. A., 2000. Analysis and interpretation of the continuous hourly monitoring data for 26 C_2-C_8 hydrocarbons at 12 United Kingdom sites during 1996. Atmospheric Environment, 34, 297-312.

Derwent, R. G., Simmonds, P. G., Manning, A. J., Spain, T. G., 2007b. Trends over a 20-year period from 1987 to 2007 in surface ozone at the atmospheric research station, Mace Head, Ireland. Atmospheric Environment, 41, 9091-9098.

Derwent, R.G., Jenkin, M.E., Passant, N.R.,et al., 2007a. Reactivity-basedstrategiesforphotochemical ozone control in Europe. Environment Science and Policy10, 445-453.

Derwent, R.G., Jenkin, M.E., Saunders, S.M., Pilling, M.J., 1998. Photochemical ozone creation potentials for organic compounds in northwest Europe calculated with a master chemical mechanism. Atmospheric Environment 32, 2429-2441.

Di Carlo, P., Brune, W.H., Martinez, M., Harder, H., Lesher, R., Ren, X.R., Thornberry, T., Carroll, M.A., Young, V., Shepson, P.B., Riemer, D., Apel, E., Campbell, C., 2004. Missing OH reactivity in a forest: evidence for unknown reactive biogenic VOCs. Science 304, 722–725.

Ding, A. J., Wang, T., Thouret, V., Cammas, J. P., Nédélec, P., 2008. Tropospheric ozone climatology over Beijing: analysis of aircraft data from the MOZAIC program. Atmospheric Chemistry and Physics 8, 1-13.

Ding, A., Wang, T., Zhao, M., Wang, T., Li, Z., 2004. Simulation of sea-land breezes and a discussion of their implications on the transport of air pollution during a multi-day ozone episode in the Pearl River Delta of China. Atmospheric Environment, 38, 6737-6750.

Dodge, M. C., 1977. Combined use of modeling techniques and smog chamber data to derive ozone-precursor relationships. International Conference on Photochemical Oxidant Pollution and its Control: Proceedings, Vol.II B, EPA/600/3-77-001b. U.S. Environmental Protection Agency, Research Triange Park, NC, 881-889,.

Done, J., Davis, C., Weisman, M., 2004. The next generation of NWP: Explicit forecasts of convection using the Weather Research and Forecast (WRF) model, Atmospheric Science Letter 5, 110–117, doi:10.1002/asl.72.

Doran, J. C., Berkowitz, C. M., Coulter, R. L., Spicer, C. W., and Shaw, W.J., 2003. The 2001 Phoenix Sunrise experiment: vertical mixing and chemistry during the morning transition in Phoenix, Atmospheric Environment 37, 2365-2377.

Du, L., Xu, Y.F., Ge, M.F., Jia, L., Wang, G.C., Wang, D.X., 2007. Smog chamber simulation of atmospheric photochemical reactions of acetylene and NO_x (in Chinese). Environmental Science 28, 482-488.

Durana, N., Navazo, M., GÓmez, M.C., Alonso, L., García, J.A., Ilardia, J.L., Gangoiti, G., Iza, J., 2006. Long term hourly measurement of 62 non-methane hydrocarbons in an urban area: main results and contribution of non-traffic sources. Atmospheric Environment 40, 2860-2872.

Dusanter, S., Vimal, D., Stevens, P.S., Volkamer, R., Molina, L.T., Baker, A., Meinardi, S., Blake, D., Sheehy, P., Merten, A., Zhang, R., Zheng, J., Fortner, E.C., Junkermann, W., Dubey, M., Rahn, T., Eichinger, B., Lewandowski, P., Prueger, J., Holder, H., 2009. Measurements of OH and HO_2 concentrations during the MCMA-2006 field campaign-Part 2: model comparison and radical budget. Atmospheric Chemistry and Physics 9, 6655-6675.

Edgerton, S.A., Holdren, M.W., Smith, D.L., Shah, J.J., 1989. Interurban comparison of ambient volatile organic compound concentrations in U.S. cities. Journal of Air and Waste Management Associate 44, 881-899.

Ehhalt, D.H., Rohrer, F., Wahner, A., Prather, M.J., Blake, D.R., 1998 On the use of hydrocarbons for the determination of tropospheric OH concentrations, Journal of Geophysical Research 103, 18981-18997.

Emmerson, K.M., Carslaw, N., Carslaw, D.C., Lee, J.D., McFiggans, G., Bloss, W.J., Gravestock, T., Heard, D.E., Hopkins, J., Ingham, T., Pilling, M.J., Smith, S.C., Jacob, M., Monks, P.S., 2007. Free radical modeling studies during the UK TORCH campaign in summer 2003. Atmospheric Chemistry and Physics 7, 167-181.

Environmental Protection Agency (EPA), 2004. Emission inventory improvement programs, Technical report series, Technology transfer network clearinghouse for inventories and emission factors. http://www.epa.gov/ttn/chief/eiip/techreport.

Environmental Protection Agency (EPA), 2008. EPA Positive Matrix Factorization (PMF) 3.0 fundamentals and user guide.

Eric, G., Reinhold, A.R., Daniel, G., 1998. Ambient levels of gas phase pollutants in Porto Alegre, Brazil. Atmospheric Environment 32 (20), 3371-3379.

Evtyugina, M. G., Nunes, T., Alves, C., Marques, M. C., 2009. Photochemical pollution in a rural mountainous area in the northeast of Portugal. Atmospheric Research, 92, 151-158.

Evtyugina, M.G., Pio, C., Nunes, T., Pinho, P.G., Costa, C.S., 2007. Photochemical ozone formation at Portugal West Coast under sea breeze conditions as assessed by master chemical mechanism model. Atmospheric Environment 41, 2171-2182.

Fan, S., Wang, B., Tesche, M., Engelmann, R., Althausen, A., Liu, J., Zhu, W., Fan, Q., Li, M., Ta, N., Song, L., Leong, K., 2008. Meteorological conditions and structures of atmospheric boundary layer in October 2004 over Pearl River Delta area. Atmospheric Environment 42, 6174-6186.

Feng, X. Q, Peng, K., Ling, Z. H, Zheng, J .Y, Guo. H., 2013. Source apportionments and characteristics of VOCs from 2005 to 2010 in Hong Kong. Acta Scientiae Circumstantiae, 33(1):173-180. (in Chinese)

Finlayson-Pitts B. J. and N. Pitts, 1993. VOCs, NOx and ozone production. Journal of Air and Waste Management Association 43, 1093-1101, 1993.

Fiore, A.M., Levy, H., Jaffe, D.A., 2011. North American isoprene influence on intercontinental ozone pollution. Atmospheric Chemistry and Physics, 11, 1697-1710.

Fu, P.Q., Kawamura, K., Kanaya, Y., Wang, Z.F., 2010. Contributions of biogenic volatile organic compounds to the formation of secondary organic aerosols over Mt. Tai, Central East China, Atmospheric Environment, 44, 4817-4826.

Gao, J., Wang, T., Ding, A. J., Liu, C. B., 2005. Observational study of ozone and carbon monoxide at the summit of mount Tai (1534m a.s.l.) in central-eastern China. Atmospheric Environment, 39, 4779-4791.

Gilge, S., Plass-Duelmer, C., Fricker, W., Kaiser, A., Ries, L., Buchmann, B., Steinhacher, M., 2010. Ozone, carbon monoxide and nitrogen oxides time series at four alpine GAW mountain stations in central Europe. Atmospheric Chemistry and Physics, 10, 12295-12316.

Gilman, J. B., Kuster, W. C., Goldan, P. D., Herndon, S. C., Zahniser, M. S., Tucker, S. C., Brewer, W. A., Lerner, B. M., Williams, E. J., Harley, R. A., Fehsenfeld, F. C., Warneke, C., de Gouw, J. A., 2009. Measurements of volatile organic compounds during the 2006 TexAQS/GoMACCS campaign: industrial influences, regional characteristics, and diurnal dependencies of the OH reactivity. Journal of Geophysical Research, 114, D7, doi: 10.1029/2008JD011525.

Godish, T., 2004. Air Quality. 4th edition Lewis Publishers, Boca Raton, USA.

Grell, G. A., and Dévényi, D., 2002. A generalized approach to parameterizing convection combining ensemble and data assimilation techniques. Geophysical Research Letter 29, 1693. doi:10.1029/2002GL015311.

Grosjean, E., Rasmussen, R. A., Grosjean, D., 1998. Ambient levels of gas phase pollutants in Porto Alegre, Brazil. Atmospheric Environment, 32, 3371-3379.

Guangdong Provincial Environmental Protection Monitoring Centre (GDEMC), and Environmental Protection Department of Hong Kong (HKEPD), 2005–2012.Pearl River Delta Regional Air Quality Monitoring Network Report (in Chinese). http://sc.epd.gov.hk/gb/www.epd.gov.hk/.

Guo, H., Cheng, H.R., Ling, Z.H., Louie, P.K.K., Ayoko, G., 2011a. Which emission sources are responsible for the volatile organic compounds in the atmosphere of Pearl River Delta? Journal of Hazardous Materials 188, 116-124.

Guo, H., Jiang, F., Cheng, H. R., Simpson, I. J., Wang, X. M., Ding, A. J., Wang, T. J., Saunders, S. M., Wang, T., Lam, S. H. M., Blake, D. R., Zhang, Y. L., Xie, M., 2009. Concurrent observations of air pollutants at two sites in the Pearl River Delta and the implication of regional transport. Atmospheric Chemistry and Physics 9, 7343-7360.

Guo, H., Lee, S. C., Louie, P. K. K., Ho, K. F., 2004a. Characterization of hydrocarbons, halocarbons and carbonyls in the atmosphere of Hong Kong. Chemosphere 57, 1363-1372.

Guo, H., Ling, Z. H., Simpson, I. J., Blake, D. R., Wang, D. W., 2012. Observations of isoprene, methacrolein (MAC) and methyl vinyl ketone (MVK) at a mountain site in Hong Kong, Journal of Geophysical Research 117, D19303, doi:10.1029/2012JD017750.

Guo, H., Ling, Z.H., Cheung, K., Jiang, F., Wang, D.W., Simpson, I.J., Barletta, B., Meinardi, S., Wang, T.J., Wang, X.M., Saunders, S.M., Blake, D.R., 2013a. Characterization of photochemical pollution at different elevations in

mountainous areas in Hong Kong. Atmospheric Chemistry and Physics 13, 3881-3898.

Guo, H., Ling, Z.H., Cheung, K., Wang, D.W., Simpson, I.J., Blake, D.R., 2013b. Acetone in the atmosphere of Hong Kong: abundance, sources and photochemical precursors. Atmospheric Environment 65, 80-88.

Guo, H., So, K. L., Simpson, I. J., Barletta, B., Meinardi, S., Blake, D. R., 2007. C_1-C_8 volatile organic compounds in the atmosphere of Hong Kong: Overview of atmospheric processing and source apportionment. Atmospheric Environment 41, 1456-1472.

Guo, H., Wang, T., Blake, D. R., Simpson, I. J., Kwok, Y. H., Li, Y. S., 2006. Regional and local contributions to ambient non-methane volatile organic compounds at a polluted rural/coastal site in Pearl River Delta, China. Atmospheric Environment 40, 2345-2359.

Guo, H., Wang, T., Louie, P. K. K., 2004b. Source apportionment of ambient non-methane hydrocarbons in Hong Kong: Application of a principal component analysis/absolute principal component scores (PCA/APCS) receptor model. Environmental Pollution 129, 489-498.

Guo, H., Zou, S.C., Tsai, W.Y., Chan, L.Y., Blake, D.R., 2011b. Emission characteristics of nonmethane hydrocarbons from private cars and taxis at different driving speeds in Hong Kong. Atmospheric Environment. doi:10.1016/j.atmosenv.2011.02.053.

He, J., Chen, H.X., Liu, X.X., Hu, J.H., Li, Q.L., He, F.Q., 2002. The analysis of various volatile solvents used in different industries in Zhongshan (in Chinese). South China Journal of Preventive Medicine 28 (6), 26-27.

Health Canada, 1993. Indoor Air Quality in Office Buildings: a Technical Guide. Department of National Health and Welfare, Canada.

Hidy, G. M., 2000. Ozone process insights from field experiments - part I: overview. Atmospheric Environment 34, 2001-2022.

HKCSD (Hong Kong Census and Statistics Department), 2010. Hong Kong Energy Statistics: Annual Report. http:// www.censtatd.gov.hk.

HKCSD (Hong Kong Census and Statistics Department), 2012. Available at website: http://www.censtatd.gov.hk/hkstat.

HKEPD (Environmental Protection Department of Hong Kong), 2005. Determination of Suspended Particulate and VOC Emission Profiles for Vehicular Sources in

Hong Kong. Environmental Protection Department (Hong Kong Special Administrative Region Government).

HKEPD (Hong Kong Protection Department), 2010. Final report on review on the effectiveness of VOC control programme in Hong Kong. http://www.epd-asg.gov.hk/english/report/aqr.html.

HKEPD (Hong Kong Protection Department), 2012a. Air Quality in Hong Kong 2011.http://www.epd-asg.gov.hk/english/report/aqr.html.

HKEPD (Hong Kong Protection Department), 2012b. Integrated Data Analysis and Characterization of Photochemical Ozone in Hong Kong.http://www.epd-asg.gov.hk/english/report/aqr.html.

HKTD (Hong Kong Transport Department), 2011. The Annual Traffic Census. http:// http://www.td.gov.hk/filemanager.

Ho, K. F., Lee, S. C., Guo, H., Tsai, W. Y., 2004. Seasonal and diurnal variations of volatile organic compounds (VOCs) in the atmosphere of Hong Kong. Science of Total Environment, 322, 155–166.

Ho, K.F., Lee, S.C., Ho, W.K., Blake, D.R., Cheng, Y., Li, Y.S., Ho, S.S.H., Fung, K., Louie, P.K.K., Park, D., 2009. Vehicular emission of volatile organic compounds (VOCs) from a tunnel study in Hong Kong. Atmospheric Chemistry and Physics 9, 7491-7504.

Hofzumahaus, A., Rohrer, F., Lu, K., Bohn, B., Brauers, T., Chang, C.C., Fuchs, H., Holland, F., Kita, K., Kondo, Y., Li, X., Lou, S., Shao, M., Zeng, L., Wahner, A., Zhang, Y., 2009. Amplified trace gas removal in the troposphere. Science 324, 1702.

Hong Kong Environmental Protection Department (HKEPD): Air Quality in Hong Kong 2011 (Preliminary Report), Air Science Group, Environmental Protection Department, the Government of the Hong Kong Special Administrative Region, 2012.

HKEPD (Hong Kong Environmental Protection Department): An overview on air quality and air pollution control in Hong Kong, 2012c. http://www.epd.gov.hk/epd/english/environmentinhk/air/air_maincontent.html.

Hong, S.Y., Dudhia, J., Chen, S.H., 2004. A revised approach to ice-microphysical processes for the bulk parameterization of cloud and precipitation. Monthly Weather Review 132, 103–120, 2004.

Hong, S.Y., Noh, Y., Dudhia, J., 2006. A new vertical diffusion package with explicit treatment of entrainment processes. Monthly Weather Review 134, 2318–2341, 2006.

Hopke, P.K., 2003. Recent developments in receptor modeling.Chemometr.Intell. Lab.17,255-265.

Hough, A.M., 1988. The calculation of photolysis rates for use in global tropospheric modeling studies. AERE Report R-13259 (HMSO) London.

Hua, W., Chen, Z.M., Jie, C.Y., Kondo, Y., Hofzumahaus, A., Takegawa, N., Chang, C.C., Lu, K.D., Miyazaki, Y., Kita, K., Wang, H.L., Zhang, Y.H., Hu, M., 2008. Atmospheric hydrocarbon peroxide and organic hydroperoxides during PRIDE-PRD'06 China: their concentration, formation mechanism and contribution to secondary aerosols. Atmospheric Chemistry and Physics 8, 6755-6773.

Huang, J. P., Fung, J. C. H., Lau, A. K. H., 2006. Integrated processes analysis and systematic meteorological classification of ozone episodes in Hong Kong. Journal of Geophysical Research, 111, D20, doi: 10.1029/2005JD007012.

Huang, J. P., Fung, J. C. H., Lau, A. K. H., Qin, Y., 2005. Numerical simulation and process analysis of typhoon-related ozone episodes in Hong Kong. Journal of Geophysical Research, 110, D5, doi: 10.1029/2004JD004914.

IPCC (Intergovernmental Panel on Climate Change), 2007. Climate Change 2007: The Physical Science Basis. Contribution of Working Group I to the Fourth Assessment Report of the Intergovernmental Panel on Climate Change, Cambridge Univ. Press, Cambridge, U. K..

Jackson, A.V. and Hewitt, C.N., 1999. Atmospheric hydrogen peroxide and organic hydroperoxides: a review. Critical Reviews in Environmental Science and Technology 29, 2, 175-288.

Jacob, D. J., Logan, J. A., Murti, P. P., 1999. Effect of rising Asian emissions on surface ozone in the United States. Geophysical Research Letters, 26, 2175-2178.

Jaffe, D., Price, H., Parrish, D., Goldstein, A., Harris, J., 2003. Increasing background ozone during spring on the west coast of North America. Geophysical Research Letters, 30, 4.

Jaffe, D., Ray, J., 2007. Increase in surface ozone at rural sites in the western US. Atmospheric Environment, 41, 5452-5463.

Jenkin, M. E. and Clemitshaw, K. C., 2000. Ozone and other secondary photochemical pollutants: chemical processes governing their formation in the planetary boundary layer. Atmospheric Environment, 34, 2499-2527.

Jenkin, M. E., 2008. Trends in ozone concentration distributions in the UK since 1990: Local, regional and global influences. Atmospheric Environment 42, 5434-5445.

Jenkin, M. E., Saunders, S. M., Wagner, V., and Pilling, M. J., 2003. Protocol for the development of the master chemical mechanism MCMv3 (Part B): Tropospheric degradation of aromatic volatile organic compounds, Atmospheric Chemistry and Physics 3, 181-193. 2003.

Jenkin, M. E., Saunders, S. M., Wagner, V., and Pilling, M. J., 1997. The tropospheric degradation of volatile organic compounds: A protocol for mechanism development. Atmospheric Environment 31, 81-107, 1997.

Jiang, F., Guo, H., Wang, T. J., Cheng, H. R., Wang, X. M., Simpson, I. J., Ding, A. J., Saunders, S. M., Lam, S. H. M., and Blake, D. R., 2010. An ozone episode in the Pearl River Delta: Field observation and model simulation, J. Geophys. Res., 115, D22305, doi:10.1029/2009JD013583.

Jiang, F., Wang, T., Wang, T., Xie, M., Zhao, H., 2008. Numerical modeling of a continuous photochemical pollution episode in Hong Kong using WRF-chem. Atmospheric Environment 42, 8717-8727.

Jobson, B.T., Mckeen, S.A., and Parrish, D.D., 1998. Spatial and temporal variability of nonmethane hydrocarbon mixing ratios and their relation to photochemical lifetime, Journal of Geophysical Research 103 (D11), 13557-13567, 1998.

Jorquera, H., Rappengluck, B., 2004. Receptor modeling of ambient VOC at Santiago, Chile. Atmospheric Environment 38, 4243-4263.

Kim, S., Guenther, A., Karl, T. and Greenberg, J., 2011. Contributions of primary and secondary biogenic VOC to total OH reactivity during the CABINEX (Community Atmosphere-Biosphere INteractions EXperiments)-09 field campaign, Atmospheric Chemistry and Physics 11, 8613–8623, doi:10.5194/acp-11-8613-2011.

Kim, S., Wolfe, G.M., Mauldin, L., Cantrell, C., Guenther, A., Karl, T., Turnipseed, A., Greenberg, J., Hall, S.R., Ullmann, K., Apel, E., Hornbrook, R., Kajii, Y., Nakashima, Y., Keutsch, F.N., Digangi, J.P., Henry, S.B., Kaser, L., Schnitzhofer, R., Graus, M., Hansel, A., Zheng, W., Flocke, F.F., 2013. Evaluation of HOx sources and cycling using measurement-constrained model calculations in a

2-methyl-3-butene-2-ol (MBO) and monoterpene (MT) dominated ecosystem. Atmospheric Chemistry and Physics 13, 2031-2044.

Kleinman, L.I., 2000. Ozone process insights from field experiments - part II: Observation-based analysis for ozone production. Atmospheric Environment 34, 2023-2033.

Kleinman, L.I., 2005. The dependence of tropospheric ozone production rate on ozone precursors. Atmospheric Environment 39, 575–586.

Krzyscin, J., Krizan, P., Jaroslawski, J., 2007. Long-term changes in the tropospheric column ozone from the ozone soundings over Europe. Atmospheric Environment, 41, 606-616.

Kurokawa, J., Ohara, T., Uno, I., Hayasaki, M., Tanimoto, H., 2009. Influence of meteorological variability on interannual variations of springtime boundary layer ozone over Japan during 1981-2005. Atmospheric Chemistry and Physics 9, 6287-6304.

Kurtenbach, R., Becker, K.H., Gomes, J.A.G., Kleffmann, J., Lörzer, J.C., Spittler, M., Wiesen, P., Ackermann, R., Geyer, A., Platt, U., 2001. Investigations of emissions and heterogeneous formation of HONO in a road traffic tunnel. Atmospheric Environment 35 (20), 3385-3394.

Kwon, K.D., Jo, W.K., Lim, H.J., Jeong, W.S., 2007. Characterization of emissions composition for selected household products available in Korea. Journal of Hazardous Materials 148, 192-198.

Lai, C.H., Chang, C.C., Wang, C.H., Shao, M., 2009. Emissions of liquefied petroleum gas (LPG) from motor vehicles. Atmospheric Environment 43, 1456–1463.

Lam, K.S., Wang, T.J., Chan, L.Y., Wang, T., Harris, J., 2001. Flow patterns influencing the seasonal behavior of surface ozone and carbon monoxide at a coastal site near Hong Kong. Atmospheric Environment, 35, 3121-3135.

Lam, K.S., Wang, T.J., Wang, T., Tang, J., Kajii, Y., Liu, C.M., Shim, S.G., 2004. Overview of Surface Ozone variability in East Asia – North Pacific Region during IGAC/APARE (1994 – 1996). Journal of Environmental Sciences 16 (4), 599-609.

Lam, K.S., Wang, T.J., Wu, C.L., Li, Y.S., 2005. Study on an ozone episode in hot season in Hong Kong and transboundary air pollution over Pearl River Delta region of China. Atmospheric Environment 39, 1967-1977.

Lam, S.H.M., Saunders, S.M., Guo, H., Ling, Z.H., Jiang, F., Wang, X.M., Wang, T.J., 2013. Modelling VOC source impacts on high ozone episode days observed at a mountain summit in Hong Kong under the influence of mountain-valley breezes. Atmospheric Environment 81, 166-176.

Latella, A., Stani, G., Cobelli, L., Duane, M., Junninen, H., Astorga, C., 2005. Semicontinous GC analysis and receptor modeling for source apportionment of ozone precursor hydrocarbons in Bresso, Milan, 2003. Journal of Chromatography A 1071, 29-39.

Lau, A. K. H., Yuan, Z. B., Yu, J. Z., Louie, P. K. K., 2010. Source apportionment of ambient volatile organic compounds in Hong Kong. The Science of the Total Environment, 408, 4138-4149.

Lauz, V.A., Henne, S., Staehelin, J., et al., 2009. Statistical analysis of anthropogenic non-methane VOC variability at a European background location (Jungfraujoch, Switzerland).Atmos. Chem. Phys.9, 3445-3459.

Lauz, V.A., Hueglin, C., Buchmann, B., et al., 2008. Receptor modeling of C2-C7 hydrocarbon sources at an urban background site in Zurich, Switzerland: changes between 1993-1994 and 2005-2006.Atmos. Chem. Phys.8, 2313-2332.

Lee, S.C., Chiu, M.Y., Ho, K.F., Zou, S.C., Wang, X., 2002b. Volatile organic compounds (VOCs) in urban atmosphere of Hong Kong. Chemosphere, 48(3), 375-82.

Lee, S., Akimoto, H., Nakane, H., Kurnosenko, S., Kinjo, Y., 1998. Lower tropospheric ozone trend observed in 1989-1997 at Okinawa, Japan. Geophysical Research Letters, 25, 1637-1640.

Lee, Y.C. and Hills, P. R., 2003. Cool season pollution episodes in Hong Kong, 1996-2002. Atmospheric Environment, 37, 2927-2939.

Lee, Y.C., Calori, G., Hills, P., Carmichael, G. R., 2002a. Ozone episodes in urban Hong Kong 1994-1999. Atmospheric Environment, 36, 1957-1968.

Lei, W., Zavala, M., de Foy, B., Volkamer, R., Molina, M.J., Molina, L.T., 2009. Impact of primary formaldehyde on air pollution in the Mexico City Metropolitan Area. Atmospheric Chemistry and Physics 9, 2607-2618.

Leung, D.Y.C., Wong, P., Cheung, B.K.H., et al., 2010. Improved land cover and emission factors for modeling biogenic volatile organic compounds emissions from Hong Kong. Atmos. Environ. 44, 1456-1468.

Lelieveld, J., Bulter, T.M., Crowley, J.N., Dillon, T.J., Fischer, H., Ganzeveld, L., Harder, H., Lawrence, M.G., Martinez, M., Taraborrelli, D., Williams, J., 2008. Atmospheric oxidation capacity sustained by a tropical forest. Nature 452, 737-740.

Li, J., Pochanart, P., Wang, Z. F., Liu, Y., Yamaji, K., Takigawa, M., Kanaya, Y., and Akimoto, H., 2008. Impact of chemical production and transport on summertime diurnal ozone behavior at a mountainous site in North China Plain. Sola, 4, 121-124.

Lin, C.H., Lai, C.H., Wu, Y.L., Lai, H.C., and Lin, P.H., 2007. Vertical ozone distributions observed using tethered ozonesondes in a coastal industrial city, Kaohsiung, in southern Taiwan. Environmental Monitoring and Assessment 127, 253-270, 2007.

Lin, C. Y. C., Jacob, D. J., Munger, J. W., Fiore, A. M., 2000. Increasing background ozone in surface air over the United States. Geophysical Research Letters 27, 3465-3468.

Lin, W., Xu, X., Zhang, X., Tang, J., 2008. Contributions of pollutants from North China Plain to surface ozone at the Shangdianzi GAW Station, Atmos. Chem. Phys., 8, 5889-5898, 2008.

Ling, Z.H., Guo, H., Cheng, H.R., Yu, Y.F., 2011. Sources of ambient volatile organic compounds and their contributions to photochemical ozone formation at a site in the Pearl River Delta, southern China. Environmental Pollution 159, 2310-2319.

Ling, Z.H. and Guo, H., 2013. Contribution of VOC sources to photochemical ozone formation and its control policy implication in Hong Kong. Submitted to Environmental Science and Policy.

Ling, Z.H., Guo, H., Zheng, J.Y., Louie, P.K.K., Cheng, H.R., Jiang, F., Cheung, K., Wong, L.C., Feng, X.Q., 2013. Establishing a conceptual model for photochemical ozone pollution in subtropical Hong Kong. Atmospheric Environment 76, 208-220.

Liu, H.P, Chan, J.C.L., Cheng, A.Y.S., 2000. Internal boundary layer structure under sea-breeze conditions in Hong Kong, Atmospheric Environment, 35, 683-692.

Liu, H.P., Chan, J.C.L., 2002. Boundary layer dynamics associated with a severe air-pollution episode in Hong Kong. Atmospheric Environment, 36, 2013-2025.

Liu, Y., Shao, M., Fu, L.L., Lu, S.H., Zeng, L.M., Tang, D.G., 2008a. Source profiles of volatile organic compounds (VOCs) measured in China: Part I. Atmospheric Environment, 42, 6247–6260.

Liu, Y., Shao, M., Kuster, W.C., Goldan, P.D., Li, X.H., Lu, S.H., and de Gouw, J.A., 2009. Source identification of reactive hydrocarbons and oxygenated VOCs in the summertime in Beijing Environmental Science and Technology 43, 75-81, 2009.

Liu, Y., Shao, M., Lu, S. H., Chang, C. C., Wang, J. L., Chen, G., 2008b. Volatile Organic Compound (VOC) measurements in the Pearl River Delta (PRD) region, China. Atmospheric Chemistry and Physics, 8, 1531-1545.

Liu, Y., Shao, M., Lu, S. H., Chang, C. C., Wang, J. L., Fu, L. L., 2008c. Source apportionment of ambient volatile organic compounds in the Pearl River Delta, China: Part II. Atmospheric Environment, 42, 6261-6274.

Liu, Z., Wang, Y., Gu, D., Zhao, C., Huey, L.G., Sticker, R., Liao, J., Shao, M., Zhu, T., Zeng, L., Amoroso, A., Costabile, F., Chang, C.C., Liu, S.C., 2012. Summertime photochemistry during CAREBeijing-2007: ROx budgets and O3 formation. Atmospheric Chemistry and Physics 12, 7737-7752.

Lou, S., Holland, F., Rohrer, F., Lu, K., Bohn, B., Brauers, T., Chang, C.C., Fuchs, H., Häseler, R., Kita, K., Kondo, Y., Li, X., Shao, M., Zeng, L., Wahner, A., Zhang, Y., Wang, W., Hofzumahaus, A., 2010. Atmospheric OH reactivities in the Pearl River Delta – China in summer 2006: measurement and model results. Atmospheric Chemistry and physics, 10, 11243-11260.

Louie, P.K.K., Ho, J.W.K., Tsang, R.C.W., et al., 2012. VOCs and OVOCs distribution and control policy implications in Pearl River Delta region, China. Atmos. Environ., doi: 10.1016/j.atmosenv.2012.08.058.

Loyd, A., 1979. Tropospheric chemistry of aldehydes. NBS Spec. Publ. U.S. 557, 27-48, 1979.

Lü, H., Cai, Q. Y., Chi, Y., Guo, S., Sheng, G., Fu, J., 2010. Seasonal and diurnal variations of carbonyl compounds in the urban atmosphere of Guangzhou, China. Science of the Total environment, 408, 3523-3529.

Lu, K.D., Zhang, Y.H., Su, H., Brauers, T., Chou, C.C., Hofzumahaus, A., Liu, S.C., Kita, K., Kondo, Y., Shao, M., Wahner, A., Wang, J.L., Wang, X.S., Zhu, T., 2010. Oxidant (O_3 + NO_2) production processes and formation regimes in Beijing. Journal of Geophysical Research 115, D07303, doi:10.1029/2009JD012714.

Lu, K.D., Rohrer, F., Holland, F., Fuchs, H., Bohn, B., Brauers, T., Chang, C.C., Häseler, R., Hu, M., Kita, K., Kondo, Y., Li, X., Lou, S.R., Nehr, S., Shao, M., Zeng, L.M., Wahner, A., Zhang, Y.H., Hofzumahaus, A., 2012. Observation and modeling of OH and HO_2 concentrations in the Pearl River Delta 2006: a missing OH source in a VOC rich atmosphere. Atmospheric Chemistry and Physics 12, 1541-1569.

Ma., Z. Q., Zhang, X. L., Xu, J., Zhao, X. J., and Wei, M.: Characteristics of ozone vertical profile observed in the boundary layer around Beijing in autumn, J. Environ. Sci., 23 (8), 1316-1324, 2011.

Madronic, S., 2012. NCAR/ACD TUV: Tropospheric ultraviolet & visible radiation model. Available at the website: http://cprm.acd.ucar.edu/models/TUV.

Martinez, M., Harder, H., Kovacs, T.A., Simpas, J.B., Bassis, J., Lesher, R., Brune, W.H., Frost, G.J., Williams, E.J., Stroud, C.A., Jobson, B.T., Roberts, J.M., Hall, S.R., Shetter, R.E., Wert, B., Fried, A., Alicke, B., Stutz, J., Young, V.L., White, A.B., Zamora, R.J., 2003. OH and HO_2 concentrations, sources, and loss rates during the Southern Oxidants Study in Nashville, Tennessee, summer 1999. Journal of Geophysical Research 108, D19, 4617, doi:10.1029/2003JD003551.

Mauzerall, D. L., Wang, X., 2001. Protecting agricultural crops from the effects of tropospheric ozone exposure-reconciling science and standard setting. Annual Review of Energy and Environment, 26, 237–268.

McKeen, S. A., Trainer, M., Hsie, E. Y., Tallamrayu, R. K., Liu, S. C.: On the indirect determination of atmospheric OH radical concentrations from reactive hydrocarbon measurements. J. Geophys. Res., 95 (D6), 7493–7500, 1990.

Milford, J., Gao, D., Sillman, S., Blossey, P., Russell, A.G., 1994. Total reactive nitrogen (NO_y) as an indicator for the sensitivity of ozone to NO_x and hydrocarbons. Journal of Geophysical Research 99, 3533-3542.

Miller, S. L., Anderson, M. J., Daly, E. P., Milfrod, J. B., 2002. Source apportionment of exposures to volatile organic compounds. I. Evaluation of receptor models using simulated exposure data. Atmospheric Environment, 36, 3629-3641.

Mlawer, E. J., Taubman, S. J., Brown, P. D., Iacono, M. J. and Clough, S. A.: Radiative transfer for inhomogeneous atmospheres: RRTM, a validated correlated-k model for the longwave. J. Geophys. Res., 102D, 16663–16682, 1997.

Mlawer, E.J., Taubman, S.J., Brown, P.D., Iacono, M.J., Clough, S.A., 1997. Radiative transfer for inhomogeneous atmospheres: RRTM, a validated correlated-k model for the longwave. Journal of Geophysical Research 102D, 16663–16682, 1997.

Monks, P. S., 2000. A review of the observations and origins of the spring ozone maximum. Atmospheric Environment 34, 3545-3561.

Monteiro, A., Strunk, A., Carvalho, A., Tchepep, O., Miranda, A. I., Borrego, C., Saavedra, S., Rpdríguez, A., Souto, J., Casares, J., Friese, E., and Elbern, H., 2012. Investigating a high ozone episode in a rural mountain site. Environmental Pollution, 162, 176-189.

Morikawa, T., Wakamatsu, S., Tanaka, M., Uno, I., Kamiura, T., Maeda, T., 1998. C2-C5 hydrocarbon concentrations in central Osaka. Atmospheric Environment, 32, 2007-2016.

Mugica, V., Vega, E., Sánchez, G., Reyes, E., Arriaga, J.L., Chow, J.,Watson, J., Egami, R., 2001. Volatile organic compounds emissions from gasoline and diesel powered vehicles. Atmósfera 14, 29-37. Website: http://www.ejournal.unam.mx/atm/Vol14-1/ATM14103.pdf.

Na, K., Kim, Y.P. 2007. Chemical mass balance receptor model applied to ambient C2-C9VOC concentration in Seoul, Korea: Effect of chemical reaction losses. Atmos. Environ. 41, 6715-6728.

NESCAUM (Northeast States for Coordinated Air Use Management), 1995: Preview of 1994

NRC(National Research Council), 1991. Rethinking the Ozone Problem in Urban and Regional Air Pollution. National Academic Press, Washington, DC.

Oltmans, S. J., Lefohn, A. S., Harris, J. M., Galbally, I., Scheel, H. E., Bodeker, G., Brunke, E., Claude, H., Tarasick, D., Johnson, B. J., Simmonds, P., Shadwick, D., Anlauf, K., Hayden, K., Schmidlin, F., Fujimoto, T., Akagi, K., Meyer, C., Nichol, S., Davies, J., Redondas, A., Cuevas, E., 2006. Long-term changes in tropospheric ozone. Atmospheric Environment, 40, 3156-3173.

Oltmans, S. J., Lefohn, A. S., Harris, J. M., Shadwick, D. S., 2008. Background ozone levels of air entering the west coast of the US and assessment of longer-term changes. Atmospheric Environment, 42, 6020-6038.

Ou Yang, C. F., Liu, N. H., Sheu, G. R., Lee, C. T., and Wang, J. L., 2012. Seasonal and diurnal variations of ozone at a high-altitude mountain baseline station in East Asia. Atmospheric Environment, 46, 279-288.

Paatero, P., 1997. Least squares formulation of robust non-negative factor analysis. Chemometrics and Intelligent Laboratory Systems 37, 23-35.

Paatero, P., 2000a. User's Guide for Positive Matrix Factorization Programs PMF2 and PMF3, Part 1: Tutorial. Prepared by University of Helsinki, Finland (February).

Paatero, P., 2000b. User's Guide for Positive Matrix Factorization Programs PMF2 and PMF3, Part 2: Reference. Prepared by University of Helsinki, Finland (February).

Paatero, P., Tapper, U., 1994. Positive matrix factorization: a non-negative factor model with optimal utilization of error estimates of data values. Environmetrics 5, 111-126.

Parrish, D. D., Buhr, M. P., Trainer, M., Northon, R. B., Shimshock, J. P., Fehsenfeld, F. C., Anlauf, K. G., Bottenheim, J. W., Tang, Y. Z., Wiebe, H. A., Roberts, J. M., Tanner, R. L., Newman, L., Bowersox, V. C., Olszyna, K. J., Bailey, E. M., Rodgers, M. O., Wang, T., Berresheim, H., Roychowdhury, U. K., and Demerjiani, K.L., 1993. The total reactive oxidized nitrogen levels and their partitioning between the individual species at six rural sites in eastern North America. Journal of Geophysical Research 98(D2), 2927-2939.

Parrish, D. D., Dunlea, E. J., Atlas, E. L., Schauffler, S., Donnelly, S., Stroud, V., Goldstein, A. H., Millet, D. B., Mckay, M., Jaffe, D. A., Price, H. U., Hess, P. G., Flocke, F., Roberts, J. M., 2004. Changes in the photochemical environment of the temperate North Pacific troposphere in response to increased Asian emissions. Journal of Geophysical Research, 109, D23, doi: 10.1029/2004JD004978.

Parrish, D. D., Millet, D. B., Goldstein, A. H., 2009. Increasing ozone in marine boundary layer inflow at the west coasts of North America and Europe. Atmospheric Chemistry and Physics, 9, 1303-1323.

Pinho, P.G., Lemos, L.T., Pio, C.A., Evtyugina, M.G., Nunes, T.V., Jenkin, M.E., 2009. Detailed chemical analysis of regional-scale air pollution in western Portugal using an adapted version of MCM v3.1. Science of the Total Environment 407, 2024-2038.

Pochanart, P., Akimoto, H., Kajii, Y., Potemkin, V. M., and Khodzher, V. T., 2003. Regional background ozone and carbon monoxide variations in remote Siberia/east Asia. Journal of Geophysical Research, 108, D1, doi: 10.1029/2001JD001412.

Poisson, N., Kanakidou, M., Crutzen, P.J., 2000. Impact of non-methane hydrocarbons on tropospheric chemistry and the oxidizing power of the global troposphere: 3-dimensional modelling results. Journal of Atmospheric Chemistry 36, 157-230.

PORG (Photochemical Oxidants Review Group): Ozone in the United Kingdom, Fourth Report of the UK photochemical Oxidants review group, Department of the Environment, Transport and the Regions, London, 1997.

Pun, B.K., Louis, J.F., Seigneur, C., 1998. A conceptual model for ozone formation in the San Joaquin Valley. Atmospheric Environmental Research, Inc.

Reeves, C. E., Slemr, J., Oram, D. E., Worton, D., Penkett, S. A., Stewart, D. J., Purvis, R., Watson, N., Hopkins, J., Lewis, A., Methven, J., Blake, D. R., and Atlas, E., 2007. Alkyl nitrates in outflow from North America over the North Atlantic during Intercontinental Transport of Ozone and Precursors 2004. Journal of Geophysical Research 112, doi:10.1029/2006JD007567, 2007.

Ren, X.R., Brune, W.H., Mao, J.Q., Mitchell, M.J., Lesher, R.L., Simpas, J.B., Metcalf, A.R., Schwab, J.J. Cai, C.X., Li, Y.Q., Demerjian, K.L., Felton, H.D., Boynton, G., Adams, A., Perry, J., He, Y., Zhou, X.L., Hou, J., 2006. Behavior of OH and HO2 in the winter atmosphere in New York City. Atmospheric Environment 40, S252-S263.

Ren, X.R., Olson, J.R., Crawford, J.H., Brune, W.H., Mao, J.Q., Long, R.B., Chen, Z., Chen, G., Avery, M.A., Sachse, G.W., Barrick, J.D., Diskin, G.S., Huey, L.G., Fried, A., Cohen, R.C., Heikes, B., Wennberg, P.O., Singh, H.B., Blake, D.R., Shetter, R.E., 2008. HOx chemistry during INTEX-2004: observation, model calculation, and comparison with previous studies. Journal of Geophysical Research,

Ren, X.R., van Duin, D., Cazorla, M., Chen, S., Mao, J.Q., Zhang, L., Brune, W.H., Flynn, J.H., Grossberg, N., Lefer, B.L., Rappenglück, B., Wong, K.W., Tsai, C., Stutz, J., Dibb, J.E., Jobson, B.T., Luke, W.T., Kelley, P., 2013. Atmospheric oxidation chemistry and ozone production: results from SHARP 2009 in Houston, Texas. Journal of Geophysical Research 118, 1-11, doi:10.1002/jgrd.50342.

Roberts, J. M., Bertman, S. B., Parrish, D. D., Fehsenfeld, F. C., Jobson, B. T., and Niki, H.: Measurement of alkyl nitrates at Chebogue Point, Nova Scotia during the 1993 North Atlantic Regional Experiment (NARE) intensive, J. Geophys. Res., 103, 13569-13580, 1998.

Russell, A., Dennis, R., 2000. NARSTO critical review of photochemical models and modelling. Atmospheric Environment 34, 2283-2324.

Ryerson, T. B., Trainer, M., Angevine, W. M., Brock, C. A., Dissly, R. W., Fehsenfeld, F. C., Frost, G. J., Goldan, P. D., Holloway, J. S., Hübler, G., Jakoubek, R. O., Kuster, W. C., Neuman, J. A., Nicks Jr, D. K., Parrish, D. D., Roberts, J. M., Sueper, D. T., Atlas, E. L., Donnelly, S. G., Flocke, F., Fried, A., Potter, W. T., Schauffler, S., Stroud, V., Weinheimer, A. J., Wert, B. P., Wiedinmyer, C., Alvarez, R. J., Banta, R. M., Darby, L. S., Senff, C. J., 2003. Effect of petrochemical industrial emissions of reactive alkenes and NO_x on tropospheric ozone formation in Houston, Texas. Journal of Geophysical Research, 108, D8, doi: 10.1029/2002JD003070, 2003.

Sander, S.P., Friedl, R.R., Ravishankara, A.R., Golden, D.M., Kurylo, M.J., Molina, M.J., Moortgat, G.K., Keller-Rudek, H., Finlayson-Pitts, B.J., Wine, P.H., Huie, R.E., Orkin, V.L., 2006. Chemical Kinetics and Photochemical Data for Use in Atmospheric Studies. Evaluation Number 15.

Saunders, S. M., Jenkin, M. E., Derwent, R. G., and Pilling, M. J., 2003. Protocol for the development of the master chemical mechanism MCMv3 (Part A): Tropospheric degradation of non-aromatic volatile organic compounds. Atmos. Chem. and Phys., 3, 161-180.

Sauvage, S., Plaisance, H., Locoge, A., Wroblewski, A., Coddeville, P., Galloo, J.C., 2009. Long term measurement and source apportionment of non-methane hydrocarbons in three French rural areas. Atmospheric Environment 43, 2430-2441.

Scott, B. and Ahmet, P., 2009. Influence of synoptic and mesoscale meteorology on ozone pollution potential for San Joaquin Valley of California. Atmospheric Environment, 43, 1779-1788.

Seila, R.L., Main, H.H., Arriaga, J.L., Martinez, G.V., Ramadan, A.B., 2001. Atmospheric volatile organic compounds measurements during the 1996 Paso del Norte ozone study. Science of the Total Environment 276, 153-169.

Seinfeld, J.H. and Pandis, S.N., 2006. Atmospheric Chemistry and Physics: from air pollution to climate change, 2nd edition. Wiley Publisher, New Jersey, USA.

Shao, M., Lu, S., Liu, Y., Xie, X., Chang, C., Huang, S., Chen, Z., 2009a. Volatile organic compounds measured in summer in Beijing and their role in ground-level ozone formation. Journal of Geophysical Research, 114, D00G06, doi: 10.1029/2008JD010863.

Shao, M., Zhang, Y. H., Zeng, L. M., Tang, X. Y., Zhang, J., Zhong, L. J., Wang, B. G., 2009b. Ground-level ozone in the Pearl River Delta and the roles of VOC and NOx in its production, Journal of Environmental Management, 90, 512-518, 2009.

Shirley, T.R., Brune, W.H., Ren, X., Mao, J., Lesher, R., Cardenas, B., Volkamer, R., Molina, L.T., Molina, M.J., Lamb, B., Velasco, E., Jobson, T., Alexander, M., 2006. Atmospheric oxidation in the Mexico City Metropolitan Area (MCMA) during April 2003. Atmospheric Chemistry and Physics 6, 2753–2765.

Shiu, C.J., Liu, S.C., Chang, C.C., Chen, J.P., Chou, C.C.K., Lin, C.Y., Young, C.Y., 2007. Photochemical production of ozone and control strategy for Southern Taiwan. Atmospheric Environment 41, 9324-9340.

Sillman, S., 1999. The relation between ozone, NOx and hydrocarbons in urban and polluted rural environments. Atmospheric Environment 33, 1821-1845.

Sillman, S., He, D.Y., and Pippin, M.R., 1998. Model correlations for ozone, reactive nitrogen, and peroxides for Nashville in comparison with measurements: Implications for O3-NOx-hydrocarbon chemistry, Journal of Geophysical Research 103 (D17), 22629-22644, 1998.

Sillman, S., Vautard, R., Menut, L., Kley, D., 2003. O_3-NO_x-VOC sensitivity and NOx-VOC indicators in Paris: Results from models and atmospheric pollution over the Paris Area (ESQUIF) measurements. Journal of Geophysical Research 108, D17, 8563, doi:10.1029/2002JD001561, 2003.

Simmonds, P. G., Derwent, R. G., Manning, A. L., Spain, G., 2004. Significant growth in surface ozone at Mace Head, Irland, 1987-2003. Atmospheric Environment, 38, 4769-4778.

Simpson, D., 1995. Hydrocarbon reactivity and ozone formation in Europe. Journal of Atmospheric Chemistry, 20, 163-177.

Simpson, I. J., Blake, N. J., Barletta, B., Diskin, G. S., Fuelberg, H. E., Gorham, K., Huey, L. G., Meinardi, S., Rowland, F. S., Vay, S. A., Weinheimer, A. J., Yang,

M., and Blake, D. R.: Characterization of trace gases measured over Alberta oil sands mining operations: 76 speciated C_2-C_{10} volatile organic compounds (VOCs), CO_2, CH_4, CO, NO, NO_2, NO_y, O_3 and SO_2, Atmospheric Chemistry and Physics 10, 11931-11954, 2010.

Simpson, I. J., Rowland, F. S., Meinardi, S., Blake, D. R., 2006. Influence of biomass burning during recent fluctuations in the slow growth of global tropospheric methane. Geophysical Research Letter, 33, L22808, doi: 10.1029/2006GL027330.

Sin, D. W. M., Wong, Y. C., Louie, P. K. K., 2000. Monitoring of ambient volatile organic compounds at two urban sites in Hong Kong from 1997 to 1998. Indoor and Built Environment, 9, 216–227.

Singh, H. B., M. Kanakidou, P. J. Crutzen, D. J. Jacob, 1995. High concentrations and photochemical fate of oxygenated hydrocarbons in the global troposphere. Nature, 378, 50-54.

Singh, H. B., Salas, L. J., Chatfield, R. B., Czech, E., Fried, A., Walega, J., Evans, M. J., Field, B. D., Jacob, D. J., Blake, D., Heikes, B., Talbot, R., Sachse, G., Crawford, J. H., Avery, M. A., Sandholm, S., Fuelberg, H., 2004. Analysis of the atmospheric distribution, sources, and sinks of oxygenated volatile organic chemicals based on measurements over the Pacific during TRACE-P. Journal of Geophysical Research, 109, D15, doi: 10.1029/2003JD003883.

Singh, H., Chen, Y., Staudt, A., Jacob, D., Blake, D., Heikes, B., Snow, J., 2001. Evidence from the Pacific troposphere for large global sources of oxygenated organic compounds. Nature, 410, 1078-1082.

Singh, H.B., Salas, L.J., Smith, A.J., Shigeishi, H., 1981. Measurements of some potentially hazardous organic chemicals in urban environments. Atmospheric Environment 15, 601-612.

Skamarock, W.C. and Klemp, J.B., 2008. A time split non hydrostatic atmospheric model for weather research and forecasting applications, Journal of Computational Physics 227, 7, 3465-3485.

So, K. L. and Wang, T., 2003. On the local and regional influence on ground-level ozone concentrations in Hong Kong. Environmental Pollution 123, 307-317.

So, K. L. and Wang, T., 2004. C_3-C_{12} non-methane hydrocarbons in subtropical Hong Kong: spatial-temporal variations, source-receptor relationships and photochemical reactivity. Science of the Total Environment, 328, 161-174.

Solomon, P., Cowling, E., Hidy, G., Furiness, C., 2000. Comparison of scientific findings from major ozone field studies in North America and Europe. Atmospheric Environment, 34, 1885-1920.

Sommariva, R., Haggerstone, A.L., Carpenter, L.J., Carslaw, N., Creasey, D.J., Heard, D.E., Lee, J.D., Lewis, A.C., Pilling, M.J., Zádor, J., 2004. OH and HO2 chemistry in clean marine air during SOAPEX-2. Atmospheric Chemistry and Physics 4, 839-856.

Song, Y., Dai, W., Shao, M., et al., 2008. Comparison of receptor models for source apportionment of volatile organic compounds in Beijing, China. Environ. Pollut. 156, 174-183.

Song, Y., Shao, M., Liu, Y., Lu, S.H., Kuster, W., Goldan, P., 2007. Source apportionment of ambient volatile organic compounds in Beijing. Environmental Science and Technology 41, 4348-4353.

Starn, T. K., Shepson, P. B., Riemer, D. D., Zika, R. G. and Olzyna, K., 1998. Nighttime isoprene chemistry at an urban-impacted forest site. Journal of Geophysical Research 103, 22437-22447, 1998.

Steinbacher, M., Zellweger, C., Schwarzenbach, B., Bugmann, S., Buchmann, B., Ordónez, C., Prevot, A., and Hueglin, C.: Nitrogen oxide measurements at rural sites in Switzerland: Bias of conventional measurement techniques, J. Geophys. Res., 112, D11307, 2007.

Steven, E.K., Benjamin, S.G., McGinley, J.A., Brown, J.M., Schultz, P., Szoke, E.J., Smirnova, T.G., Shaw, B.L., Birkenheuer, D., Albers, S., Peckham, S., Grell, G., 2004. Real-time Applications of the WRF Model at the Forecast Systems Laboratory, 84th AMS Annual Meeting, Seattle, U. S.A., Jan 10-15, 2004.

Stohl, A., 1998. Computation, accuracy and application of trajectories – A review and bibliography. Atmospheric Environment, 32, 6, 947-966.

Tan, J.H., Guo, S.J., Ma, Y.L., Yang, F.M., He, K.B., Yu, Y.C., Wang, J.W., Shi, Z.B., Chen, G.C., 2012. Non-methane hydrocarbons and their ozone formation potentials in Foshan, China. Aerosol and Air Quality Research, 12, 387–398.

Tang, G., Wang, Y., Li, X., Ji, D., Hsu, S., and Gao, X., 2012. Spatial-temporal variations in surface ozone in Northern China as observed during 2009-2010 and possible implications for future air quality control strategies, Atmospheric Chemistry and Physics 12, 2757-2776, 2012.

Tang, J.H., Chan, L.Y., Chan, C.Y., Li, Y.S., Chang, C.C., Liu, S.C., Wu, D., Li, Y.D., 2007a. Regional and local contributions to ambient non-methane volatile organic compounds at a polluted rural/coastal site in Pearl River Delta, China. Atmospheric Environment, 41, 8620-8632.

Tang, J.H., Chan, L.Y., Chan, C.Y., et al., 2008. Implications of changing urban and rural emissions on non-methane hydrocarbons in the Pearl River Delta region of China. Atmos. Environ. 42, 3780-3794.

Tang, J.H., Chan, L.Y., Chan, C.Y., Li, Y.S., Chang, C.C., Liu, S.C., Wu, D., Li, Y.D., 2007b. Characteristics and diurnal variations of NMHCs at urban, suburban, and rural sites in the Pearl River Delta and a remote site in South China. Atmospheric Environment 41, 8620-8632.

Tang, X.Y., Zhang, Y.H., Shao,M., 2006. Atmospheric Environmental Chemistry, Higher Education Press, China, 2nd edition, 58-60.

Tanimoto, H., 2009. Increase in springtime tropospheric ozone at a mountainous site in Japan for the period 1998-2006. Atmospheric Environment 43, 1358-1363.

Tanimoto, H., Furutani, H., Kato, S., Matsumoto, J., Makide, Y., Akimoto, H., 2002. Seasonal cycles of ozone and oxidized nitrogen species in northeast Asia - 1. Impact of regional climatology and photochemistry observed during RISOTTO 1999-2000. Journal of Geophysical Research, 107, D24, doi: 10.1029/2001JD001496.

Tarasova, O. A., Senik, I. A., Sosonkin, M. G., Cui, J., Staehelin, J., Prévôt., 2009. Surface ozone at the Caucasian site Kislovodsk high mountain station and the Swiss Alpine site Junfraujoch: data analsis and trends (1990-2006). Atmospheric Chemistry and Physics, 9, 4257-4175.

Thornton, J.A., Wooldridge, P.J., Cohen, R.C., et al., 2002. Ozone production rates as a function of NOx abundances and Hox production rates in the Nashville urban plume. J. Geophys. Res. 107 (D12), 4146, doi :10.1029/2001JD000932.

Tiwari, S., Rai, R., Agrawal, M., 2008. Annual and seasonal variations in tropospheric ozone concentrations around Varanasi. International Journal of Remote Sensing 29, 4499-4514.

Tom, D., Richard, F., Robert, H., Iyad, K., Gary, K., Paul, M., Leah, W., 2006. The nature of the ozone air quality problem in the ozone transport region: a conceptual description. Prepared for the ozone transport commission. NESCAUM, Boston, MA.

Tsai, W.Y., Chan, L.Y., Blake, D.R., Chu, K.W., 2006. Vehicular fuel composition and atmospheric emissions in South China: Hong Kong, Macau, Guangzhou, and Zhuhai. Atmospheric Chemistry and Physics 6, 3281-3288.

Tseng, K. H., Chen, C. L., Lin, M. D., Chang, K. H., and Tsuang, B. J.: Vertical profile of ozone and accompanying air pollutant concentrations observed at a downwind foothill site of industrial and urban areas, Aerosol Air Qual. Res., 9, 421-434, 2009.

Tsui, J.K.Y., Guenther, A., Yip, W.K., Chen, F., 2009. A biogenic volatile organic compound emission inventory for Hong Kong. Atmospheric Environment 43, 6442-6448.

Turnipseed, A.A., Anderson, D.E., Burns, S., Blanken, P.D., and Monson, R.K.:, 2004. Airflows and turbulent flux measurements in mountainous terrain Part 2: mesoscale effects, AGR. Forest Meterology 125, 187-205.

Vingarzan, R., 2004. A review of surface ozone background levels and trends. Atmospheric Environment 38, 3431-3442.

Vingarzan, R., Taylor, B., 2003. Trend analysis of ground level ozone in the greater Vancouver/Fraser Valley area of British Columbia. Atmospheric Environment 37, 2159-2171.

Volkamer, R., Sheehy, P., Molina, L.T., Molina, M.J., 2010. Oxidative capacity of the Mexico City atmosphere-Part 1: A radical source perspective. Atmospheric Chemistry and Physics 10, 6969–6991.

Vrekoussis, M., Mihalopoulos, N., Gerasopoulos, Kanakidou, E., M., Crutzen, P.J. and Lelieveld, J., 2007. Two-year of NO_3 radical observations in the boundary layer over the Eastern Mediterranean. Atmospheric Chemistry and Physics 7, 315–327, doi:10.5194/acp-7-315-2007.

Wang, H.Q., Jacob, D.J., Le Sager, P., Streets, D.G., Park, R.J., Gilliland, A.B., van Donkelaar, A., 2009. Surface ozone background in the United States: Canadian and Mexican pollution influences. Atmospheric Environment 43, 1310-1319.

Wang, J.L., Wang, C.H., Lai, C.H., Chang, C.C., Liu, Y.L., Zhang, Y.H., Liu, S., Shao, M., 2008. Characterization of ozone precursors in the Pearl River Delta by time series observation of non-methane hydrocarbons. Atmospheric Environment, 42, 6233-6246.

Wang, T. and Kwok, J.Y.H., 2003. Measurement and analysis of a multi-day photochemical smog episode in the Pearl River Delta of China. Journal of Applied Meteorology 42, 404-416.

Wang, T.J., Lam, K.S., Xie, M., Wang, X.M., Carmichael, G., Li, Y.S., 2006a. Integrated studies of a photochemical smog episode in Hong Kong and regional transport in the Pearl River Delta of China. Tellus Ser. B-Chem. Phys. Meteorol. 58, 31-40.

Wang, T., Cheung, V.T.F., Lam, K.S., Kok, G.L., and Harris, J.M., 2001. The characteristics of ozone and related compounds in the boundary layer of the South China coast: temporal and vertical variations during autumn season, Atmospheric Environment 35, 2735-2746.

Wang, T., Guo, H., Blake, D.R., Kwok, Y.H., Simpson, I.J., Li, Y.S., 2005. Measurements of trace gases in the inflow of South China Sea background air and outflow of regional pollution at Tai O, Southern China. Journal of Atmospheric Chemistry, 52, 295-317.

Wang, T., Lam, K.S., Lee, A.S.Y., Pang, S.W., Tsui, W.S., 1998. Meteorological and chemical characteristics of the photochemical ozone episodes observed at Cape D'Aguilar in Hong Kong. Journal of Applied Meteorology 37, 1167-1178.

Wang, T., Poon, C.N., Kwok, Y.H., Li, Y.S., 2003. Characterizing the temporal variability and emission patterns of pollution plumes in the Pearl River Delta of China. Atmospheric Environment, 37, 25, 3539-3550.

Wang, T., Wei, X.L., Ding, A.J., Poon, C.N., Lam, K.S., Li, Y.S., Chan, L.Y., Anson, M., 2009. Increasing surface ozone concentrations in the background atmosphere of Southern China, 1994-2007. Atmospheric Chemistry and Physics, 9, 6217-6227.

Wang, T., Wong, H.L.A., Tang, J., Ding, A., Wu, W. S., and Zhang, X.C., 2006b. On the origin of surface ozone and reactive nitrogen observed at remote site in the northeastern Qinghai-Tibetan Plateau, western China, Journal of Geophysical Research, 111, D08303, doi: 10.1029/2005JD006527.

Wang, Y., Zhang, Y., Hao, J., Luo, M., 2011. Seasonal and spatial variability of surface ozone over China: contributions from background and domestic pollution. Atmospheric Chemistry and Physics, 11, 3511-3525.

Ward, J.H., 1963. Hierarchical grouping to optimize an objective function. Journal of the American Statistical Association 48, 236-244.

Warneke, C. and de Gouw, J.A., 2001. Organic trace gas composition of the marine boundary layer over the northwest India Ocean in April 2000. Atmospheric Environment 35, 5923-5933.

Warneke, C., Gouw, J.A., Goldan, P.D., Kuster, W.C., Williams, E.J., Lerner, B.M., Jakoubek, R., Brown, S.S., Stark, H., Aldener, M., Ravishankara, A.R., Roberts, J.M., Marchewka, M., Bertman, S., Sueper, D.T., Mckeen, S.A., Meagher, J.F., Fehsenfeld, F.C., 2004. Comparison of daytime and nighttime oxidation of biogenic and anthropogenic VOCs along the New England coast in summer during New England Air Quality Study. Journal of Geophysical Research-Atmospheres, 109, D10.

Watson, J.G., Chow, J.C., Fujita, E.M., 2001. Review of volatile organic compound source apportionment by chemical mass balance. Atmospheric Environment 35, 1567-1584.

Wennberg, P.O., Hanisco, T.F., Jaegle, L., Jacob, E.J., Hintsa, E.J., Lanzendorf, J.G., Anderson, J.G., Gao, R.S., Keim, E.R., Donnelly, S.G., 1998. Hydrogen radicals, nitrogen radicals, and the production of ozone in the upper troposphere. Science, 279, 49-53.

Xie, Y.L. and Bekowitz, C.M., 2006. The use of positive matrix factorization with conditional probability functions in air quality studies: An application to hydrocarbon emissions in Houston, Texas. Atmospheric Environment 40, 3070-3091.

Xu, X., Lin, W., Wang, T., Yan, P., Tang, J., Meng, Z., Wang, Y., 2008. Long-term trend of surface ozone at a regional background station in eastern China 1991-2006: enhanced variability. Atmospheric Chemistry and Physics, 8, 2595-2607.

Xu, Z., Wang, T., Xue, L.K., Louie, P., Luk, C., Gao, J., Wang, S.L., Chai, F.H., Wang, W.X., 2013. Evaluating the uncertainties of thermal catalytic conversion for measuring atmospheric nitrogen dioxide at four polluted sites in China, Atmospheric Environment, doi:10.1016/j.atmosenv.2012.09.043.

Xue, L. K., Wang, T., Zhang, J. M., Zhang, X. C., Delig-Geer, Poon, C. N., Ding, A. J., Zhou, X. H., Wu, W. S., Tang, J., Zhang, Q. Z., and Wang, W. X., 2011. Source of surface ozone and reactive nitrogen speciation at Mount Waliguan in Western China: New insights from the 2006 summer study. Journal of Geophysical Research, 116, D07306, dio:10.1029/2010JD014735.

Yoshino, A., Sadanaga, Y., Watanabe, K., Kato, S., Miyakawa, Y., Matsumoto, J., Kajii, Y., 2006. Measurement of total OH reactivity by laser-induced pump and probe technique – comprehensive observations in the urban atmosphere of Tokyo. Atmospheric Environment 40, 7869-7881.

Yuan, B., Chen, W. T., Shao, M., Wang, M., Lu, S. H., Wang, B., Liu, Y., Chang, C. C., Wang, B., 2012b. Measurements of ambient hydrocarbons and carbonyls in the Pearl River Delta (PRD), China. Atmospheric Research, 116, 93–104.

Yuan, Z. B., Zhong, L. J., Lau, A. K. H., Yu, J. Z., Louie, P. K. K., 2012a. Volatile organic compounds in the Pearl River Delta: Identification of source regions and recommendations for emission-oriented monitoring strategies. Atmospheric Environment, http://dx.doi.org/10.1016/j.atmosenv.2012.11.034.

Yuan, Z.B., Lau, A.K.H., Shao, M., Louie, P.K.K., Liu, S.C., Zhu, T., 2009. Source analysis of volatile organic compounds by positive matrix factorization in urban and rural environments in Beijing. Journal of Geophysical Research 114, D00G15, doi:10.1029/2008JD011190.

Zanis, P., Ganser, A., Zellweger, C., Henne, S., Steinbacher, M., Staehelin, J.: Seasonal variability of measured ozone production efficiencies in the lower free troposphere of central Europe, Atmos. Chem. Phys., 7, 223-236, doi:10.5194/acp-7-223-2007, 2007.

Zellweger, C., Forrer, P., Nyeki, S., Schwarzenbach, B. M. M., Weingarter, E., Ammann, M., and Baltensperger, U., 2003. Partitioning of reactive nitrogen (NO_y) and dependence on meteorological conditions in the lower free troposphere. Atmospheric Chemistry and Physics, 3, 779-796, 2003.

Zhang, D., Anthes, R.A., 1982. A high-resolution model of the planetary boundary layer—sensitivity tests and comparison with SESAME-79 data. Journal of Applied Meteorology 21, 1594–1609.

Zhang, J., Wang, T., Chameides, W. L., Cardelino, C., Blake, D. R., Streets, D. G., 2008. Source characteristics of volatile organic compounds during high ozone episodes in Hong Kong, Southern China. Atmospheric Chemistry and Physics, 8, 4983-4996.

Zhang, J., Wang, T., Chameides, W. L., Cardelino, C., Kwok, J., Blake, D. R., Ding, A. J., So, K. L., 2007. Ozone production and hydrocarbon reactivity in Hong Kong, Southern China. Atmospheric Chemistry and Physics 7, 557-573.

Zhang, L. F., and Zhang, M., 1997. Study of the sea-land breeze system in Hong Kong, Hong Kong Meteorological Science Bulletin, 7, 22-42.

Zhang, Y. H., Su, H., Zhong, L. J., Cheng, Y. F., Zeng, L. M., Wang, X. S., Xiang, Y. R., Wang, J. L., Gao, D. F., Shao, M., Fan, S. J., Liu, S. C., 2008. Regional ozone pollution and observation-based approach for analyzing ozone-precursor relationship during the PRIDE-PRD2004 campaign. Atmospheric Environment 42, 6203-6218.

Zhang, Y.L., Wang, X.M., Barletta, B., Simpson, I.J., Blake, D.R., Fu, X.X., Zhang, Z., He, Q. F., Liu, T.Y., Zhao, X.Y., Ding, X., 2013. Source attributions of hazardous aromatic hydrocarbons in urban, suburban and rural areas in the Pearl River Delta (PRD) region. Journal of Hazardous Materials, 250-251, 403-411.

Zhang, Y.L., Wang, X.M., Blake, D.R., Li, L.F., Zhang, Z., Wang, S.Y., Guo, H., Lee, S.C., Gao, B., Chan, L.Y., Wu, D., Rowland, F.S., 2012. Aromatic hydrocarbons as ozone precursors before and after outbreak of the 2008 financial crisis in the Pearl River Delta region, south China. Journal of Geophysical Research, 117, D15306, doi: 10.1029/2011JD017356, 2012.

Zhao, Y., Shao, M., Wang, C., Wang, B.G., Lu, S.H., Zhong, L.J., 2011. Characterizing spatial patterns of NO_x, SO_2 and O_3 in Pearl River Delta by Passive Sampling, Environmental Science 32, 324-329.

Zhao, Y., Shao, M., Wang, C., Wang, B.G., Lu, S.H., Zhong, L.J., 2011. Characterizing spatial patterns of NOx, SO2 and O3 in Pearl River Delta by Passive Sampling, Environmental Science 32, 324-329.

Zheng, J.Y., Shao, M., Che, W.W., Zhang, L.J., Zhong, L.J., Zhang, Y.H., Streets, D., 2009b. Speciated VOC emission inventory and spatial patterns of ozone formation potential in the Pearl River Delta, China. Environmental Science and Technology 43, 8580-8586.

Zheng, J.Y., Zhang, L.J., Che, W.W., et al., 2009a. A highly resolved temporal and spatial air Pollutant emission inventory for the Pearl River Delta region, China and its uncertainty assessment. Atmospheric Environment 43, 5112-5122.

Zheng, J.Y., Yu, Y.F., Mo, Z.W., Zhang, Z., Wang, X.M., Yin, S.S., Peng, K., Yang, Y., Feng, X.Q., Cai, H.H., 2013. Industrial sector-based volatile organic compound (VOC) source profiles measured in manufacturing facilities in the Pearl River Delta, China. Science of the Total Environment, 456-457, 127-136.

Zheng, J. Y., Zhong, L. J., Wang, T., Louie, P. K. K., Li, Z. C., 2010a. Ground-level ozone in the Pearl River Delta region: analysis of data from a recently established regional air quality monitoring network. Atmospheric Environment 44, 814-823.

Zheng, J.Y., Zheng, Z. Y., Yu Y. F., Zhong, L. J., 2010b. Temporal, spatial characteristics and uncertainty of biogenic VOC emissions in the Pearl River Delta region, China. Atmospheric Environment, 44, 1960-1969.

Zhong, L., Louie, P.K.K., Zheng, J., et al., 2013. Science-policy interplay: air quality management in the Pearl River Delta region and Hong Kong. Atmos. Environ., doi: 10.1016/j.atmosenv.2013.03.012.